(12)

RADC-TR-75-134
Final Technical Report
May 1975

THERMOMECHANICAL TESTING TECHNIQUES FOR MICROCIRCUITS

Motorola, Inc.

Rome Air Development Center
Air Force Systems Command
Griffiss Air Force Base, New York 13441

Thia report has been reviewed by the RADC Information Office (OI) and ia releaaable to the National Technical Information Service (NTIS). At NTIS it will be releasable to the general public, including foreign nationa.

Thia technical report has been reviewed and approved for publication.

APPROVED: Alfred L. Tamburrino

ALFRED L. TAMBURRINO
Project Engineer

APPROVED: Lester E Treankler

LESTER E. TREANKLER, Lt Col, USAF
Acting Asaistant Chief
Reliability & Compatibility Diviaion

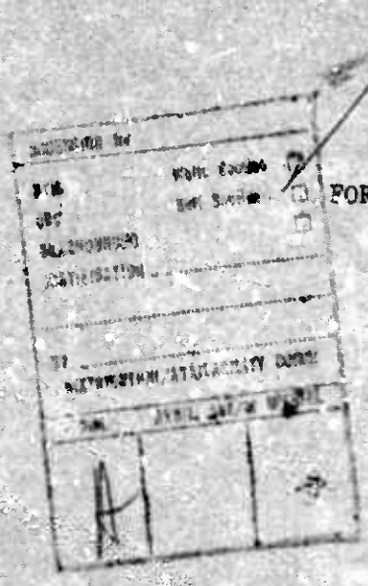

FOR THE COMMANDER: John P. Huss

JOHN P. HUSS
Acting Chief, Plans Office

Do not return this copy. Retain or deatroy.

DISCLAIMER NOTICE

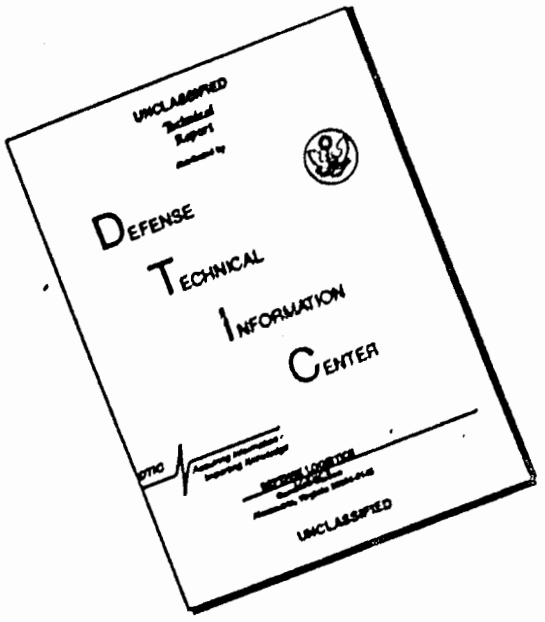

THIS DOCUMENT IS BEST QUALITY AVAILABLE. THE COPY FURNISHED TO DTIC CONTAINED A SIGNIFICANT NUMBER OF PAGES WHICH DO NOT REPRODUCE LEGIBLY.

UNCLASSIFIED

SECURITY CLASSIFICATION OF THIS PAGE (When Data Entered)

REPORT DOCUMENTATION PAGE

READ INSTRUCTIONS BEFORE COMPLETING FORM

1. REPORT NUMBER: RADC-TR-75-134	2. GOVT ACCESSION NO.
3. RECIPIENT'S CATALOG NUMBER	
4. TITLE (and Subtitle): THERMOMECHANICAL TESTING TECHNIQUES FOR MICROCIRCUITS.	5. TYPE OF REPORT & PERIOD COVERED: Final Report. Mar 72 — Dec 74
	6. PERFORMING ORG. REPORT NUMBER: N/A
7. AUTHOR(s): M. R. Carpenter, W. Fitch	8. CONTRACT OR GRANT NUMBER(s): F30602-72-C-0251
9. PERFORMING ORGANIZATION NAME AND ADDRESS: Motorola, Inc., Semiconductor Products Division, 5005 East McDowell Road, Phoenix AR 85008	10. PROGRAM ELEMENT, PROJECT, TASK AREA & WORK UNIT NUMBERS: AF-5519, 55190[illegible]
11. CONTROLLING OFFICE NAME AND ADDRESS: Rome Air Development Center (RBRP), Griffiss AFB NY 13441	12. REPORT DATE: May 75
	13. NUMBER OF PAGES: 275
14. MONITORING AGENCY NAME & ADDRESS (if different from Controlling Office): Same	15. SECURITY CLASS. (of this report): UNCLASSIFIED
	15a. DECLASSIFICATION/DOWNGRADING SCHEDULE: N/A

16. DISTRIBUTION STATEMENT (of this Report)

Approved for public release; distribution unlimited.

17. DISTRIBUTION STATEMENT (of the abstract entered in Block 20, if different from Report)

Same

18. SUPPLEMENTARY NOTES

RADC Project Engineer:
Alfred L. Tamburrino (RBRP)

DDC

19. KEY WORDS (Continue on reverse side if necessary and identify by block number)

Reliability, Microcircuits, Hermetic, Plastic, Thermal Shock, Temperature Cycling, Screening

20. ABSTRACT (Continue on reverse side if necessary and identify by block number)

This study investigated the performance of more than 3,000 plastic and hermetic 14-lead integrated circuits in various temperature cycling and thermal shock step stress and extended cycle test sequences; interaction between thermal shock preconditioning on temperature cycling; and wire bond and seal strength degradation when subjected to more than 1,000 thermal cycles. Thermal analysis of 14-lead ceramic DIP was also studied. Glass transition temperature of the various plastics was measured. The latest plastic integrated circuit with large diameter wires was the best package on long term (>4,000 cycles)

DD FORM 1 JAN 73 1473 EDITION OF 1 NOV 65 IS OBSOLETE

UNCLASSIFIED

SECURITY CLASSIFICATION OF THIS PAGE (When Data Entered)

thermal cycling. Flat packages were the best hermetic package. Major failure modes were grain boundry fracture in plastic integrated circuits and wire flex failures in hermetic. Temperature cycling affects the bonding wires whereas thermal shock affects the package hermeticity. Mean wire pull strength does degrade approximately 10% in 1,000 cycles, with some zero strength bonds occurring after 240 cycles. The ceramic dual-in-line glass seal shows an average degradation of 6.4 in-lbs/1,000 cycles in strength with extended cycling. The mean number of cycles to failure was 7,800.

TABLE OF CONTENTS

TABLE OF CONTENTS (Cont'd)

TABLE OF CONTENTS (Cont'd)

TABLE OF CONTENTS (Cont'd)

LIST OF TABLES

LIST OF TABLES (Cont'd)

LIST OF ILLUSTRATIONS

LIST OF ILLUSTRATIONS (Cont'd)

LIST OF ILLUSTRATIONS (Cont'd)

LIST OF ILLUSTRATIONS (Cont'd)

LIST OF ILLUSTRATIONS (Cont'd)

EVALUATION

Thermal tests such as air-to-air temperature cycling and liquid-to-liquid thermal shock are important environmental requirements for microcircuit devices. This study has comprehensively investigated the response of a wide variety of modern microcircuit types in both hermetic and plastic packages to many variations of these stresses for many thousands of cycles. We have learned which package types are strongest, how wire bonds degrade, which tests (and at what range and number of cycles) result in device degradation, and how effective are screening tests using temperature cycling and/or thermal shock.

This data may be used to estimate failure rate under cycled conditions, to improve screening and qualification specifications, to improve device design for greater environmental strength, and to evaluate the capabilities of various package types.

Regarding the plastic vs. hermetic controversy, it will be found that although it is shown that plastic molded parts may behave quite well under cycled temperature environments, they may also perform very poorly. Because of this variability, lack of general confidence in the plastic package remains. However, the high frequency of hermeticity failures of the ceramic dual-in-line package is also cause for concern, and RADC's emphasis on package strength, hermeticity and cleanliness continues.

Alfred L. Tamburrino

ALFRED L. TAMBURRINO
Chief, Reliability Physics Section
Reliability Branch

SECTION I

1.0 INTRODUCTION

Thermal mechanical tests, temperature cycling and thermal shock have long been used to evaluate and screen integrated circuits. The mechanical stresses at the temperature extremes used in these tests induced by the differences in the thermal expansion coefficients of the materials used to fabricate a complete integrated circuit, become concentrated at material defects such as cracks and voids. This increased stress may rupture or fracture the material at the point of defect or cause fatigue-type failures upon repeated application of the stress through repeated cycling. Since these stresses are most critical at material interfaces, these tests have been used to detect bad wire bonds and die bonds, poor metallization, marginal package seals. The repeated application of the mechanical stresses characteristic of these tests will also cause propagation of cracks in brittle materials.

Temperature cycling is an air-to-air test. Method 1010 of MIL-STD-883 defines a test where the devices are alternately placed in a hot chamber and then a cold chamber until 10 exposures at each extreme are completed. The devices remain a minimum of 10 minutes after the test chamber temperature has stabilized to assure that the devices reach thermal equilibrium with the air in the chamber under these conditions. The transfer between chambers may be abrupt or the devices may sit at room temperature for 5 minutes. The temperature of the device, while changing rapidly, is essentially the same throughout the device at any instant; that is, the temperature gradients inside the device are very small.

Thermal shock as defined by Method 1011 of MIL-STD-883 specifies hot and cold baths of a suitable liquid. The devices are immersed in each bath for a period of 5 minutes and the transfer time must be less than 10 seconds. In this test, the change of temperature is much more rapid and temperature gradients may exist within the device, inducing mechanical stresses which are beyond the strength of the materials in the device.

Historically, thermal shock has been called a glass strain test (MIL-STD-750 Method 1056.1) and has been used to evaluate the quality of glass packages and glass-to-metal seals. Temperture cycling has been the test used for thermomechanical screening.

There exists differences of opinion as to which test, temperature cycling or thermal shock, provides the most efficacious and cost-effective thermomechanical screening test. Some device manufacturers are interested in using thermal shock for 100% screening because of the shortened cycle times afforded by the test. Some organizations believe that thermal shock provides a more effective screen than does temperature cycling, while others believe that temperature gradients induced in the package by thermal shock tests have the potential of causing excessive stress in the glass-to-metal seal areas, which can produce latent hermeticity failures. The ability of different package designs to withstand thermal shock stresses varies widely.

There are differences of opinion as to the critical parameters of thermomechanical testing. Some work has indicated that the temperture range is more critical than the rate of change of

temperature. Often, however, there appears to be little correlation between thermal shock and temperature cycling test results when performed using the same temperature extremes.

The parameters of thermomechanical testing should be better defined. The failure mechanisms activated by these stresses must be determined with greater precision.

In March 1972, Motorola initiated a program to investigate thermomechanical testing. This effort was sponsored by the Rome Air Development Center, Griffiss Air Force Base, New York under Air Force Contract #F30602-72-C-0251. This report presents the results of this program.

1.1 PROGRAM OBJECTS

The objects of this effort were:

(1) To evaluate the ability of state-of-the-art packages to withstand the mechanical stresses induced by temperature cycling and thermal shock.

(2) To determine if a relationship exists between the effects of temperature cycling and thermal shock test methods to end-use conditions.

(3) To assess the value of thermal shock and temperature cycling as stresses which may be used to accelerate those failure mechanisms which are activated by the temperature changes characteristic of normal use environment.

(4) To study those physical principles governing thermal mechanical testing which will establish guidelines for testing future devices.

1.2 PROGRAM OUTLINE

To accomplish the objectives of the program the following major tasks were established.

1.2.1 Test Sample Selection

A total of 3,168 samples of 14 vendor package combinations were used in this program. The package types and number of vendors for each package are shown in Table I-1.

Throughout this report vendor means manufacturer. . i.e., the company who made the product, not the company that sold the product.

The 7400 type TTL quad 2 input NAND Gate was chosen as the test vehicle for all 14 pin packages. An 1103 type random access MOS memory was used for the test vehicle in the 18 pin silicone package. The 40-pin Vendor 12 LSI package was used with a 112 Gate Array, three level metallization, patterned for a multiplexer unit. Vendor 13 LSI packages were dummies.

1.2.2 Basic Studies

Thermal coefficients of expansion and the glass transition temperature of the epoxy and phenolic molding compounds were determined experimentally.

The thermal mechanical data on the materials used in the fabrication of the ceramic glass devices were obtained from the leterature and materials manufacture. This data was utilized in performing a heat flow analysis and a thermomechanical stress

Package type/style	Materisl	Vendor Designation	Total Samples
14 Pin Plastic dual-in-line	Type 1 (A) Epoxy	Vendor #1	216
		Vendor #3	217
	Type 2 (B) Epoxy	Vendor #2	215
	Phenolic	Vendor #4	214
18 Pin Plastic dual-in-line	Silicone	Vendor #14	46
14 Pin Flat Package	Metal Glass	Vendor #5	276
	Ceramic Solder Glass	Vendor #6	240
		Vendor #7	277
14 Pin Ceramic dual-in-line	Ceramic Solder Glass	Vendor #8	342
		Vendor #9	341
		Vendor #10	339
	Ceramic, Metal Cap	Vendor #11	275
40 Pin Ceramic dual-in-line LSI	Ceramic Metal Base Metal Cap	Vendor #12	115
	Ceramic Metal Base Metal Cap Dummy	Vendor #13	55
TOTAL SAMPLE SIZE			3,168

Notes:

(A) Type 1 epoxy is a Phenol Cured, Epoxy Novolac.
(B) Type 2 epoxy is an Anhydride Cured, Bisphenol-A, epoxy.

TABLE I-1

Package Classification By Vendor

analysis on the dual-in-line ceramic package using the Motorola "MELTA" program for heat flow analysis. The results of this analysis were used to perform a static load stress analysis using the Mechanics Research Inc., Stardyne Computer Program.

Studies were performed, using thermal diode techniques, to determine heating and cooling rates at the die when the device undergoes temperature cycling and thermal shock in accordance with methods 1010 and 1011 of MIL-STD-883.

The final study was to determine the effect on the package seal when exposed to the fluids normally used in thermal shock.

1.2.3 Thermomechanical Stress Matrices

The thermomechanical stress matrices are shown in Table 1-2. With the exception of the tests in Matrix I, the Temperature Cycling Thermal Shock Step Stress Matrix, all test cycles performed in accordance with the applicable test methods of MIL-STD-883. The thermal shock test was modified to 10 cycles per step to coincide with temperature cycling requirements. The temperature cycling temperature limits were modified for plastic packages because at temperatures above 200°C the plastic material degrades rapidly. End-point measurements were performed after each step to detect electrical and package failures.

The Multiple Cycle Temperature Cycle and Thermal Shock Matrix (Test Matrix II) consists of 2000 cycles minimum of thermal shock and temperature cycling, as defined in MIL-STD-883 Method 1011 and 1010 at levels shown. Test cells were truncated after greater than 60% of the sample had failed. End-point measurements were made periodically to detect electrical and package failures.

TABLE 1-2

Thermomechanical Stress Matrices

	Test Description		Vendor #	MIC	Type 1 Epoxy 1	Type 2 Epoxy 2	Type 1 Epoxy 3	Phenolic 4	Metal Glass 14 Pin Flat 5	Ceramic Solder-Glass 24 Pin Flat 6	7	Ceramic Solder-Glass 14 Pin Dual-in-Line 8	9	10	Ceramic Metal 14 Pin Dual-in-Line 11	40 Pin LSI Ceramic Metal Dual-in-Line 12	40 Pin LSI Ceramic Metal Dummy 13	18 Pin Silicone 14	Total
I	Temp Cyc - Step Level			A	24	24	25	24	25	25	25	25	25	24	25	15		10	296
	Ther Sh - Step Level			B	25	25	25	25	25	25	25	25	25	23	25	15		10	298
II	Temperature Cycle - Extended Cycle Mil-Std-883 Method		1010B	C	25	24	25	24											98
			1010C	D	25	25	25	24	25	25	25	25	25	25	23	25		15	312
			1010D	E					25	23	25	25	25	25	25	25			198
			1010E	F					24	25	25	25	24	25	25				173
	Thermal Shock Extended Cycle Mil-Std-883 Method		1011A	G	15	15	15	15				15	15	15	15	15			135
			1011C	H	15	15	15	15	15	15	15	15	15	15	15	15		11	191
			1011D	I					15	15	15								45
III	Thermal Shock/ Temp Cycle Interaction Matrix	Pre-condition 1011A 15 Cyc	1010B	J	8	8	8	8	8	8	8	8	8	8	8		5		93
			1010C	K	8	8	8	8	8	8	8	8	8	8	8		5		93
			1010D	L	8	8	8	8	8	8	8	8	8	8	8		5		93
		Pre-Cond 1011B 15 Cyc	1010B	M	8	8	8	8	8	8	8	8	8	8	8		5		93
			1010C	N	8	8	8	8	8	8	8	8	8	8	8		5		93
			1010D	P	8	8	8	8	8	8	8	8	8	8	8		5		93
		Pre-Cond 1011C 15 Cyc	1010B	Q	8	8	8	8	8	8	8	8	8	8	8		5		93
			1010C	R	8	8	8	8	8	8	8	8	8	8	8		5		93
			1010D	S	8	8	8	8	8	8	8	8	8	8	8		5		93
IV	Wire Bond	Control Group		T					5		5	(5)	(5)	5	(5)				30
	Dey	1010C/1K Cyc		U					15		15	(15)	(15)	15	(15)				90
		1011C/1K Cyc		V					15		5	(15)	(15)	15	(15)				90
V	Seal	Torque		W								15	15	15					45
	Strength	1011A + Torque		X								50	50	50					150
	Ther Shock Fluid Studies			Y	5	5	5	5	5	5	5	5	5	5	5	5			60
				Z	10	10	10	10	10	10	10	10	10	10	10		10		120
	TOTALS				216	215	217	214	276	240	277	342	341	339	275	115	55	46	3168

The purpose of this matrix was to determine the differences, if any, in failure modes and failure distributions.

The Thermal Shock Temperature Cycle Inter-action Matrix (Matrix 3) was designed to detect any latent defects which might be induced by thermal shock when used as a 100% screen. The devices were preconditioned by subjecting them to 15 cycles of thermal shock per Method 1011, MIL-STD-883, at the levels shown, and then subjecting the devices to extended temperature cycling. End-point measurements were made after thermal shock and at intervals during the extended temperature cycling to detect electrical and package failures.

The Wirebond Degradation Matrix (Matrix IV) was designed to determine the effect of thermal shock and temperature cycling on the pull strength of the internal lead wires and wire bonds. Devices were subjected to temperature cycling and thermal shock as shown in Table I-2. End-point measurements in both tests were performed at 30, 60, 120, 510, 1020 cycles. Two units and the five units of the control group were decapped and all undamaged wires were pulled. Breaking force and failure mode were recorded for each wire.

The Seal Strength Degradation Test was performed to determine if the glass seal of the Cerdip package would be degraded by subjecting the device to thermal shock at Test Condition A of Method 1011, MIL-STD-883. End-point measurements were performed at 15, 45, 90, 495 and 1005 cycles. At each end point 10 devices were removed from the test lot. These devices plus a 15-piece correlation sample were subjected to a torque stress in the seal area. The value of torque required to fracture the package was recorded for each broken device.

End-point measurements for the foregoing stress tests consisted of DC and functional tests at 25°C, continuity tests at temperature extremes and, in the case of the 14 pin plastics, a Monitored Temperature Cycle Test over the temperature range of -65°C to 150°C. All hermetic packages were subjected to seal tests per MIL-STD-883, Method 1014, Test Conditions A and C.

All confirmed failures were analyzed to determine the causative mechanism. Special techniques used in decapsulating plastic packages are presented in Section V.

Analysis of the data, in some cases, presented some special problems. The data does not always fit the distributions usually used in analysis. For that reason the results of the tests in Matrix I and Matrix II are presented as linear plots with respect to the number of cycles. The statistical techniques used to analyze each major matrix and the data presentation employed are discussed in the body of this report.

SECTION II

2.0 SUMMARY

A variety of thermo-mechanical stress tests were performed on a variety of package styles from several different manufacturers. The single most obvious result was the widely different failure responses observed from vendor-to-vendor within the same package styles.

Plastic dual-in-line devices using the latest epoxy and large internal wires (Vendor 1) out-performed all package styles, hermetic and plastic on long-term temperature cycling (greater than 3000 cycles, -65/+150°C) and thermal shock (greater than 2500 cycles, -65/+150°C). Devices from another vendor (Vendor 3), using the new epoxy but smaller internal wires, did very well on both these stress sequences but not as well as Vendor 1. Interaction Matrix results indicated Vendor 4 had a perfect record, with Vendor 1 next, then Vendor 3. The failure mode for plastic devices was intermittents or opens at 25°C due to grain boundry fracture or intergranular fracture in the wire above the bond.

Ceramic flat packages were the best performers of the hermetic package styles, especially on the thermal shock stress tests. These packages are small and strong and retain their hermeticity through the toughest environments. They did experience slightly more bond failures throughout the extended thermal cycling than did the best plastic, but fewer than the ceramic dual-in-line samples. In the Interaction Matrix, Vendor 7 had a perfect record, with Vendor 5, a metal flat, next, and Vendor 6, with noticeably poorer performance than 5 or 7.

The ceramic dual-in-line package style gave intermediate-to-poor performance results, experiencing much greater hermeticity failure and bond failures throughout these test sequences. The hermeticity performance depends directly on the type and strength of the sealing glass with the newer glasses performing much better than the old glasses. In all cases, thermal shock is destructive to the hermeticity of these packages due to the relatively weak glass and thermal mismatch of the DIP construction. In general, long-term temperature cycling does not affect hermeticity but does cause extensive wirebond failure within the first few thousand cycles. The failure distribution appears to be "wearout". The failure mode is "open at 25°C" due to wireflex failure.

Thermal shock, 0 - 100°C can cause progressive weakening of the sealing glass, as shown by the torque test results, and temperature cycling does cause a degradation in wirebond strength as well as the number of wireflex failures.

The heat flow study shows that 5-minute dwell for Thermal Shock, Method 1011, Conditions A, B, or C is adequate for 14 pin plastic and ceramic dual-in-line and the 40 pin dual-in-line LSI package. Actual temperature measurements, using substrate isolation diodes, indicate the computer heat flow analysis is conservative.

Ethylene glycol is shown to chemically attack the sealing glass used to seal dual-in-line packages. For long-term thermal shock sequences, polyalkylene glycol (UCON OIL) was used. This material caused much less glass attack than did the ethylene glycol. This test sequence demonstrated the importance of the bath fluid in obtaining accurate long-term thermal cycling results.

SECTION III

3.0 CONCLUSIONS

3.1 PLASTIC DEVICES

(1) Plastic devices are capable of good performance when subjected to temperature cycling step stress provided they have heavy wires (i.e., 1.5 mil).

(2) The major difference in thermal cycling response was due to the difference in wire bond size (i.e., 1.0 mil vs 1.5 mil).

(3) Phenolic performed better than epoxy above 125°C since the glass transition point for phenolic is considerably higher than that of epoxy (i.e., ~200°C vs ~145°C).

(4) Thermal cycling plastic above its glass transition point is not immediately destructive, but not recommended.

(5) There was a strong vendor-to-vendor difference - Vendor 2 having significantly poorer performance than Vendor 3, using same bonding system (1.0 mil gold ball bonds) but a different epoxy.

(6) There are significant differences in thermal cycling performance due to differences in epoxy. Type 1 epoxy performed better than Type 2.

(7) Various distributions of the failures were found. No one failure distribution appears to be predominant.

(8) Thermal cycled plastic devices fail as intermittents and hard opens. Those that failed for intermittent operation would eventually fail as hard opens after additional cycling. The failure mode was predominantly grain boundry fracture and intergranular fracture.

(9) 3000 thermal cycles was not far enough to generate 50% failures on several samples. The sample sizes were too small to allow meaningful extrapolation.

(10) Plastic devices showed higher failure rates with thermal shock, Condition A than with Condition C, even though Condition C had a greater delta temperature and higher maximum temperature. The higher failure rate was due to the use of water in Condition A rather than UCON oil as used in the other conditions. The water would penetrate into the devices and cause corrosion of the aluminum. The UCON oil would not.

(11) Thermal shock (10 cycles) preconditioning did not influence the subsequent long-term temperature cycling performance but there was a significant temperature cycles-vs-vendors interaction as well as a vendor-to-vendor difference.

(12) The vendor with the lowest glass transition point and 1.3 mil wires (Vendor 2) had the highest failure rate under all thermal cycling conditions. This fact would be consistent with the assumption of weakened wirebonds due to stress relaxation combined with high tension forces on these wires by the surrounding plastic as it expands.

(13) In liquid-to-liquid thermal shock, 5-minute dwell time at each extreme is adequate for plastic packages to reach equilibrium temperature.

3.2 CERAMIC DUAL-IN-LINE PACKAGES

(1) The media study confirmed that ethylene glycol attacks the seal glass used in the fabrication of dual-in-line

ceramic packages. Type 1 glass suffered more chemical attack than did Type 2 glass.

(2) In liquid-to-liquid thermal shock, 5-minute soak time at each temperature extreme is adequate for these packages to reach thermal equilibrium.

(3) The computer analysis shows that the sealing glass (Type 1 in particular) is the weakest material in this structure. The calculated 5000 PSI tensile strength in the glass is only slightly higher than the 4330 PSI stress incurred at steady state cool-down to -65°C.

(4) Some long-term loss in strength of the sealing glass occurs with repeated thermal shock to Method 1011, Condition A (0 - 100°C). The strength loss is greater in Type 1 glass than in Type 2 glass.

(5) Thermal shock is more detrimental to package integrity (hermeticity) than to wire bonds. Thermal shock, Method 1011, Condition A (0 - 100°C) resulted in helium fine leakers whereas Condition C (-65/+150°C) generated gross leakers. The distribution of leak test failures was essentially the same pattern in both cases (i.e., a weak distribution below 100 cycles and a strong distribution above 100 cycles).

(6) Dual-in-line ceramics suffered much greater hermeticity reject rates than did ceramic flat packages when thermal cycled.

(7) A strong vendor-to-vendor difference was noted in nearly all test sequences. Vendor 9 had the strongest Cerdip but weakest bonding. Vendor 8 did poorly overall; Vendor 10 had a weak package but good wire-bonding.

(8) Temperature cycling affects wirebonds and bond strength much more than does thermal shock.

(9) Wirebond strength is affected by prolonged thermal cycling, especially Method 1010, Condition C, temperature cycling. The bond strength starts to degrade from the start and continues fairly linearly with either log (cycles) or log (time at 150°C).

(10) At higher stress levels, Method 1010, Condition D (-65°C/+200°C) some stress relaxation takes place, improving the failure rate over that of Condition C.

(11) If residual glass is left on the bonding pads, wires bonded through this glass will be more likely to fail as lifted bonds upon thermal cycling. Expansion of this glass causes the bond-to-pad to develop fractures and eventually to lift off the pad (LD's).

(12) The strong bonds degrade the least while the weak bonds degrade the most when subjected to extended thermal cycling. Zero wire pulls were obtained from 240 cycles on. Greater degradation occurs with gold-aluminum bonds than with the all-aluminum bonding system.

(13) The main failure mode for these thermal cycled parts was break at the heel due to wire flex.

(14) Thermally cycled wedgebonds fail sooner than ball bonds and if it is a gold-aluminum wedge bond, it will fail sooner than an aluminum-aluminum bond.

(15) Gold wire had a significantly greater number of center wire breaks than did aluminum wire samples. The high capping temperature of the Cerdips increased the annealing of the aluminum wires and resulted in more centerwire breaks than in the sidebraze dip sealed at the lower temperature.

(16) The direction of bonding had a significant effect on failure mode. Vendors 8 and 9 used up-bonding and experienced 94% of their failures with the first bond - the one on the die (BD's). Vendors 10 and 11 used down-bonding and experienced 85% of their failures with the first bond - the one on the post (BP's).

(17) There were no interactions between ceramic dual-in-line packages and no significant main effects on DC electrical performance when parts were preconditioned with thermal shock and then given extended temperature cycling. There was a significant interaction between thermal shock response and vendors, and a strong independent effect due to thermal shock alone, on hermeticity performance (Indicated Leakers). After confirming the leakers, there remained a significant (@ 0.1%) main effect between levels of thermal shock. Test Condition C, thermal shock, is particularly destructive to all Cerdip parts on hermeticity, but not DC electrical.

3.3 SIDEBRAZE

(1) The sidebraze package is very strong and does very well in temperature cycling and thermal shock up to 325°C. At this temperature the solder seal melts and the device fails catastrophically. It had the best hermeticity response to thermal shock of all the dual-in-lines.

(2) The wire bond reliability was not as good as with other dual-in-line packages since down-bonding was used from a gold-plated post to the aluminum pad on the die. The post bond was weak because it was the first bond made and because it developed intermetallics, which are also weak.

(3) This package didn't appear to undergo stress relaxation since the post bond was the weakest link and it did not anneal. Therefore Condition D results are consistent with test Condition C results.

(4) This package went 1500 thermal cycles (offset) prior to onset of failure. From that point on, it began failing (opens) very quickly. 50% of the sample had failed by 3000 cycles.

(5) In the interaction matrix, the sidebraze package (Vendor 11) with its gold-aluminum post bonds, showed a much higher failure rate to preconditioning level C combined with temperature cycle life to Condition D, than did any of the other dual-in-line parts. However, on hermeticity, it was the only package with a perfect record - no failures.

(6) With improvements in wirebonding to this package, the sidebraze could be a very good high reliability package for use in thermal cycling operation

3.4 FLAT PACKAGES

(1) Flat packages, both ceramic and metal, were the best performers throughout all test sequences.

(2) On the interaction matrix test, Vendor 6 was significantly worse than Vendors 5 and 7 on DC failures but was still better than the best ceramic dual-in-line. There were no leak test failures.

(3) Stress relaxation is evident in these flat package groups also, with bond failures to test Condition D being less than to test Condition C (Temperature Cycling, Method 1010).

(4) In the wirebond degradation study, no hermeticity failures occurred to any of the flat packages subjected to either 1020 cycles of temperature cycling or thermal shock, Condition C (-65/+150°C) in both cases. There were also no failures on electrical or mechanical evaluations.

(5) Vendor 7 was the best performer across the board with no hermetic, mechanical, electrical, or zero wire pulls throughout the entire 1020 cycles of the wirebond degradation study.

(6) For thermal cycling reliability, the ceramic flat package is best.

3.5 LSI PACKAGE

(1) Because of the large size of these packages, this package tended to trap helium more often and to a greater extent than most dual-in-lines. When confirmation tests were run, very few of these 40 pin packages would confirm as leakers. Only dummy packages were used in the interaction matrix.

(2) Up to 200°C, these LSI packages did well on both temperature cycling and thermal shock step stress test sequences. Since they had a solder seal, stresses above 325°C caused hermeticity failures.

(3) Due to continuous electrical readout problems with LSI chips, these parts did not progress as planned. Vendor 14 only reached 500 cycles of thermal shock, Condition C, but was 100% failed at 30 cycles of Condition C, temperature cycling, due to electrical opens.

(4) Vendor 12 made 2000 cycle readout with 12% electrical failures. As with the other dual-in-lines, more failures were found to temperature cycling, Condition C, and to Condition D, a higher stress. This indicates that stress relaxation predominated over an intermetallic formation of the post bonds.

3.6 GENERAL CONCLUSIONS

(1) Temperature cycling affects wirebonds, whereas thermal shock affects hermeticity.

(2) The greatest difference observed over all test sequences was vendor-to-vendor differences.

(3) Hermetic parts tended to fail for break at the heel due to wireflex.

(4) Plastic parts generally failed for grain boundry fracture above the bond due to tension on the captive wire by the plastic.

(5) Thermal shock, Method 1011, Condition A, does cause fine leak failures even with 15 cycles. To screen the entire weak distribution would require approximately

100 cycles, and result in a 30 to 45% loss. This test appears to be destructive to the integrity of the package and should not be used as a 100% screen.

(6) Thermal shock preconditioning (15 cycles) using Condition A, B, or C, does not modify the subsequent performance of ceramic dual-in-line or ceramic flat packages to extended temperature cycling at Conditions B, C, or D. There is no interaction between thermal shock and temperature cycling.

(7) Differences in choice of materials and methods of processing can cause different response to thermal cycling.

(8) Hermetic parts were approaching wearout at 4000 temperature cycles, Method 1010, Condition C (-65/+150°C). Two plastic lots both having 1.5 mil wire went 4000 cycles at the same test conditions without any failures.

SECTION IV

4.0 TEST PROGRAM

4.1 SAMPLE DESCRIPTION AND END POINT TESTS

The 7400 quad 2 input NAND gate was chosen as the test vehicle for all 14 pin packages. This device is covered by military specification. It is a mature device, available from many vendors in all packages of interest. To obtain a better measure of the effectiveness of the thermo-mechanical stresses screens, commercial grade product was procured.

The device used in the LSI packages, Vendor 12, is a Multiplex Circuit derived from a 112 gate array. This circuit uses three levels of metallization to form the functional interconnect on the die. The package used was a 40 pin dual-in-line package. Dummy packages, designated Vendor 13, were used in the interaction matrix to reduce costs.

The Vendor 14 device was an 18 pin silicone dual-in-line package containing a P channel MOS 1024 bit random access memory.

The method of procurement for the sample used is shown below.

Franchise Distributor Stock	Vendors 2, 5, 6, 7, 8, 9
Direct Factory Order	Vendors 1, 3, 4, 7, 10, 11, 12, 13
Government Furnished Sample	Vendor 14

Details of the design and construction for each of the devices used are shown in the following paragraphs.

4.1.1 Dual-In-Line Plastic Packages

Five plastic packages were chosen for the program. They include four 14 pin packages and one 18 pin package. Table IV-1 presents a comparison of the material and assembly techniques.

One sample of the five plastic packages were subjected to X-ray to show the details of lead frame and mounting bar design. Figure 4-1 shows the X-ray photograph of the packages from vendors 1, 2, 3, 4 and 14. As shown in the figure, each vendor uses an isolated die bond flag. Figures 4-2 through 4-5, SEM micro-photographs of samples of Vendors 1, 2, 3 and 14, show internal construction detail. To prepare the samples for these micro-photographs the encapsulant was chemically removed so as not to disturb the wires relative to the die and lead frame. All die bonds were of the gold eutectic type. From the amount of material in the filled area on the Vendor 14 die it is deduced that Vendor 14 uses a gold preform in the die bond process.

As shown in Figure 4-1, the lead frame geometry of Vendors 1 and 4 are identical. Vendor 4 uses a silastic die coat. Figure 4-6 pictures a Vendor 4 device in cross section showing the geometry of the silastic die coat in relation to the die and lead frame. Other than the differences in bonding techniques and wire size, the geometries of the internal wires do not vary significantly among Vendors 1, 2, 3 and 4. The minor differences shown in Figures 4-2, 4-3, 4-4 and 4-5 are typical of what was observed in the analysis of the failures generated by the test program, and as will be shown in later sections, wire dress had no bearing on the ability of these devices to withstand the stresses of the environment.

CHARACTERISTIC	VENDOR 1	VENDOR 2	VENDOR 3	VENDOR 4	VENDOR 14
Molding Compound	Phenol Cured Epoxy Novolac	Anhydride Cured Bisphenol-A Epoxy	Phenol Cured Epoxy Novolac	Phenolic	Silicone
Die Coat	NONE	NONE	NONE	"silastic"	NONE
Lead Frame Mat'l.	Nickel	Kovar	Kovar	Nickel	Kovar
Number of Leads	14	14	14	14	18
Lead Finish	Acid-Tin	Silver Alloy	Acid-Tin	Gold Plate	Gold Plate
Post Plating	Gold	Gold	Gold	Gold	Gold
Wire Material	Gold	Gold	Gold	Gold	Gold
Wire Size (dia)	0.0015 in (38.1μm)	0.001 in (25.4μm)	0.001 in (38.1μm)	0.0015 in (25.4μm)	0.001 in (25.4μm)
Post Bond Type	T-C Wedge	T-C Wedge	T-C Wedge	T-C Wedge	T-C Wedge
Pad Bond Type	T-C Wedge	T-C Ball	T-C Ball	T-C Wedge	T-C Ball
Pad Metallization	Aluminum	Aluminum	Aluminum	Aluminum	Aluminum
Glassivation	YES	NO	YES	YES	YES
Wafer Type	Bipolar	Bipolar	Bipolar	Bipolar	P-MOS
Circuit Function	7400 NAND Gate	7400 NAND Gate	7400 NAND Gate	7400 NAND Gate	1024 Bit RAM

TABLE IV-1

Plastic Dual In Line Package Material Characteristics

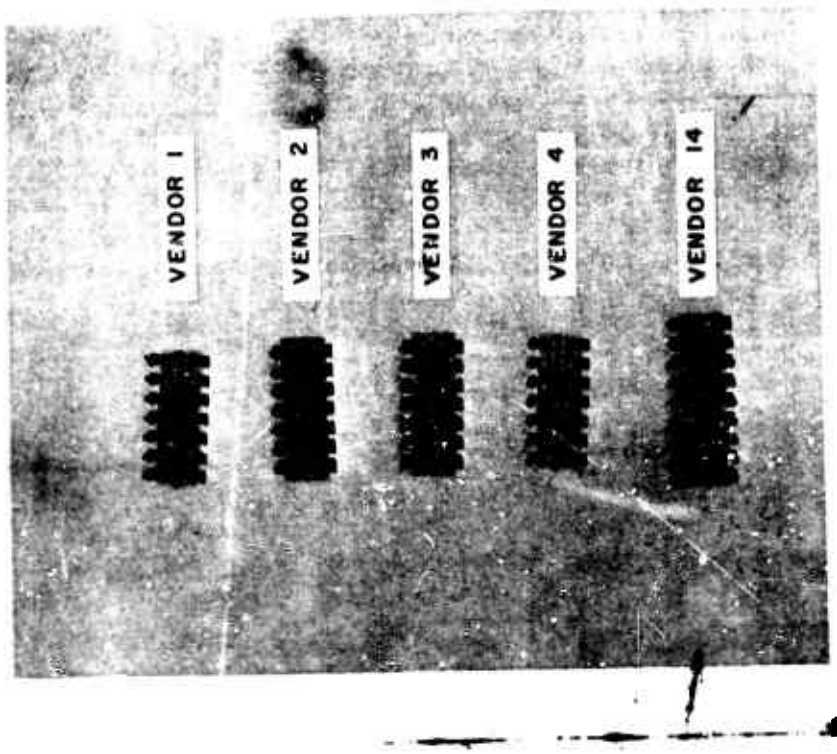

Figure 4-1. X-Ray of Plastic Dual-In-Line Package

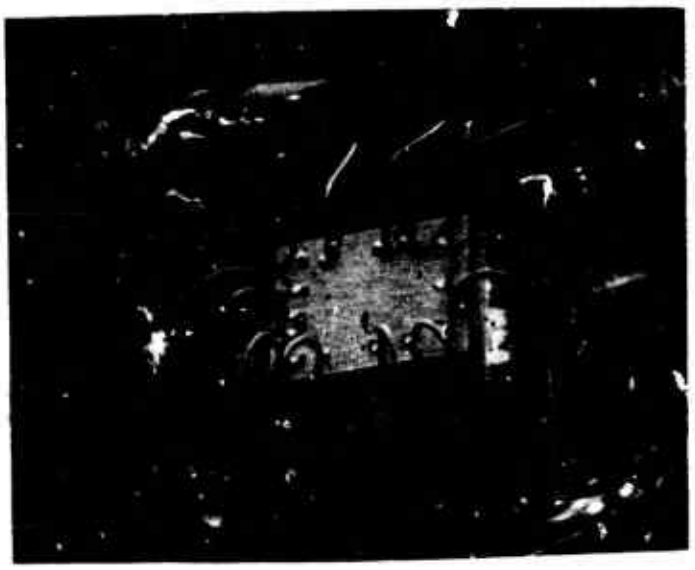

Figure 4-2. SEM Microphotograph. Vendor 1 Wire and Lead Frame Assembly After Partial Chemical Removal of Encapsulant.

Figure 4-3. SEM Photograph. Vendor 2 Device Wire and Lead Frame Assembly after Partial Chemical Removal of Encapsulant.

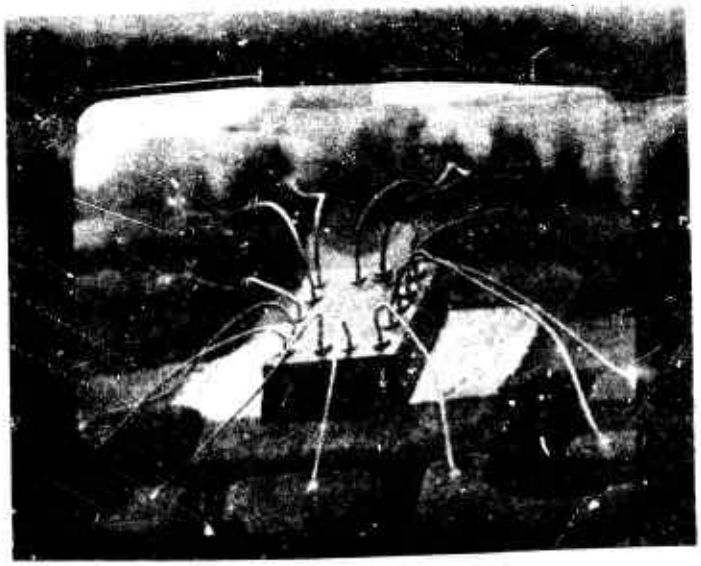

Figure 4-4. SEM Photograph, Vendor 3 Device Wire and Lead Frame Assembly After Chemical Removal of Encapsulant.

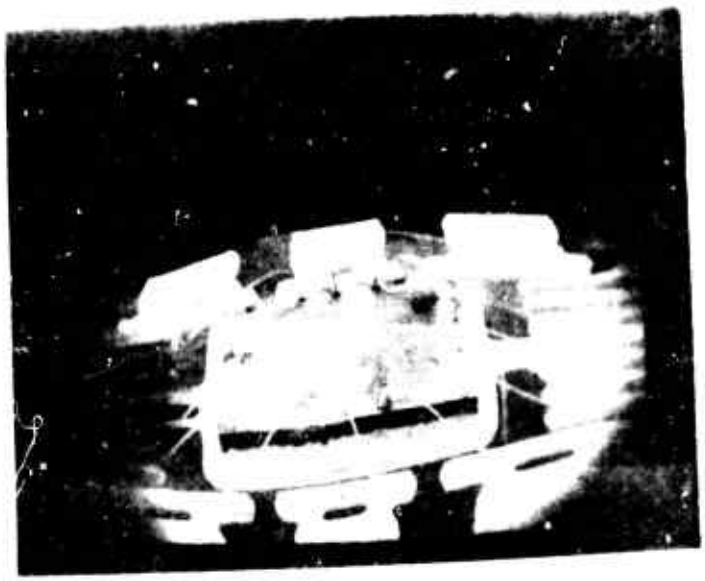

[illegible] SEM [illegible] Vendor [illegible] After [illegible]

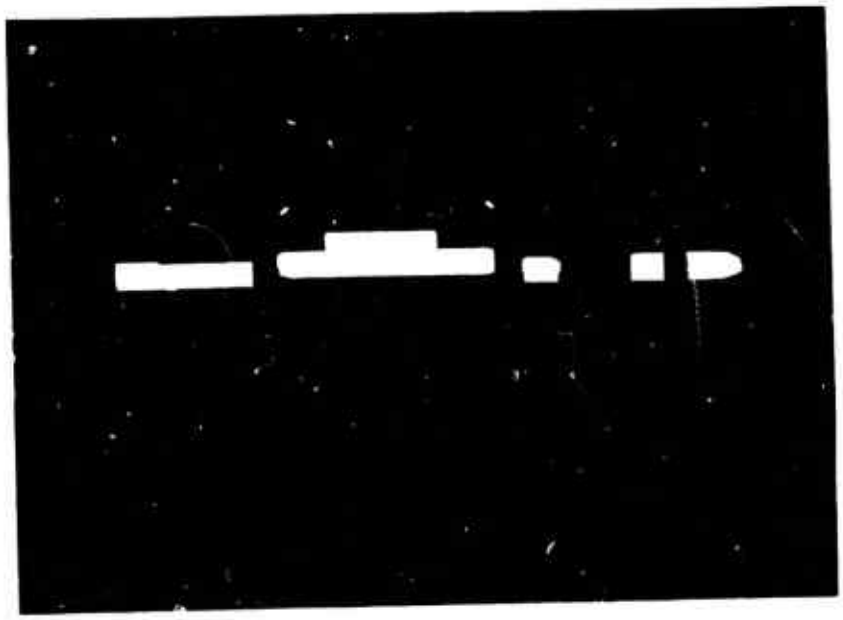

13.5 X

4-6(A)

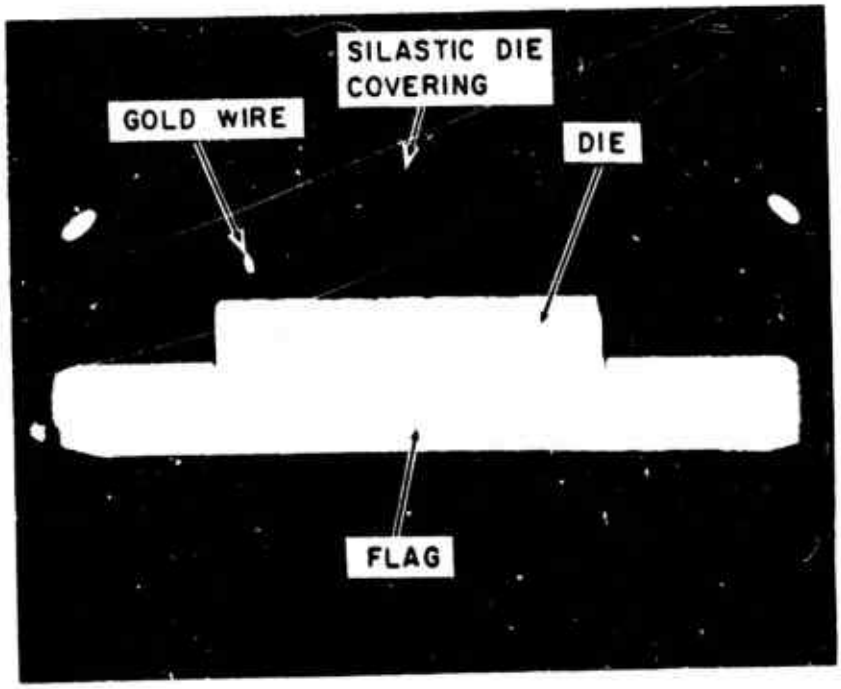

48X

4-6(B)

Figure 4-6. Cross Section of Vendor 4 14 Pin P_astic Dual-In-Line Package

4.1.2 Flat Packages

Three flat packages were chosen for this program. They represent the three most popular case outlines in the 14 pin configuration. The case outlines designations and material and construction characteristics are shown in Table IV-2.

The Vendor 5 package is a metal glass package having a Kovar body and cap with glass seals between the leads and body. Final sealing is achieved by welding the cap to the body or base. All metal parts of the package are gold plated.

Vendor 6 and Vendor 7 flat packages have essentially the same construction, differing only in outline dimension of the package body. These packages consist of a ceramic cap and base, each of which is selectively glazed with a crystallizing solder glass. Assembly and sealing is achieved by heating the base to soften the glass at which time the lead frame is imbedded in the glass of the base, and the die bond is made. The temperature at which this takes place is in the range of 350°C to 400°C depending on the type of glass used. The time of exposure at this temperature is short so that little, if any, devitrification (crystallization) of the glass occurs. After wire bonding, the cap is placed on the base and lead frame and the entire assembly is rapidly heated to 450°C to 500°C. This temperature is maintained for a period on the order of 5 to 10 minutes. The glass on the base and cap flows together around the leads and crystallizes (devitrifies), forming the lead and final seal at the same time. Each of the foregoing steps must be precisely controlled to assure the correct properties of the glass. This is the same process used to seal the ceramic glass dual-in-line package.

Characteristic	Vendor 5	Vendor 6	Vendor 7
Case Style (1)	F-3 (1/4" x 1/8")	F-2 (1/4" x 3/8")	F-1 (1/4" x 1/4")
Cap	Kovar	Al_2O_3 Ceramic	Al_2O_3 Ceramic
Base	Kovar	Al_2O_3 Ceramic	Al_2O_3 Ceramic
Base Metalization (2)	Gold Plated Kovar	Gold Frit	Gold Frit
Lead Frame Mat'l.	Kovar	Kovar	Alloy 42
Lead Finish	Au Plated	Bright Acid Tin	Bright Acid Tin
Lead Seal	Glass-Metal	Type 2* Glass	Type 1 Glass
Final Seal	Metal Weld	Type 2* Glass	Type 1 Glass
Post Finish	Au Plated	Aluminum Clad	Aluminum Clad
Wire Material	Gold	Aluminum	Aluminum, 1% Silicon
Wire Diameter	0.001 in. (25.4um)	0.001 in. (25.4um)	0.001 in. (25.4um)
Post Bond Type	T-C Wedge	Ultrasonic	Ultrasonic
Pad Bond, Type	T-C Ball	Ultrasonic	Ultrasonic
Pad Metalization	Aluminum	Aluminum	Aluminum
Die Bond	Au-Si Eutectic	Au-Si Eutectic	Au-Si Eutectic
Glassivation	YES	YES	YES

Notes:

(1) Case style letter designation are per Mil-M-38510
(2) Base Metalization refers to Metalization in Die Bond Area

*Similar to Type 2

TABLE IV-2

Flat Package Material and Construction Characteristics

The solder glasses are based on lead oxide (PbO). Various materials are added to control the properties of the glass, such as the devitrifying temperature and the temperature coefficient of expansion. Tables IV-3 and IV-4 give the results of a chemical analysis of a typical lot of each of two types of solder glasses found in this program. As shown by these analyses, many elements and their oxides are found in these glasses either as dopants or impurities.

4.1.3 Dual-In-Line Ceramic Packages

Four 14 pin dual-in-line ceramic packages were chosen for this program. Three of these, Vendors 8, 9 and 10, were of the ceramic-solder glass type. The fourth, Vendor 11, was of the metal ceramic lead seal type. Table IV-5 shows a comparison of materials and assembly techniques used to fabricate these packages. The ceramic glass packages are assembled in the same manner as the ceramic flat packages. Heating rates and times may be adjusted slightly to account for the larger thermal mass of the dual-in-line package.

The ceramic metal sealed package is fabricated in the following manner. First, a metal film patterned to form the leads through the package and the die mounting area is placed on a thin piece of green (dried but not fixed) ceramic. The metal used is usually molybdenum or a similar material which will stand ceramic firing temperatures and bonds to the ceramic. Then, a second piece of green ceramic with a window cut to form the die cavity is placed over the first piece. Then both halves are fuzed together, forming a seal around the lead pattern.

The lead pattern is extended to the edge of the package. The external package leads or pins are brazed to the edge of the

Silica (SiO_2)	4.62
Mixed Oxides (Al_2O_3, Fe_2O_3, etc.)	1.91
Calcia (CaO)	0.00
Magnesia (MgO)	0.00
Baria (BaO)	0.00
Soda (Na_2O)	0.08
Potassa (K_2O)	0.00
Sulfate (SO_3)	0.00
Fluoride (F_2)	0.00
Boron Oxide (B_2O_3)	9.73
Zinc Oxide (ZnO)	15.10
Lead Oxide (PbO)	68.36
Titanium Oxide (TiO_2)	0.13
Lithium Oxide (Li_2O)	0.15
TOTAL	100.08

TABLE IV-3

Results of Chemical Analysis of a Typical Lot of Type 1 Crystallizing Solder Glass

Silica (SiO_2)	4.06
Alumina (Al_2O_3)	2.86
Iron Oxide (Fe_2O_3)	0.002
Calcia (CaO)	0.00
Magnesia (MgO)	0.00
Baria (BaO)	2.71
Fluoride (F_2)	0.00
Titanium Oxide (TiO_2)	0.040
Vanadium Oxide (V_2O_5)	0.00
Lead Oxide (PbO)	65.56
Boron Oxide (B_2O_3)	8.83
Zinc Oxide (ZnO)	8.80
Zirconium Oxide (ZrO_2)	7.02
TOTAL	99.88

TABLE IV-4

Results of Chemical Analysis of a Typical Lot of Type 2 Crystallizing Solder Glass

Characteristic	Vendor 8	Vendor 9	Vendor 10	Vendor 11
Case Outline (1)	D-1 (1/4" x 3/4")	D-1 (1/4" x 3/4")	D-1 (1/4" x 3/4")	D-1 (1/4" x 3/4")
Cap	Al_2O_3 Ceramic	Al_2O_3 Ceramic	Al_2O_3 Ceramic	Iron-Nickel Alloy
Base	Al_2O_3 Ceramic	Al_2O_3 Ceramic	Al_2O_3 Ceramic	Al_2O_3 Ceramic
Base Metallization (2)	Gold Frit	Gold Frit	Gold Frit	Au Plated Moly
Lead Frame Mat'l.	Kovar	Kovar	Alloy 42	Kovar
Lead Finish	Bright Acid Tin	Bright Acid Tin	Bright Acid Tin	Gold Plate
Lead Seal	Type 1 Glass	Type 2 Glass	Type 1 Glass	Ceramic-Metal
Final Seal	Type 1 Glass	Type 2 Glass	Type 1 Glass	Au-Sn eutectic Braze
Post Finish	Aluminum Clad	Aluminum Glad	Aluminum Glad	Gold Plate
Wire Material	Aluminum	Aluminum	Aluminum 1% Si	Aluminum 1% Si
Wire Material	0.001 in (25.4μm)	0.001 in (25.4μm)	0.001 in (25.4μm)	0.001 in (25.4μm)
Post Bond Type	Ultrasonic	Ultrasonic Split Wedge	Ultrasonic	Ultrasonic
Pad Bond Type	Ultrasonic	Ultrasonic Split Wedge	Ultrasonic	Ultrasonic
Pad Metallization	Aluminum	Aluminum	Aluminum	Aluminum
Die Bond	Au-Si eutectic	Au-Si Eutectic	Au-Si Eutectic	Lead Indium Tin Solder
Glassivation	No	Yes	Yes	Yes

Notes: (1) Case outline designation per Mil-M-38510
(2) Base Metallization refers to Metallization in Die Bond Area

TABLE IV-5

Dual-in-line Ceramic Package Material Characteristics

package giving the package the popular name of "Sidebraze." A metallized strip is also laid down around the opening in the top to facilitate capping with a metal lid. All exposed metal parts are then gold plated.

In assembling devices in this package Vendor 11 used a furnace die bond method with a lead-indium tin solder to bond the die to the package. Final sealing was performed by brazing the Kovar cap to the package with a gold-tin eutectic braze at 325°C.

4.1.4 LSI Package

The 40 pin LSI package chosen for this program is a ceramic filled glass package featuring a Kovar base plate and top plate, both of which extend the full length and width of the package. Figure 4-7 shows the completed package. The package is constructed by laying up in a proper fixture the base plate, a ceramic filled glass preform, and the top plate. All metal parts are oxidized to provide a metal glass seal. The glass preforms have windows cut into the center to form the package cavity. The window in the top preform is larger so that the lead frame tip which forms the wire bonding posts are exposed and supported by the bottom layer of glass. The assembly is then fired at 1100°C to 1200°C to fuse the parts together. After firing, the metal parts are cleaned and gold plated.

When assembled into a completed circuit, the die is mounted directly to the base plate using either a gold silicon eutectic bond or a solder preform. The Kovar lid is brazed to the top of the package with a gold tin eutectic.

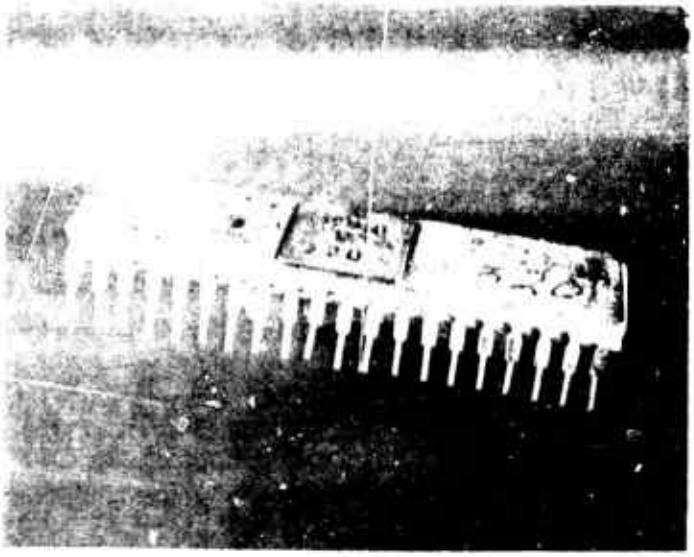

Figure 4-7. Dual-In-Line LSI Package

4.1.5 End-Point Measurements

The tests and measurements to which all samples were subjected initially, and at specific intervals throughout the test program, are shown in Tables IV-6 and IV-7.

4.1.5.1 Electrical Tests and Measurements

DC parameters for the 7400 product (Table IV-6) consisted of first a threshold continuity test where the ground pin was biased positive and the current sensed between all other pins and ground. The value of bias was 1 volt, so that the possibility of healing an open bond by arc over was minimized. After threshold testing, the DC parameters were measured. These measurements included all specified parameters for the commercial 7400 TTL NAND gate. The applied sequence of input and output forcing functions and measurements were sufficient to assure the device was functional. These tests were programmed on a Fairchild 4000M integrated circuit tester. The continuity tests were programmed to occupy the first track of the tester memory disc. This allows the use of the 4000M to be used for continuity tests at -65 and 125°C. The 125°C continuity tests were performed on plastic dual-in-line packages using Motorola's test system dedicated for that purpose. The test method applies a positive voltage at ground pin and ground all other pins through a detector circuit which activates a signal light for each pin.

A special electrical test circuit was designed for the monitored temperature cycle test. This test, used on plastic dual-in-line packages, monitors the current through all pins of the device as the device is exposed first to -65 and then to 150°C.

Test or Measurement	HERMETIC			PLASTIC		
	Initial	Interim	1000 Cycle	Initial	Interim	1000 Cycle
Seal Test Method 1014 A & C	YES	YES	YES			
Monitored Temp. Cycle; -65°C to 150°C				YES	YES	YES
Continuity 125°C				YES	YES	YES
Continuity 150°C	YES	YES	YES			
Continuity -65°C	YES	YES	YES			
DC Parameters 25°C	R & R(1)	R & R	R & R	R & R	R & R	R & R
DC Parameters 70°C	R & R		R & R	R & R		R & R
DC Parameters 0°C	R & R		R & R	R & R		R & R

Notes: (1) R & R stands for read and record parameter values

TABLE IV-6

End Point Tests and Measurements For
7400 TTL NAND Gates

Test or Measurement	Hermetic Bipolar LSI			Plastic P-MOS 1103 RAM		
	Initial	Interim	1000 Cycle	Initial	Interim	1000 Cycle
Seal Test Method 1014 A & C	YES	YES	YES			
DC Parameters 25°C	R & R(1)	GNG	R & R	GNG	GNG	GNG
DC Parameters 70°C	GNG(2)	GNG	GNG			
DC Parameters 0°C	GNG	GNG	GNG			
Functional Test 25°C	(3)			YES	YES	YES
Continuity 125°C				YES	YES	YES
Continuity -55°C				YES	YES	YES

Notes: (1) R & R means Read and Record parameter value
(2) GNG means Device Tested to Parameter Limits Only No Recorded Data
(3) Functional Testing is Incorporated into DC Parameter Tests

TABLE IV-7

End Point Tests and Measurements for LSI and Memory Devices

A schematic diagram of the sense and indicating circuits is shown in Figure 4-8. Current is forced through the substrate diodes of the device under test (not shown) by connecting Vcc = 5.00 to pin 7, the device ground pin. If all internal connections are intact, this current flows out the pins under test (pins 1 through 6, and 8 through 14). This current, on the order of 100 microamperes, is sufficient to saturate each Q1 hold in each Q2 cutoff. This impresses 4 volts to each input of the 13 input positive NAND gate formed by the MC1803P and the 5 expander diodes holding pin 8 of the MC1803P low, which extinguishes the LED indicator. If any pin opens, the corresponding Q2 transistor goes into saturation, forcing pin 8 of the 1803P high, turning the LED on. The LED remains on as long as any pin remains open.

These circuits were mounted on a multilayer etched circuit board. These boards were plugged into a card edge connector on removable temperature chamber door. The devices, under test, were plugged into test sockets mounted on a small etched circuit board which plugged into a card edge connector on the inside of the oven door. Devices are temperature cycled by changing the oven door from the cold chamber to the hot chamber. The test operator observes the LEDS during the temperature cycle and records those which come on momentarily during the cycle and those that are on as the devices stabilize at 150°C. In this way, we were able to differentiate window intermittents, i.e., those units which show open wire bonds over a small portion of the cycle, from those devices which remain open circuited at 150°C (or -65°C).

The minimum response time of the system is dependent on the visual response of the operator, which is in the range of 0.1 to 0.01 second. Since the maximum rate of change of temperature was on the order of 1 degree per second, the minimum temperature window we could have detected was less than 1 degree.

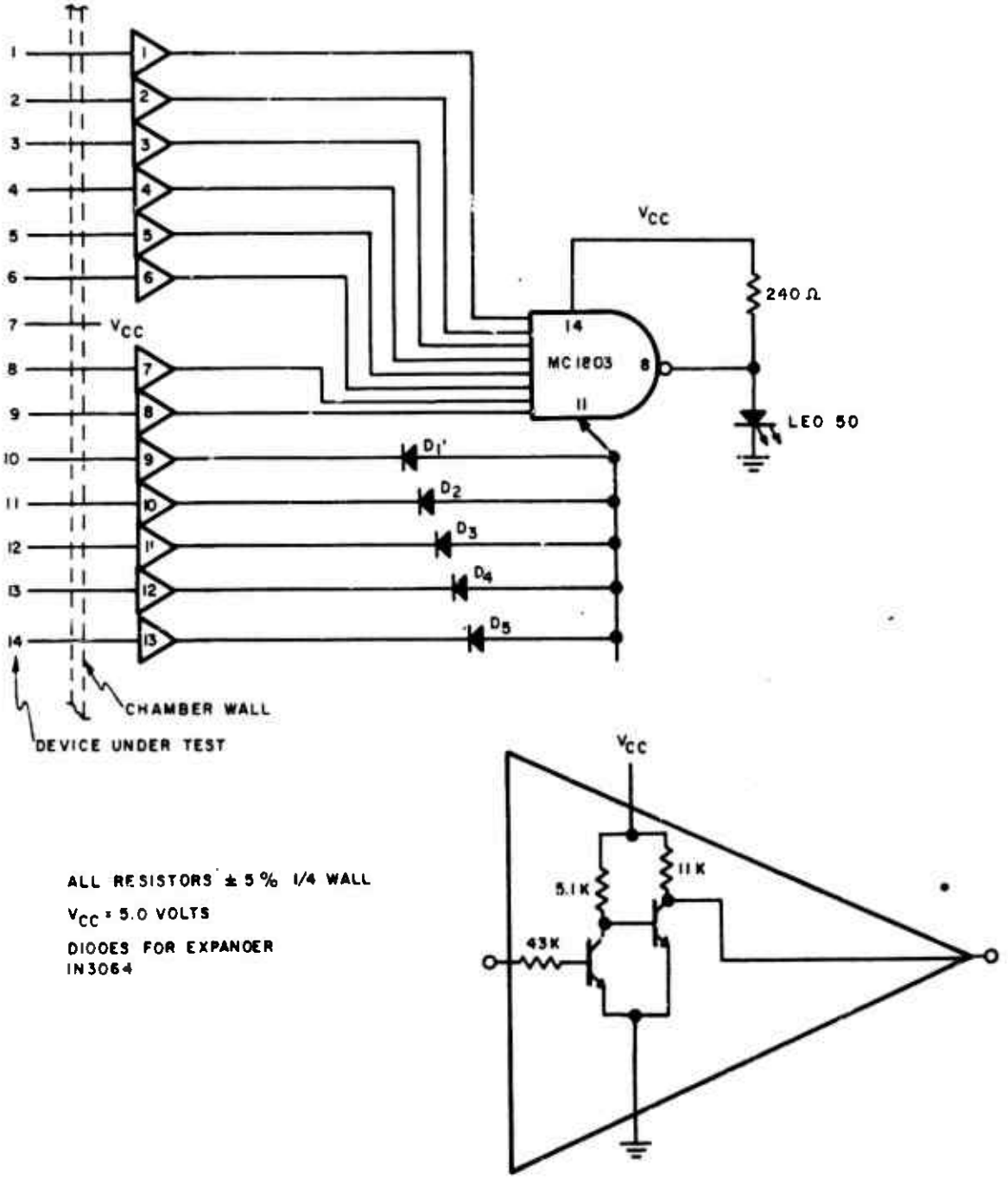

Figure 4-8. Thermal Intermittant Test Circuit Schematic

The DC electrical parameters of the bipolar 112 Gate Array (see Table IV-7) were measured on a proprietary LSI tester. Pass-fail criteria for input and output parameters were essentially the same as commercial TTL logic limits adjusted to account for fanout loading. Initial parameter limits were used throughout the program. Since the circuit used was a multichannel multiplexer, this device was functionally tested in the process of setting the output states during parameter measurement. These measurements were taken at 0°C, 25°C and 70°C at each readout.

DC parameter measurements on the 1103 P-MOS Random Access Memory were performed in accordance with the commercial specification on a proprietary MOS Memory/LSI Tester. Functional tests were performed on a Microdyne Memory Exerciser.

High and low temperature continuity tests were performed in a manner similar to the other plastic devices. The substrate and protective diodes are forward biased and the current is sensed at every pin. The temperature extremes were established by immersing the device under test in a "florinert" bath maintained at the specified temperature (-55°C and 125°C).

Functional testing was performed after DC parameter and continuity testing to detect any static electrical discharge damage induced by handling. Maximum rate of change of temperature was on the order of 1 degree per second. The minimum temperature window of intermittent contact we would have detected is less than 1 degree Celcius.

All electrical rejects were verified by retest and curve tracer analysis as applicable. Since the dominant failure modes of plastic encapsulated integrated circuits in the thermal cycling

environment has been intermittent open and open circuit failures caused by fracture of the internal lead wires and wire bonds, all thermal intermittent failures were left on test until 25°C failures developed or until the end of the test sequence. Then the failed units were removed for failure analysis. This was done to determine the time stress relationship between the onset of thermal intermittent failures and complete open circuit conditions.

4.1.6 Seal Tests

Seal tests were performed on all hermetically sealed devices using procedures per MIL-STD-883, Method 1014, Condition A, for fine leaks and Condition C for gross leaks, initially and at every readout. The limit for fine leak was 5×10^{-8} atm-cc/sec helium. The relative leak rate was recorded for all rejects. Indicated fine leak rejects were allowed to remain on test. Indicated gross leak rejects were removed and subjected to red dye verification. The procedure for this is found in Appendix I.

4.2 PLASTIC THERMAL EXPANSION CHARACTERISTICS

4.2.1 Discussion

The ability of a plastic encapsulated device to withstand temperature cycling and thermal shock is directly related to the thermal expansion coefficient over the temperatures of interest. The thermal expansion coefficient is not constant with temperature. It increases with temperature monotonically until a critical temperature is reached where the rate of change of the temperature coefficient of expansion increases dramatically. The temperature or range of temperatures where this abrupt change in the thermal expansion coefficient takes place is called the glass transition temperature (T_g) of the material. These changes in secondary thermodynamic properties are indicative of changes of material at the molecular level.

In addition, composite metal/plastic structures and almost all fiber filled molding compounds exhibit anisotropic thermal expansion characteristics. In general, the coefficient of thermal expansion is smaller in the direction of material flow during molding than is the coefficient of expansion in a direction normal to the flow axis. This phenomena is due in part to the ordering of the filler fibers parallel to the axis of flow.

Another factor which contributes to the anistropy in thermal expansion of a plastic encapsulated integrated circuit is the orientation of the lead frame with respect to the axis of measurement. This latter factor would be the primary cause of anistropic thermal expansion in silica filled molding compounds, the silica filler being generally in the form of small spheroids. Expansion measurements were taken in three orthogonal directions on each package to determine if any TEC differences existed due to filler orientation or molding conditions.

4.2.2 Theory of Measurement

Thermal expansion of the polymer materials used to encapsulate IC's can be determined by placing a piece of the polymer of known dimension in a thermomechanical analyzer (TMA) and measuring its change in length (ΔL) as a function of temperature (T). Thermal expansion coefficient (TEC) is determined from the slope of the ΔL-T plot using the following mathematical relationship:

$$TEC = \frac{1}{L_o} \cdot \frac{\Delta L}{\Delta T} = \frac{1}{L_o} \cdot \frac{dL}{dT} \qquad (1)$$

L_o = initial specimen height at room temperature
L = specimen height at T
$\Delta L = L - L_o$

Equation (1) is a definition of expansion coefficient which has the units: mm expanded per mm of original length per degree.

L_o is measured before subjecting the polymer specimen to testing, and the temperature and rate of heating are controlled by conditions set up on the TMA. The problem then becomes one of determining the slope of the ΔL-T curve so the TEC can be calculated from equation (1).

The measurements for this program were taken on a "Dupont 900" Thermal Analyzer with a Dupont 941 Thermal Mechanical Analyzer (TMA). This instrument monitors the movement of a probe placed against the sample under test as the sample is heated, thus measuring the change in length. The critical test variables in these measurements are probe loading and sample heating rates. The Dupont 941 TMA has provisions built into it to vary the load on the probe on the specimen from approximately 0 grams to 100 grams. Motorola's experience in testing the thermoset polymers used for encapsulating integrated circuits has shown that varying the loading on the specimen from 1 to 20 grams on a 0.635MM (0.025 inch) diameter probe did not cause any significant change in the derived thermal expansion coefficients.

The 20 gram loading produces a compression stress of 6.2×10^5 Newtons per square meter (approx 90 psi) which is less than 0.5 percent of the compressive strength of the molding compound used. A load of 5 grams was chosen for the TEC measurements in this program. This load gives an average compressive stress at the probe contact of 1.55×10^5 Newtons per square meter (approximately 22.5 psi). This reduces the error in measurements due to deformation and creep in the specimen at the elevated temperature to essentially zero.

Specimen heating rate must be established and controlled as the accuracy of the results depend on temperature uniformity within material. When considering the specimen heating rate, the size and thermal conductivity of the material must be considered. Large specimens or specimens with low thermal conductivity require low heating rates to obtain the degree of temperature uniformity required for accurate thermal expansion coefficient determination. However, if the rate of heating is too low, molecular flow of the material, particularly at temperatures above the glass transition, may produce erroneous results as well as consume an excessive amount of time. The specimen heating rate in the Dupont Thermo Mechanical Analyzer can be controlled accurately over the range of 2.5°C/min to 50°C/min. Experience in testing a large number of polymeric materials is that the errors in the thermal expansion coefficient caused by heating rates are negligible over the range of 2.5°C/min to 20°C/min when using a specimen of nominal size 6.35mm long by 6.35mm wide by 2.5mm thick (0.25 in by 0.25 in by 0.1 in).

The glass transition temperature, T_g can be estimated from a plot (Graph) of change in length vs temperature or thermal expansion coefficient vs temperature. In either case, the value is determined by extrapolating best fit straight lines to the curve above and below the breakpoint or knee of the curve until they intersect. The point of intersection defines the estimate of T_g. Figure 4-9 shows this construction on a hypothetical thermal expansion coefficient - temperature curve.

4.2.3 Experimental Procedure

Thermal expansion coefficient measurements were made on specimens from five 14 pin plastic dual-in-line packages of the vendor types shown below.

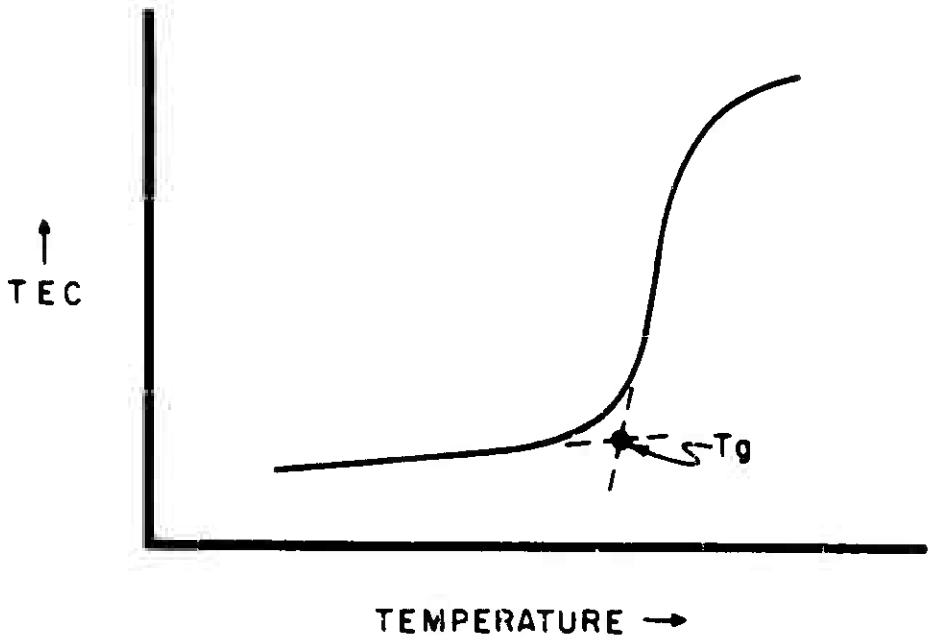

Figure 4-9. Determination of Glass Transition Temperature from Thermal Expansion Coefficient vs Temperature Plot

Vendor Number	Resin Type
1	Epoxy Type 1
2	Epoxy Type 2
3	Epoxy Type 1
4	Phenolic

A specimen was prepared from each device (five specimens per vendor) by sawing a block from one end of the package as shown in Figure 4-10. Each specimen is a composite structure of molding compound and lead frame. Thermal expansion measurements were performed on the Dupont Model 900 Thermal Analyzer with the Dupont Model #941 Thermal Mechanical Analyzer attachment. The test parameters were:

Probe	0.635mm (0.025 in)
Load	5 grams
Heating Rate	20°C/min.
Atmosphere	Dry N2

Each specimen was cycled through the thermal analyzer two times, without removal, for each of the three orientations. The first run from room temperature to 245°C has the effect of setting the probe firmly against the specimen. After reaching 245°C, the specimen is cooled to -80°C and the second run then made, again to 245°C.

The thermal expansion coefficient is determined from the thermal analyzer output using a five-point numerical differentiation formula, using computer processing of the data[1]. The TEC is determined as a function of temperature from -70 to 240°C.

The data is shown on Figures 4-11, 4-12, 4-13, and 4-14 from -50°C to 200°C. Each point is an average of five separate measurements.

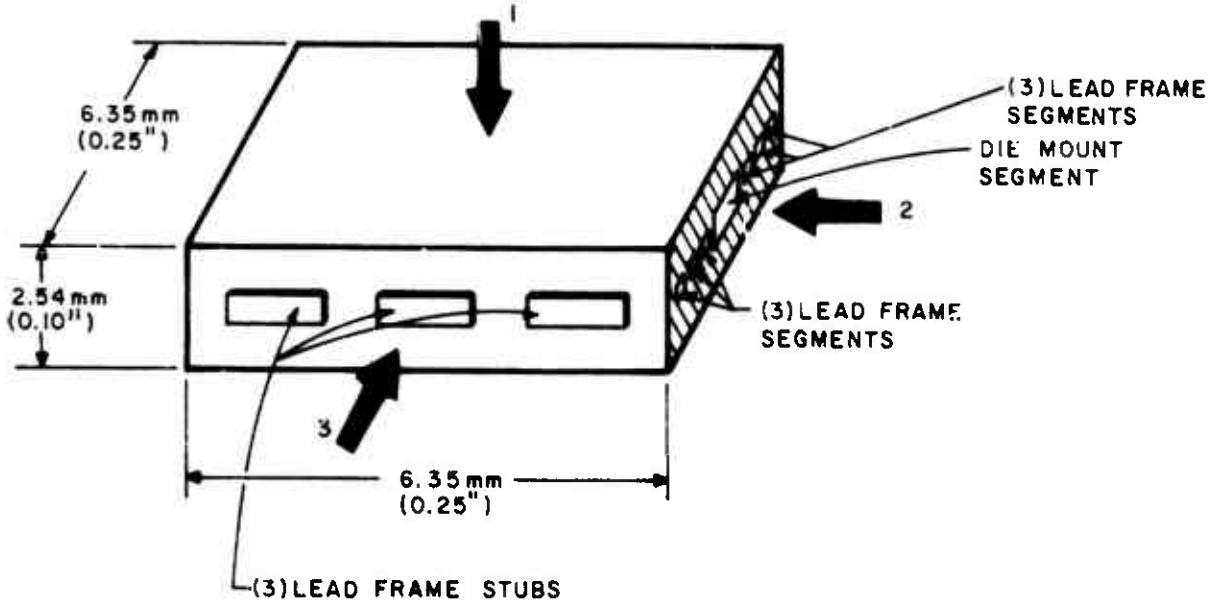

Position	1	Perpendicular to the lead frame
Position	2	Parallel to the long axis of the package
Position	3	Perpendicular to positions 1 and 2

Figure 4-10. Orientation of Expansion Measurements with Respect to IC Package Geometry

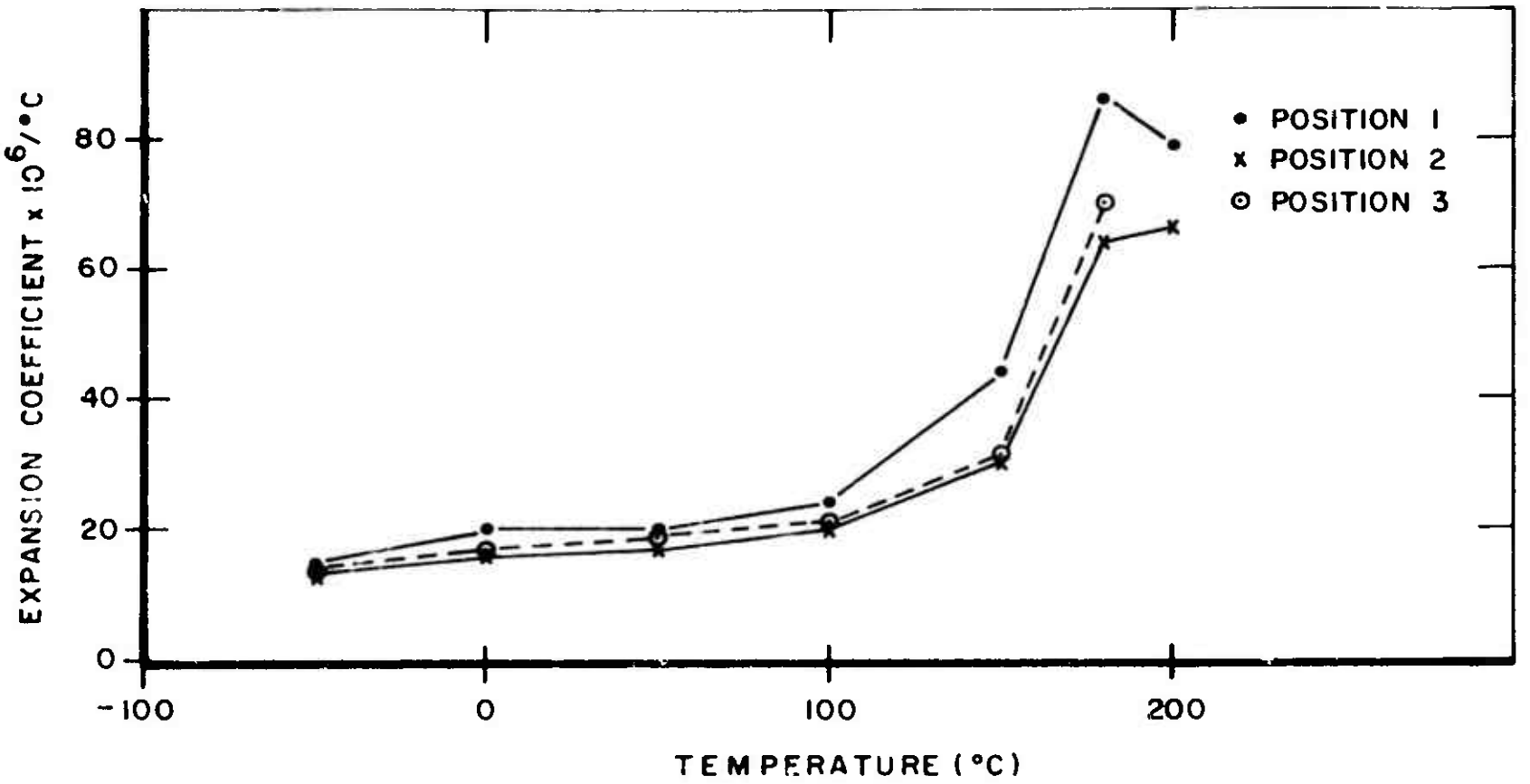

Figure 4-11. Thermal Expansion Coefficient vs Temperature for Vendor 1 Type 1 Epoxy

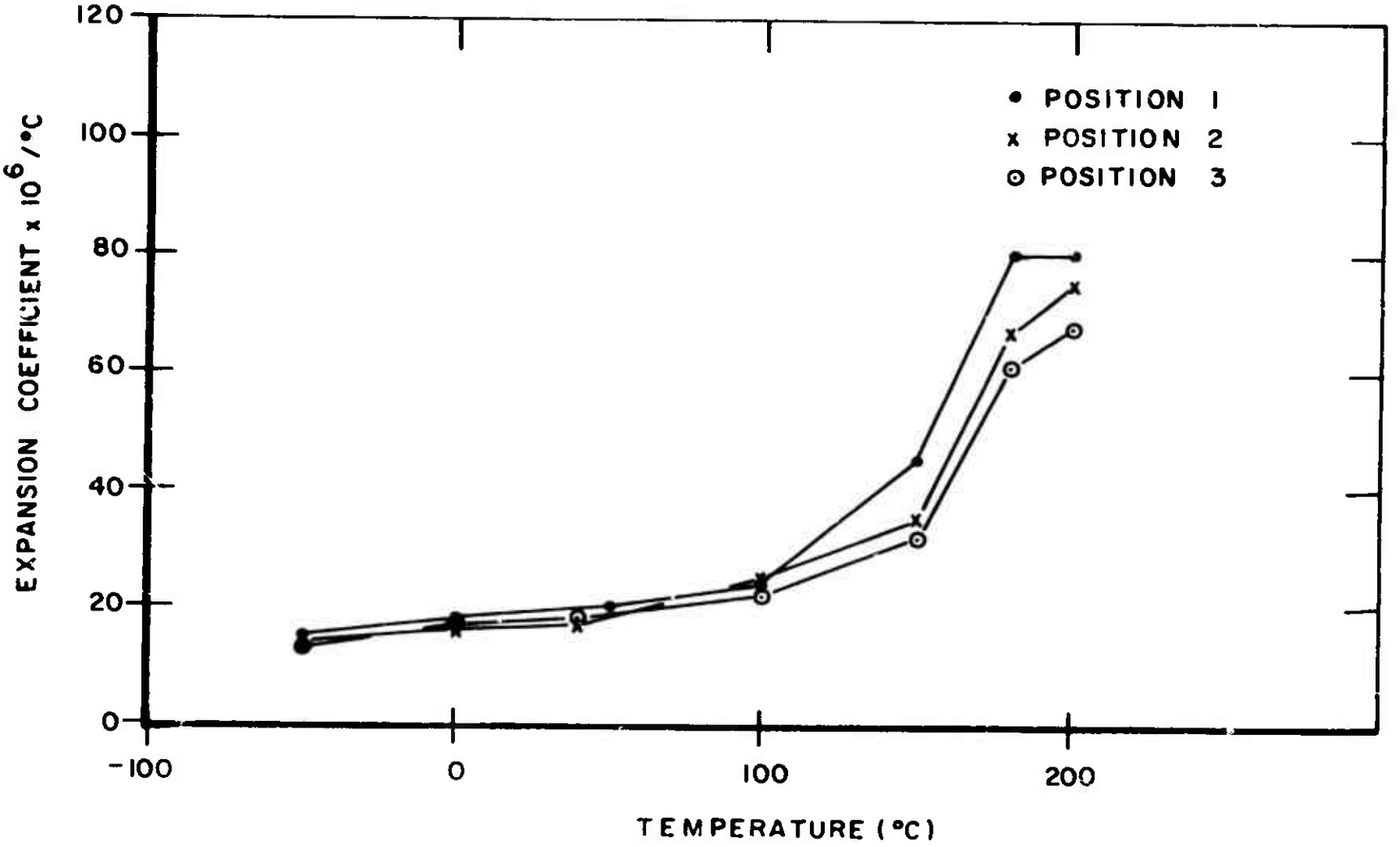

Figure 4-12. Thermal Expansion Coefficient vs Temperature for Vendor 3 Type 1 Epoxy

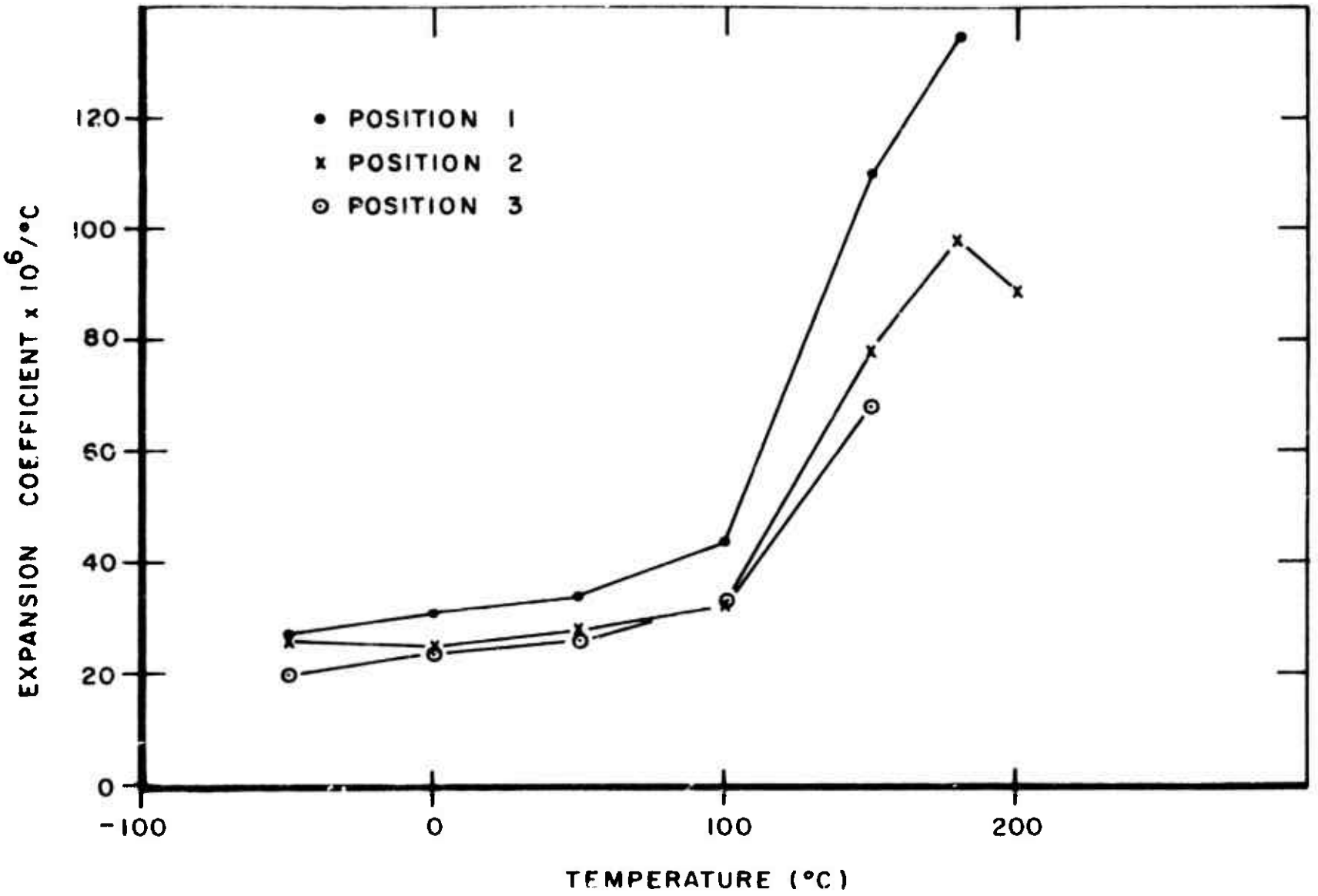

Figure 4-13. Thermal Expansion Coefficient vs Temperature for Vendor 2 Type 2 Epoxy

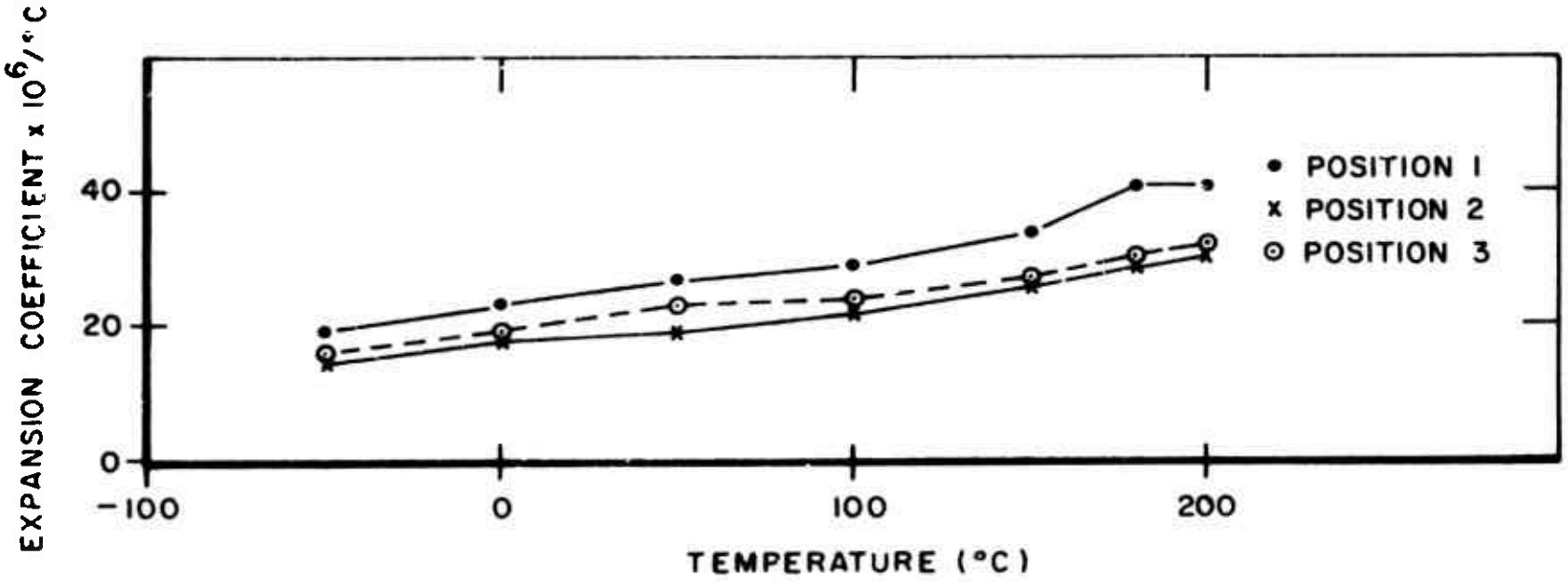

Figure 4-14. Thermal Expansion Coefficient vs Temperature for Vendor 4, Phenolic

4.2.4 Results

Examination of Figures 4-11 through 4-14 show some small difference in the TEC for each of the three mutually perpendicular directions. These differences are primarily due to lead frame orientation. As a consequence of sample preparation, each TEC measurement represents a composite of leadframe, and resin expansion, and the data is thus representative of the complete integrated circuit package.

Comparison of the Vendor 1 and 3 expansion curves show them to be identical. This is not surprising since Type 1 molding resin is used for both parts. Vendor 4 phenolic has the lowest thermal expansion coefficient. Vendor 2 type 2 devices have a higher thermal expansion coefficient than the others.

Expansion coefficients for epoxies increase as the temperature rises. The point at which this increase becomes rapid is the glass transition temperature (T_g). Estimated values for each package system are given below:

System	T_g (^oC)
Vendor 1 Type 1 Epoxy	150
Vendor 3 Type 1 Epoxy	150
Vendor 2 Type 2 Epoxy	100-120
Vendor 4 Phenolic	180-200

Differences in the orthogonal TEC measurements are attributed to differences in lead-frame orientation. These differences, while small, are real and become larger above the glass transition temperature.

Vendor 1 and Vendor 3 Type 1 epoxy units have identical TEC-temperature curves which are the result of using similar molding compounds. Lead frame design differences between the units does not cause a detectable difference in the TEC results.

4.3 THERMOMECHANICAL STRESS

This section covers the thermomechanical analysis of the Microelectronics Package Study. Section 4.3.1 discusses the detailed thermal analysis aspects and 4.3.2 discusses the mechanical aspects. The analysis was concentrated on a 14 lead ceramic dual-in-line package since this package is the most susceptible to thermal shock stresses. Stress levels near the package leads were predicted for typical cool-down and warm-up thermal shock conditions. Basically, the results indicated that the maximum stress levels would occur during a cool-down from 400°C (i.e., the stress free temperature) to -65°C. The results also indicated that the glass material with a tensile stress of 4330 psi would be very close to its allowable limit (5000 psi @ 25°C).

4.3.1 Thermal Analysis

During the cold and hot temperature shock tests required by MIL-STD-883, the microelectronics package is subject to severe temperature extremes (i.e., -65°C to +150°C). These sudden temperature changes produce stress levels in the package that may cause degradation or catastrophic failure of the lead/glass seal interface. To predict these stress levels, it is necessary to know the thermal gradients throughout the package as a function of time. A detailed computer thermal analysis was made to determine transient temperature profiles for both a sudden warm-up and cool-down of a typical 14 lead ceramic dual-in-line package (CDIP).

4.3.1.1 Thermal Model

Prior to making the analysis, it was necessary to model the DIP as a series of finite element subvolumes (nodes). Because of symmetry, only one quarter of the package was modeled. A total of 716 nodes were used to represent the one quarter model of the 14 lead CDIP. The package was basically divided into eight layers as described below:

LAYER NO.	MATERIAL	DEPTH(Inches)
1	Ceramic	0 to .025
2	Ceramic	.025 to .050
3	Glass	.050 to .063
4	Glass/Lead Frame	.063 to .073
5	Glass	.073 to .085
6	Ceramic	.085 to .110
7	Ceramic	.110 to .135
8	Ceramic	.135 to .160

Each layer, with the exception of layer No. 4, contained at least seventy-five 0.025 in. wide x 0.025 in long nodes. The glass/lead frame layer (No. 4) had many small irregular shaped nodes due to the variations in the widths of the leads. After completing the nodal model, the intra-nodel thermal resistances and the thermal capacitance (Wcp) for each node were determined. In order to calculate these values, the thermophysical properties of the various materials must be known. The material properties that were used are listed in Table IV-8.

TABLE IV-8 Material Properties for Thermal Analysis

Material	Density Lb/Ft^3	Specific Heat BTU/Lb-^oF	Thermal Conductivity BTU/Hr-Ft-^oF
Ceramic (Al_2O_3)	235	0.20	11.0
Glass Type 1	374	0.03	0.33
Lead Frame (Alloy 42)	510	0.11	10.0
*Lead Frame (Alloy 200)	555	0.105	36.0
Silicon	145	0.18	80.0
Plastic (Phenall 8700)	110	0.30	0.64

*Used with plastic package.

After completing the above calculations, the data was input to the Motorola SIGMA 5 computer in conjunction with the in-house thermal analyzer program (MELTA) and a sample free convection steady-state problem was run for the ceramic package to verify the adequacy of the thermal model. The results agreed with past experimental data and indicated that the model was suitable. The next step was to include boiling heat transfer from the surface of the package and the leads.

4.3.1.2 Heat Transfer Coefficients

During a typical thermal shock test, the DIP is subjected to a sudden plunge from a 150^oC soak into a -65^oC methyl alcohol bath. Boiling occurs the instant the DIP is submerged in the bath. The boiling heat transfer rate is a function of the temperature difference between the surface temperature of the DIP and the liquid's saturation

temperature (65°C for methyl alcohol at sea level). The boiling heat transfer equations also include a constant that is dependent upon the surface-fluid interface combination. This constant can only be determined experimentally. Since it was not within the scope of this effort to determine the boiling heat transfer rates for methyl alcohol, the following approach was taken. The data of Reference 2 presents the boiling heat transfer equations and empirical data for cooling integrated circuit packages in Freon. These equations were modified for use in the present analysis by substituting the appropriate property values for methyl alcohol in place of those for Freon. A check was then made to determine if the boiling heat transfer coefficients that were obtained as a function of temperature were reasonable. The results are shown in Figure 4-15. Note that the heat transfer coefficient ranges from 10 BTU/Hr-Ft^{2}-°F to 25 BTU/Hr-Ft^{2}-°F in the free convection region and increases to approximately 9000 BTU/Hr-Ft^{2}-°F in the boiling region. It should be mentioned that the free convection coefficients are determined via a subroutine in the main heat transfer program. The equations involved for these calculations are straightforward and can be found in most heat transfer text books.

4.3.1.3 Computer Analysis and Results

The first problem that was run on the computer was the cool-down of a 150°C ceramic DIP when plunged into a -65°C methyl alcohol bath. After completing the ceramic DIP run, the properties and model were changed to represent a plastic DIP and the problem was rerun. The results showed that the most severe thermal gradients occurred in the ceramic package. Figures 4-16 and 4-17 show the cool-down curves at sections taken through the center and near pin 7, respectively, of the ceramic DIP. Note that the cool-down response

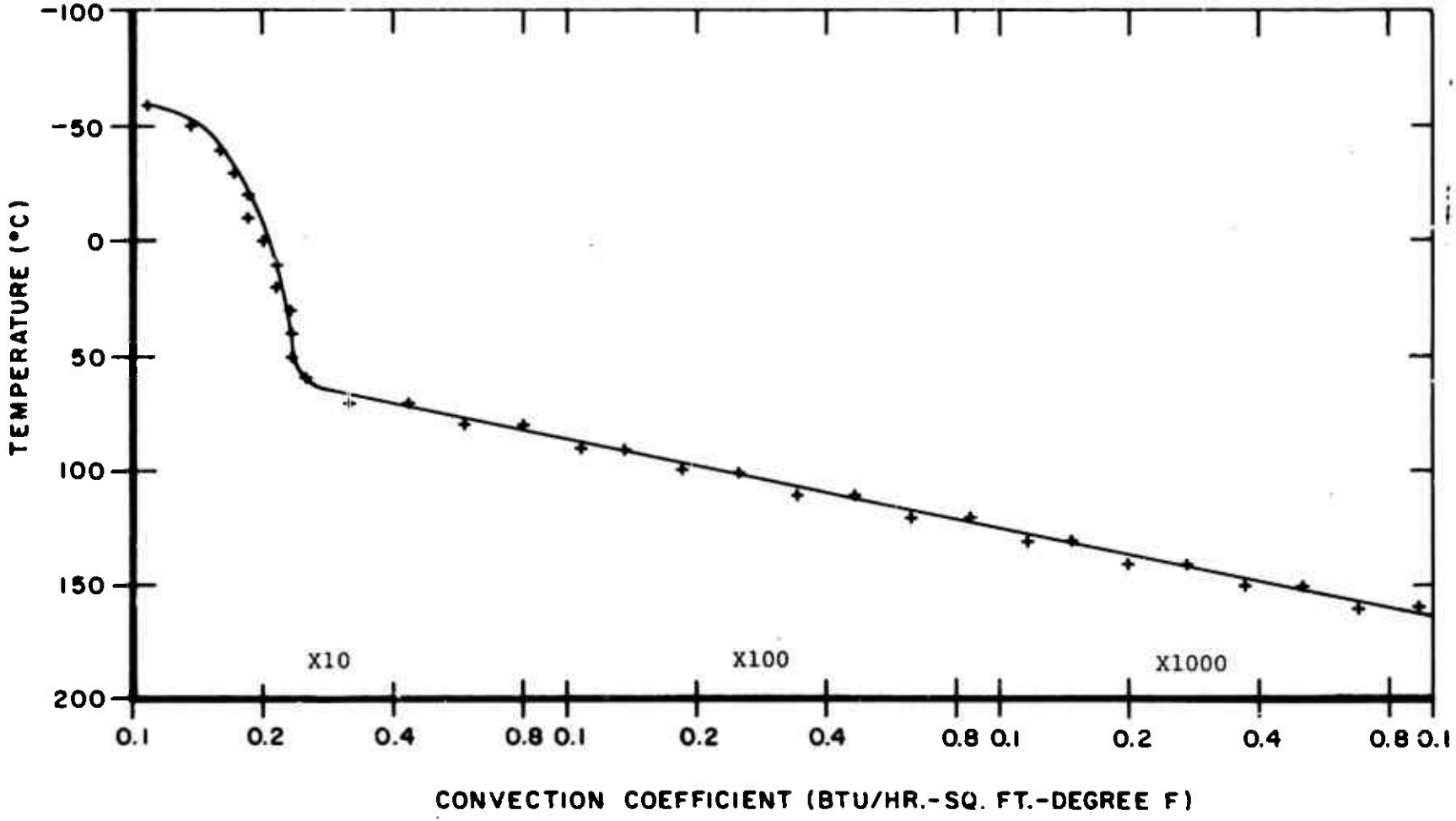

Figure 4-15. Coefficient of Heat Transfer vs Surface Temperature of Cooling Body for Methanol

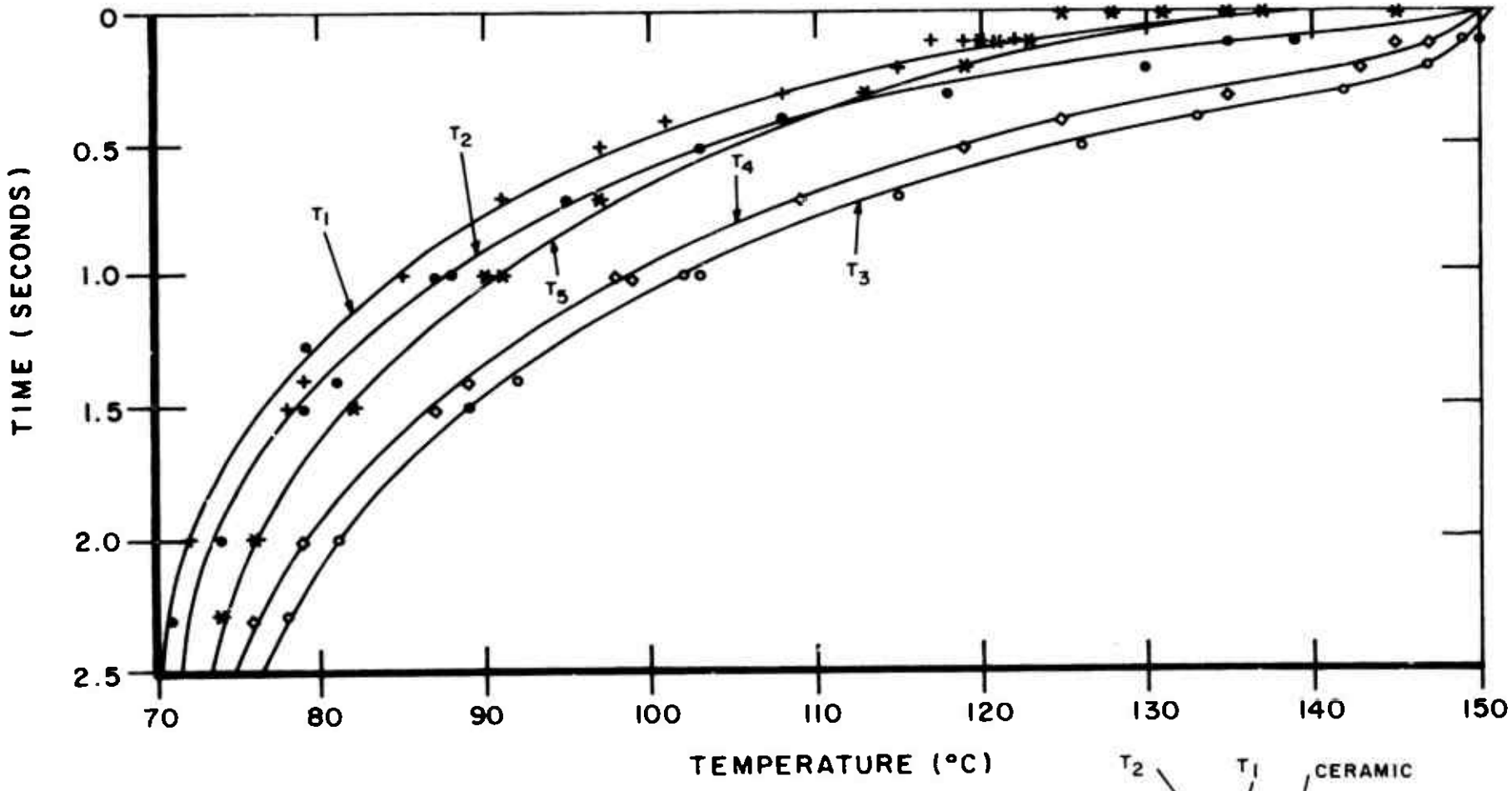

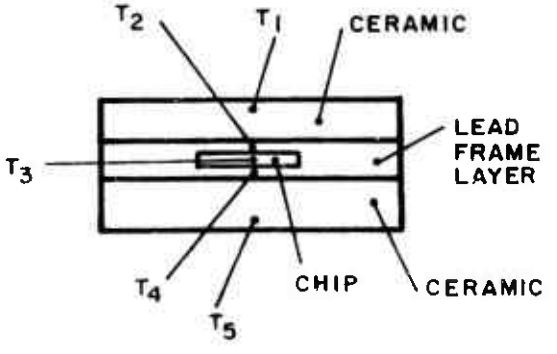

Figure 4-16. Temperature History of DIP for Cool-Down in Methyl Alcohol (150° to -65°C)

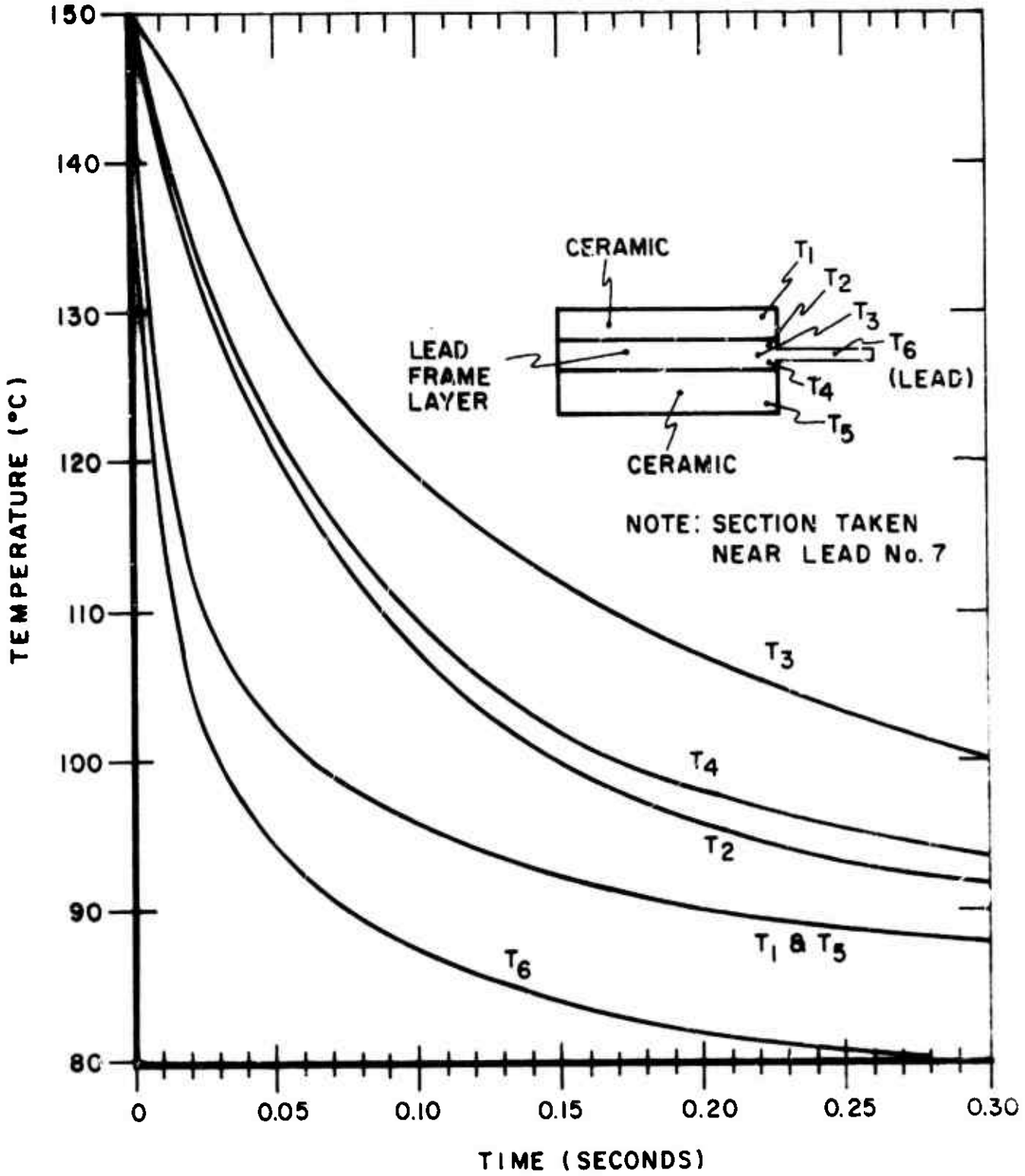

Figure 4-17. Cool-Down of DIP in Methyl Alcohol

near pin 7 is much more rapid than near the center of the package. Figure 4-17 also indicates that gradients of up to 50°C occur in the ceramic DIP within 20 milliseconds.

After completing the cold-shock analyses, the warm-up problem was investigated. The hot thermal shock occurs when a DIP is suddenly immersed in a 150°C oil bath after a cold soak at -65°C. The hot bath used was UCON OIL 50 HB280X, a poly alkylene glycol. Thermal properties for this oil can be found in Reference 3. Figures 4-18 and 4-19 show the thermal gradients in the ceramic DIP during warm-up at sections taken through the center and near pin 7, respectively. It can be seen in Figures 4-18 and 4-19 that the warm-up response of the package in oil is much less rapid than the cool-down in the methyl alcohol. This is what one would expect since the boiling heat transfer coefficients in methyl alcohol are significantly larger than the convection heat transfer coefficients in the oil. Note, however, that gradients of up to about 60°C occur between pin 7 and the glass seal near the edge of the package.

4.3.1.4 Discussion of Results

Both the cool-down and warm-up transient temperature response data was supplied as input data for the computer stress analysis of the package. However, prior to discussing the stress analysis, it is appropriate to make some additional comments concerning the thermal analysis. First, it was very difficult to obtain thermophysical properties of the Type 1 glass. The manufacurer indicated that the specific heat of the glass, as noted in Table IV-8 was 0.03 BTU/lb-°F. This valuc is highly suspect

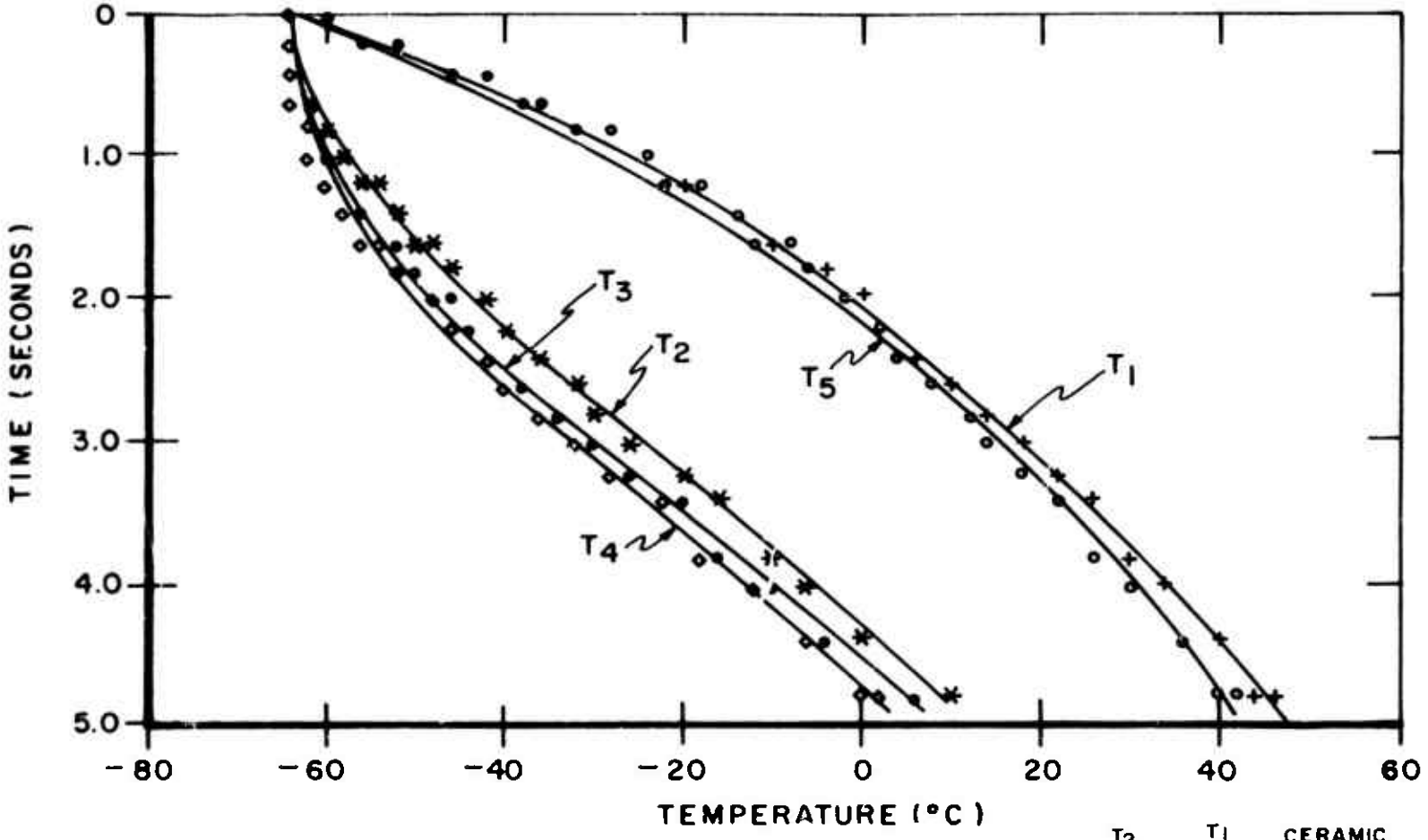

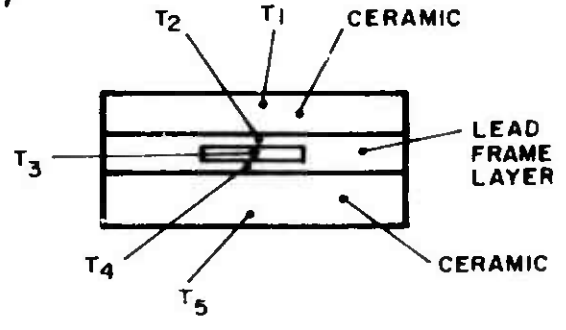

Figure 4-18. Temperature History of DIP for Warm-Up in Ucon Oil (-65°C to 150°C)

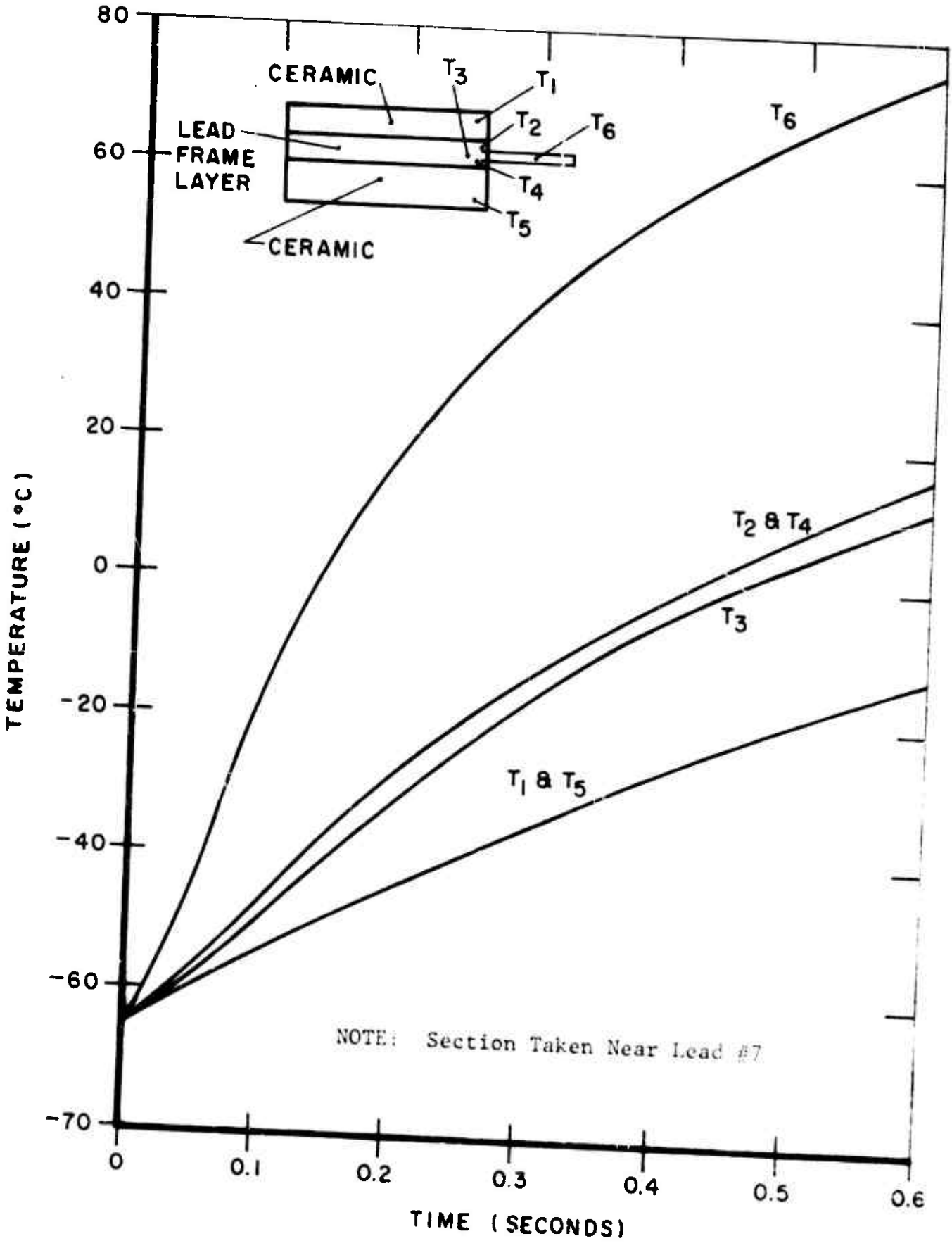

Figure 4-19. Warm-Up of DIP in Ucon Oil

since conflicting data from another source indicates that this value should be about 0.2 BTU/lb-^{o}F. The higher specific heat value would tend to make the gradients between the glass and the lead frame less than indicated in the present analysis. Secondly, the nodal division used for the model may not be small enough to "sense" the temperature gradients near the outer surface of the package. Hand calculations based on the infinite slab assumption indicate that the thermal gradients can be as large as 45^{o}C through the first 10 mils of the package after 6 milliseconds of submersion in the cold bath. This would undoubtedly increase the stress levels at the lead/glass interface near the surface of the pins. Finally, it was assumed that no voids existed in the thermal model. Voids could have several effects. If the void were between a surface node and an interior node, the node near the surface would change temperature more rapidly than it should. This in essence means that a larger gradient would occur than was indicated by the thermal analyses.

Most of the above mentioned "problems" tend to produce results that will make the stresses more severe. However, these points may indicate that the analysis is in the "ballpark" if the computer stress analysis produces results that are near the stress limits of the materials.

4.3.2 Mechanical Analysis

A mechanical structural analysis of the ceramic, 14 lead dual-in-line package was proposed. With the resulting temperature profiles and gradients from the thermal analysis as input, the predicted stress levels in the package were to be computed. These results would then be evaluated in comparison with the material allowable strengths to determine if failures could be expected.

The package was ultimately modeled in the local area of lead 7 and consisted of 81 "cube" elements making up five layers of materials. The materials were Type 1 glass, Alloy 42 lead material, and alumina ceramic.

With the use of Mechanics Research Inc. STARDYNE structural/dynamic system, the stress levels were predicted for three load cases:

(1) Steady state cool-down from 400°C to -65°C.

(2) A run considering temperature gradients in the package after being immersed in an alcohol bath at -65°C, following a stabilizing soak at 150°C.

(3) Temperature gradients in the package after being immersed in oil at 150°C, following a stabilizing soak at -65°C.

The results of the analyses show a maximum stress condition during the steady state cool-down from 400°C to -65°C. The maximum stresses occurring in the glass were greater than 4000 psi in tension. Comparing with a room temperature strength value of 5000 psi in tension yields the qualitative observation that a trend is established for a possible failure in the glass.

4.3.2.1 Procedure

The ceramic, 14 lead dual-in-line package was modeled structurally with hexahedron ("cube") finite elements while taking into account the package's inherent quarter symmetry. Figure 4-20 shows the package configuration used in the model. The model consisted of 646 "cube" elements which made up five layers of materials.

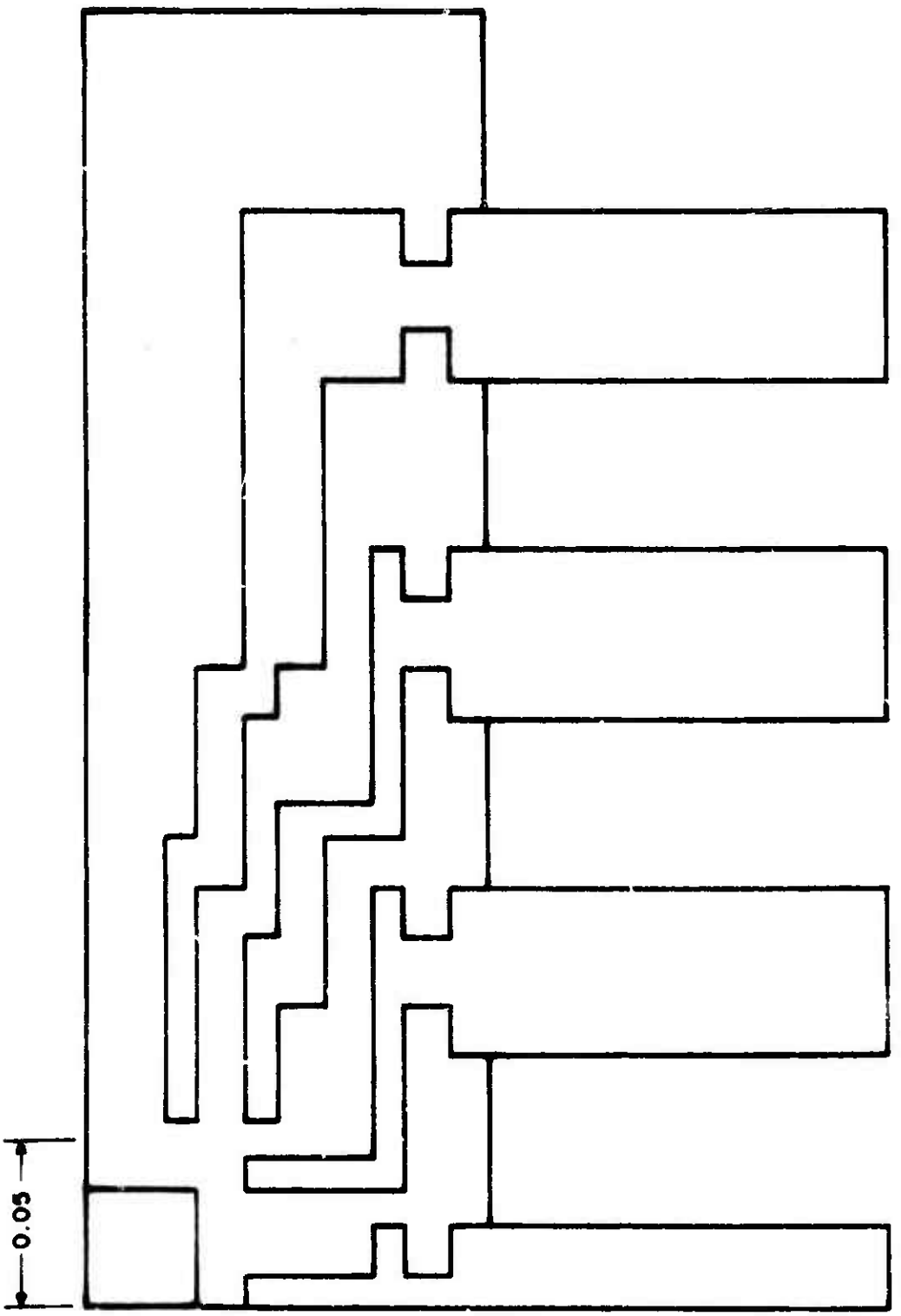

Figure 4-20. Plan View of Initial Package Model

The two outer layers were alumina ceramic, the two layers surrounding the middle layer were Type 1 glass, and the center layer consisted of glass and Alloy 42 lead material.

Because of the large number of degrees-of-freedom required for the 646 element model, and since several load cases would be required for a reasonable analysis, the decision was made to re-evaluate the original model. Following evaluation of the temperature profiles in the package and information from actual package test data, the model was reduced in size to the local area of lead number 7. Figure 4-21 illustrates the portion of the package which was modeled. As with the original model, the revised model consisted of the same five layers of the same three materials. Figure 4-22 shows the finite element model consisting of 81 "cubes". The figure also shows the numbering schemes used for the elements.

The revised geometry and temperature data obtained from the thermal analysis discussed in section 4.3.1 were used as input data for three static load cases. The cases were run using the Mechanics Research Inc.'s STARDYNE computer program. STARDYNE is a general-purpose finite element computer program which can be used to evaluate a wide variety of static and dynamics problems. It offers several three-dimensional elements of which the hexahedron is one. This particular element has the following built in assumptions:

(1) The element is linear, homogenous, elastic, and isotropic.
(2) The element undergoes small deformations.
(3) The element has non-zero volume.
(4) The displacement of the element is restricted to three translations at each node.
(5) The element requires eight nodes for representing the cube shape.

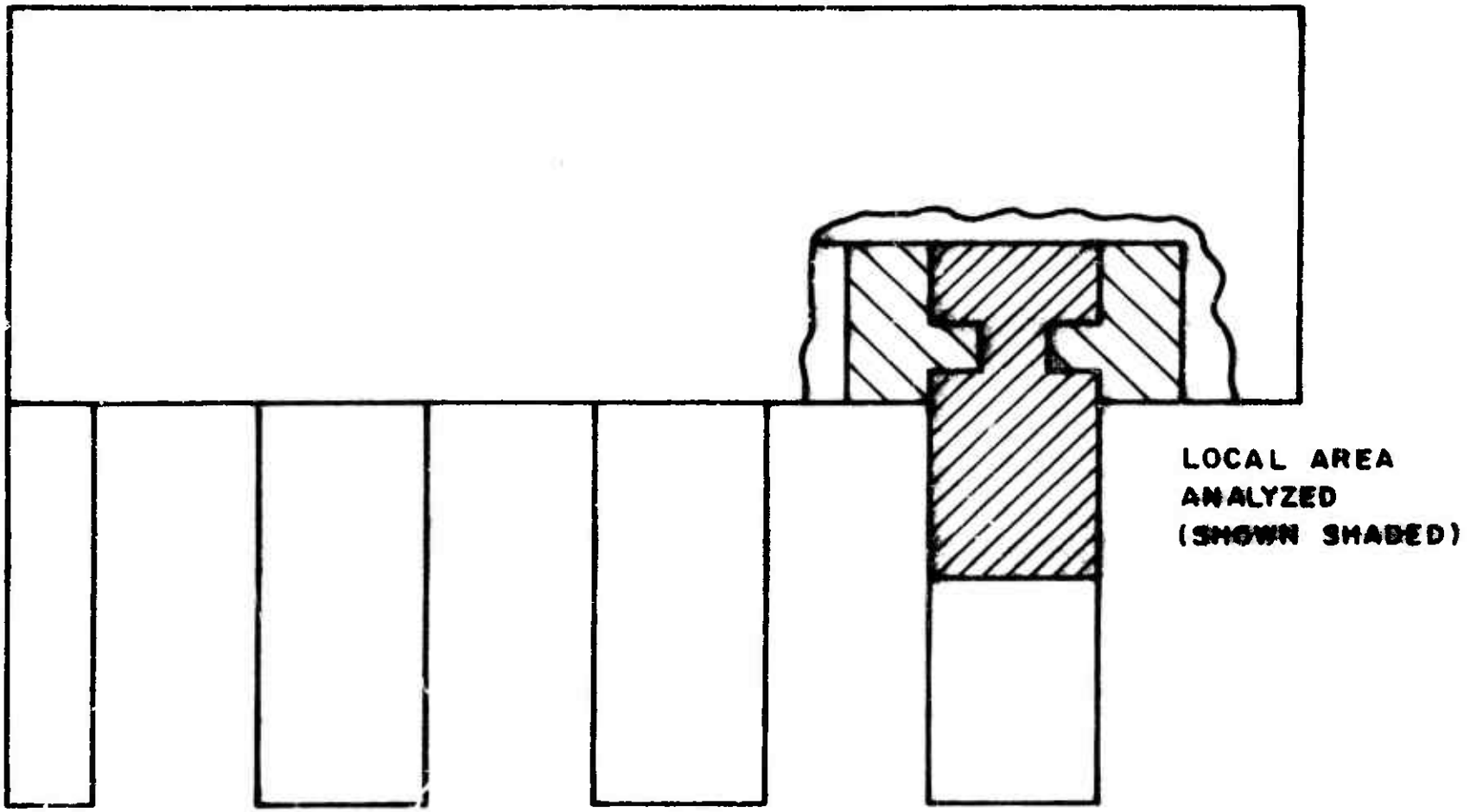

Figure 4-21. Revised Model at Lead 7

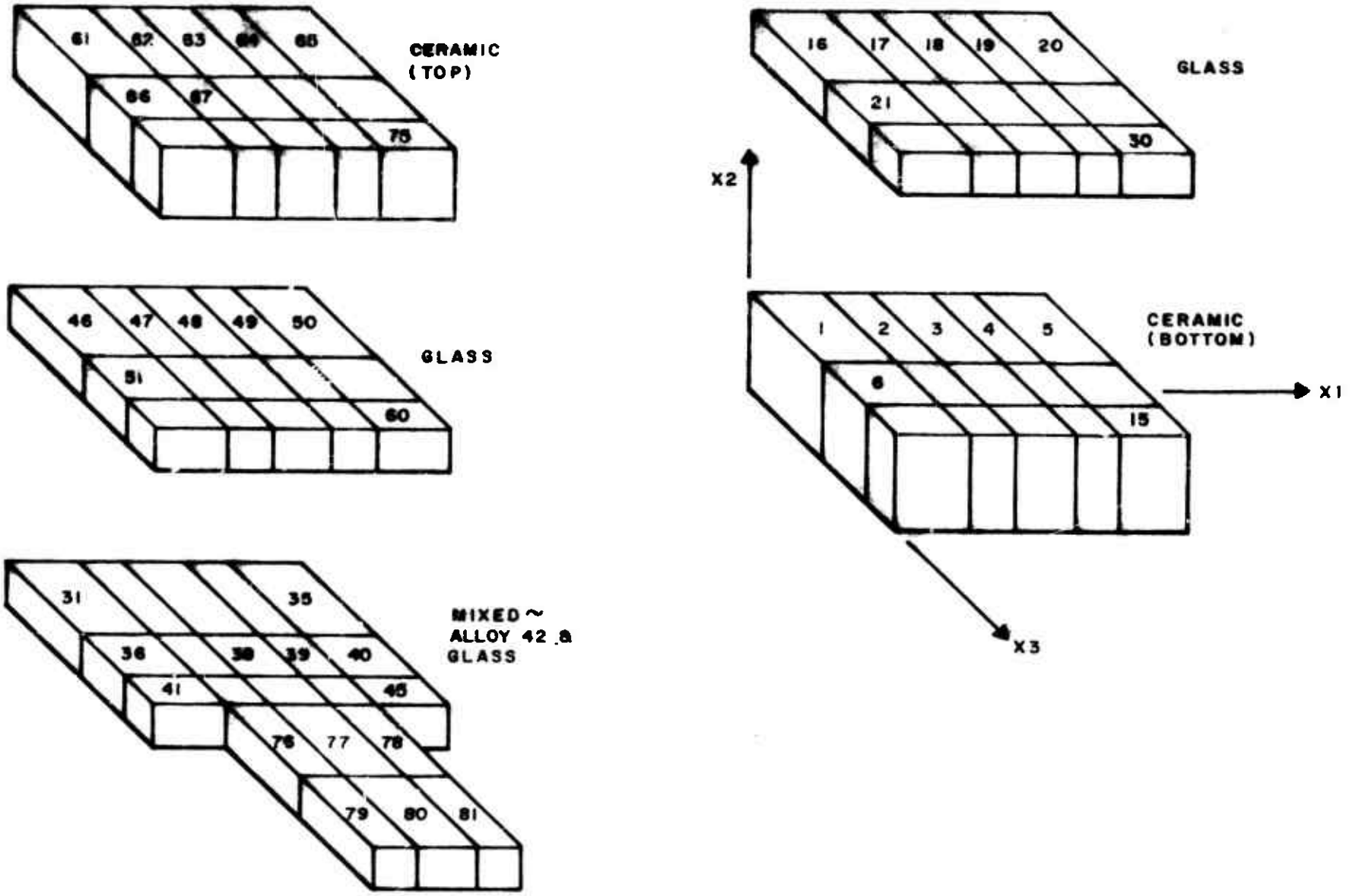

Figure 4-22. 81 Element Model with Element Ordering

For the three materials making up the model, the following values for the material properties were assumed:

	GLASS	ALLOY 42	ALUMINA
Elastic Modulus, psi	7.34×10^6	22×10^6	48×10^6
Poisson's Ratio	.294	.29	.28
Coefficient of Thermal Expansion, /°C	7.7×10^{-6}	6.8×10^{-6}	7.1×10^{-6}

The three cases considered for the study were:

(1) Steady state cool-down from 400°C to -65°C.

(2) A run considering the temperature gradients through the package at 0.029 seconds after being immersed in a -65°C alcohol bath. The package was previously soaked at 150°C prior to immersion in the alcohol.

(3) A run considering temperature gradients 0.678 second after having been immersed in a 150°C oil bath. The soak temperature for this case was -65°C.

In all three cases, a stress-free temperature state was taken to be 400°C. This temperature is based upon the assumption that during the cool-down stage of the assembly process of the package, the glass has solidified sufficiently at 400°C to begin a build up of residual stresses in the materials. The particular chosen times were based upon an examination of graphs of temperatures at various locations within the package versus time. The two subject times were judged to be representative of the maximum temperature gradients throughout the package.

For the temperature gradient cases (case 2 and 3), the temperatures at various locations in the package were obtained from the temperature profiles computed during the thermal analysis discussed previously. Because the thermal element requires less than one-tenth the number of degrees of freedom that a corresponding mechanical finite element requires, a much finer element breakdown was possible with the thermal model. Thus, the temperatures used for many of the elements were obtained by averaging several temperatures within the element in question. The temperatures used in the two temperature gradient cases are shown in Tables IV-9 and IV-10.

4.3.2.2 Results

An examination of the results of the computer runs for the three static load cases shows a maximum stress condition occurs during the steady state cool-down environment with the case 3 temperature gradient (warm-up) environment running a close second. For the three load conditions, the following table shows the maximum stress and its corresponding material. The plus (+) and minus (-) signs indicate tensile and compressive stresses, respectively.

CASE 1		CASE 2		CASE 3	
Thermal Cool-Down 400°C to -65°C		At Peak Temp. Gradient -65°C Bath		At Peak Temp Gradient 150°C Bath	
Material	Stress,psi	Material	Stress,psi	Material	Stress,psi
Glass	+4330	Ceramic	+2110	Glass	+3780
Alloy 42	-7940	Alloy 42	-6580	Alloy 42	-7990

For the glass, the maximum stresses occur in "cubes" 39, 67, and 19 for cases 1, 2, and 3, respectively.

TABLE IV-9 ELEMENT TEMPERATURES
AT MAXIMUM TEMPERATURE
GRADIENT IN -65°C BATH. CASE 2

ELEMENT	TEMPERATURE, °C	ELEMENT	TEMPERATURE, °C
1	135.7	42	129.0
2	|	43	129.0
3	|	44	129.6
4	|	45	142.6
5	135.7	46	148.0
6	119.2	47	|
7	|	48	|
8	|	49	|
9	|	50	148.0
10	|	51	130.5
11	|	52	|
12	|	53	|
13	|	54	|
14	|	55	|
15	119.2	56	|
16	148.7	57	|
17	|	58	|
18	|	59	|
19	|	60	130.5
20	148.7	61	131.5
21	131.0	62	|
22	|	63	|
23	|	64	|
24	|	65	131.5
25	|	66	115.5
26	|	67	|
27	|	68	|
28	|	69	|
29	|	70	|
30	131.0	71	|
31	149.6	72	|
32	149.0	73	|
33	149.0	74	|
34	149.0	75	115.5
35	149.5	76	100.6
36	142.6	77	|
37	141.8	78	|
38	139.8	79	|
39	141.8	80	|
40	142.6	81	100.6
41	142.6		

TABLE IV-10 ELEMENT TEMPERATURES
AT MAXIMUM TEMPERATURE
GRADIENT IN THE +150°C BATH. CASE 3

ELEMENT	TEMPERATURE, °C	ELEMENT	TEMPERATURE, °C
1	-45.2	42	41.8
2	-44.2	43	41.8
3	-44.2	44	41.8
4	-44.2	45	5.1
5	-40.4	46	-48.8
6	-21.2	47	-37.5
7	-19.5	48	-37.5
8	|	49	-37.5
9	|	50	-44.2
10	-19.5	51	0.0
11	-21.2	52	21.3
12	-19.5	53	21.3
13	|	54	21.3
14	|	55	1.9
15	-19.5	56	0.0
16	-51.1	57	21.3
17	-40.1	58	21.3
18	-40.1	59	21.3
19	-40.1	60	1.9
20	-46.5	61	-39.1
21	- 1.9	62	-37.7
22	20.5	63	-37.7
23	20.5	64	-37.7
24	20.5	65	-34.3
25	0.0	66	-14.5
26	- 1.9	67	-12.4
27	20.5	68	|
28	20.5	69	|
29	20.5	70	-12.4
30	0.0	71	-14.5
31	-43.9	72	-12.4
32	-17.7	73	|
33	-17.7	74	|
34	-17.7	75	-12.4
35	-39.3	76	80.0
36	3.5	77	|
37	15.0	78	|
38	16.2	79	|
39	15.4	80	|
40	5.1	81	80.0
41	3.5		

As a comparative example of the stresses at a particular location in the model, "cube" 29 was chosen. The following table depicts the stresses for each of the three load cases:

CASE	STRESS, psi
1 - Steady state cool-down	+4330
2 - Cool-down from 150°C	+2000
3 - Warm-up from -65°C	+2500

For comparison, the following table lists the allowable strengths for the three materials which make up the package. Lacking data for the materials at 150°C or -65°C, the values shown are for room temperature.

MATERIAL	ALLOWABLE STRENGTH, psi
Type 1 Glass	5,000 (Tensile)
Alloy 42	68,000 (Tensile)
Alumina	26,000 (Tensile) 300,000 (Compressive)

It is seen that the glass is the only material which apparently is stressed near its allowable strength. While this observation is more qualitative than quantitative, the trend is established for the glass material as the weak link in the package.

Areas which might affect the accuracy of these results are:

(1) Fineness of the structural model. An investigation of the stability of the solution versus the number of finite elements used for a given model would have been advantageous but most probably very costly.

(2) The temperature gradients chosen. Based upon data from initial computer runs, one particular time was chosen for cases 2 and 3. Perhaps temperature gradients over a short distance or at the surface could contribute to high stresses. This ties in with the fineness of the structural model.

(3) Inherent in the package are re-entrant corners at the interface of the leads and the glass which encases it. These are areas of stress concentrations which are difficult to account for.

(4) Material properties. Since the computer program will handle only static load cases, the material properties chosen were taken to be constant for a given base temperature. The fact that the actual test conditions for the package entail transient conditions most probably affects the accuracy of the modeled results.

4.3.2.3 Conclusions

The results indicate that failure of the dual-in-line ceramic package would most likely occur either:

(1) during heating from -65°C due to thermal gradients which create stress in the glass additive to the internal stress at -65°C, or

(2) at thermal equilibrium at -65°C due to the residual stresses at that temperature.

4.4 HEAT FLOW AND THERMAL SHOCK FLUID COMPATIBILITY STUDIES

The experiments discussed in this section were designed to provide information in two areas: (1) Is the thermal shock cycle, defined in MIL-STD-883, Method 1011, adequate to achieve temperature stabilization at each extreme for all packages at the standard test levels? (2) Are the fluids popularly used compatible with the materials of the packages used in integrated circuit production? That is, do these fluids chemically attack the glass or metal parts of the package?

4.4.1 Heat Flow Studies

To determine the rate of change of temperature of the integrated circuit die during the thermal shock cycle, the voltage drop of the substrate isolation diode was monitored on an X-Y recorder as the device was transferred from one bath to the other. To establish this voltage, a constant current on the order of 100 microamperes was injected into the ground pin of the device under test and the circuit returned through the Vcc or power supply pin.

The packages studied included the 14 pin flat packages; 14 pin dual-in-line, ceramic and plastic; and the 40 pin dual-in-line LSI package. Fluids studied were water, methonol and dry ice mixture (-65^{o}C bath), poly alkylene glycol, and the "flourinerts."

The results of the study indicate, for the baths and packages tested, the currently specified 5 minutes dwell at each temperature extreme is adequate to stabilize the temperature throughout all packages. The LSI package was, of course, the

slowest to reach thermal equilibrium with the bath, stabilizing in approximately three minutes in ice water after being transferred from boiling water (Test Level A). This particular sequence proved to give the longest stabilization time for all packages.

Comparison of the measured rate of cool-down from 150°C to -65°C, in methanol and dry ice mixture, to that which was predicted by the thermal analysis showed that the cooling rates established by the computer analysis were conservative. The curve in Figure 4-16 shows cool-down to approximately 78°C in 2.5 seconds, whereas measurements determined that this temperature was reached in less than 1 second. The main source of difference is most likely to be due to the agitation of the bath when the devices are plunged into it. (The computer analysis assumed boiling, cooling, and free convection.)

The data generated by these experiments indicate that while the 5 minute dwell or method is approximately five times the stabilization time for 14 pin packages, these data are insufficient to suggest any change in the cycle currently defined.

4.4.2 Fluid Compatibility Studies

Two samples each from Vendors 6, 7, 8, 9, 10, 11, and 13 were subjected to a high temperature soak in ethylene glycol and poly alkylene glycol for 400 hours in accordance with the conditions shown in Table IV-11 below.

	125°C	150°C	200°C
Ethylene Glycol	X	X	
Poly Alkylene Glycol		X	X

TABLE IV-11. High Temperature Soak Matrix

The samples were visually examined and subjected to fine and gross seal tests every 40 hours.

The results show severe hermeticity loss in the ethylene glycol soaks. Failure of some vendors occurred at 40 hours and glass sealed ceramic parts had failed gross seal test by 200 hours at 125°C, and 120 hours at 150°C. These failures appear to be the result of chemical attack of the sealing glass by the ethylene glycol. Figure 4-23, 4-24, and 4-25 show the evidence of chemical attack of the sealing glsss. This attack was more apparent on Type 1 glass than or Type 2 glass.

There was some evidence that the poly alkylene glycol reacted with the sealing glass to a degree. Indicated fine leak failures were noted after 120 hours on some units. These failures were adjudged to be due to trapping helium at the surface of the glass.

The sidebraze (Vendor 11) package and the LSI package did not suffer any confirmed gross leaks in either fluid. Indicated fine leak failures were observed in the ethylene glycol soaked LSI packages after 120 hours at 150°C. The problem was trapping at the metal ceramic interface indicating some reaction in this area.

From this data it appears that ethylene glycol makes a poor fluid for thermal shock of ceramic packages.

4.5 THERMAL CYCLING STEP STRESS MATRIX

Step stress testing was performed to determine the limits of stress which can be applied to the packages tested in

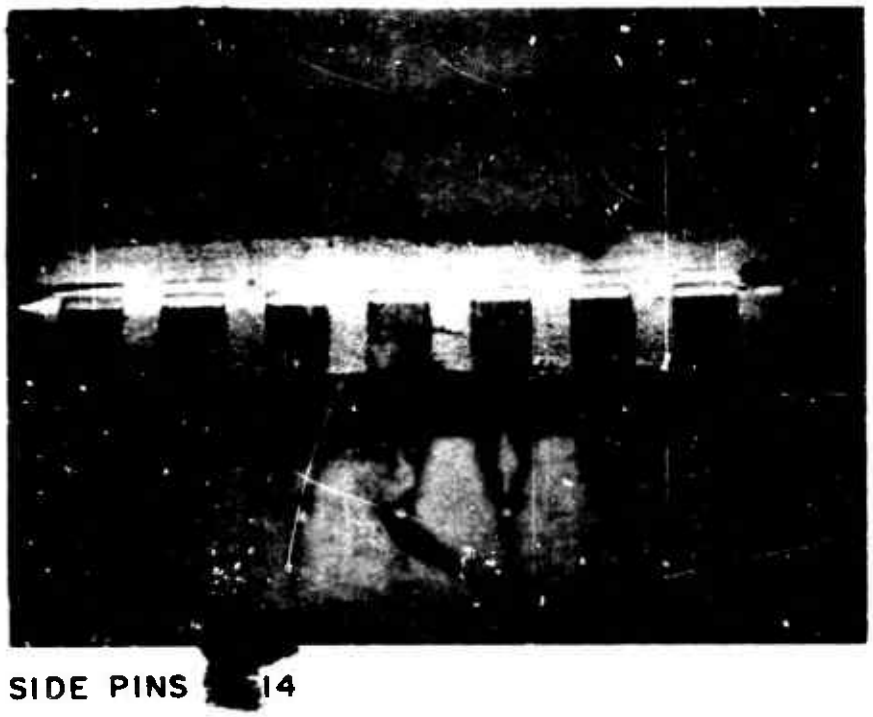

Figure 4-23. Unit #1195 Vendor 10 after 40 Hours in Ethylene Glycol at 125°C

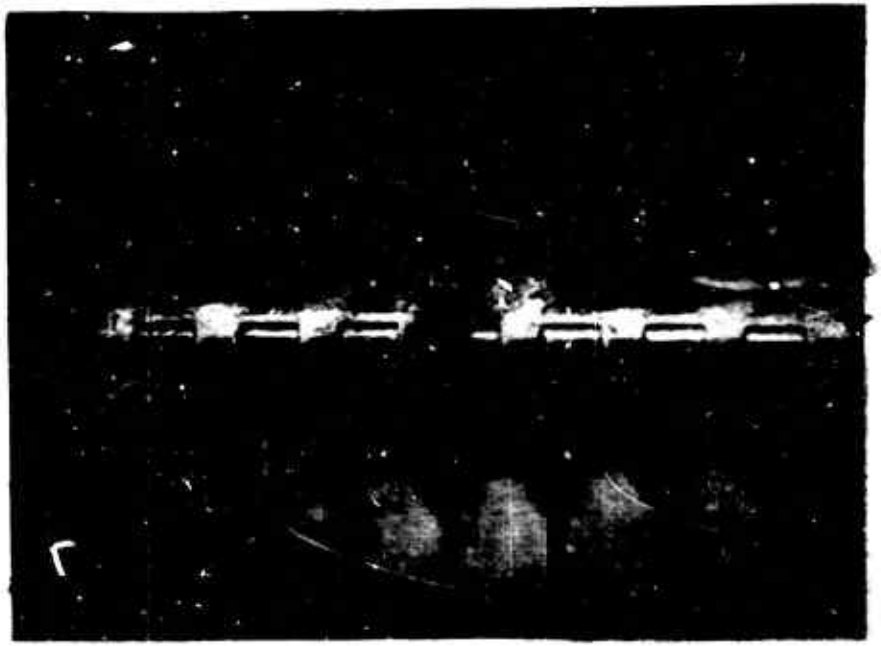

SIDE PINS 1-7

END PINS 1 & 14

Figure 4-24. Unit #1196 after 120 Hours in Ethylene Glycol at 150°C

SIDE PINS 8 - 14

END PINS 7 & 8

this program. Two thermal cycling step stress sequences were established: (1) A temperature cycle step stress sequence in which the devices were subject to each level defined by MIL-STD-883, Method 1010, Conditions B through F. The values of T_{max} for the steps above, test Condition D, (-65°C to 200°C) were modified for plastic devices because of the high temperature limitations of the molding compounds. Table IV-12 shows the test sequence used for this test; (2) A thermal shock step stress sequence was established which subjects devices to increasing levels of thermal shock as defined in MIL-STD-883, Method 1011, Test Condition A through F. The test, as defined in Method 1011, was modified to reduce the cycles per step to 10 from the specified 15. End point measurements were performed after each step. Figure 4-26 shows the flow of samples through this test.

In the analysis of this data, attempts to define the failure-stress distributions were unsuccessful due to the number of data points. The presentation of data has been designed to indicate the dominant failure modes for each package type. Sample sizes for each vendor is indicated in each figure.

4.5.1 Results on the Plastic Package

Figure 4-27 shows the thermal cycling step stress results for all plastic packages. The bar charts show the accumulated percent failures at the end of each step.

These charts show that the main effect of the thermal cycling is maximum temperature, rather than the difference between T-high and T-low, or rate of change of temperature. This would indicate that from the standpoint of package assembly strength the

10 Cycles Per Step STEP	TEMPERATURE CYCLING			THERMAL SHOCK	
	HERMETIC PACKAGES		Plastic Packages Temperature Range	Temperature Range	Method 1011 Level
	Temperature Range	Method 1010 Level			
1	-55°C to 125°C	B	-55°C to 125°C	0°C to 100°C	A
2	-65°C to 150°C	C	-65°C to 150°C	-55°C to 125°C	B
3	-65°C to 200°C	D	-65°C to 200°C	-65°C to 150°C	C
4	-65°C to 350°C	E	-65°C to 225°C	-65°C to 200°C	D
5	-65°C to 500°C	F	-65°C to 250°C	-195°C to 150°C	E
6	-65°C to 500°C	F	-65°C to 300°C	-195°C to 200°C	F

TABLE IV-12

TEMPERATURE CYCLING-THERMAL SHOCK
STEP STRESS MATRIX.

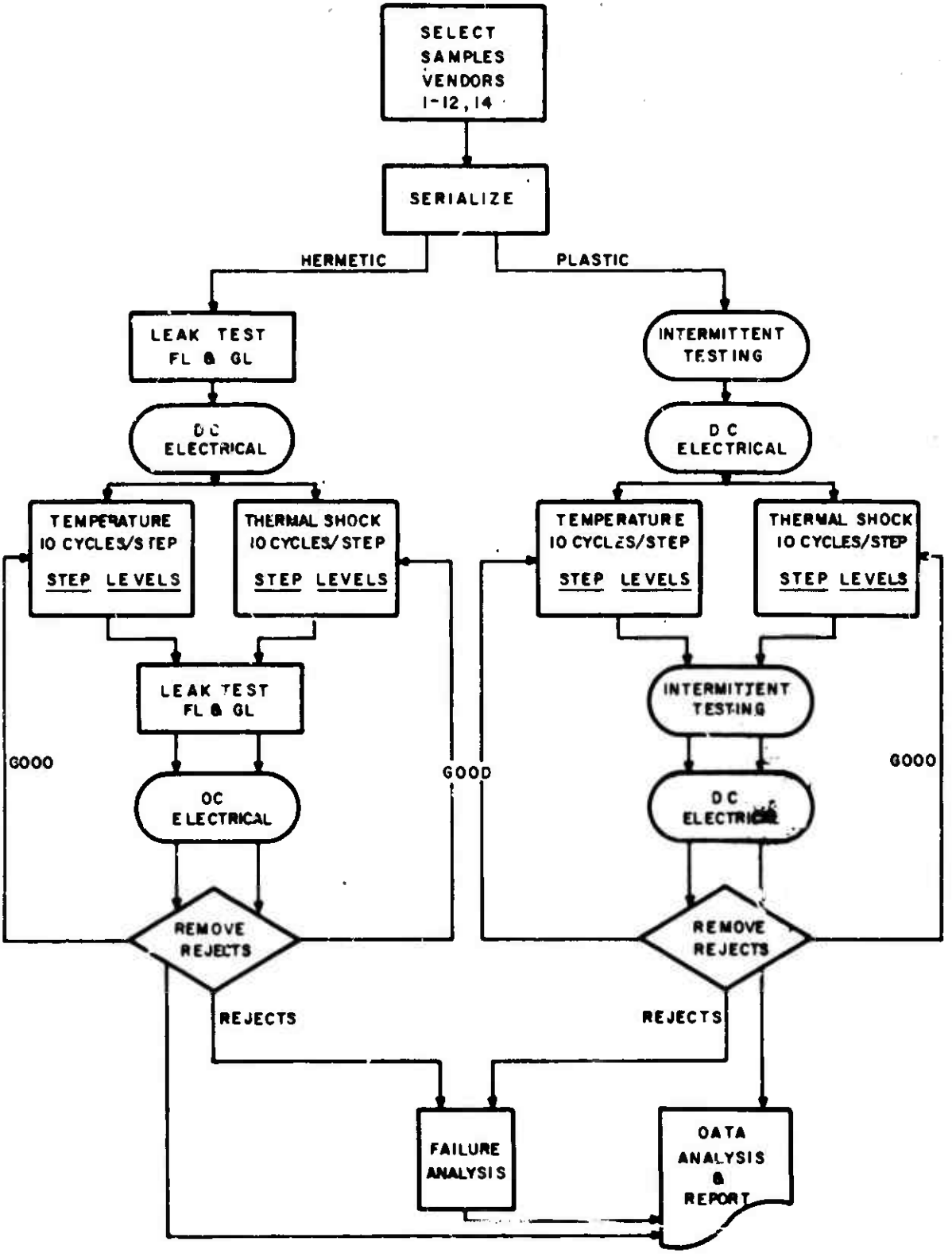

Figure 4-26. Thermal Cycling Step Stress Test Plan

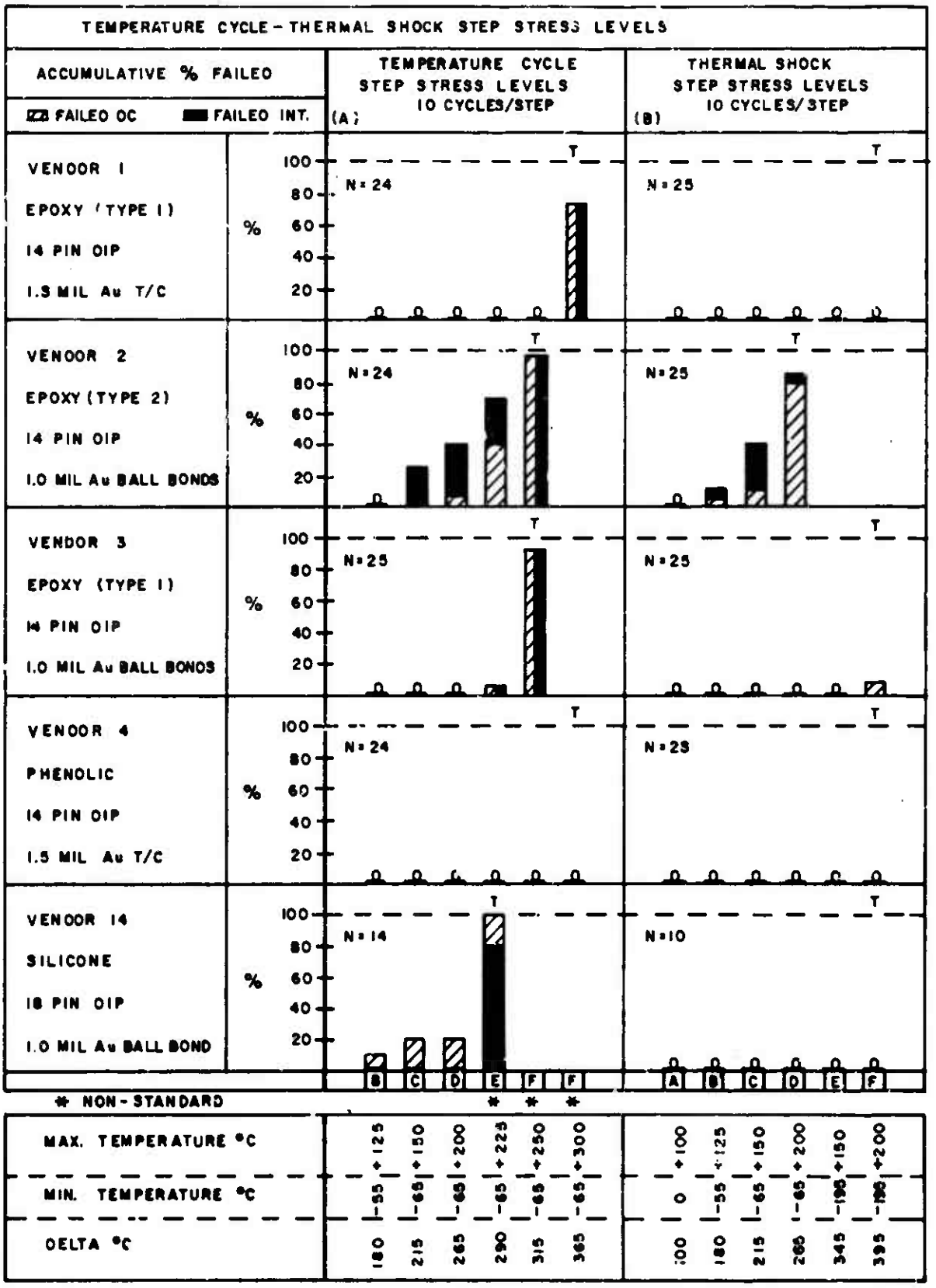
TEMPERATURE CYCLE - THERMAL SHOCK STEP STRESS LEVELS
ACCUMULATIVE % FAILED
FAILED OC
FAILED INT.
TEMPERATURE CYCLE STEP STRESS LEVELS 10 CYCLES/STEP (A)
THERMAL SHOCK STEP STRESS LEVELS 10 CYCLES/STEP (B)
VENDOR 1
EPOXY (TYPE 1)
14 PIN DIP
1.5 MIL Au T/C
N = 24
N = 25
VENDOR 2
EPOXY (TYPE 2)
14 PIN DIP
1.0 MIL Au BALL BONDS
N = 24
N = 25
VENDOR 3
EPOXY (TYPE 1)
14 PIN DIP
1.0 MIL Au BALL BONDS
N = 25
N = 25
VENDOR 4
PHENOLIC
14 PIN DIP
1.5 MIL Au T/C
N = 24
N = 25
VENDOR 14
SILICONE
18 PIN DIP
1.0 MIL Au BALL BOND
N = 14
N = 10
%
100
80
60
40
20
T
A B C D E F
* NON-STANDARD
MAX. TEMPERATURE °C
MIN. TEMPERATURE °C
DELTA °C
+125 +150 +200 +225 +250 +300
-55 -65 -65 -65 -65 -65
180 215 265 290 315 365
+100 +125 +150 +200 +150 +200
0 -55 -65 -65 -150 -200
100 180 215 265 345 395

Figure 4-27.

critical reliability factors relating to plastic dual-in-line packages in the thermal cycling environment would be (1) temperature coefficient of expansion of the plastic, (2) glass transition temperature (T_g) of the plastic, and (3) size and strength of the internal wire interconnect system.

The data shows that Vendor 4 had the strongest package in this test, followed by Vendor 1, then 3 and 2 for the 14 pin devices. Vendor 14 shows weaker than Vendor 2 on temperature cycling, but far superior in thermal shock. If we consider the thermal expansion coefficients (TEC) of the materials tested in Section 4.2, we find that Vendor 4 has the lowest TEC (25 ppm at 100°C) and highest T_g (180°C to 200°C) followed by Vendors 1 and 3, both with a T_g of 150°C and approximately the same TEC (23 ppm at 100°C).

Vendor 2 (type 2 epoxy) has a TEC of approximately 33 ppm at 100°C, and a T_g of 100° to 120°C.

Vendor 14 (silicone) was not included in the plastic thermomechanical studies. Studies at Motorola, and other studies reported in the literature, indicate that the TEC of the material is on the order of 30 to 50 ppm at 25°C. Although the T_g of the silicone is very high, over 250°C, the TEC at temperatures of 200 + 225°C is approximately 10 to 20% higher (33 to 60 ppm).

The differences in the TEC and the glass transition temperatures (T_g's) partially explains the differences in performance of the five venodrs in the temperature cycling step stress.

The failures observed were caused by opens in the internal lead wires. Neglecting residual stresses, the stress in these wires during the high temperature half of the temperature cycle is a function of the TEC of the material at that temperature. Assuming equivalent wire and bond strengths, these data indicate that the type 2 epoxy and the silicone have nearly equal TEC's at 200 to 250°C, even though the low temperature TEC's and T_g's of the two materials are different.

The results from Vendor 2 in both thermal cycling stresses indicate a double distribution. The weak distribution generally failed due to lifted ball bonds at the die. The stronger, representing wearout or excessive mechanical stress, generally failed by breaks at the ball and in some cases breaks at the heel of the post bond. The mechanisms of wire and bond fracture in plastics are discussed in more detail in Section V.

To explain the differences in the performance of Vendor 1 and Vendor 3, we must look at the mechanisms of failure. All failures of Vendor 3 were wire breaks - 1 to 3 wire diameters above the ball. The wire appeared to have fractured along a grain boundary. Evidence of large grain formation in the gold wire was observed by optical microscope and confirmed with the scanning electron microscope. Failures of Vendor 1 devices did not occur until the -65°C to 300°C step and resulted from wire fracture due to the stress, which occurred when the epoxy started to disintegrate at the high temperature. The wire broke as a result of excessive tensile stress. Some intergranular fracture was evident.

Since the molding compounds were the same, the wire size and bonding method must account for the difference in response in

this test sequence. As shown in Table IV-1, Vendor 1 uses 0.0015 in (38.1μm) wire, while Vendor 3 uses 0.001 inch wire (25.4μm). This gives Vendor 1 a stronger wire bonding system. The grain boundry fracture phenomena is discussed in more detail in Section V, Failure Analysis.

With the exception of Vendor 2, thermal shock had little effect on these devices. Vendor 3 had 1 device which failed due to electrochemical corrosion of the aluminum bonding pad on the die, which is caused by moisture penetrating to the die and not directly related to the thermomechanical stresses.

The greater effects found in temperature cycling are related to two factors: (1) the maximum temperatures are higher, reaching the point where the plastics begin to disintegrate; (2) the time at temperature is greater under temperature cycling than the time at extreme temperature by a factor of almost 2 As will be shown in Section 4.8, this appears to be the dominant factor in wire bond degradation at a given temperature rather than the rate of change of temperature.

4.5.2 Flat Package Results

The performance of the flat packages tested in the thermal cycling step stress matrix tends to duplicate the results of the plastic package in that the temperature cycling step stress produced the greater number of failures. In this case, however, the maximum temperature (T_{HIGH}) was stepped in accordance with the stress levels of Method 1010, MIL-STD-883, from level B through level F. Level F was repeated as the sixth step to balance the matrix. The results of testing are plotted in Figure 4-28.

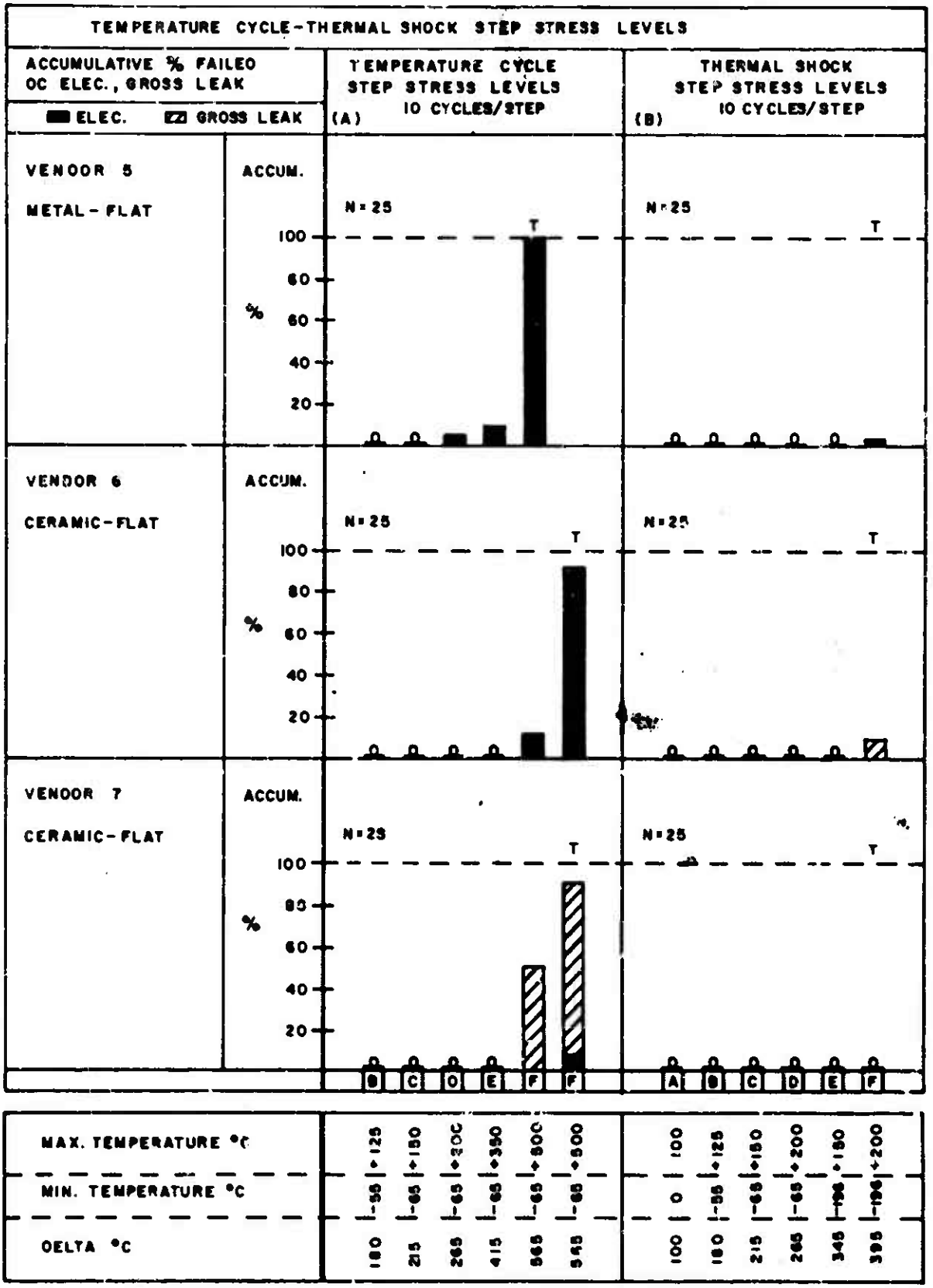
TEMPERATURE CYCLE-THERMAL SHOCK STEP STRESS LEVELS
ACCUMULATIVE % FAILED OC ELEC., GROSS LEAK
ELEC.
GROSS LEAK
TEMPERATURE CYCLE STEP STRESS LEVELS 10 CYCLES/STEP (A)
THERMAL SHOCK STEP STRESS LEVELS 10 CYCLES/STEP (B)
VENDOR 5
METAL-FLAT
VENDOR 6
CERAMIC-FLAT
VENDOR 7
CERAMIC-FLAT
ACCUM.
%
N=25
T
100
80
60
40
20
B C D E F F
A B C D E F
MAX. TEMPERATURE °C
MIN. TEMPERATURE °C
DELTA °C
-55 +125
-65 +150
-65 +300
-65 +350
-65 +500
-65 +500
100
0
-55 +125
-65 +150
-65 +200
-65 +150
-196 +200
180
215
265
415
565
565
100
180
215
265
345
396

Figure 4-28.

The Vendor 5 failures were predominately bond failures and shorts caused by massive intermetallic reaction which were detected after step 5 (-65 to 500°C). The two failures occurred prior to that step--one device after test condition D, which failed due to an oxide flaw at bonding, and one device after test condition E, which failed due to a fractured die bond. These failures represent a typical device and are due to mechanisms normally activated by thermomechanical stresses.

One failure was observed in the thermal shock step stress sequence. The failure, detected after step 6 (-196° to 200°C), was caused by a cracked die.

Vendor 6 devices failed due to lifted post bonds at the condition F level temperature cycle (-65° to 500°C). The lifted bonds were caused by separation of the aluminum cladding from the post.

The two failures of Vendor 6 units in thermal shock were due to cracks forming in the seal area as a result of the stresses induced by the -196° to 200° thermal shock. The units were subjected to a red dye penetrant test (see Appendix I). One unit showed penetration of the dye into the cavity of the device. The other unit showed penetration of die around the fracture surface to an extent greater than 50% of the seal length.

All of the Vendor 7 failures were gross leakers. In all cases, the leakage occurred in the interface between the solder glass and the base of the package.

The electrical rejects were caused by lifted post bonds, caused by depletion of the aluminum cladding at the post. The thermal shock step stress induced no failures in the Vendor 7 units.

4.5.3 Dual-In-Line Ceramic Package Results

The results of the thermal cycling step stress matrix are shown in Figure 4-29.

The Glass Sealed Ceramic Packages (Cerdip) show a high susceptibility to thermal shock at the -65 to 200°C level. Thirty-two of the seventy three devices tested were damaged in the basket used for thermal shock or during end point measurements. Figure 4-30 shows the condition of the Vendor 9 units after completion of 10 cycles of test condition D. (The devices which remained intact were removed for hermeticity testing prior to taking the photograph.)

Temperature cycling did not affect the hermeticity of Cerdip packages until level 1010F was reached. Since most solder glasses are sealed at 475° to 500°C it is not surprising that the T_{HIGH} = 500°C of Level F degrades the seal.

The final seal of both the 14 pin metallized ceramic sidebraze package and the LSI package is made by brazing a metal cap to the package with a gold-tin eutectic which has a melting point of 325°C. Exposure of these devices to any temperature above 325°C will cause the braze to reflow, allowing the lid to shift on the package. Maintenance of hermeticity is a matter of piece parts orientation and chance. At any stress level of 1010E or above, the LSI package would tend to be the first to lose hermeticity, because of the larger, heavier lid.

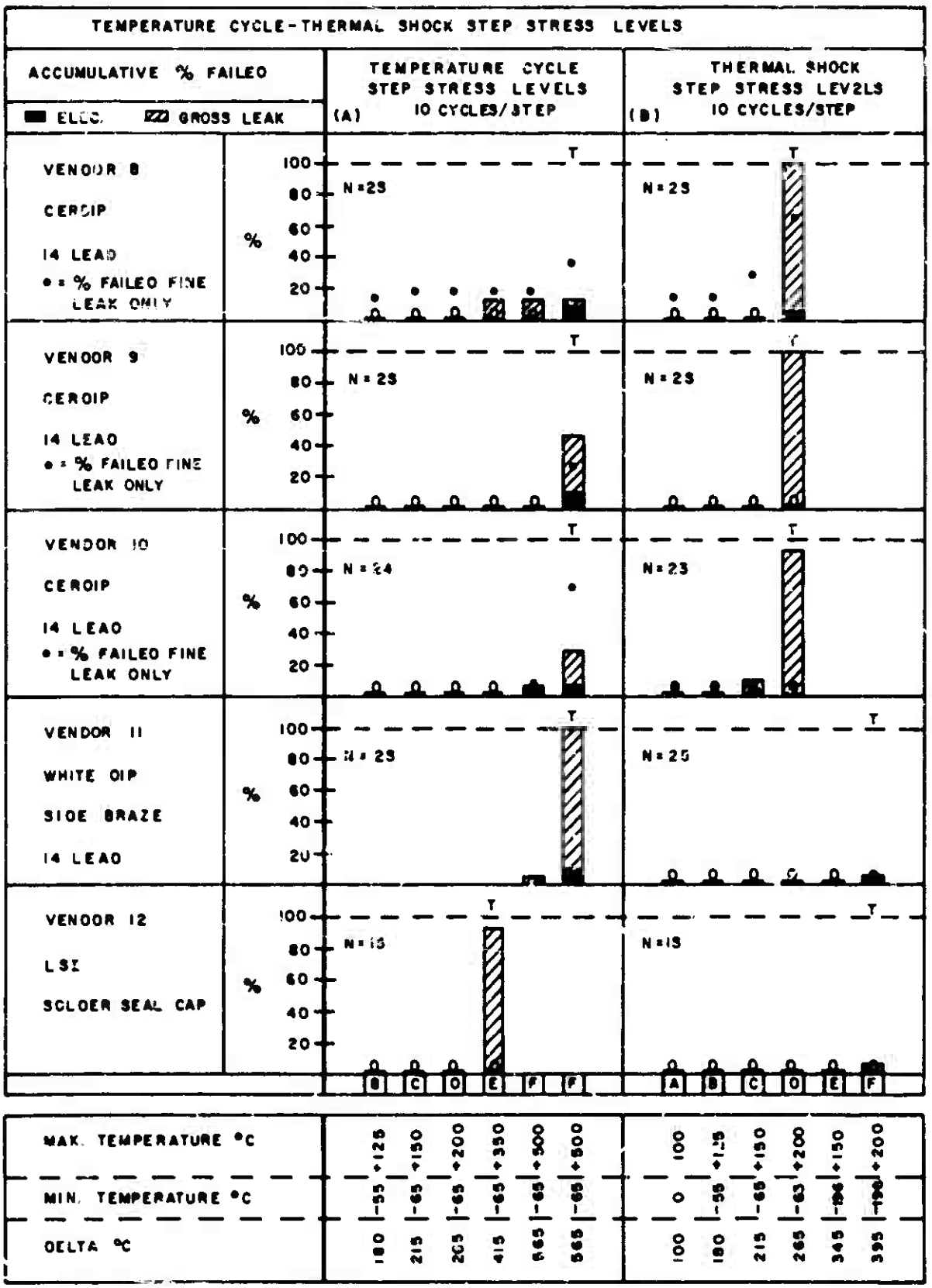
TEMPERATURE CYCLE-THERMAL SHOCK STEP STRESS LEVELS
ACCUMULATIVE % FAILED
ELEC.
GROSS LEAK
TEMPERATURE CYCLE STEP STRESS LEVELS (A) 10 CYCLES/STEP
THERMAL SHOCK STEP STRESS LEVELS (B) 10 CYCLES/STEP
VENDOR 8
CERDIP
14 LEAD
• = % FAILED FINE LEAK ONLY
VENDOR 9
CERDIP
14 LEAD
• = % FAILED FINE LEAK ONLY
VENDOR 10
CERDIP
14 LEAD
• = % FAILED FINE LEAK ONLY
VENDOR 11
WHITE DIP
SIDE BRAZE
14 LEAD
VENDOR 12
LSI
SOLDER SEAL CAP
%
100
80
60
40
20
N=25
N=24
N=23
N=15
T
A
B
C
D
E
F
MAX. TEMPERATURE °C
MIN. TEMPERATURE °C
DELTA °C
+125
+150
+200
+350
+500
-55
-65
180
215
265
415
565
100
0
-55
-65
-85
-150
-200
100
180
215
265
345
365

Figure 4-29.

Figure 4-30. Vendor 9 Devices After 10 Cycles Thermal Shock Method 1010D (-65°C to 200°C)

Electrical failures of Vendor 8 and 10 devices were predominantly heel breaks at the post. One Vendor 8 unit failed in temperature cycling due to an oxide flow.

The Vendor 11 electrical failures were caused by loss of hermeticity and contamination of the aluminum wire. Aluminum hydroxide was detected on the failed wires. Excessive intermetallic formation was also noted.

4.5.4 Summary of Results

Considering ceramic flat packages and Cerdips this step stress matrix shows that thermal shock weakens or degrades seals. Temperature cycling has more effect on wires and bonds and some die related failures provided the maximum temperatures are limited to the capabilities of the packaging system. The failure mechanisms detected in this matrix will be described in Section V.

4.6 MULTIPLE THERMAL CYCLE STRESS MATRIX

This matrix (matrix 2 of Table 2) consists of subjecting samples from each vendor (except 14) to different levels of thermal cycling (Temperature Cycle and Thermal Shock) and extending the number of cycles until 50% of the sample had failed or a minimum of 1000 cycles had been achieved. The stress levels chosen were per MIL-STD-883 Methods 1010 and 1011 except for the number of cycles. The stress levels at which each package type was tested are shown in Table IV-13.

TABLE IV-13

		Test Lot	Dual-in-Line Plastic	Dual-in-Line Ceramic	Flat Packages	LSI Pkg.
Method	B	C	X			
1010	C	D	X	X	X	X
Level	D	E		X	X	X
	E	F		X	X	
Method	A	G	X	X		X
1011	C	H	X	X	X	X
Level	D	I			X	

End Point	1	2	3	4	5	6	7	8
Thermal Shock	0	15	30	60	105	300	510	1005
Temp. Cycle	0	10	30	60	100	300	510	1000

Multiple Thermal Cycle Matrix

The schedule of endpoint tests, as specified in 4.1.2, through the first 1,000 thermal cycles were as shown in Table IV-13. After the first 1,000 cycles endpoint tests were performed every 500 cycles. As shown in Table I-2, 15 samples of Vendor 14 devices were included in Lot D (Temperature Cycle, Method 1010 Level C) and 11 Vendor 14 devices were included in Lot H (Thermal Shock, Method 1011 Level C). The flow of samples through these tests is shown in Figure 4-31.

4.6.1 Data Presentation

The data from this test matrix was first analyzed to determine the distribution of failures with respect to total cycles. Several distribution plots were attempted, including Normal, Log Normal, Weibull, and Hazard plots. The data seemed

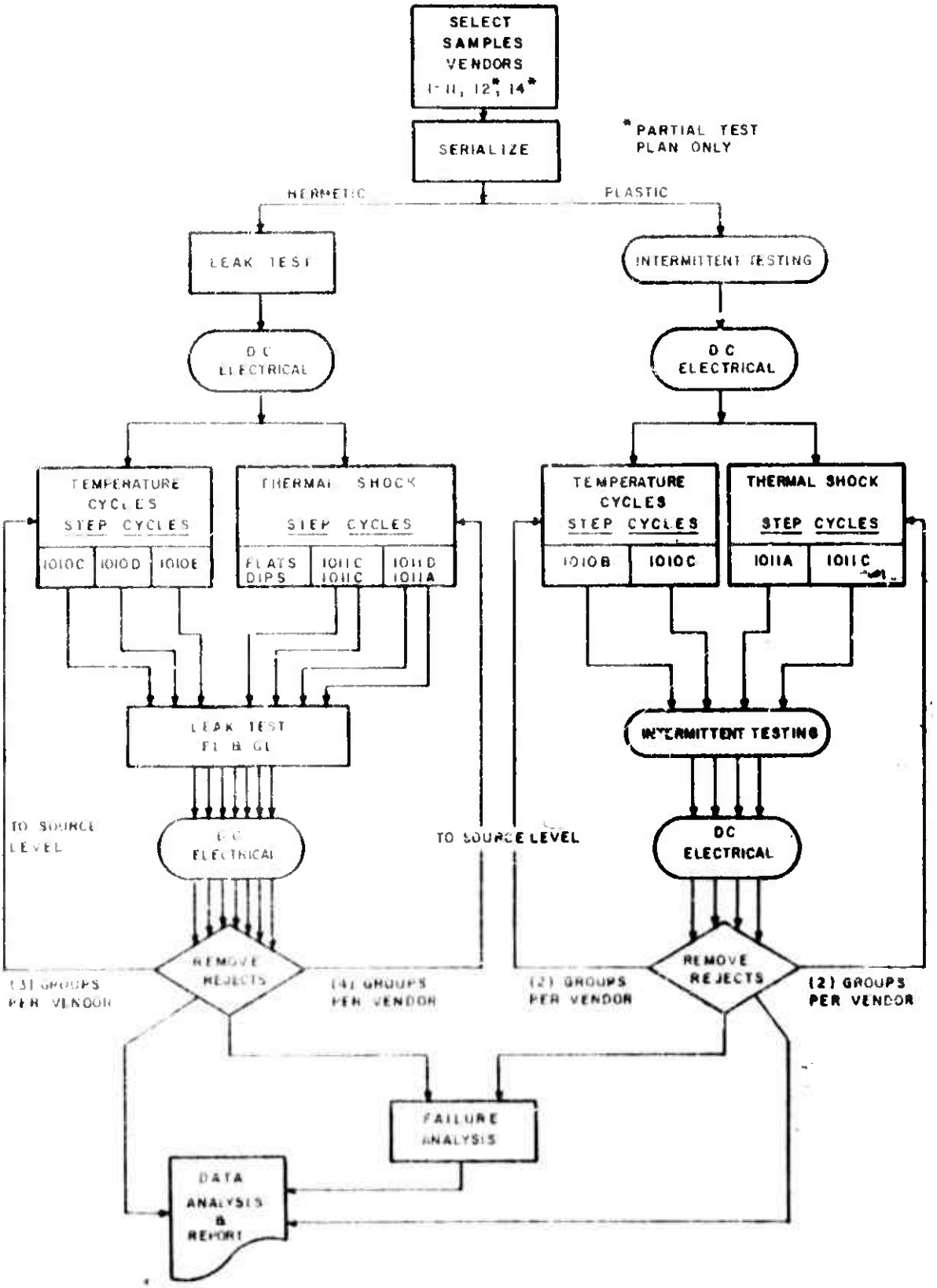

Figure 4-31. Multiple Thermal Cycle Matrix Test Plan

to fit a linear plot of accumulative percent failure versus number of cycles. This method of presentation was chosen. All curves are labeled with an alpha-numeric designator which indicates stress level and vendor. Thus, Curve C-2 represents Lot C. (Temperature Cycle per Method 1010, Level B, -55°C to 125°C), Vendor 2. This nomenclature, derived from Table I-2, is carried throughout this and subsequent sections.

4.6.2 Plastic Results

All electrical failures of the plastic encapsulated integrated circuits were due to open wires or bonds. Thus, the DC failures at 25°C also failed the monitored temperature cycle (intermittence) test.

All intermittent failures were left in the test program until the testing on the particular cell was completed or until they became 25°C DC electrical failures. Almost all intermittent failures, except those which failed the last readout, became electrical opens at 25°C after additional temperature cycling. The data indicates that wires and bonds fail first during the high temperature portion of the cycle. Repeated cycling tends to cause sufficient separation of the wire end(s) at the break, such that the device shows an electrical open type of failure at 25°C. This phenomena occurred at all levels of thermal cycling. All intermittent failures failed over the high temperature portion of the monitored cycle. Few temperature windows, opens occurring only over a temperature range of a few degrees Celcius, were observed and in all cases these devices were open circuited at 150°C.

Where a significant difference exists between the accumulation of total failures and 25°C DC parameter failures, both are plotted.

4.6.2.1 Temperature Cycling Results

Figures 4-32 and 4-33 show the results of Temperature Cycling, Method 1010, Level B (-55°C to 125°C) and Level C (-65°C to 150°C). These curves present the total electrical failures and DC electrical failures at 25°C as a function of temperature cycles completed. Comparison of Figure 4-32 and 4-33 shows acceleration of failures at the higher stress level (Level C). In both cells all the 25°C DC failures, through the first 30 cycles, were caused by lifted bonds. The remainder of the failures were caused by fracture along the boundary of relatively large metallurgical grains formed in the gold wire (intergranular or grain boundary fracture). These failure mechanisms are discussed in Section V, Failure Analysis.

4.6.2.2 Thermal Shock Results

The results of repeated thermal shock cycling per Method 1011 Level A and Level C are shown in Figures 4-34 and 4-35. A comparison of these Figures shows that as the stress level increased from Test Condition A to Test Condition C, the failures were apparently accelerated in Vendor 2 and Vendor 3 devices at the higher stress level. Vendor 4 devices, however, showed greater susceptibility to Test Condition A Thermal Shock than to Test Condition C. The reasons for this are related to the historic susceptibility of the phenolic package to moisture (water is used

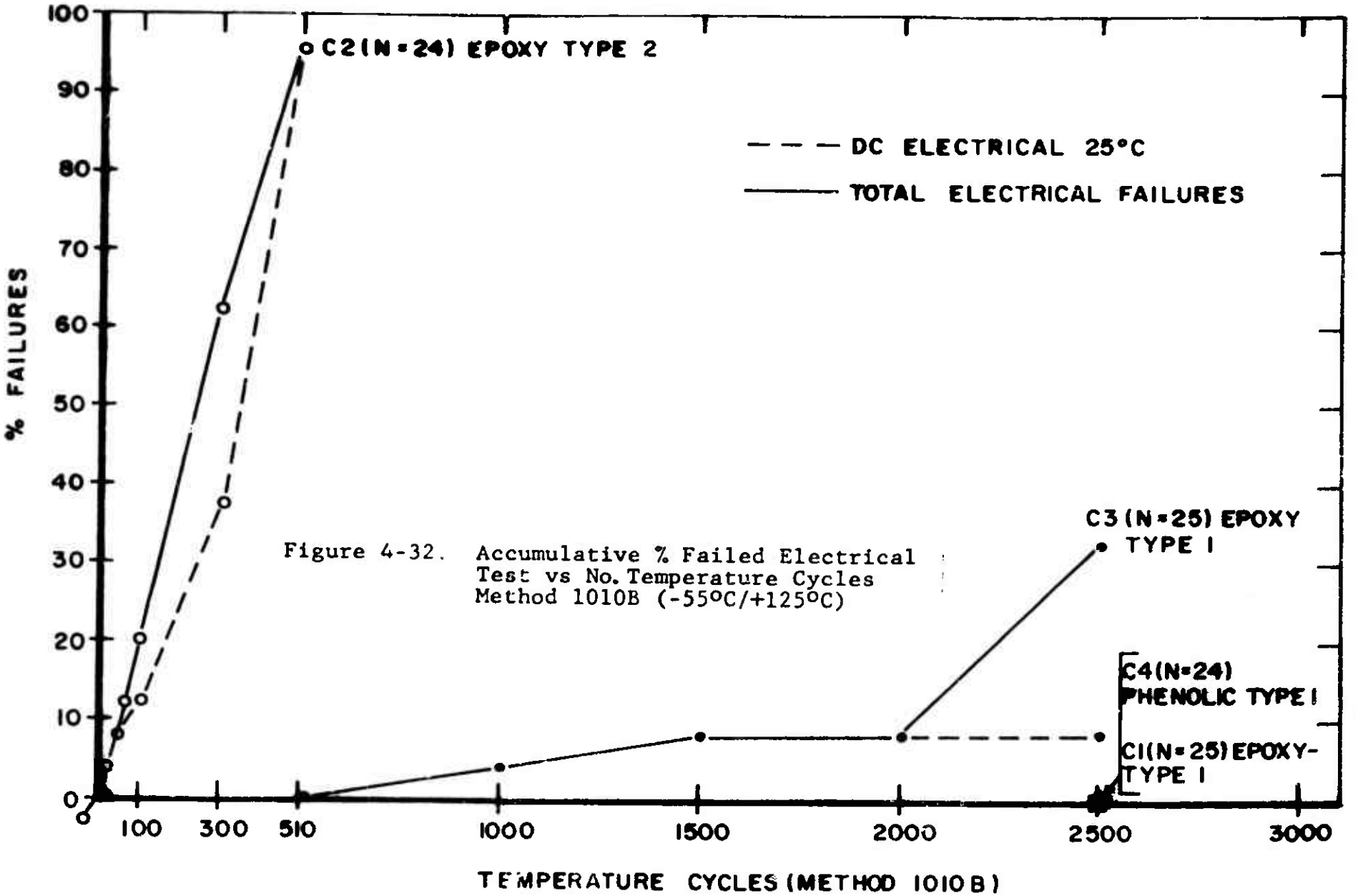

Figure 4-32. Accumulative % Failed Electrical Test vs No. Temperature Cycles Method 1010B (-55°C/+125°C)

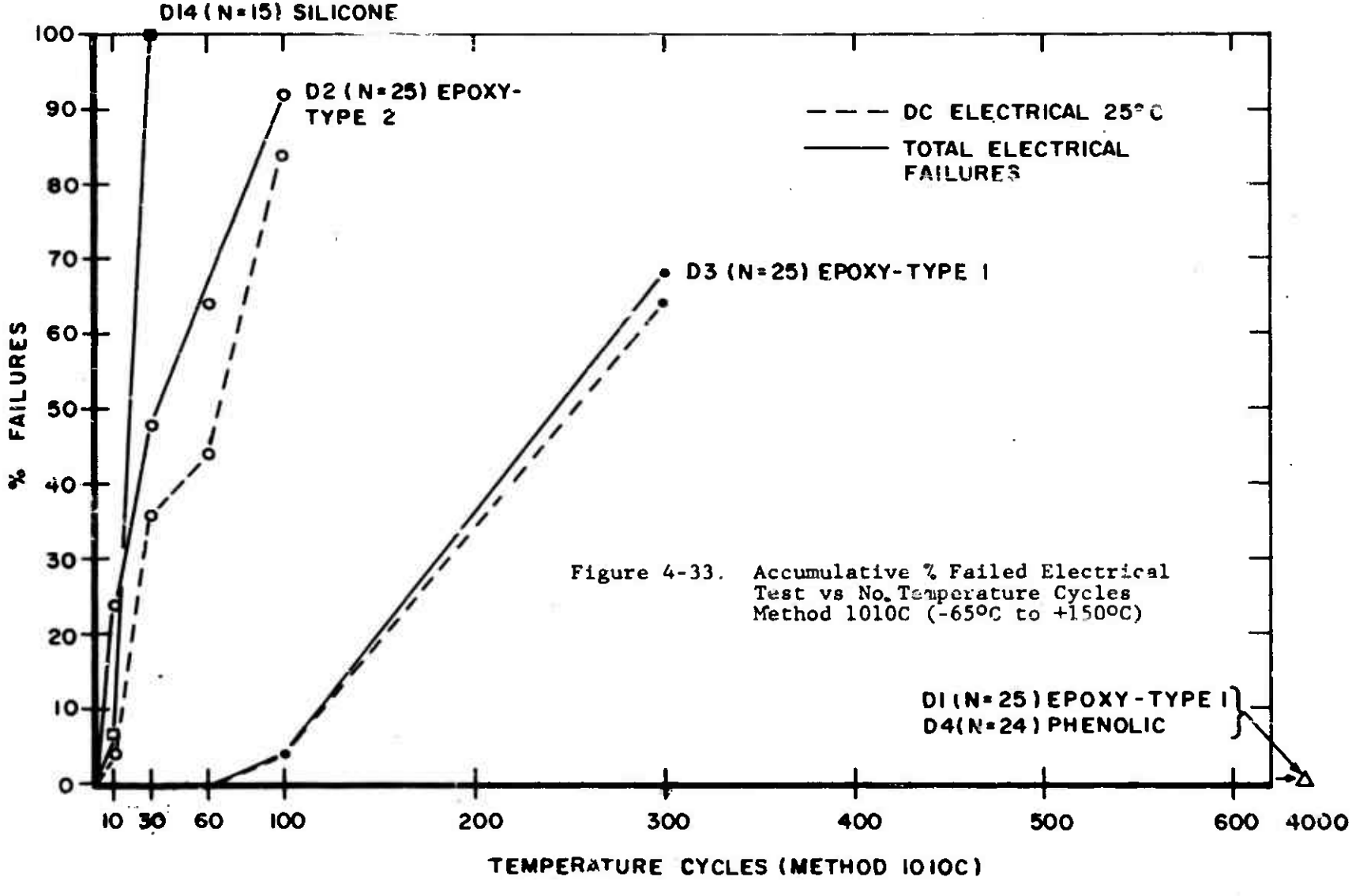

Figure 4-33. Accumulative % Failed Electrical Test vs No. Temperature Cycles Method 1010C (-65°C to +150°C)

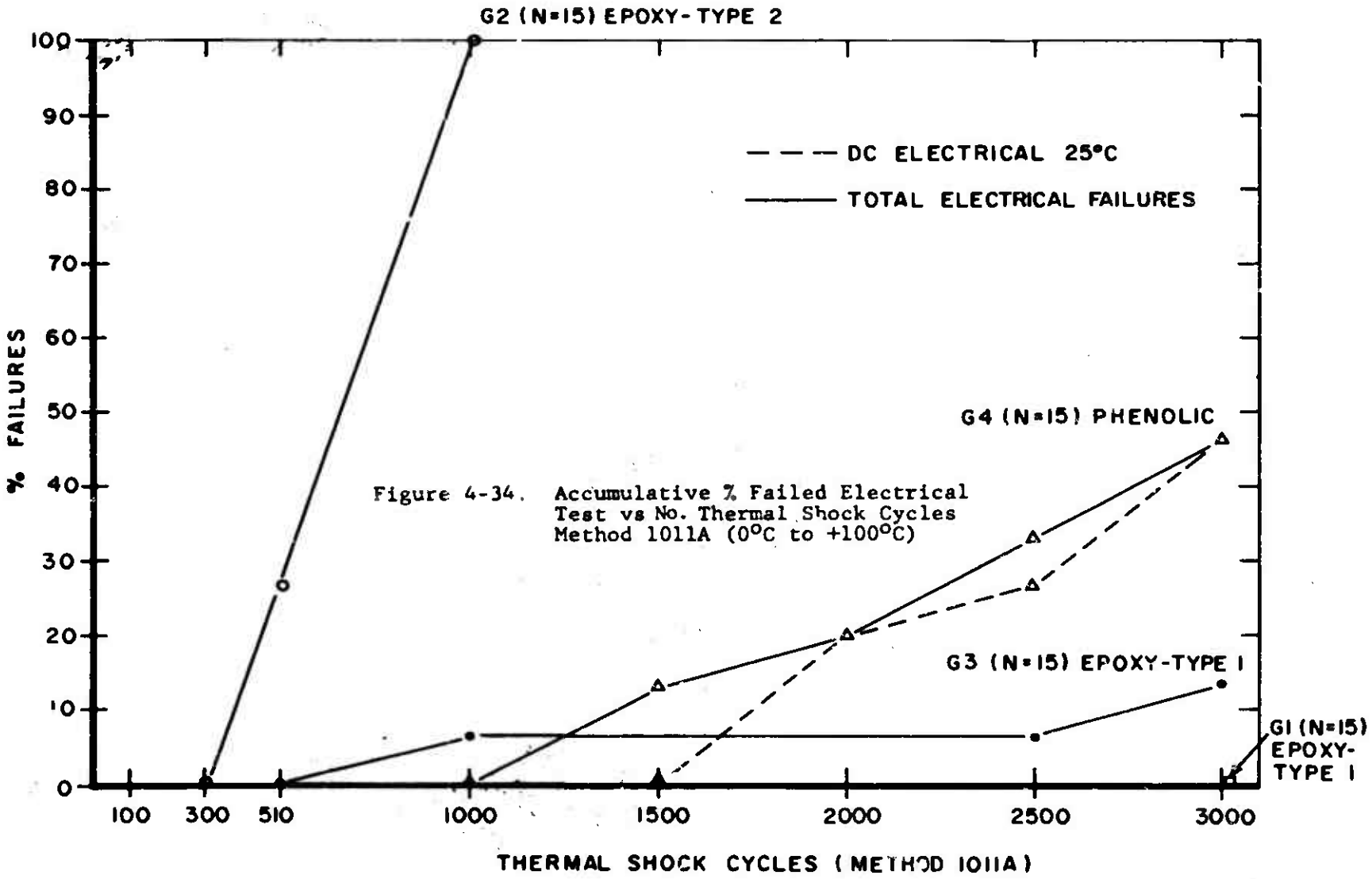

Figure 4-34. Accumulative % Failed Electrical Test vs No. Thermal Shock Cycles Method 1011A (0°C to +100°C)

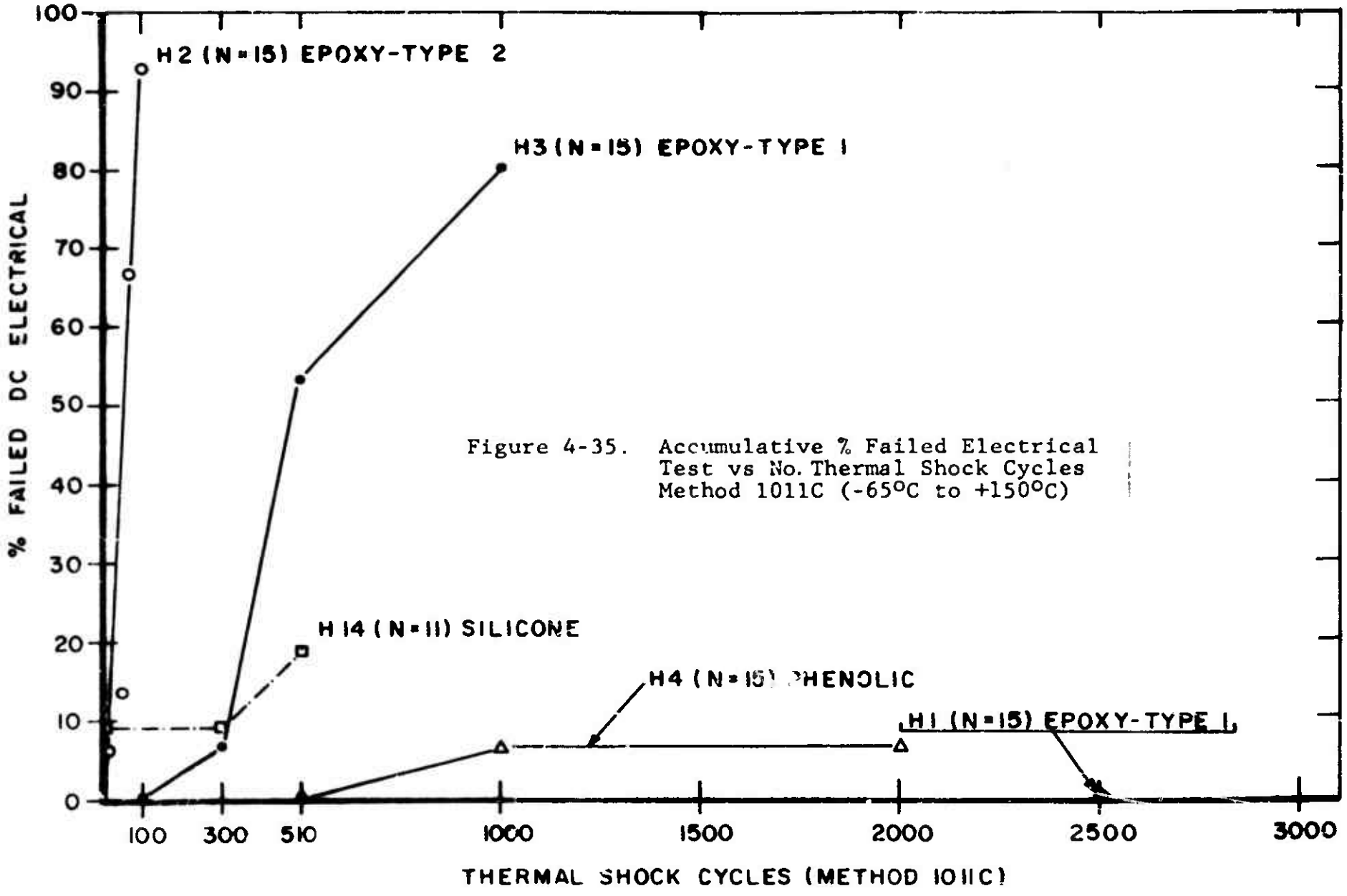

Figure 4-35. Accumulative % Failed Electrical Test vs No. Thermal Shock Cycles Method 1011C (-65°C to +150°C)

for both baths of Test Condition A). All the Vendor 4 failures in Test Condition A showed evidence of electrochemical corrosion of the aluminum pad. Metallization of the die showed that moisture had penetrated the package. By 1500 cycles, this corrosion had progressed sufficiently to weaken the bonds at the die to the extent that failures occurred due to lifted bonds.

Since the thermal shock fluids used for Test Level A were ice water and boiling water, some water penetration occurred as evidenced by the presence of electrochemical corrosion at the pads of the failed devices.

The baths used to perform thermal shock at Level C were Methonal and dry ice for the -65°C bath and "UCON Oil", a polyalkylene glycol, for the 150°C bath. Both the high viscosity and the surface tension (with respect to water) of the UCON Oil inhibits penetration along the lead encapsulated interface. Thus, the transport of moisture and other contaminants to the die surface is much slower than is the case where water is used as the thermal fluid.

All the failures in Lot G (Test Condition A, Method 1011) except one (Vendor 3 at 3,000 cycles) were caused by lifted bonds at the die. Electrochemical corrosion was noted in all lifted bond failures. (See Section V.)

The response to Level C Thermal Shock was similar to the response to Level C Temperature Cycle. All DC failures detected through the first 30 cycles were due to lifted bonds. The rest, with one exception, were due to intergranular fracture in the gold wire near the ball bond at the die. The lone exception was the

failure of the Vendor 4 device at 1,000 cycles. This unit failed due to a lifted bond at the die. No corrosion of the pad metal was evident. Since there were no further failures of Vendor 4 devices at this level through 2,000 cycles, this device was most likely a sport, or abnormal device.

Because of the presence of electrochemical corrosion at the pads of all failures in Level A Thermal Shock, the difference between the response to Level A and Level C does not represent a true acceleration due to thermomechanical stresses.

The original test plan called for a minimum of 1,000 thermal cycles at each thermal cycle or 50% failure of the test sample. Because of the loss of four Vendor 14 devices, (MOS Memory) due to test and handling damage, test cell H14 was truncated at 510 cycles.

4.6.2.3 Discussion of Thermal Shock and Temperature Cycling Results

The overall response of the samples from the 5 vendors confirm that which was predicted from the thermomechanical expansion data and the step stress results of Section 4.5. The Type 2 epoxy of Vendor 1 and the silicone of Vendor 14 tend to fail fastest under all conditions of thermal cycling, while Vendors 2 and 4 are relatively unaffected by thermal cycling except for the corrosion mechanisms found in the phenolic package (Vendor 4) as a result of Thermal Shock per Method 1011 Test Condition A. Vendor 3 devices fail all groups faster than would be predicted from the temperature coefficient of expansion data. The failures were due to fracture along the boundaries of rather large grains formed in the wire near the ball bond at the die. The difference in response between Vendor 1 and Vendor 3 is attributed to the difference in wire size and bonding method. This phenomenon is discussed in Section 5.

The DC failures of Vendors 2, 3 and 14 in Level C of both thermal shock and temperature cycling are shown in Figure 4-36. Both these tests have the same temperature extremes, -65°C to 150°C, differing only in the time at tempereture and rate of change of temperature of the device. From the curves of Figure 4-36 it can be seen that temperature cycling has a greater effect than does thermal shock for Vendors 14 and 3. This would indicate that the time at temperature is more critical than is the rate of change of temperature.

There is little difference, however, in the response of Vendor 2 devices to temperature cycling and thermal shock at level C. This may be a result of the high temperature portion of the cycle; 150°C is much greater than the glass transition temperature and the net thermal expansion coefficient at 150°C is high, creating sufficient stress in the wire to mask the effects of time at temperature. The mechanics of the system and the electrical test data indicate that the failures in the wires and bond occur during the high temperature portion of the cycle.

4.6.3 Dual-In-Line Ceramic Results

As has been shown by the thermomechanical stress analysis presented in Section 4.3, the thermally induced stress in the ceramic dual-in-line package may reach critical levels with respect to the ultimate strength of the sealing glass. The temperature gradients present during the thermal shock cycle enhance these stresses.

If thermal shock or temperature cycling tests are to be used for screening stresses, it is critical to learn the effects

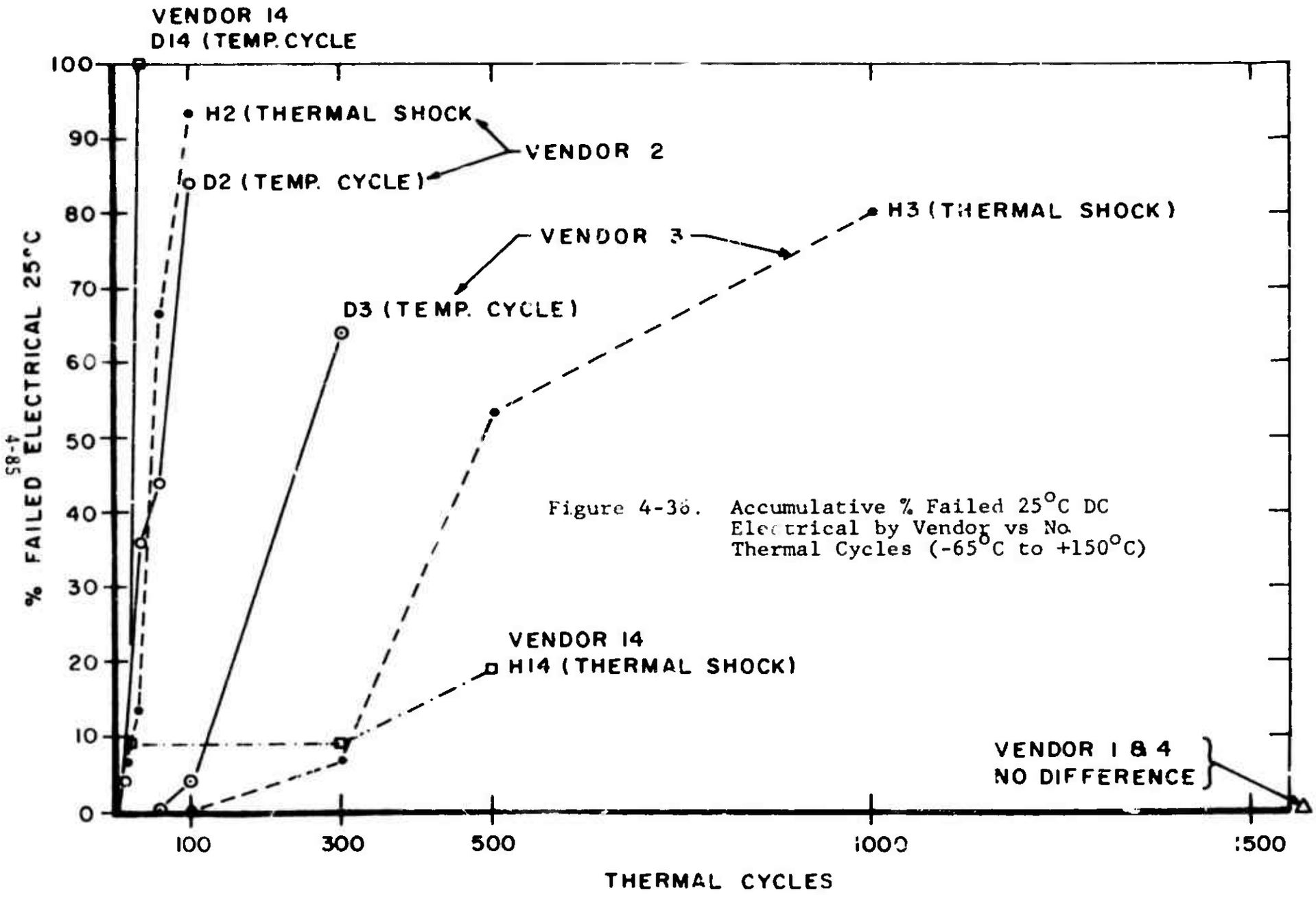

Figure 4-36. Accumulative % Failed 25°C DC Electrical by Vendor vs No. Thermal Cycles (-65°C to +150°C)

such tests will have on the integrity of the package seal, as well as on those mechanisms which directly affect the electrical performance of the device. We have chosen, therefore, to study the effects on the package seal separately from the electrical failures.

4.6.3.1 Seal Test Results

The pattern of seal failure, noted in all cells, was first failure to pass the fine leak criteria of 5×10^{8} atm-cc per sec., helium. These indicated fine leak failures were subjected to future thermal cycling until they became gross leakers or electrical failures. A tendency was shown for these helium leak test readings on these devices to increase to the range of 10^{-6} atm-cc/sec. In many cases these devices would then pass the helium leak test and gross leak tests on a subsequent end point, only to fail gross leak tests on the following end point. This response was most prevalent in the thermal shock cells.

All gross leak failures were subjected to destructive penetrant dye tests for confirmation of leak. All electrical rejects were subjected to the pressure and bake cycles prior to submission to failure analysis. The development of the dye was performed as part of the failures analysis procedure (see Section V). All of the indicated helium rejects were verified at the end of the test. Evidence of dye penetrating to greater than 50% of the distance from the outside lead surface to the edge of the package cavity was classified as confirmed leaks. The results of this analysis indicated that the seal degradation starts at the surface of the seal, evidenced as small cracks around the leads. The cracks tend to propagate to the cavity with repeated thermal

cycling. This phenomenon was more prevalent in thermal shock. Most unconfirmed rejects were due to trapping of helium gas at the surface of the sealing glass.

Figures 4-37, 4-38, 4-39, and 4-40 show the gross leak failures of Vendors 8, 9, 10, and 11 dual-in-line ceramic packages as a function of thermal cycles. Total indicated seal test failures are plotted for Lots H-9 (-65°C to 150°C thermal shock, Vendor 9) and G-10 (0°C to 100°C thermal shock, Vendor 10).

These curves show that the accumulation of seal failures in Vendors 8, 9, and 10 packages are much more rapid in thermal shock than in temperature cycling. Seal degradation at level C of thermal shock was so great that some of the packages of Vendors 8, 9, and 10 fell apart, being unable to withstand the forces of insertion and withdrawal in the test sockets.

Vendors 8 and 10, both using Type 1 glass, were highly susceptable to level A thermal shock, while Vendor 9 (Type 2 glass) was unaffected at this test level.

With the exception of Vendor 8, whose units indicated a typical response for that manufacturer in all hermeticity tests, temperature cycling at levels C and D had little effect on the package seal for any of the dual-in-line packages. Because of the extreme high temperature, 350°C, level E, catastrophic effects occurred in the sidebraze package because of reflow of the cap brazing material during the 350°C portion of the level E cycle. This caused 100% seal failure within 30 cycles. The material, a gold-tin eutectic melts at 325°C. The extreme high temperature limit of level E also affects the hermeticity of the glass sealed ceramic packages (Vendors 8, 9, and 10). It will be shown in the next section that these affects are overshadowed by the affects on the die bond.

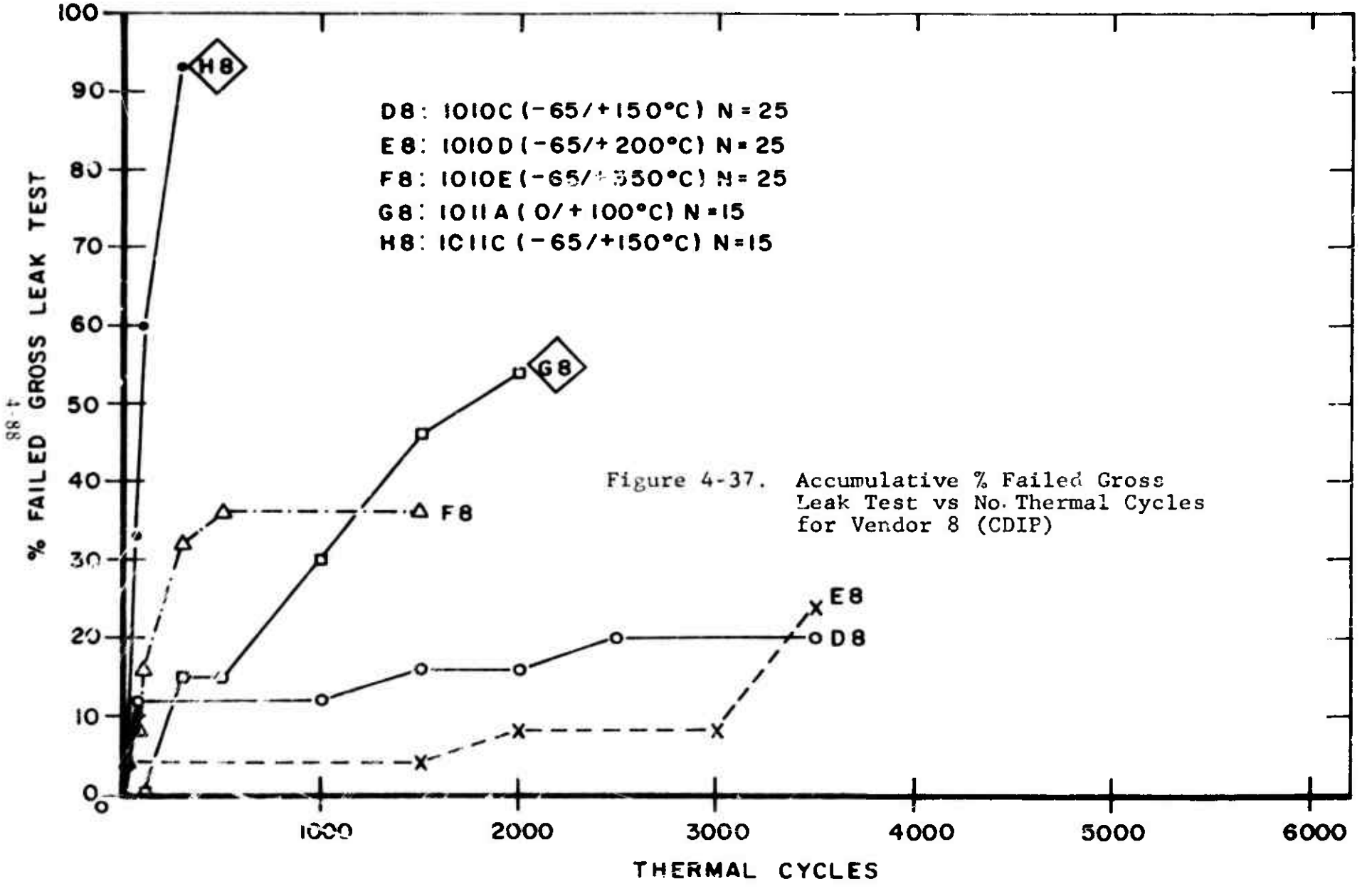

Figure 4-37. Accumulative % Failed Gross Leak Test vs No. Thermal Cycles for Vendor 8 (CDIP)

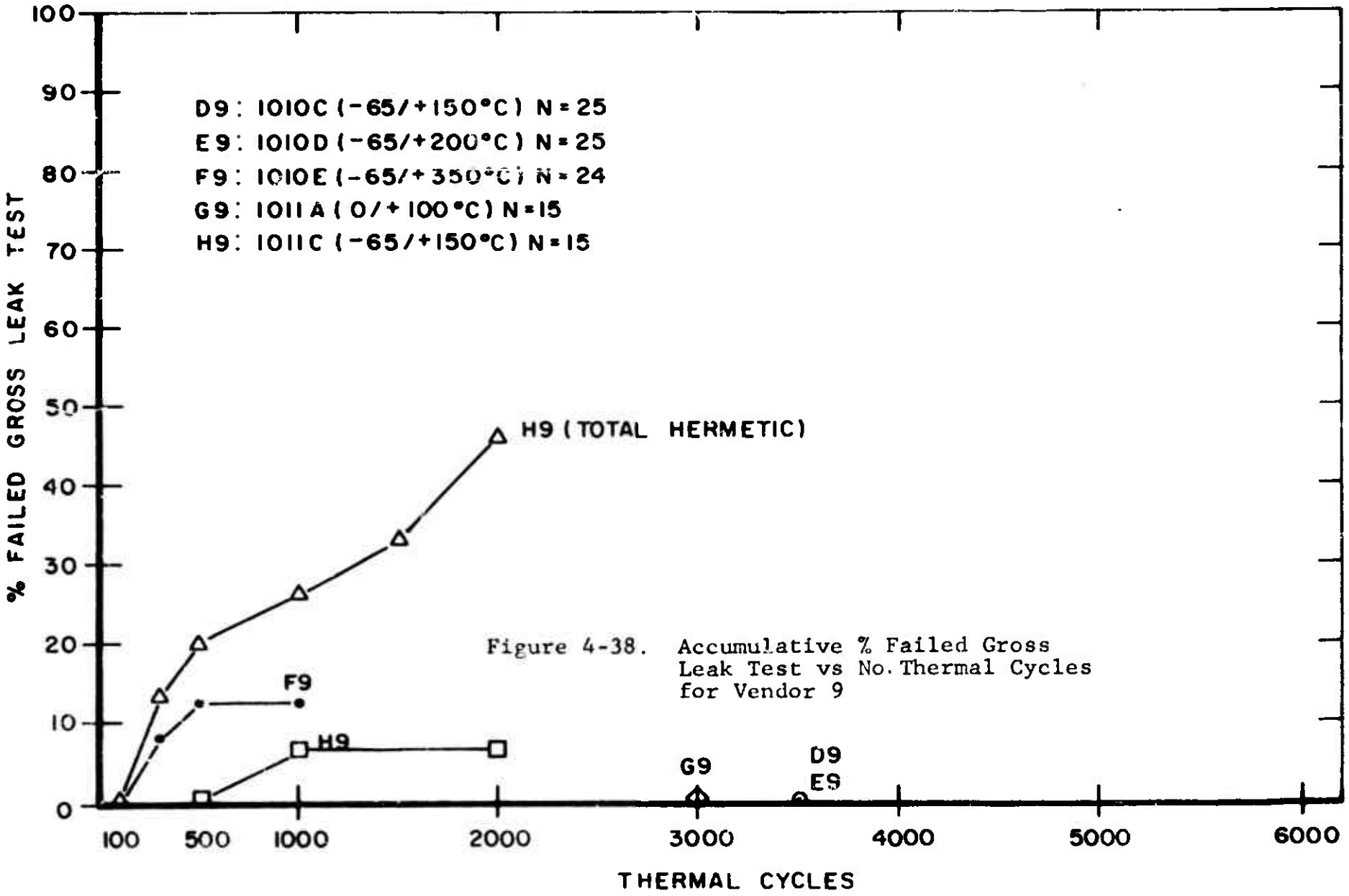

Figure 4-38. Accumulative % Failed Gross Leak Test vs No. Thermal Cycles for Vendor 9

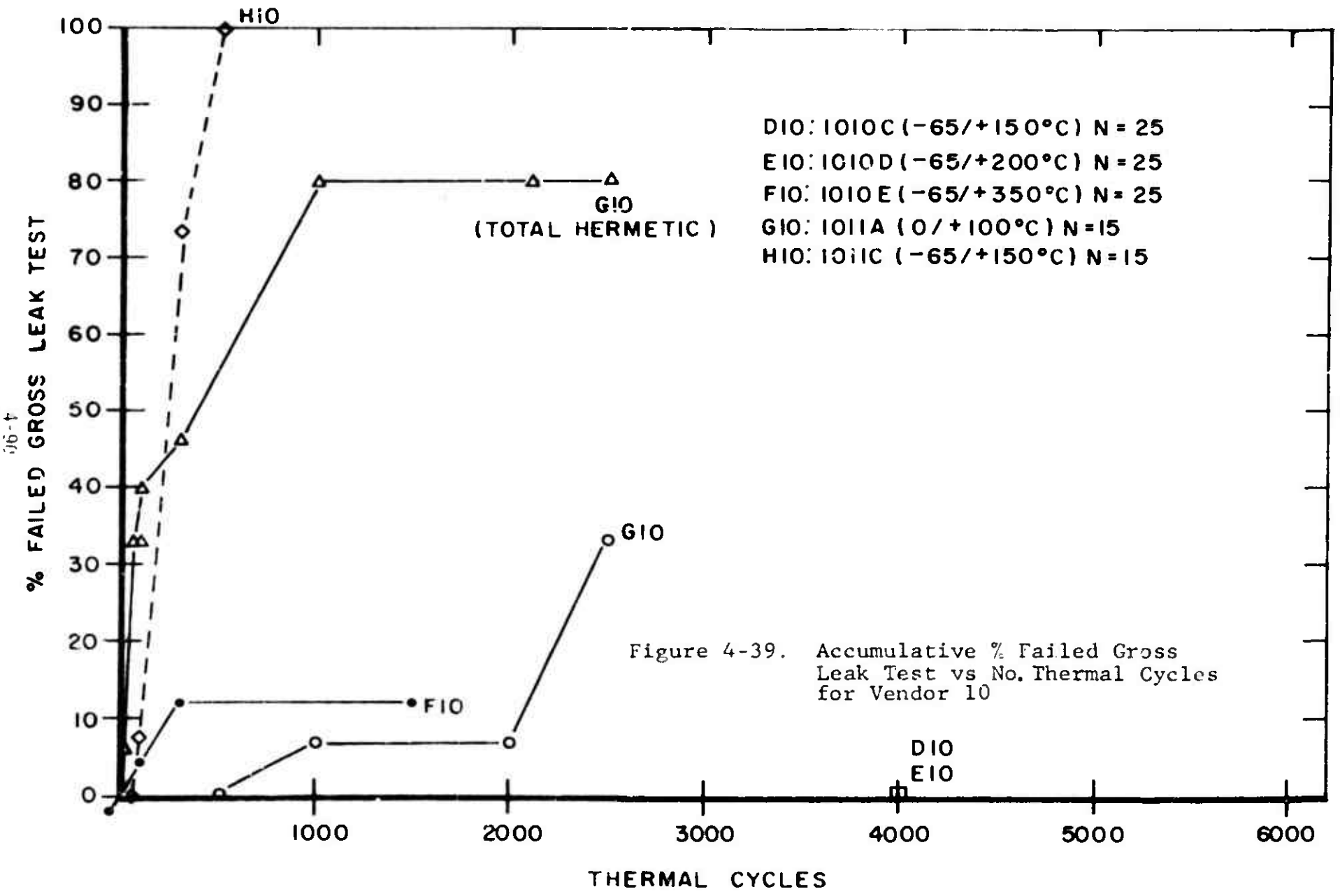

Figure 4-39. Accumulative % Failed Gross Leak Test vs No. Thermal Cycles for Vendor 10

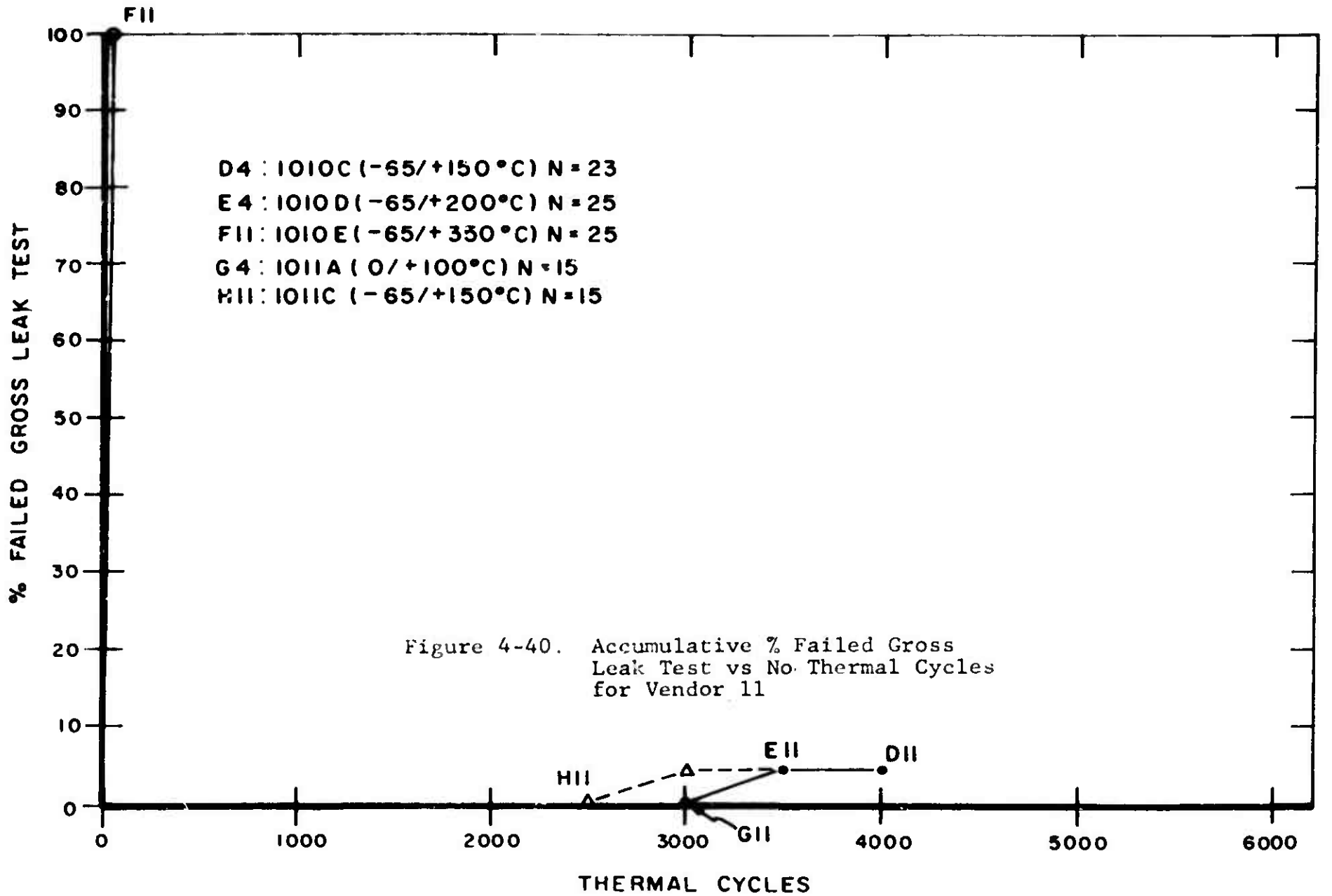

Figure 4-40. Accumulative % Failed Gross Leak Test vs No. Thermal Cycles for Vendor 11

The LSI package had no gross leak failures in this matrix; however, 19 units failed the fine leak test due to trapping in the metal ceramic interface at the surface of the seal area. Three units from Log H-12 (thermal shock, level C) were confirmed to be fine leak failures at 1000 cycles by using penetrant die techniques. The units were found to be leaking at the metal ceramic interface at the corner of the cavity. Trapping of helium around the lead and at the surface of the metal plate ceramic seal was a characteristic mode for this package for all thermal cycle cells, though very few of the packages were verified leakers.

4.6.3.2 Electrical Test Results

The electrical end point test results for Vendors 8, 9, 10, 11, and 12 are shown in Figures 4-41, 4-42, 4-43, 4-44, and 4-45 respectively.

The general response pattern of dual-in-line ceramic packages to the temperature cycling tests (Codes D, E, and F for each vendor) is characterized by an offset, or a number of cycles completed with zero failures, and then a nearly linear increase of failures with increasing cycles.

As noted in the preceding section, Vendor 11 suffered total loss of hermeticity within the first 30 cycles at test condition F (-65°C to 350°C) temperature cycling, causing truncation of the test on that device at that point. The dominant cause of failure of the other samples (Vendors 8, 9, and 10) tested at this level was degradation of the die bonds, resulting in loose die in the package.

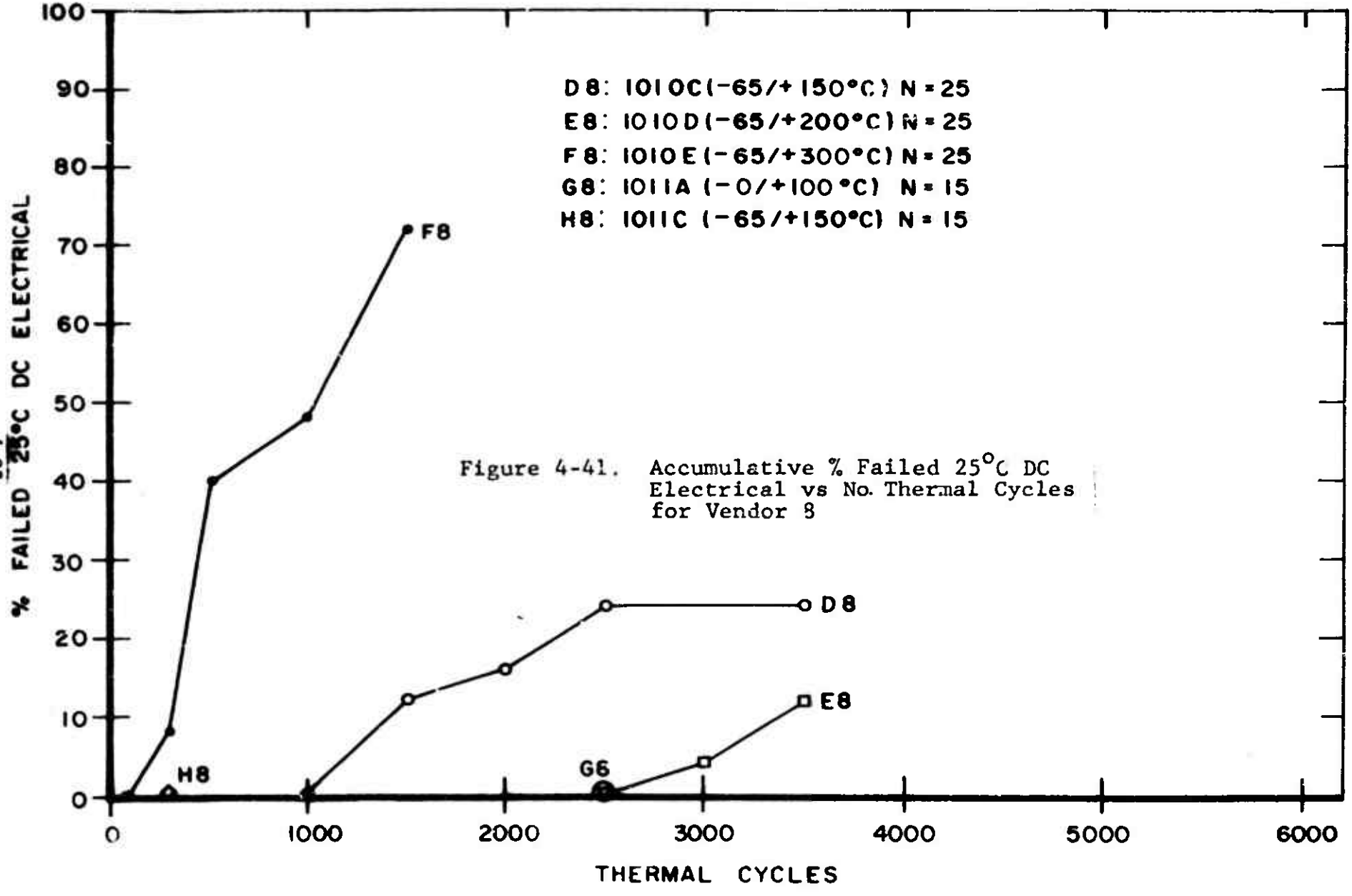

Figure 4-41. Accumulative % Failed 25°C DC Electrical vs No. Thermal Cycles for Vendor 8

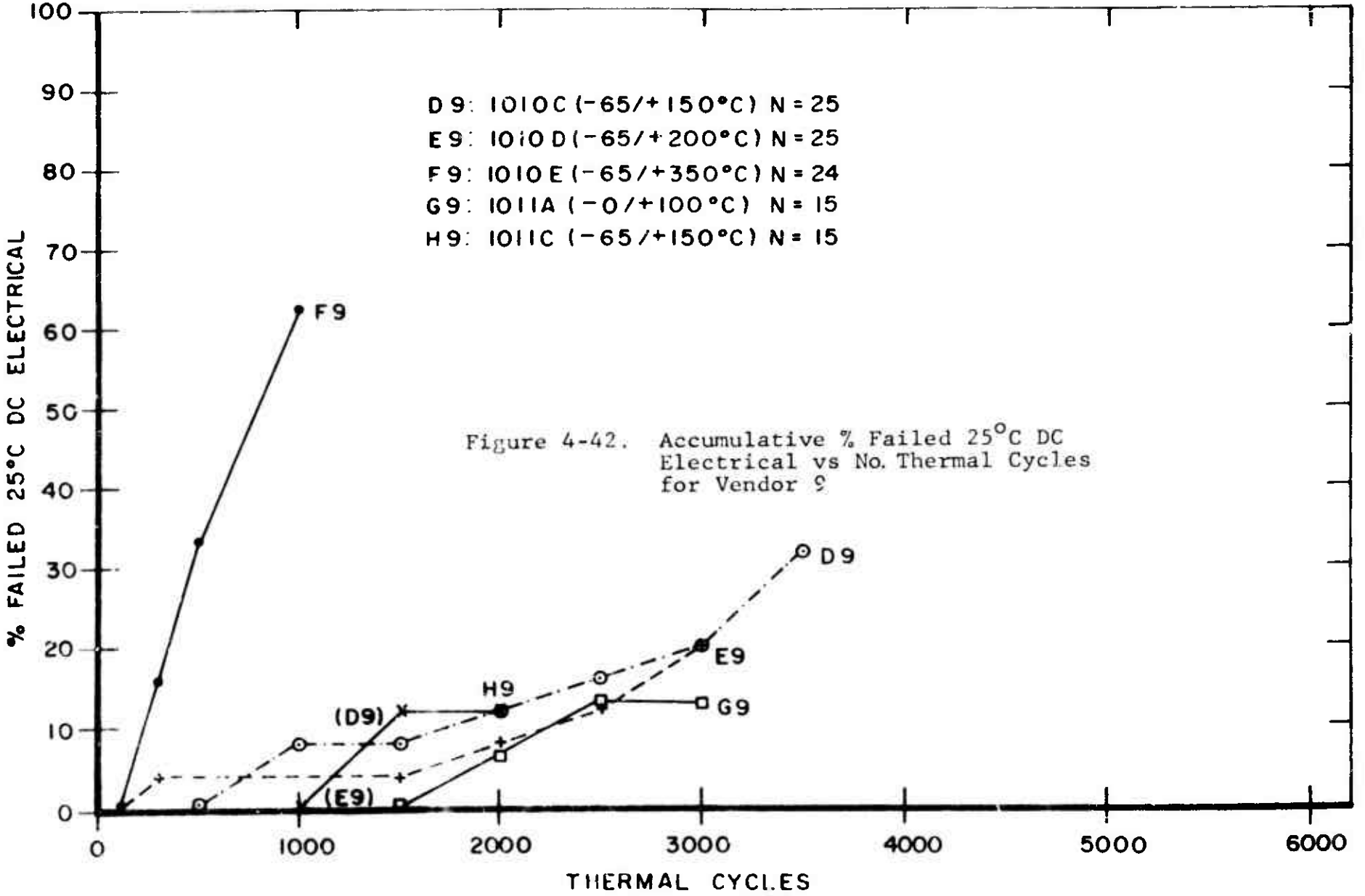

Figure 4-42. Accumulative % Failed 25°C DC Electrical vs No. Thermal Cycles for Vendor 9

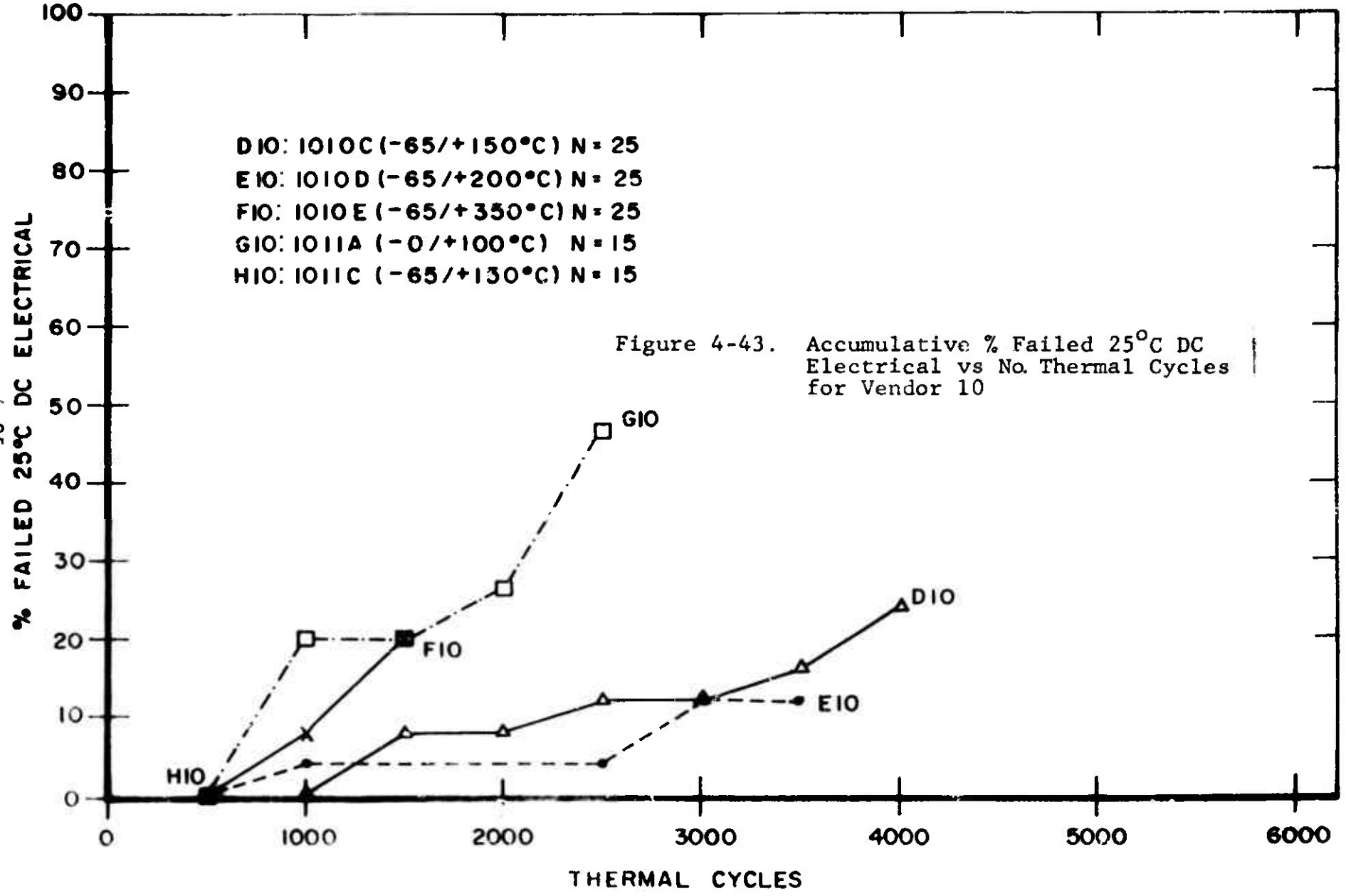

Figure 4-43. Accumulative % Failed 25°C DC Electrical vs No. Thermal Cycles for Vendor 10

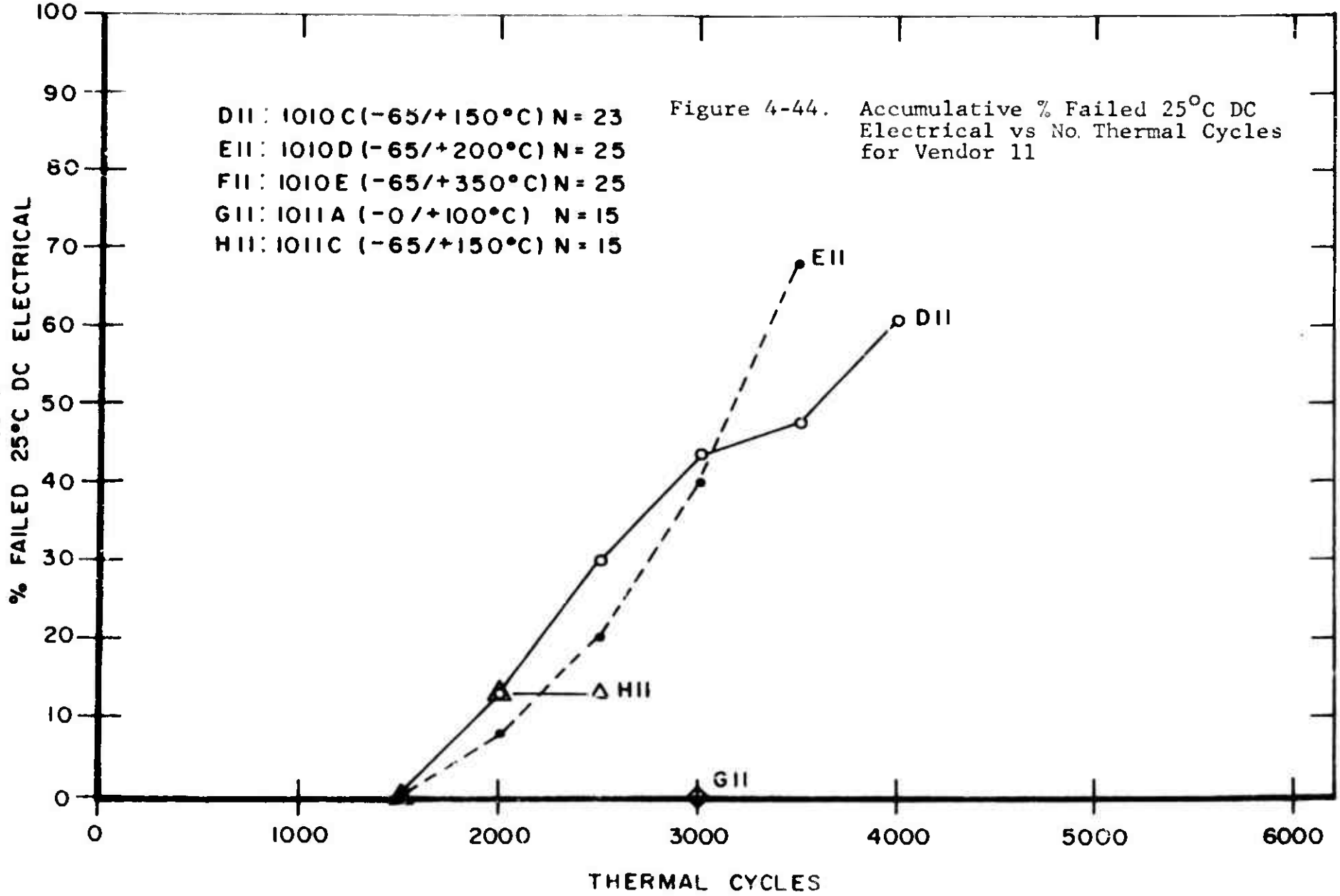

Figure 4-44. Accumulative % Failed 25°C DC Electrical vs No. Thermal Cycles for Vendor 11

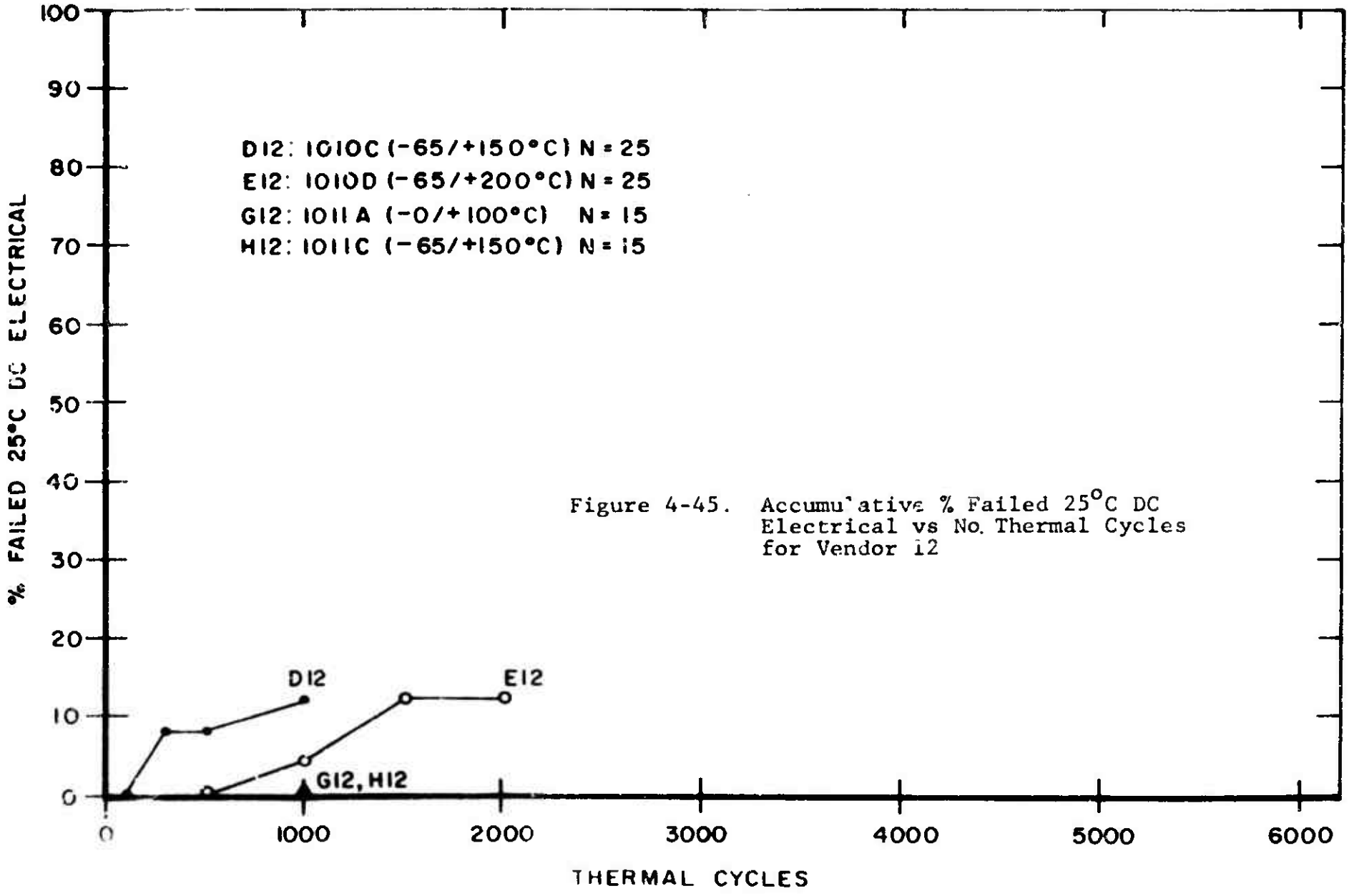

Figure 4-45. Accumulative % Failed 25°C DC Electrical vs No. Thermal Cycles for Vendor 12

The dominant cause of electrical failure for all devices at levels C and D of temperature cycle and level A and C of thermal shock was broken wires at the heel of the first bond, caused by mechanical fatigue. In the case of Vendor 8 this mechanism was accelerated at test Condition A, thermal shock, by chemical attack of the aluminum wire. This chemical reaction is a result of the loss of hermeticity which allowed contaminated moisture to enter the package and react with the aluminum.

On all other packages the longer wires tended to fail first, with Vendor 12 LSI devices having the longest span and failing first, followed by the sidebraze and then the ceramic glass packages. Vendor 9 wire bonds had a higher degree of deformation at the heel of the first bond which makes them more susceptable to early failure in thermal mechanical testing. These mechanisms and the physical geometries which effect them will be discussed in Section V.

4.6.3.3 Discussion of Results

There is an apparent anomaly in the response of Vendors 8, 9, and 10 devices to temperature cycling at levels C and D. One would expect that level D would cause more failures with fewer cycles than level C. Considering the temperature range of the two test levels, -65°C to 200°C for D and -65°C to 150°C for level C, only Vendor 11 (Figure 4-44) shows the expected response and even here the accumulated percent failure of level D (Curve E11) lags level C (Curve D11) until approximately 3000 cycles.

Referring to Figure 4-37 we see that the number of gross leak test failures at Condition C, (Curve D8), temperature cycle, is higher than at Condition D, (Curve E8), temperature cycle, through 3000 cycles. From the thermomechanical stress analysis, the critical stress in the seal of the devices occurs at -65°C (the low temperature for both test levels). Therefore, the close tracking of Lots E-8 and D-8 are not surprising and the sample error may well explain any difference in seal test results.

Electrical test results are not so easily disposed. The difference between levels C and D of temperature cycling are consistent across all vendors except Vendor 11. As will be seen later, this phenomena is also observed in the response of Vendor 6 flat package to these temperature cycling levels.

Considering only fatigue type bond failures, the temperature cycling test data and failure analysis results indicate that the metallurgical system showing the greatest decelleration with increasing temperature cycling level from C to D is the aluminum bonding system. Further, the minimum recrystallization temperature of aluminum is 150°C. This means that at 200°C, the rate of annealing of aluminum wire proceeds rapidly. While such annealing does reduce the tensile strength of the wire, it decreases the hardness and increases the ductility. It appears then, that at test level D of temperature cycling, the work hardening induced at this heel of the bond is partially annealed during the dwell at 200°C. This phenomena will be further dilated upon in Section V.

A comparison of the effects of thermal shock and temperature cycling from the standpoint of electrical failures can only be done with Vendor 9 and Vendor 11 devices. Vendors 8 and

10 suffered extensive hermeticity fallout at test condition C. The units failed gross leak tests before the onset of failure of the wire bonds.

A comparison of the results of temperature cycling and thermal shock at test level C (-65°C to 150°C) indicates that temperature cycling is more effective in inducing wire and bond failures than is thermal shock.

Thermal shock has a great effect on seals, particularly on Type 1 glass seals. Type 2 glass is affected to a lesser degree, though one device with Type 2 glass fractured during electrical readouts at the 1005 cycle end point at test level C.

4.6.4 14 Pin Flat Package Results

There was only one seal test failure among the 14 pin flat packages as a result of the thermal cycling in this matrix. The single failure was a Vendor 6 device, which was destroyed during electrical testing during the 1500 cycle readout at test condition F temperature cycle (-65°C to 350°C). The seal separated at the interface between the sealing glass and the ceramic base. This unit also had a lifted die and is included in the electrical failure vs cycle curves.

4.6.4.1 Electrical Test Results

The electrical test results are given in Figures 4-46, 4-47 and 4-48 for Vendors 5, 6 and 7, respectively.

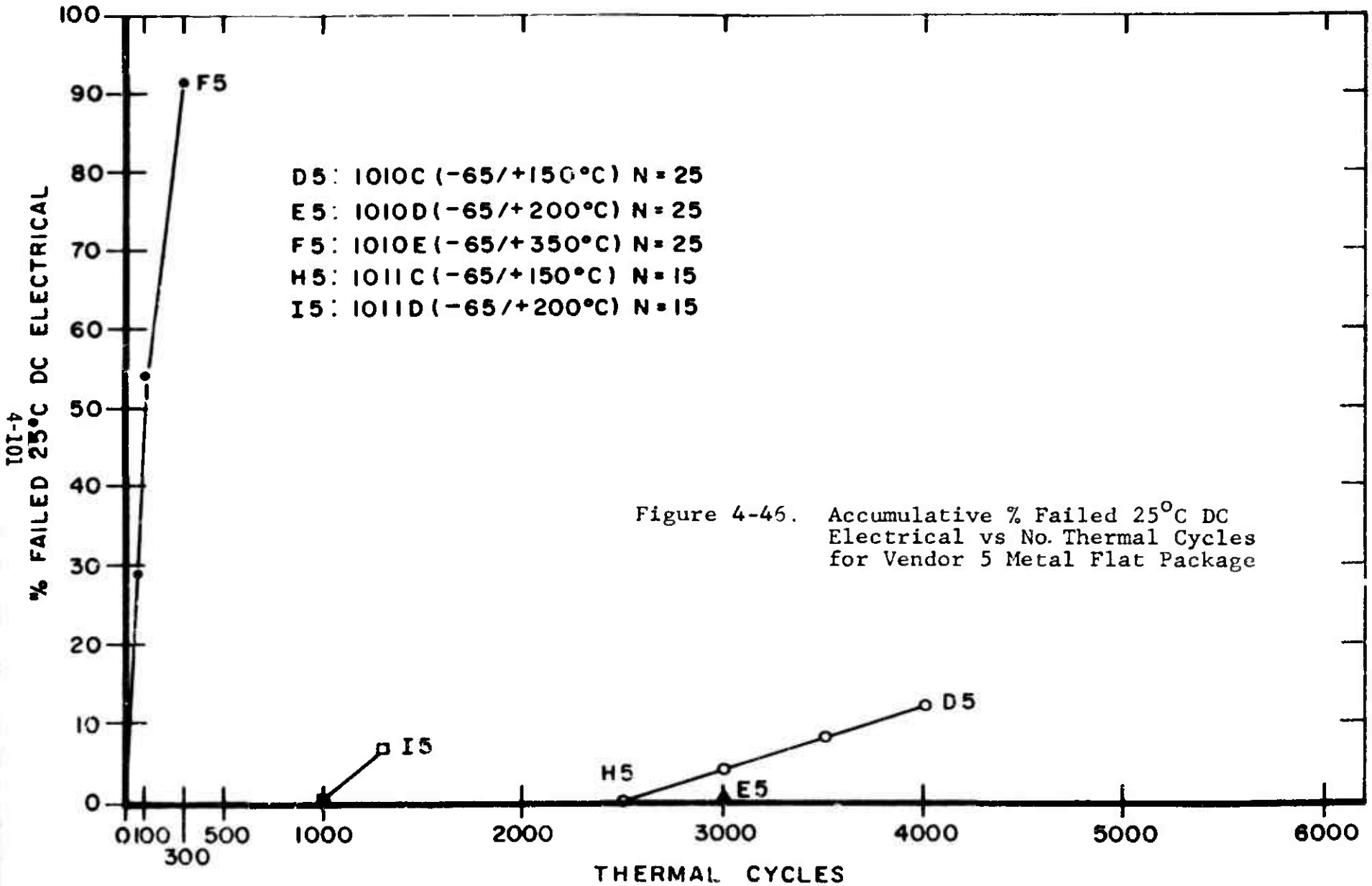

Figure 4-46. Accumulative % Failed 25°C DC Electrical vs No. Thermal Cycles for Vendor 5 Metal Flat Package

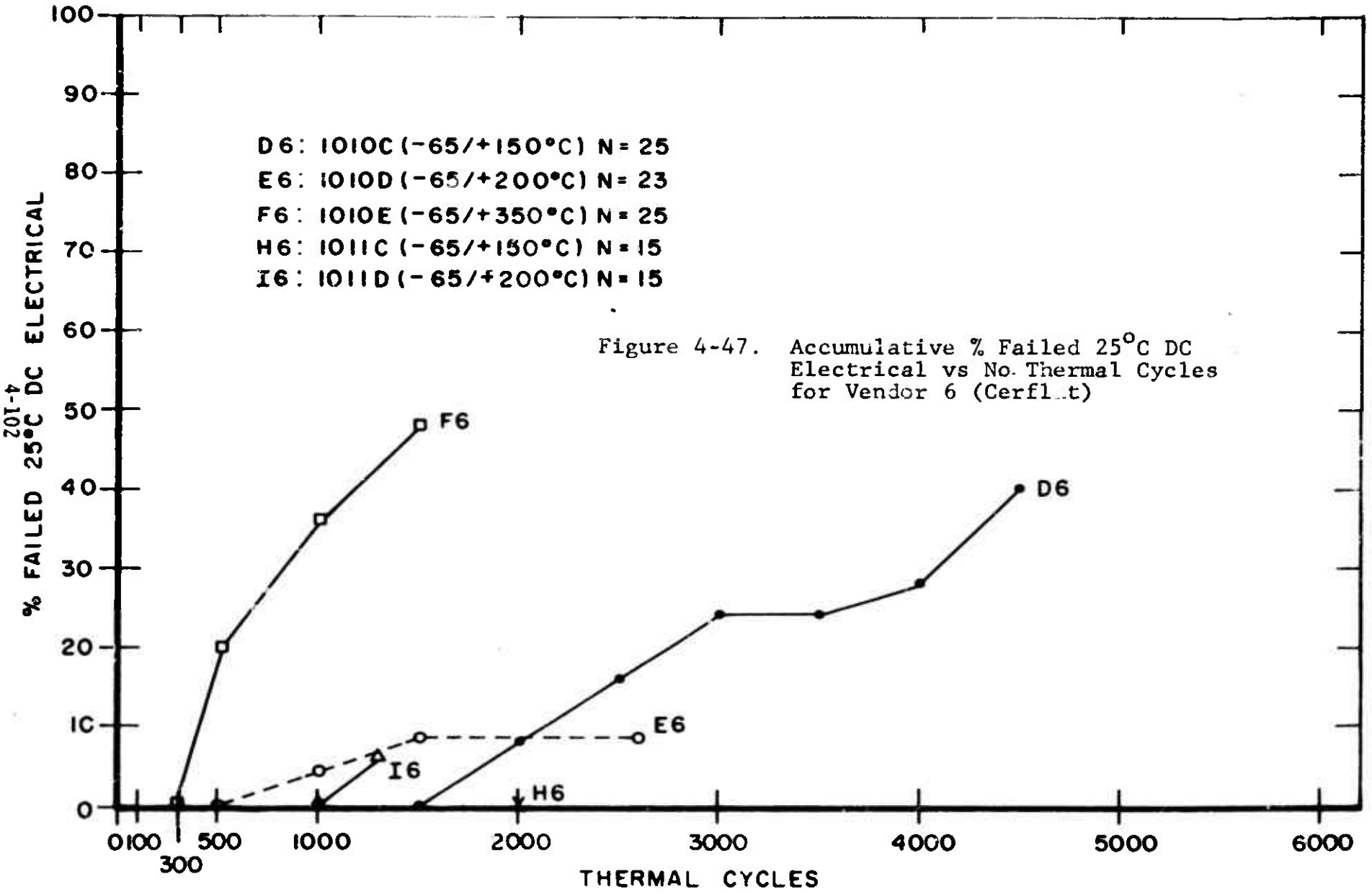

Figure 4-47. Accumulative % Failed 25°C DC Electrical vs No. Thermal Cycles for Vendor 6 (Cerfl..t)

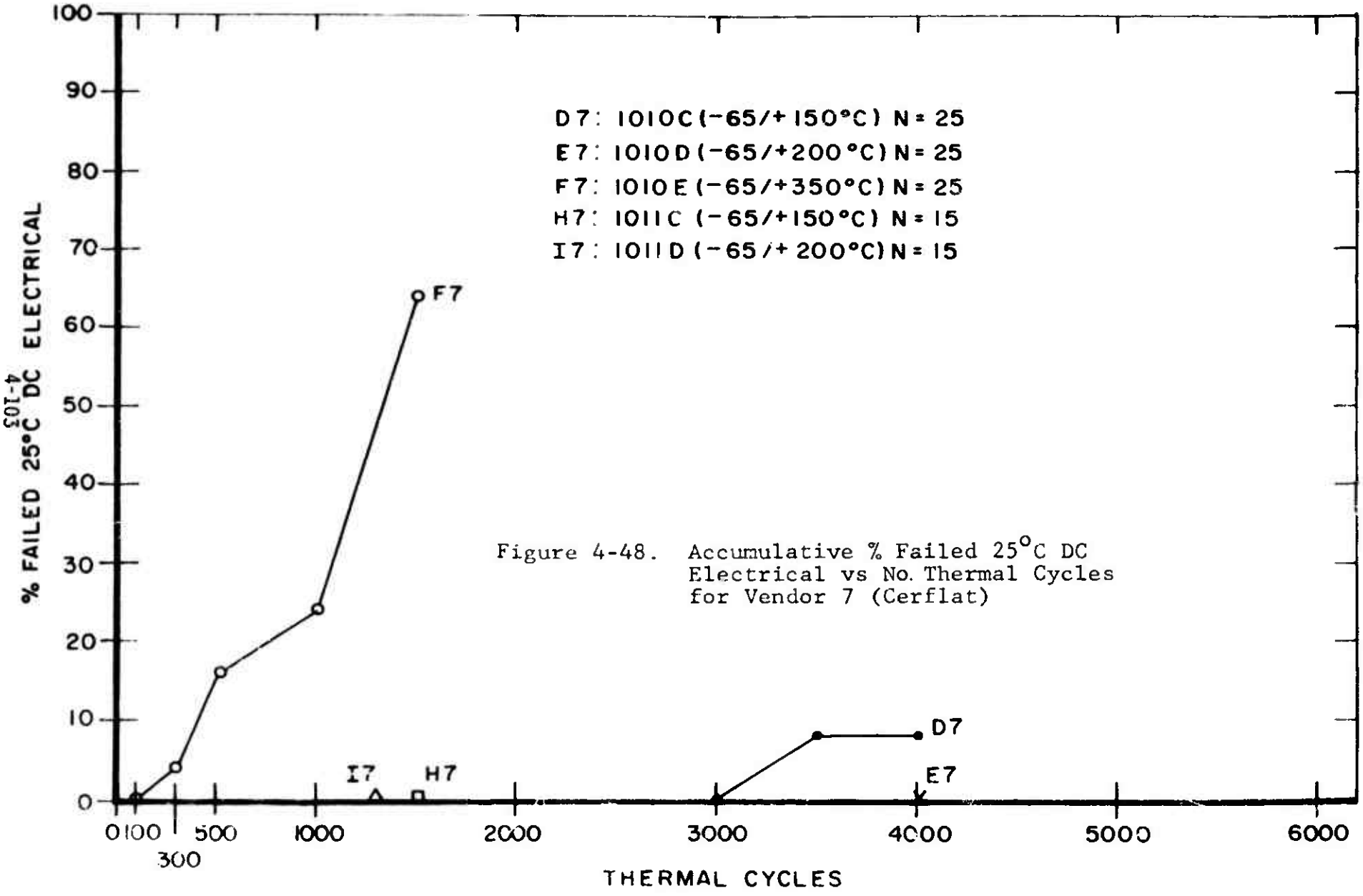

Figure 4-48. Accumulative % Failed 25°C DC Electrical vs No. Thermal Cycles for Vendor 7 (Cerflat)

The patterns of failure and failure modes of Vendors 6 and 7 are similar to those which were observed in the dual-in-line ceramic packages.

The dominant failure modes for test level F of temperature cycle were lifted die bonds. Vendor 5 devices, however, failed due tc intermetallic formation between the gold ball bonds and the aluminum metallization.

The response of the units of Vendor 5 and 6 to test levels C and D of temperature cycling and thermal shock is characterized by a number of cycles without failure (offset) followed by a nearly linear increase in the accumulated percent failures with increasing cycles. Vendor 7 was relatively unaffected by thermal cycling at these levels over the first 3000 cycles.

Comparison of the effect on ceramic flat packages of temperature cycling at level C with respect to level D shows (as was shown by the dual-in-line ceramic) that in terms of fatigue type failures at the heel of the bond, test level C is apparently more severe than level D. As indicated in paragraph 4.6.3 3 and in section 5.2, this could be due to the rate of annealing of the aluminum wire at 200°C.

No significant comparison can be made between temperature cycling and thermal shock. The logistics of performing multiple thermal shock cycles forced the truncation of the thermal shock sequences prior to establishing the failure pattern caused by thermal shock.

4.6.5 Discussion of Results

This thermal cycle matrix was designed with two purposes in mind. First was to examine the effects of increasing the high temperature in temperature cycling and thermal shock, and second was to compare the effect of temperature cycle and thermal shock when these tests are extended to greater than 1000 cycles.

While the differences in results are not dramatic, temperature cycling has a greater effect on wires and bonds than does thermal shock. This difference was most significant in plastic devices and in the sidebraze 14 pin ceramic package (Vendor 11). The other 14 pin dual-in-line ceramic package tended to fail gross leak before the onset of thermal mechanical fatigue.

A comparison of all hermetic vendors at test level C temperature cycling is shown in Figure 4-49. This family of curves shows that the flat packages are definitely stronger than the ceramic daul-in-line packages in temperature cycling. Vendor 12 is the worst performer although this device has 42 wires rather than 14, and the average wire length is much greater than in the 14 pin dips.

From the results shown for the dual-in-line ceramic package, thermal shock affects the package seal while temperature cycle has the greatest effect on wires and bonds.

In addition, long term cycling induces mechanical fatigue failure at the heel of the bonds in ceramic devices, giving rise to a wearout characteristic which is approximately linear with respect to the number of cycles.

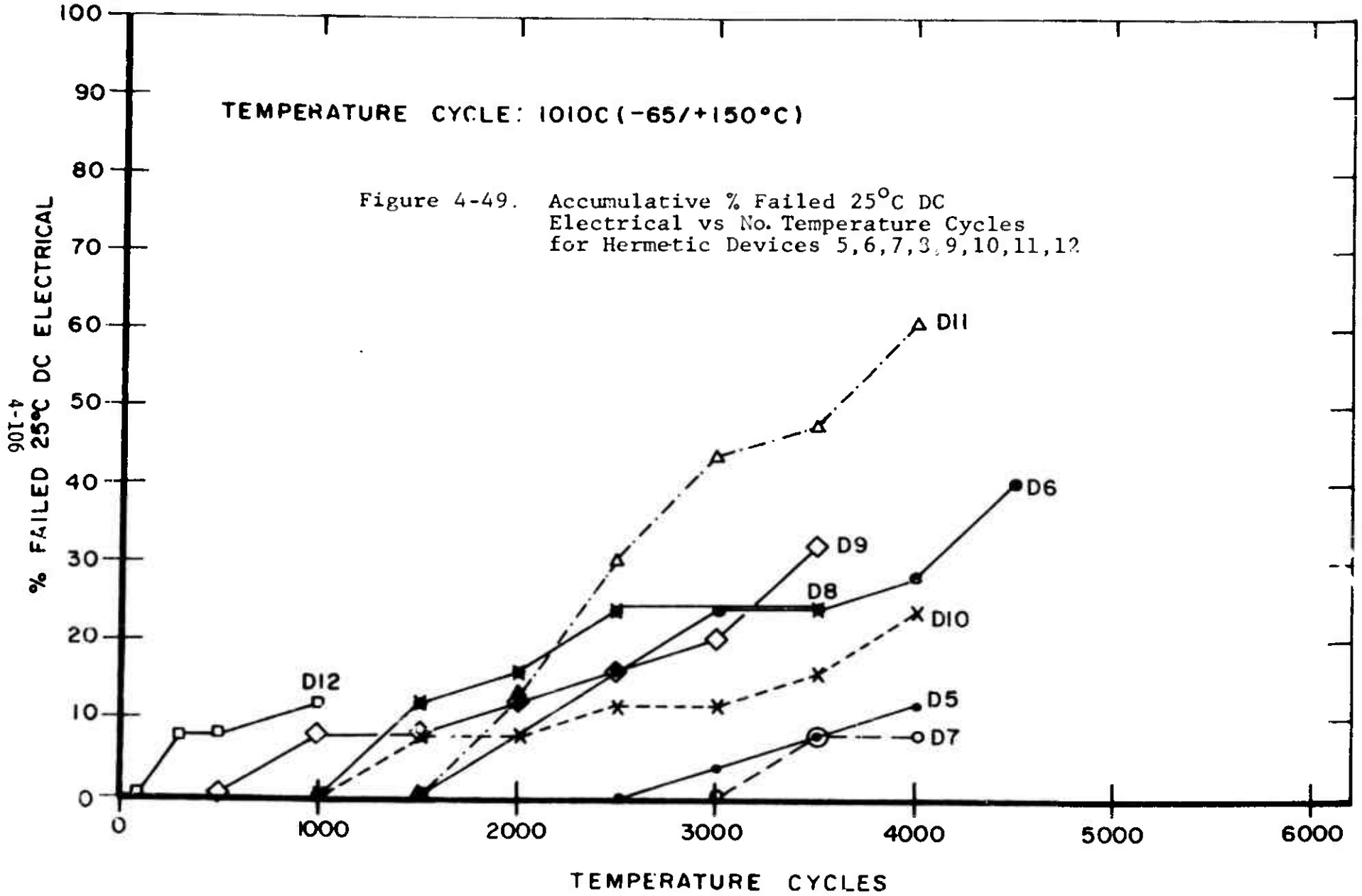

Figure 4-49. Accumulative % Failed 25°C DC Electrical vs No. Temperature Cycles for Hermetic Devices 5,6,7,8,9,10,11,12

Other mechanisms causing failures in this matrix were oxide shorts, which generally occurred between 1000 and 1500 cycles, on Vendor 6 Cerflat and Vendor 9 Cerdip. These two vendors also showed the greater deformation at the heel of the bond, thus rendering the devices more susceptable to fatigue fracture at the heel of the first bond.

4.7 THERMAL SHOCK/TEMPERATURE CYCLING INTERACTION MATRIX

This test sequence was designed to investigate what effect, if any, a 15 cycle preconditioning thermal shock, would have on the subsequent performance of the devices subjected to extended temperature cycling. The devices would be evaluated on package integrity and circuit integrity.

The basic test plan is shown in Figure 4-50. Parts were preconditioned with 15 cycles of Method 1011A, or 1011B, or 1011C and then subjected to extended Temperature Cycling per Method 1010B or 1010C or 1010D. The results were arranged in a balanced design matrix having three rows (Temperature Cycling levels - Factor A), three columns (preconditioning Thermal Shock - Factor B), and from three to five values per cell (vendors - Factor C). See Figure 4-51.

4.7.1 Data Analysis

The three-way analysis of variance was used to analyze the interaction test results[6]. The model used was as follows:

$$X_{ijk} = \bar{X}' + A'_i + B'_j + C'_k + (AB)'_{ij} + (AC)'_{ik} + (BC)'_{jk} + E_{e(ijk)}$$

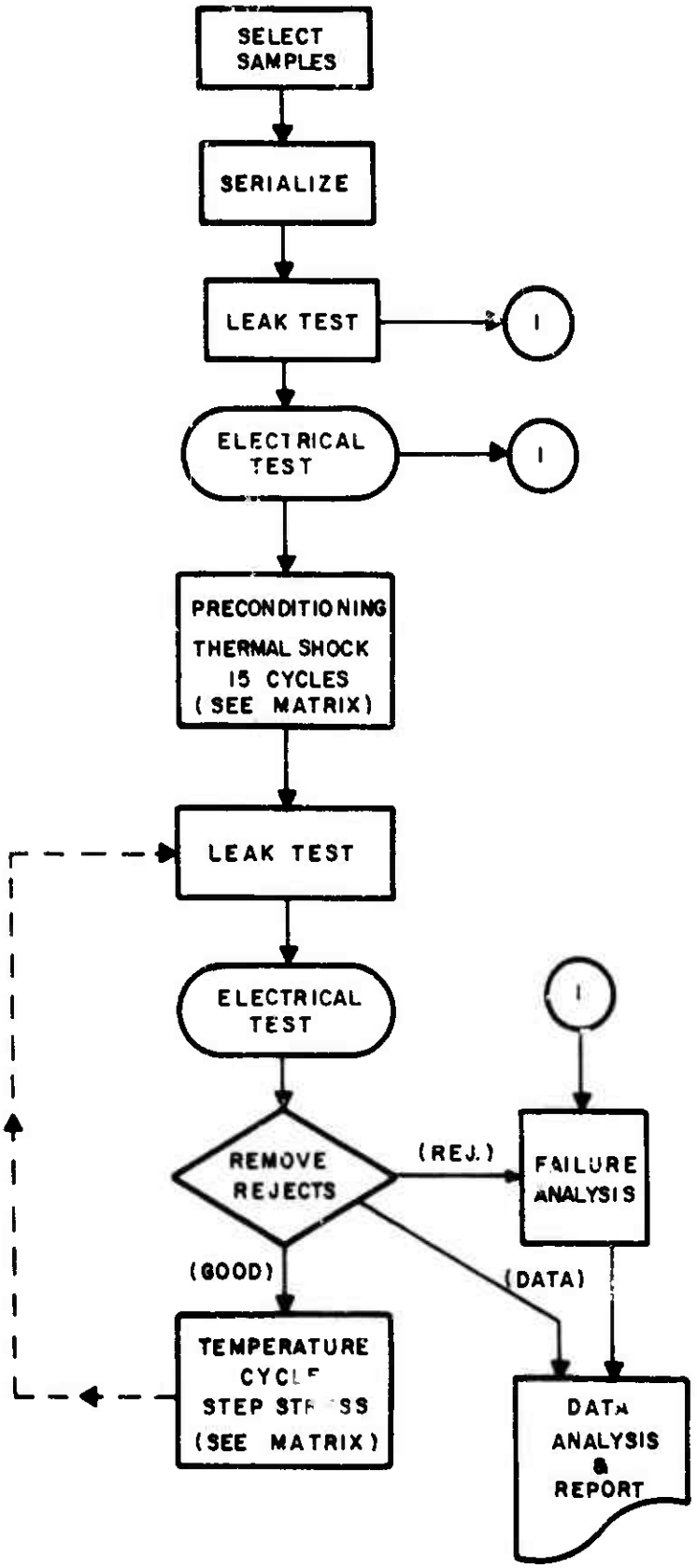

Figure 4-50. Thermal Cycling Interaction Matrix Test Plan

Interaction Matrix

Repeat for Each Vendor			
Temperature Cycle	Preconditioning Thermal Shock		
Ro: 30,60,100,500, 1000,1500,2000, 2500,3000,3500, 4000,4500	1011A 15 Cy. 0/+100°C	1011B 15 Cy -55/+125°C	1011C 15 Cy -65/+150°C
1010B (-55/+125°C)	J (J) 1, 1	M (M) 1, 2	Q (Q) 1, 3
1010C (-65/+150°C)	K (K) 2, 1	N (N) 2, 2	R (R) 2, 3
1010D (-65/+200°C)	L (L) 3, 1	P (P) 3, 2	S (S) 3, 3
Note: Control Samples - See Test Groups C (Method 1010B) D (Method 1010C) F (Method 1010D)			

Figure 4-51. Interaction Matrix Cell Identification

where

X_{ijk} = Cell value observed.

X' = Estimate of the true mean cell value.

A'_j = Effect on cell value due to temperature cycling level - Factor A.

B'_j = Effect on cell value due to preconditioning thermal shock level - Factor B.

C'_k = Effect on cell value due to vendor.

$(AB)'_{ij}$ = Effect on cell value due to an interaction between Factors A and B.

$(AC)'_{ik}$ = Effect on cell value due to an interaction between Factors A and C.

$(BC)'_{jk}$ = Effect on cell value due to an interaction between Factors B and C.

$E_{k(ijk)}$ = Random error - not accounted for in any other relationship.

Factor A - Temperature Cycling (B, C, and D) are fixed levels.
Factor B - Thermal Shock (A, B, and C) are fixed levels.
Factor C - Vendors are fixed levels (but could also be considered random levels).

The mechanics of conducting a three-way Anova are adequately covered in references (4), (6), and (7). The advantage of this type of analysis is that it does break out each of the individual factor contributions to the cell values and lists these with an estimate of their relative effect - i.e., the mean square (MS) values. It then compares each factor variance against a random error variance to obtain an "F" value. Looking up the "F" values in a handbook leads to conclusions of statistical significance. In this report, a "statistical significance at 1%" means

there is only a 1% chance that no effect difference exists - i.e., that all levels of the factor in question are equal.

4.7.2 Discussion - Choice of Variable to be Used in Analysis

To simplify the data analysis and allow comparisons of effects of temperature cycling and thermal shock, a search was made for a single number or figure of merit which could be used. One was found and used in all the data analysis of the interaction matrix results.

4.7.2.1 Figure of Merit

As the data analysis progressed, it became apparent that the typical failure response to long term thermal cycling consisted of an offset time period plus a failure period. The offset period is the number of thermal cycles from zero to the last readout with zero cycles (OA) and represents the time period of trouble-free service prior to start of failure. The failure period starts with the last zero readout and continues from there (ABCDEF).

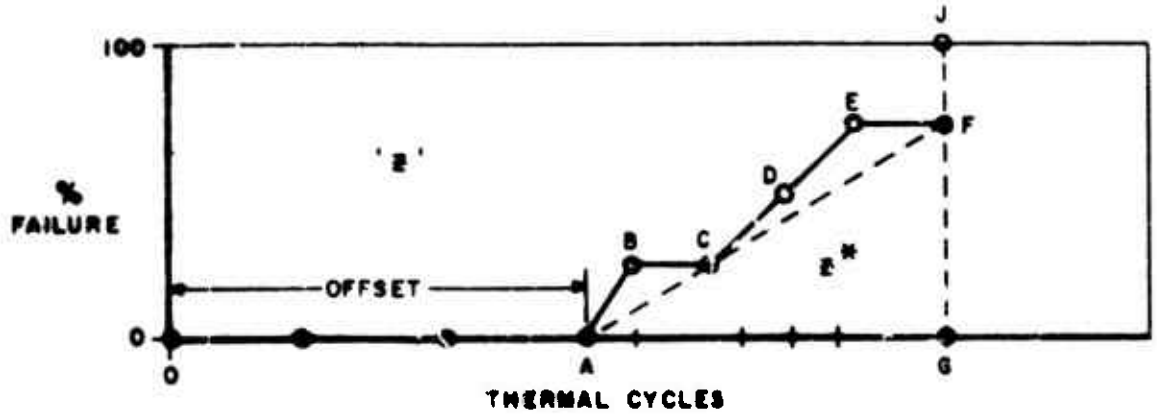

The offset period varies from none, for one vendor, to very long (for several samples). In some cases, no failures were found throughout the entire test period, these samples representing the best performance. It is believed that a long offset period is the most important characteristic to have since this represents the period of "trouble-free service". It also represents the "warrantee period" response, or period when the expected failure rate is very low.

The failure period also has varying characteristics. In one case, only one failure is found followed by several readouts with zero failures (ABCD) - very low failure rate. In other cases, the failures occur all at once going from zero failures (at point A) to 100% failures on the very next readout (point B). A response in between is shown as ABCDEF. It is felt that low failure rate is better than high failure rate.

The first figure of merit investigated, but not used, was called the "Z" value and is proportioned to the area above the curve, i.e., area OABCDEFJ100. The higher the "Z" the longer the offset and the lower the failure rate. The lower the "Z" the shorter the offset and higher the failure rate. Those Z values in between fall according to their offset vs failure rate relationship.

4.7.2.2 Truncated "Z" Values (Z*)

It became evident that Temperature Cycling Method 1010C was carried out further than any other condition and that the test results would have to be truncated at a point closer to the final readout for the remaining cells. Therefore, 3000 cycles

were chosen as the upper truncation point and all data was recalculated based on a maximum test time of 3000 cycles. It also became apparent that numbers based upon performance at 3000 cycles gave numbers whose magnitude went from 0 (no failures through 3000 cycles) to high numbers (large number of failures - high failure rate - early failures). This Z* number is proportional to the area below the curve - referenced from 3000 cycles. (Point G would be the 3000 cycle end point.)

These Z* numbers will be used throughout the interaction matrix analyses (Area of ΔAFG)

$$Z^* = 1/2\ (P\%)\ [3000 - A(\text{cycles})]/1000$$

where P% = % failure @ 3000 cycles

A = last readout cycles with zero failures

4.7.3 Hermetic Dips (DC Electrical - Z^* Values)

The 3 x 3 x 4 Anova is shown in Table IV-14. The matrix values are given in Table IV-15. Since no interactions are present the variation due just to temperature cycles - Factor A mean square is tested against the pooled residual mean square. This comparison is not significant: that is, there is no significant independent degradation due to Temperature Cycling alone in this experiment.

The interactions in A x C, Cycles vs Vendors, is almost significant due to the same sample results - sample 3, 3, 3 = 125 and sample 3, 3, 4 = 159.37. These results indicate Vendor 10 and 11 both showed higher failure rates when subjected to Method 1011C, Thermal Shock Preconditioning, and Method 1010D, Extended Temperature Cycling, than did any of the other vendors.

AVWPO

THREE WAY ANALYSIS OF VARIANCE

DC ELECTRICAL FAILURES..DIPS..'Z*' VALUES

SOURCE OF VARIATION	SS	DF	MS	F
TEMP CYCLE LEVELS...A	6698.52	2	3349.26	4.83 //2.78=ns
PRECON THER-SHOCK...B	1069.26	2	534.63	0.85 NS
VENDORS.....C	1895.13	3	631.71	1.00 NS
CYCLES VS SHOCK...A*B	6659.77	4	1664.94	2.63 NS
CYCLES VS VENDORS.A*C	12099.40	6	2016.57	3.19/2.26=NS
SHOCK VS VENDORS..B*C	6926.91	6	1154.48	1.83 NS
RESIDUAL ERROR.....	7582.32	12	631.86	
TOTAL SUM OF SQRS.....	42331.30	35		
COMMENTS Pooled=	24133.38	27	893.83	
	36232.78	33	1097.96	

TABLE IV-14

PKG: DIPS PROJECT NO: 2075

VARIABLE or PARAMETER Z* : DC

A = 3
B = 3
C = 4

TEMP. CYCLE		(TS)	VENDOR C1 8	C2 9	C3 10	C4 11	C5	Ave	Ave
A1 B	B1	A	31.25	25	0	3.12		14.84	
	B2	B	37.5	6.25	0	0		10.93	11.72
	B3	C	31.25	6.25	0	0		9.37	
A2 C	B1	A	18.75	90.62	3.13	18.75		32.81	
	B2	B	25	9.38	18.75	37.50		22.65	21.87
	B3	C	9.38	12.5	6.25	12.5		10.15	
A3 D	B1	A	31.25	31.25	0	62.5		31.25	
	B2	B	12.5	9.38	18.75	46.87		21.87	42.97
	B3	C	6.25	12.5	125	159.37		75.78	
									= TOTAL
	Ave		22.57	22.57	19.09	37.84		X =	25.52

(A * C)		C1 8	C2 9	C3 10	C4 11	C5	Ave	
A1	TC B	33.33	12.5	0	1.04		11.72	
A2	TC C	17.71	37.5	9.38	22.91		21.87	
A3	TC D	16.67	17.71	47.92	89.58		42.97	

(B * C)		C1 8	C2 9	C3 10	C4 11	C5	Ave	
B1	TS (A)	27.08	48.95	1.04	28.12		26.30	
B2	TS (B)	25	8.33	12.5	28.12		18.49	
B3	TS (C)	15.62	10.42	43.75	57.29		31.77	

(A * B)		A1 TC (B)	A2 TC (C)	A3 TC (D)	Ave	
B1	TS (A)	14.84	32.81	31.25	26.30	
B2	TS (B)	10.93	22.65	21.87	18.49	
B3	TS (C)	9.37	10.15	75.78	31.77	

REMARKS:

TABLE IV-15

Interaction Matrix (Z* values) DC Electrical - DIPS

The failure modes, Table IV-16, were heel breaks at the bond to the die (BD - Break at Die) for Vendors 8 and 9 and predominately heel breaks at the post bond (BP - Break at Post) for Vendors 10 and 11. This difference in failure mode is attributed to the difference in bonding sequence: Vendor 8 and 9 bonded die first and post last. Vendors 10 and 11 bonded post first and die last. The mechanics of bonding subjects the first bond to flexure as the bonding needle routes the wire to the final bond location. Each flexure of the bond "work hardens" it, making it more brittle and subject to failure. Consequently, subsequent expansion - contraction of the bonded wire when the device is subjected to Temperature Cycling causes the first bond to fail first. All samples had comparable 1 mil aluminum wire with ultra sonic bonds. Vendor 11 was the only one of the four with gold plated Kovar posts. A comparison between Vendor 10 and 11, both bonded post to pad, would indicate additional failure rate due to the presence of gold aluminum intermetallic in the post bond only. This additional weakening of the bond shows up strongly in Temperature Cycle Method 1010D (-65° to 200°C) - row 3, where 15 BP failures were obtained vs 2-BP and 1BD for Vendor 10. The abnormally high failure rates (Z* values) in samples 3, 3, 4 (Vendor 11) was due to the very early BP failures (500, 500, 1000, 1500, and 2000 cycles) compared to most other samples which did not show failures until after 1000 cycles. Sample 3, 3, 3 (Vendor 10) also had early failures (30, 1000 cycles) for the cell, causing a high failure rate (Z*) values.

As will be shown later, Vendor 11 (sidebraze) had a perfect hermeticity record but the combination of gold-aluminum posts and post to pad bonding lead to reduced electrical performance (opens) compared to the others in this test.

Overall n=288			Upbonded (Vendors 8, 9) n=144		Downbonded (Vendors 10, 11) n=144	
Mode	No	Percent	No	Percent	No	Percent
BD	34	50.75	32	94.12	2	6.06
BP	29	43.28	1	2.94	28	84.85
Corrosion	3	4.48	0	0	3	9.09
Oxide Flaw	1	1.49	1	2.94	0	0

TABLE IV-16

Failure Modes vs Bonding Direction

The 2, 4, 4 matrix, specifically run to compare the effect of preconditioning against no preconditioning, showed no significant differences between any main effects or interactions. Therefore, it can be concluded that preconditioning Thermal Shock (1011A, B or C) for 15 cycles does not significantly alter subsequent electrical performance to Temperature Cycling on hermetic DIP devices.

4.7.4 Hermetic Dips - (Leak Test Results - Z* Values)

The three-way analysis of variance for leak test failures was quite different from that for electrical failures. Two situations were analyzed:

(1) Indicated Fine Leak Failures (Table IV-17 and IV-18)
(2) Confirmed Fine Leak Failures (Table IV-19 and IV-20)

In both cases there was a significant effect due to the preconditioning thermal shock.

Taking the indicated Helium Leak Anova first, the residual error term was pooled with those of A, A x B, and A x C, to obtain the new values below the line. Testing this pooled residual against the B x C interaction showed this interaction to be highly significant at 0.5%. Therefore, the value obtained for a particular vendor was dependent upon which preconditioning column it was in. A look at the basic matrix indicated that both Vendor 10 and Vendor 13 had higher failure rates (higher Z* values)

AVWPO

THREE WAY ANALYSIS OF VARIANCE

INDICATED HELIUM LEAKERS..DIPS..'Z*' VALUES

SOURCE OF VARIATION	SS	DF	MS	F
TEMP CYCLE LEVELS...A	157.50	2	78.75	0.18 NS
PRECON THER-SHOCK...B	11569.97	2	5784.98	13.14
VENDORS.....C	9307.44	4	2326.86	5.28
CYCLES VS SHOCK...A*B	443.75	4	110.94	0.25 NS
CYCLES VS VENDORS.A*C	3572.95	8	446.62	1.01 NS
SHOCK VS VENDORS..B*C	10436.93	8	1304.62	2.96/3.49=*0.5%
RESIDUAL ERROR.....	7046.20	16	440.39	
TOTAL SUM OF SQRS.....	42534.73	44		
---	---	---	---	
COMMENTS **Pooled=**	**11220.40**	**30**	**374.10**	

TABLE IV-17

PKG: DIPS PROJECT NO: 2075

VARIABLE or PARAMETER Z* : Indicated Fine Leak

TEMP. CYCLE	(TS)	VENDOR C1 8	C2 9	C3 10	C4 11	C5 13	A = B = C = Ave	Ave
A1 B	B1 A	0	0	0	0	30	6.00	
	B2 B	18.75	12.50	15.62	0	0	9.37	19.54
	B3 C	36.25	6.25	93.75	0	80	43.25	
A2 C	B1 A	0	0	0	0	30	6.00	
	B2 B	74.25	0	0	0	5	15.85	24.07
	B3 C	75	12.5	74.25	0	89.10	50.35	
A3 D	B1 A	18.75	9.37	0	0	45	14.63	
	B2 B	6.25	0	28.12	0	30	12.87	22.67
	B3 C	18.75	56.25	112.50	0	15	40.50	
								= TOTAL
	Ave	27.56	10.76	36.03	0	36.11	X =	22.09

(A * C)		C1 8	C2 9	C3 10	C4 11	C5 13	Ave	
A1	TC B	18.33	6.25	36.46	0	36.67	19.54	
A2	TC C	49.75	4.17	24.75	0	41.67	24.07	
A3	TC D	14.58	21.87	46.87	0	30.00	22.67	

(B * C)		C1 8	C2 9	C3 10	C4 11	C5 13	Ave	
B1	TS (A)	6.25	3.13	0	0	35	8.88	
B2	TS (B)	33.08	4.17	14.58	0	11.70	12.70	
B3	TS (C)	43.33	25.00	93.50	0	61.70	44.70	

(A * B)		A1 TC (B)	A2 TC (C)	A3 TC (D)	Ave	
B1	TS (A)	6.00	6.00	14.63	8.88	
B2	TS (B)	9.37	15.85	12.87	12.70	
B3	TS (C)	43.25	50.35	40.50	44.70	

REMARKS:

TABLE IV-18

Interaction Matrix (Z* values)

Indicated Fine Leak - DIPS

AVWPO

THREE WAY ANALYSIS OF VARIANCE

CONFIRMED HELIUM LEAKERS..DIPS..'Z*' VALUES

SOURCE OF VARIATION	SS	DF	MS	F
TEMP CYCLE LEVELS...A	1791.11	2	895.56	2.01 NS
PRECON THER-SHOCK...B	8359.70	2	4179.85	9.39/8.49=*0.1%
VENDORS.....C	2422.79	4	605.70	1.36 NS
CYCLES VS SHOCK...A*B	2191.89	4	547.97	1.23 NS
CYCLES VS VENDORS.A*C	3152.15	8	394.02	0.88 NS
SHOCK VS VENDORS..B*C	4033.43	8	504.43	1.12 NS
RESIDUAL ERROR.....	7125.69	16	445.36	
TOTAL SUM OF SQRS.....	29046.77	44		
COMMENTS **Pooled=**	**20687**	**42**	**492.55**	

TABLE IV-19

PKG: DIPS PROJECT NO: 2075

VARIABLE or PARAMETER Z* : Confirmed Fine Leak

A = 3
B = 3
C = 5

TEMP. CYCLE		(TS)	VENDOR C1 8	C2 9	C3 10	C4 11	C5 13	Ave	Ave
A1	B	B1 A	0	0	0	0	0	0	2.83
		B2 B	0	0	0	0	0	0	
		B3 C	36.25	6.25	0	0	0	8.5	
A2	C	B1 A	0	0	0	0	0	0	15.26
		B2 B	9.37	0	0	0	0	1.87	
		B3 C	56.25	0	74.25	0	89.10	43.92	
A3	D	B1 A	18.75	9.37	0	0	0	5.62	16.99
		B2 B	0	0	9.37	0	15	4.87	
		B3 C	18.75	56.25	112.50	0	15	40.5	
									= TOTAL
		Ave	15.48	7.98	21.79	0	13.23	X =	11.69

(A * C)		C1 8	C2 9	C3 10	C4 11	C5 13	Ave	
A1	TC B	12.08	2.08	0	0	0	2.83	
A2	TC C	21.87	0	24.75	0	29.7	15.26	
A3	TC D	12.5	21.87	40.62	0	10	16.99	

(B * C)		C1 8	C2 9	C3 10	C4 11	C5 13	Ave	
B1	TS (A)	6.25	3.12	0	0	0	1.87	
B2	TS (B)	3.12	0	3.12	0	5	2.25	
B3	TS (C)	37.08	20.83	62.25	0	34.7	30.97	

(A * B)		A1 TC (B)	A2 TC (C)	A3 TC (D)	Ave	
B1	TS (A)	0	0	5.62	1.87	
B2	TS (B)	0	1.87	4.87	2.25	
B3	TS (C)	8.5	43.92	40.5	30.97	

REMARKS:

TABLE IV-20

Interaction Matrix (Z* values)

Confirmed Leaks - DIPS

than expected whereas Vendor 11 (Sidebraze) had a perfect record - no indicated leakers in 3000 cycles. All other vendors had consistently higher failure rates when subjected to Preconditioning Thermal Shock 1011C than to levels 1011B or 1011A. The Z* number for 1011C is nearly 4X the number for 1011B! This high value is statistically significant at 2.5%.

A study of the vendor averages, indicates that Vendor 11 is best and Vendor 9 is next. Vendor 9 was also shown to have a very strong package on the torque test sequence. Vendor 8 and 10 have similar packages and used essentially the same sealing glass but Vendor 10 has more helium trapping problems. Vendor 13 also has a trapping problem. It is of interest that the extended temperature cycling following the preconditioning had very little effect on the outcome even at much higher temperature extremes than those used for the preconditioning. The temperature cycling performance does not depend upon the level of thermal shock preconditioning.

The confirmed Helium Leakers Anova simplifies the problem further. The results are presented in Table IV-19 and IV-20. Again pooling the nonsignificant terms to obtain a better overall estimate of residual variance and testing for significance of differences between levels of Factor B (Preconditioning Thermal Shock) yields significant difference at 0.1% due to the preconditioning leak chosen. The difference between response to Method 1011C and Method 1011B is even greater than in the previous case for indicated fine leakers. The most dramatic shift in Z* values occurs in all the lower stress levels, such as Method 1010B and 1011A.

At lower levels of preconditioning, approximately 20% of the indicated helium leakers are confirmed whereas for Preconditioning Thermal Shock, Method 1011C, 69% of the indicated leakers were confirmed.

The same general pattern holds for Temperature Cycling - 14.48% of 1010B; 63.4% of 1010C and 74.9% of 1010D values were confirmed.

When comparing vendors, the results are:

Vendor	% Confirmed	
8	56.17%	
9	74.16%	Best CDIP
10	60.48%	
11	100 %	Sidebrazer-Solder Seal Lid
13	36.64%	Large 18 lead DIP

The percent confirmed correlates well with the absolute value of Z*; i.e., the lower the Z* (lower failure rate) the greater the percent confirmed. This is due to less helium trapping by the strcnger packages and better glass-to-metal and glass-to-ceramic bonding. The only gross leakers obtained were with Vendor 10 in the highest levels - 1011C Preconditioning plus 1010D Temperature Cycling.

The major observations made from these matrix tests are:

(1) Thermal shock preconditioning has a highly significant effect on helium leak performance with Method 1011C causing a significant failure rate for this failure mode. It has little effect on bond strength.

(2) Extended temperature cycling has the most effect on bond failures with an increasing failure rate with an increase in level or an increase in number of cycles. It has little effect on leak test results.

(3) Vendor 10 has the best bonding but weakest package. Vendor 11 had the best leak test performance but highest bond failure rate due to putting the first bond on the post and having a gold-aluminum post bond with intermetallics causing additional weakening of bond strength.

4.7.5 Flat Packages

Vendors 5, 6 and 7 are flat packages with Vendor 5 being a metal flat with gold ball bonds, and Vendor 6 and 7 being Cerflats with aluminum-ultrasonic bonds. There were no leak test failures for the flat packages. The small flat packages have excellent hermeticity performance throughout the entire test program. The Interaction Matrix for DC Electrical is shown in Table IV-21 and Table IV-22.

Using a pooled value for the residual, there is a significant difference between vendors at 2.5%. This difference is obviously between Vendor 6 and Vendor 7. Vendor 7 had no DC electrical failures nor any bond failures in the entire 3000 cycles. There is no significant interactions in this test. All the differences observed were due to vendor-to-vendor differences.

There is a pattern of increasing failure rate with increasing Temperature Cycling Level (Factor A) but no similar trend associated with Thermal Shock Preconditioning.

AVWPO

THREE WAY ANALYSIS OF VARIANCE

DC ELECTRICAL FAILURES..FLATS..'Z*' VALUES

SOURCE OF VARIATION	SS	DF	MS	F
TEMP CYCLE LEVELS...A	558.21	2	279.11	1.67 NS
PRECON THER-SHOCK...B	102.66	2	51.33	0.31 NS
VENDORS.....C	1243.34	2	621.67	3.73/4.95=*2.5%
CYCLES VS SHOCK...A*B	578.02	4	144.50	0.87 NS
CYCLES VS VENDORS.A*C	388.04	4	97.01	0.58 NS
SHOCK VS VENDORS..B*C	54.77	4	13.69	0.08 NS
RESIDUAL ERROR.....	1333.08	8	166.64	
TOTAL SUM OF SQRS.....	4258.12	26		
COMMENTS **Pooled=**	**3014.78**	**24**	**125.62**	

TABLE IV-21

PKG: FLATS PROJECT NO: 2075

VARIABLE or PARAMETER Z* : DC

(TS)		VENDOR C1 5	C2 6	C3 7	C4	C5	A = 3 B = 3 C = 3 Ave	Ave
		0	18.75	0			6.25	2.08
		0	0	0			0	
	C	0	0	0			0	
A2	B1 A	0	25	0			8.33	5.56
C	B2 B	0	9.38	0			3.13	
	B3 C	0	6.25	0			5.21	
A3	B1 A	12.5	0	0			4.17	12.98
D	B2 B	3.12	31.25	0			11.45	
	B3 C	15.62	54.37	0			23.33	
								= TOTAL
Ave		4.52	16.11	0			X =	6.87

(A * C)		C1 5	C2 6	C3 7	C4	C5	Ave	
A2	TC B	0	6.25	0			2.08	
A3	TC C	1.12	13.54	0			5.56	
A3	TC D	16.41	28.54	0			12.98	

(B * C)		C1 5	C2 6	C3 7	C4	C5	Ave	
B1	TS (A)	4.17	14.58	0			6.25	
B2	TS (B)	1.04	13.54	0			4.86	
B3	TS (C)	6.33	20.21	0			9.51	

(A * B)		A1 TC (B)	A2 TC (C)	A3 TC (D)	Ave	
B1	TS (A)	6.25	8.33	4.17	6.25	
B2	TS (B)	0	3.13	11.45	4.86	
B3	TS (C)	0	5.21	23.33	9.51	

REMARKS:

TABLE IV-22

Interaction Matrix (Z* values)
DC Electrical - Flats

The flat packages showed the best overall performances, as a group, to the interaction matrix testing. This package style is clearly the best "Hi Rel" package, at least for all the environments studied in this program.

4.7.6 Plastic Packages

Plastic package performance to the interaction matrix was varied. Some vendors did very well; others did poorly.

Table IV-23 and IV-24 cover the plastic results. Pooling the residual with those factors underlined gave the error mean square below the line. Testing the A x C interaction against this term showed A x C to be significant at 0.1%. Therefore, the value obtained for temperature cycling depended very strongly upon which vendor was under consideration.

Since the A x C interaction is significant the Factor A (Temp Cycle Levels Effect) and C (Between Vendors Effect) had to be tested against the interaction mean square, not the pooled residual. This testing showed a strange significant difference between vendors while the Temp Cycle Levels Effect became not significant (NS). The most surprising performance was Vendor 4 Phenolic with a perfect record - no DC electrical or intermittent failures even through 3000 Temperature Cycles of Condition D ($-65^{\circ}C/+200^{\circ}C$). The reason is thought to be: The Phenolic package had a glass transition point above $200^{\circ}C$ whereas the other three epoxy packages had glass transition points less than $150^{\circ}C$. This vendor also used 1.5 mil gold thermal compression wire bonding. Vendor 1 and 3 used the same plastic, epoxy type, but had different wire bonding systems. Vendor 1 uses 1.5 mil diameter gold thermal compression wire bonding; Vendor 3 used 1.0 mil gold ball bonding.

AVWPO

THRSE WAY ANALYSIS OF VARIANCE

DC ELECTRICAL FAILURES,,PLASTICS..'Z*' VALUES

SOURCE OF VARIATION	SS	DF	MS	F
TEMP CYCLE LEVELS...A	61960.15	2	30930.08	125.73/2.15=NS
PRECON THER-SHOCK...B	409.07	2	204.53	0.83 NS
VENDORS.....C	475640.98	3	158546.99	644.51/11.04=*1%
CYCLES VS SHOCK...A*B	267.99	4	67.00	0.27 NS
CYCLES VS VENDORS.A*C	86185.31	6	14364.22	58.39/71.46=*0.1%
SHOCK VS VENDORS..B*C	1194.90	6	199.15	2.81 NS
RESIDUAL ERROR.....	2951.97	12	246.00	
TOTAL SUM OF SQRS.....	628510.37	35		
COMMENTS **Pooled=**	**4823.93**	**24**	**201.00**	

TABLE IV-23

PKG: PLASTIC PROJECT NO: 2075

VARIABLE or PARAMETER Z* : DC

TEMP. CYCLE	(TS)	VENDOR C1 1	C2 2	C3 3	C4 4	C5	A = 3 B = 3 C = 4 Ave	Ave
A1 B	B1 A	0	247.	218.75	0		116.438	
	B2 B	0	250.	225.	0		118.75	115.114
	B3 C	0	275.	165.62	0		110.155	
A2 C	B1 A	0	273.5	233.75	0		126.813	
	B2 B	0	285.	280.	0		141.25	134.563
	B3 C	0	275.	267.5	0		135.625	
A3 D	B1 A	270.	295.	273.5	0		209.625	
	B2 B	267.5	294.37	298.5	0		215.093	211.145
	B3 C	239.37	297	298.5	0		208.718	
								= TOTAL
	Ave	86.32	276.87	251.24	0		X =	153.607

(A * C)		C1 1	C2 2	C3 3	C4 4	C5	Ave	
A1	TC B	0	257.33	203.12	0		115.114	
A2	TC C	0	277.83	260.42	0		134.563	
A3	TC D	258.96	295.46	290.17	0		211.145	

(B * C)		C1 1	C2 2	C3 3	C4 4	C5	Ave	
B1	TS (A)	90	271.83	242.	0		150.958	
B2	TS (B)	89.17	276.46	267.83	0		158.364	
B3	TS (C)	79.79	282.33	243.87	0		151.499	

(A * B)		A1 TC (B)	A2 TC (C)	A3 TC (D)	Ave	
B1	TS (A)	116.438	126.813	209.625	150.958	
B2	TS (B)	118.75	141.25	215.093	158.364	
B3	TS (C)	110.155	135.625	208.718	151.499	

REMARKS:

TABLE IV-24

Interaction Matrix (Z* values)
DC Electrical - Plastic

The poorest performance was given by Vendor 2 who had a plastic with the lowest glass transition point and 1.0 mil gold ball bonding.

The results show clearly (see A x C matrix). Through Temperature Cycling Condition C (-65°C/+150°C) 1.5 mil gold T/C bonding showed excellent performance compared to 1.0 mil gold ball bonding. Test Condition D is too much for all except Vendor 4 (Note: Vendor 4 does not make Phenolic packaged I/C at this time. The samples used throughout these tests were engineering run samples).

The failure mode for the plastic devices was detected as intermittents first and as verified DC electrical second. It sometimes took quite some time for a repeating intermittent to become a hard failure. When the failure was analyzed, the failure mode was grain boundary fracture (GBF) in the gold wire some 2-10 mils above the ball (see discussion in the Failure Analysis section). The second most common failure was failure (opens - intermittents) at the lowest intermetallic interface between the gold wire and the aluminum pad metal. This failure mode is due to Kirkendall Voiding in the Au_5 Al_2 region following fatigue cracking in the bond due to the thermal cycling[13].

There was no independent effect due specifically to the preconditioning thermal shock.

4.7.7 Overall Conclusions

The overall conclusions from analysis of the interaction results are these:

(1) Thermal shock preconditioning generates fine leak failures.

(2) Extended temperature cycling is more effective in causing wirebond failures - much less effective in causing leak test failures.

(3) There is no interaction between the preconditioning thermal shock (15 cycles) and the subsequent extended temperature cycling performance. The temp cycle performance didn't care what 15 cycle preconditioning (if any) was used.

(4) The largest overall effect across all package styles and failure modes was vendor-to-vendor differences. This testing shows the importance of evaluating each vendor on his own merits and being careful of generalization across vendors making common package styles.

(5) Flat packages showed the best overall performance, and the lowest overall average Z* value. This fact was true considering both package integrity and wire bond integrity.

(6) Plastic package can perform as well as hermetic in thermal cycling applications but is highly vendor dependent. It is also expected that lot-to-lot variations within a vendor's production would be greater for plastic and hermetic.

(7) Hermetic dual-in-lines (CDIP construction) may be convenient to use but showed greater failure rates and far greater variation from cell to cell than did the flat packages. They are particularly susceptible to package failure due to their design; i.e., uneven masses of ceramic between top and bottom, heavy lead frame reducing amount of bonding glass around the frame; large torque

forces exerted by the lead frame on the lid when the leads are compressed during insertion into the board.

(8) Dual-in-line - sidebraze showed excellent package integrity but weaker interior post bonding reliability, due to the use of a gold/aluminum structure.

4.8 WIREBOND DEGRADATION STUDY

One of the failure modes often associated with thermal cycling sequences is open bonds. It is also often assumed that the wire pull strength is affected by thermal cycling. In an effort to learn more about these possible effects, a wirebond pull strength vs thermal cycling study was performed.

The test plan flow used is given in Figure 4-52. Following each stress step, any electrical or hermeticity failures found were removed, decapped and held for wire pull. If no end point test failures were noted, two devices were pulled at random for the wire pull sample. The sample plan is given in Table IV-25.

4.8.1 End Point Test Results

The results of the End Point Tests (EPT) were the first to show the strong vendor-to-vendor difference and the severe effect of thermal shock on package integrity. The hermeticity results are shown in Tables IV-26 and IV-27, the mechanical results separately in Tables IV-28 and IV-29, and the electrical results in Tables IV-30 and IV-31.

The same temperature extremes were used for both the Thermal Shock (Method 1011C) and Temperature Cycling (Method

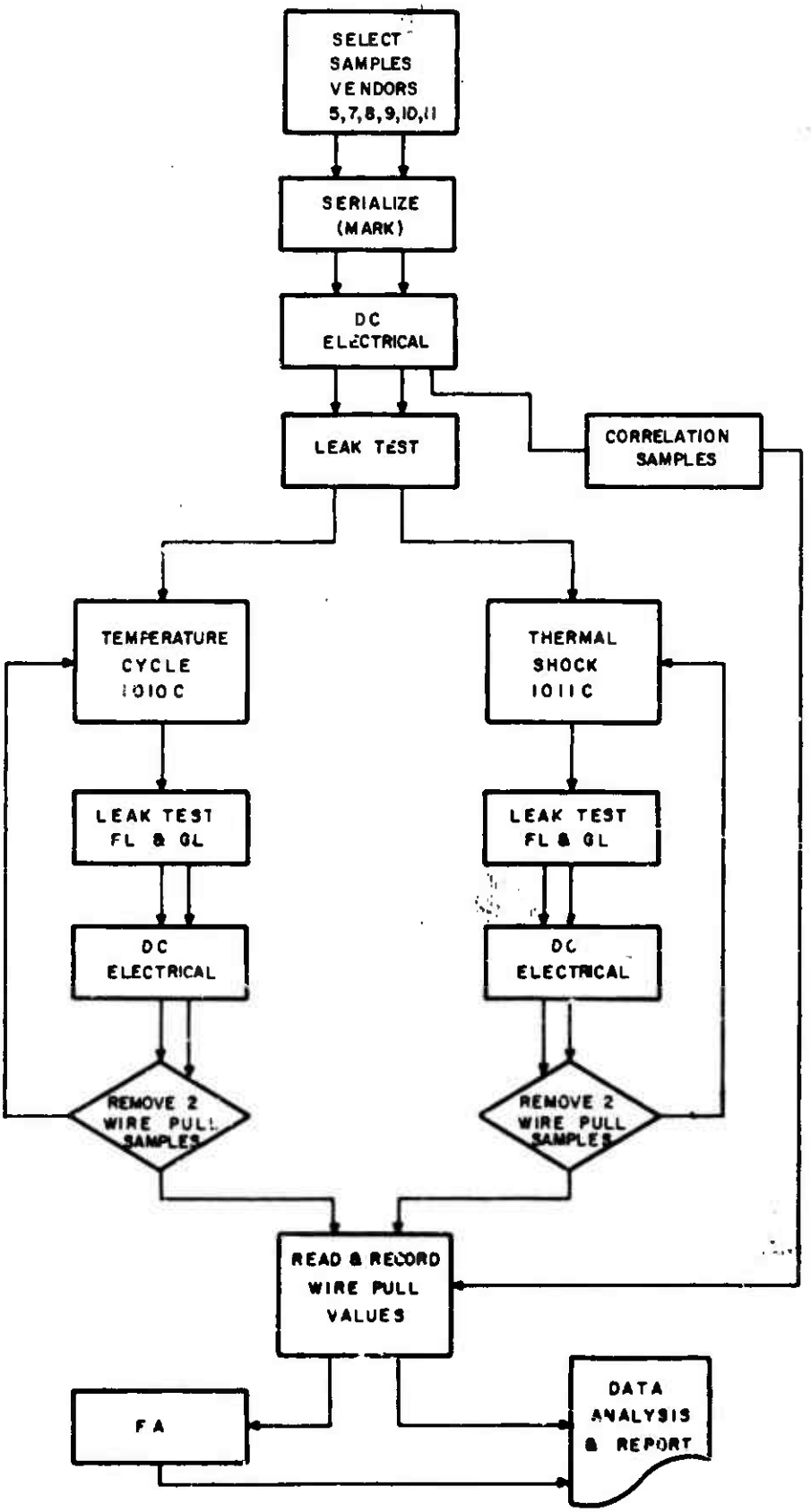

Figure 4-52. Basic Wire Pull Degradation Test Plan

	PACKAGE STYLE (All 14 Lead)											
	FLAT				DUAL IN-LINE							
	Metal		Ceramic		Ceramic		Ceramic		Ceramic		Sidebraze	
Vendor →	5		7		8		9		10		11	
Correl.	T n=5		T n=5		T n=5		T n=5		T n=5		T n=5	
u=1010C v=1011C	u	v	u	v	u	v	u	v	u	v	u	v
SS = EPT	15	15	15	15	15	15	15	15	15	15	15	15
30N, EPT Remove for Wire Pull	*	2	*	2	*	2	*	2	*	2	*	2
60N, EPT Remove for Wire Pull	4	2	4	2	4	2	4	2	4	2	4	2
120N, EPT Remove for Wire Pull	2	2	2	2	2	2	2	2	2	2	2	2
240N, EPT Remove for Wire Pull	2	2	2	2	2	2	2	2	2	2	2	2
510N, EPT Remove for Wire Pull	2	2	2	2	2	2	2	2	2	2	2	2
1020N, EPT Remove for Wire Pull	2	2	2	2	2	2	2	2	2	2	2	2

* These units not removed until after 60 cycle atep.

EPT - DC Electrical

± Helium Fine Leak (Method 1014A), 1 x 10^{-8} atm cc/sec.

- Full Fluoro Carbon (Method 1014C), with vacuum and bomb cycle.

TABLE IV-25

Wirebond Degradation Sample Plan

	Lot U	Temperature Cycling (1010C, -65°C/+150°C)						
	Hermeticity Failures vs Sample Size at Step							
	Vendor #	S.S.	No. of Cycles 30	60	120	240	510	1020	Total Hermeticity Failures
Flats	5	15	0/15	0/15	0/11	0/9	0/7	0/5	0
Flats	7	15	0/15	0/15	0/11	0/9	0/7	0/5	0
S/B CDIP	8	15	0/15	0/15	0/11	0/9	0/7	0/5	0
S/B CDIP	9	15	0/15	0/15	0/11	0/9	0/7	0/5	0
S/B CDIP	10	15	0/15	0/15	0/11	0/9	0/7	0/5	0
S/B CDIP	11	15	0/15	0/15	0/11	0/9	0/7	0/5	0
			0/90 0%	0/90 0%	0/66 0%	0/54 0%	0/42 0%	0/30 0%	0

TABLE IV-26

	Lot V	Thermal Shock - (1011C, -65°C/+150°C)						
	Hermeticity Failures va Sample Size at Step							
	Vendor #	S.S.	No. of Cyclea 30	60	120	240	510	1020	Total Hermeticity Failures
Flats	5	15	0/15	0/13	0/11	0/9	0/7	0/5	0
Flats	7	15	0/15	0/12	0/10	0/8	0/6	0/4	0
S/B CDIP	8	15	0/15	6/13	4/7	0/3	---	---	10
S/B CDIP	9	15	0/15	1/13	0/11	0/9	1/7	0/5	2
S/B CDIP	10	15	1/15	3/13	0/9	2/7	2/5	1/3	9
S/B CDIP	11	15	0/15	0/13	0/11	0/9	0/7	0/5	0
			1/90 1.11%	10/77 12.98%	4/59 6.78%	2/45 4.44%	3/32 9.38%	1/22 4.5%	21

TABLE IV-27

Lot U	Temperature Cycling (1010C, -65°C/+150°C)							
	Mechanical Failures vs Sample Size at Step							
	Vendor #	S.S.	No. of Cycles 30	60	120	240	510	1020	Total Mechanical Failures
Flats	5	15	0/15	0/15	0/11	0/9	0/7	0/5	0
Flats	7	15	0/15	0/15	0/11	0/9	0/7	0/5	0
CDIP	8	15	0/15	0/15	0/11	0/9	0/7	0/5	0
CDIP	9	15	0/15	0/15	0/11	0/9	0/7	0/5	0
CDIP	10	15	0/15	0/15	0/11	0/9	0/7	0/5	0
S/B	11	15	0/15	0/15	0/11	0/9	0/7	0/5	0
			0/90 0%	0/90 0%	0/60 0%	0/54 0%	0/42 0%	0/30 0%	0

TABLE IV-28

Lot V	Thermal Shock (1011C, -65°C/+150°C)							
	Mechanical Failures vs Sample Size at Step							
	Vendor #	S.S.	No. of Cycles 30	60	120	240	510	1020	Total Mechanical Failures
Flats	5	15	0/15	0/13	0/11	0/9	0/7	0/5	0
Flats	7	15	0/15	0/12	0/10	0/8	0/6	0/4	0
CDIP	8	15	0/15	0/13	0/7	0/3	---	---	0
CDIP	9	15	0/15	0/13	0/11	0/9	0/7	0/5	0
CDIP	10	15	0/15	1/13	0/9	0/7	0/5	1/3	2
S/B	11	15	0/15	0/13	0/11	0/9	0/7	0/5	0
			0/90 0%	1/77 1.3%	0/59 0%	0/45 0.0%	0/32 0%	1/22 4.5%	2

TABLE IV-29

	Lot U	Temperature Cycling (1010C, -65°C/+150°C)							
		Electrical Failures vs Sample Size at Step							
	Vendor #	S.S.	No. of Cycles 30	60	120	240	510	1020	Total Electrical Failures
Flats	5	15	0/15	0/15	0/11	0/9	0/7	0/5	0
Flats	7	15	0/15	0/15	0/11	0/9	0/7	0/5	0
Cdip	8	15	0/15	0/15	0/11	0/9	0/7	0/5	0
Cdip	9	15	0/15	1/15	0/11	0/9	0/7	1/5	2
Cdip	10	15	0/15	0/15	0/11	0/9	0/7	0/5	0
S/B	11	15	0/15	0/15	0/11	0/9	1/7	0/5	1
			0/90 0%	1/90 1.1%	0/66 0%	0/54 0%	1/42 2.4%	1/30 3.3%	3

TABLE IV-30

	Lot V	Thermal Shock (1011C, -65°C/+150°C)							
		Electrical Failures vs Sample Size at Step							
	Vendor #	S.S.	No. of Cycles 30	60	120	240	510	1020	Total Electrical Failures
Flats	5	15	0/15	0/13	0/11	0/9	0/7	0/5	0
Flats	7	15	0/15	0/12	0/10	0/8	0/6	0/4	0
Cdip	8	15	0/15	0/13	0/7	0/3	---	---	0
Cdip	9	15	0/15	0/13	0/11	0/9	0/7	0/5	0
Cdip	10	15	0/15	0/13	0/9	0/7	0/5	0/3	0
S/B	11	15	0/15	0/13	0/11	0/9	0/7	1/5	1
			0/90 0%	0/77 0%	0/59 0%	0/45 0%	0/32 0%	1/22 4.5%	1

TABLE IV-31

1010C, -65°C/+150°C). See Figure 4-53. The length of time at each extreme varied from 5 minutes for thermal shock to a minimum of 10 minutes (at stabilization) for temperature cycling. The major difference in stress was due to the much greater "glass strain" of the liquid-to-liquid thermal shock compared to the air-to-air temperature cycle.

4.8.1.1 Hermeticity Results

Table IV-26 indicates all lots sustained 1020 cycles of temperature cycling without any hermetic failures. However, the liquid-to-liquid thermal shock results of Table IV-27 show significant failures in the ceramic dual-in-line packages only and within this package style, significant differences between Vendor 8 and 9 and between 10 and 9. Tables IV-28 and IV-29 show mechanical fallout - packages which fall apart when handled.

Within the CDIP packages, Vendor 9 has the strongest package. This vendor uses a more elaborate locking lead frame and better glass and glass seal schedule than the other vendors. Since Vendor 8 sustained most of his failures early, it is believed that Vendor 8 has the weakest CDIP package.

The distribution of gross leak hermeticity failures was studied using Hazard Plots[9],[10]. After attempting to find a good fit of the data to several different distribution functions, the best fit was obtained using Normal paper. This result is given in Figure 4-54.

The Vendor 8 samples had gross leak failures at two readouts. The Vendor 9 sample has only one point. The Vendor 10

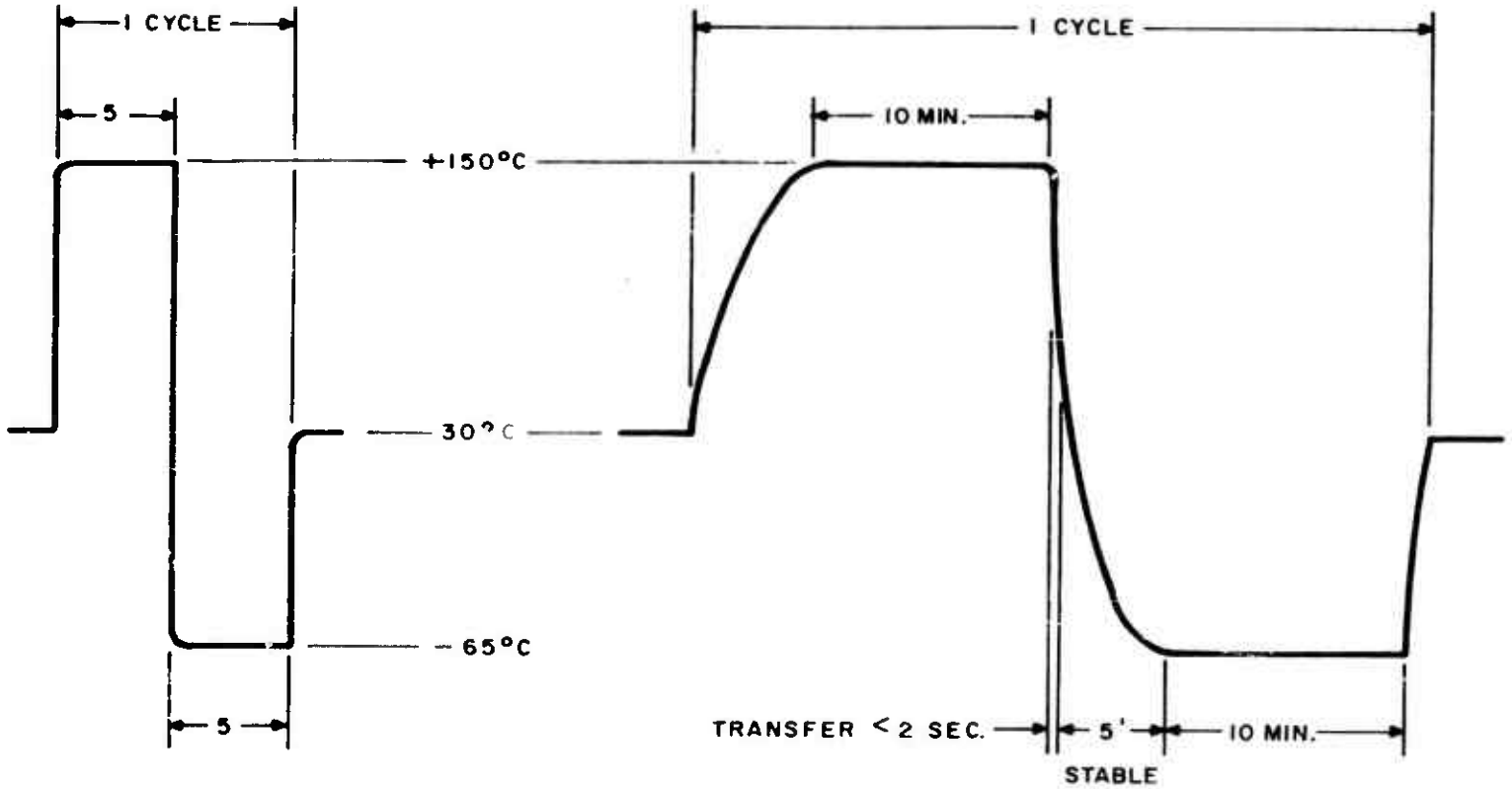

Figure 4-53 Comparison of Thermal Shock with Temperature Cycling

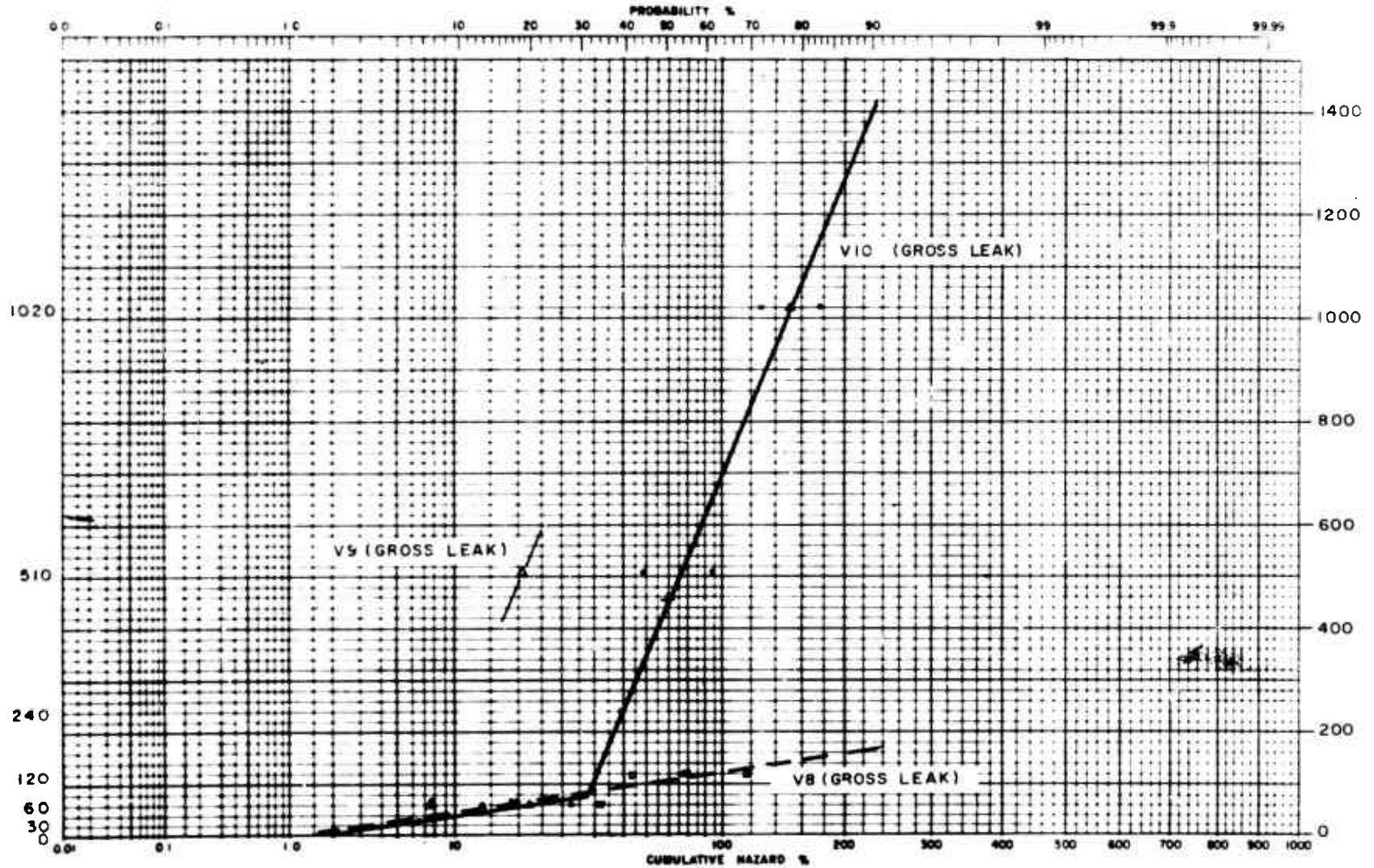

Figure 4-54. Distribution of Gross Leak Failures - Thermal Shock (1011C, -65°/+150°C)

sample had gross leak failures at all readouts, allowing a reasonable estimate to be made of the failure distribution and subsequent statistics. There appears to be a double distribution in Vendor 10. The curve above approximately 60 cycles, fits the normal distribution very well. (Note: The curves fit both normal and exponential about the same. The normal plot was picked to allow comparison with results in Section 4.9.2.1.)

From the slopes of the lines, the following statistics are obtained:

GROSS LEAK MODE	CDIP VENDORS		
Thermal Shock 1011C	V8	V9	V10
Failure Rate (%/Cycle)*	1.11	0.026**	0.135
Mean Cycles to Failure*	90	3783**	740
Actual MCTF (Observed)	135	3783**	630

*Note: Based upon exponential failure distribution with no offset. (Plot not shown.)

**Note: Estimated.

It is obvious that there were gross differences in hermeticity results following thermal shock, Method 1010C. The failure rate is constant (for Vendor 10) and assumed constant for Vendors 8 and 9. These failure rates and mean cycles to failure vary by an order of magnitude from vendor to vendor. Both Vendors 8 and 10 appear to have an offset or "freak" distribution for the first 60 cycles.

4.8.2 End Point Test Conclusions

4.8.2.1 Temperature Cycling vs Hermeticity (Table IV-26)

(1) There are no obvious differences in response between vendors or between package styles. All vendors and packages could withstand air-to-air temperature cycling without sustaining hermeticity rejects, fine leak or gross leak.

4.8.2.2 Temperature Cycling vs Electrical (Table IV-30)

(1) Flat packages had no rejects.
(2) CDIP packages had two random failures in one vendor only (Vendor 9).
(3) Sidebraze DIP package had a random failure in both the temperature cycling and thermal shock groups.
(4) Temperature cycling tends to stress wire and chip bonds more than the package integrity itself.

4.8.2.3 Thermal Shock vs Hermeticity (Table IV-27)

(1) Thermal shock is a severe test of the package.
(2) A large number of hermeticity rejects were obtained in the CDIP packages only.
(3) There were distinct differences from vendor-to-vendor with Vendor 9 having the strongest package and Vendor 8 the weakest. Vendor 10 was in between.
(4) Flats and sidebraze DIP performed well in this sequence. Both these package styles are small and lighter with much less ceramic mass than the CDIPS.

(5) The distribution of groaa leak failures for Vendor 10 is composed of an initial failure distribution and a main exponential failure distribution, with a constant failure rate of 0.135%/cycle.

(6) Leak testing is not as precise an end point as we would like. Fine leakers tend to become gross leakers eventually but not all fine leakers repeat or can be verified.

4.8.3 Wire Pull Degradation

As shown in the test plan, Table IV-25, two devices from each vendor/package were pulled and held for decapping and wire pull. Some decap problems were experienced. This was expected but was difficult to avoid. The result was that not all wires from all samples were left undamaged by the decap process. Table IV-32 shows the distribution of wires damaged during decapping. A study of this table shows that:

(1) Thermal shock caused more wire losses at decap than temperature cycling (8.8% vs 3.47%).

(2) The percent of wires lost increased with the number of cycles.

(3) The sidebraze package was the least problem. It shows the least interaction between type and length of stress and difficulty with decapping. Since this package had a soldered lid, decapping did not interact with the plane of the lead frame as it does with the CDIP package.

DISTRIBUTION OF WIRES DESTROYED DURING DECAP										
PKG.	Vendor	Stress	No. of Cycles						Ratio	% Loss
			30	60	120	240	510	1020		
FLATS	5	T.C.	--	1.	0	2	1	0	4/168	2.38
		T.S.	1	0	0	0	0	6	7/168	4.17
		Total	1	1	0	2	1	6	11/336	3.27
		Correl.*							26/70*	37.14
	7	T.C.	--	5	1	2	0	7	15/168	8.93
		T.S.	0	0	1	0	0	0	1/168	0.60
		Total	0	5	2	2	0	7	16/336	4.76
		Correl.*							7/70*	10.00
		TOTAL	1	6	2	4	1	13	27/672	4.02
CDIP	8	T.C.	--	0	0	0	0	0	0/168	0
		T.S.	*	*	*	*	*	*	*	*
		Total	--	0	0	0	0	0	0	0
		Correl.*							14/70*	20.00
	9	T.C.	--	4	2	3	4	3	16/168	9.52
		T.S.	1	4	10	8	13	7	43/168	25.60
		Total	1	8	12	11	17	10	59/336	17.56
		Correl.*							13/70*	18.59
	10	T.C.	--	0	0	0	0	0	0/168	0
		T.S.	0	3	5	7	4	4	23/168	13.69
		Total	0	3	5	7	4	4	23/336	6.85
		Correl.*							31/70*	44.29
		TOTAL	1	11	17	18	21	14	82/840	9.76
S/B	11	T.C.	--	0	0	0	0	0	0/168	0
		T.S.	0	0	0	0	0	0	0/168	0
		Total	0	0	0	0	0	0	0/336	0
		Correl.*							0/70*	0
GRAND TOTAL			2/140	17/476	19/308	22/308	22/308	27/308	109/1848	5.89
%			1.43	3.57	6.17	7.14	7.14	8.77		
T.C.			--	10	3	7	5	10	35/1008	3.47
T.S.			2	7	16	15	17	17	74/840	8.81

*All Devices Destroyed During Decap.

TABLE IV-32

(4) Vendor 9 (CDIP) has the strongest package and the hardest to open. Consequently, when this package was decapped, the lead frame tended to come out of the glass at the same time, thereby causing damage to the attached wirebonds. This resulted in a loss of 17.56% of the wires for this vendor.

(5) More failures occurred in the correlation samples than in the test groups since these were the first ones decapped and therefore because part of the "learning curve".

4.8.3.1 Wire Pull Procedure

All decapped wire pull samples were held until they could be wire pulled at one time. All samples, including the correlation devices, were wire pulled using the same electronic Transmetric Wire Pull Machine and the same operator. The machine has a linear 0-10 gram range and exerts a force on the wire at a constant rate of 3.3 gm-f/sec. The hook has a diameter of 10.0 mils. The hook is free to swivel and rotate. The pulls were made at or near the center of the wire in a vertical direction. The package was held flat by a vacuum fixture. No attempt was made to level the pad to post plane for each wire. The wire pulls were completed by vendor/package set (i.e., U8, V10, U5 etc). The correlation devices were pulled first, in order, starting with the lowest serial numbered unit within the vendor/package group selected. Next, a vendor/package group (not necessarily the same vendor/package) was selected at random and within this set a unit was selected at random. All available wires on this unit were pulled, the pull strength, failure mode and wire number noted on the data form opposite its serial

number. After all wires were pulled, another device was selected at random from the same group and its wires were pulled and the data logged. After all samples within the vendor/package group were pulled and logged another vendor/package group was selected at random. In this way, the order of the wire pull data was randomized, thus randomizing the measurement error.

Between Vendors (U8, U9, U10 etc)	Random
Between Stresses (T.C/T.S)	Random
Between No Cycles	Random
Between Devices	Random
Between Wire no.'s within devices	Semirandom

All reading nested within a vendor/package group are randomized. "Semirandom" for wires means the wires were normally pulled in some kind of order but not necessarily starting with pin 1 and ending with 14.

4.8.3.2 Data Reduction

A description of the Data Analysis is given in the Appendix.

4.8.3.3 Construction Differences

Table IV-33 gives internal wire length comparison data and Table IV-34 gives wire bonding identification information.

4.8.3.4 Mean Pull Strength Analysis

The first analysis was a three-way analysis of variance. This Anova was restricted to only Vendors 7, 9, 10 and 11, and only cycles 60 through 1020 in order to have a balanced completed

INTERNAL WIRE LENGTH (TYPICAL)							
Vendor	No. Wires	Mean Length Mils	Standard Deviation	Longest	Shortest	Range	Type
5	14	49.93	12.56	66	20	46	M. Flat
7	14	56.57	4.65	62	50	12	Cerflat
8	14	71.00	9.80	83	53	30	Cerdip
9	14	67.64	14.70	93	37	56	Cerdip
10	14	69.64	14.47	96	45	51	Cerdip
11	14	104.29	16.02	124	74	50	Sidebraze
Note: All Devices were 5400 TTL Gates.							

Table IV-33

WIRE BONDING IDENTIFICATION

Vendor	Wire		1st Bond Tail			2nd Bond No Tail			
	Diam. Mils	Mat'l.	Type	To:	Metal	Type	To:	Metal	Notes
5	1.0	Au	Ball	Pad	Al	T/C	Post	Au	(4)
7	1.0	Al	U/S	Pad	Al	U/S	Post	Al	(2)
8	1.0	Al	U/S	Pad	Al	U/S	Post	Al	(2)
9	1.0	Al	U/S	Pad	Al	U/S	Post	Al	"Black Posts" (1) (3)
10	1.0	Al	U/S	Post	Al	U/S	Pad	Al	(2)
11	1.0	Al	U/S	Post	Au	U/S	Pad	Al	(2)

(1) Notched Wedge Used.

(2) Single Wedge Used.

(3) Ground Flats on Internal Post Tips.

(4) Curved, Nonflat Post Bonding Area.

TABLE IV-34

matrix with one value per cell (the mean). Vendor 5, using gold ball bonds, was excluded since these wire pulls were almost twice as high as the others. All the others in the comparison used 1 mil diameter aluminum ultrasonic bonding. Vendor 8 and 30 cycles data were not used because of missing cells.

The Anova results are given in Table IV-35. As indicated, there is a strong "between cells" interaction and "package vs cycles" interaction. Any conclusions about these main effects cannot be made until these interactions are resolved since any observed main effects could be due to the interaction.

The Analysis Of Means[8] for the B x C interaction is given in Figure 4-55.

This method of analysis shows the cells with abnormally low readings are Vendor 9/120 cycle and Vendor 10/240 cycles; and the cells with abnormally high values are Vendor 9/510 cycles and Vendor 10/1020 cycles. Vendors 7, 9, and 10 show significant overall vendor-to-vendor differences. Only the 510 cycles point is out of limits on the analysis of cycles plot.

The overall conclusion from this analysis is that sample error is responsible for these cell-to-cell variations since separate samples had to be pulled for each cell. Therefore, the standard analysis of variance is not usable.

It is still believed that a trend does exist in mean pull strength vs amount of thermal cycling. The data was replotted four ways:

(1) Mean pull strength vs No. cycles (Figure 4-56)

AVWPO

THREE WAY ANALYSIS OF VARIANCE

WIRE PULL STRENGTH..GRAMS FORCE

SOURCE OF VARIATION	SS	DF	MS	F	
STRESS METHODS.....A	0.47	1	0.47	0.92	
VENDOR/PACKAGE.....B	34.71	3	11.57	22.42	* 0.1 %
NO OF CYCLES.....C	7.79	4	1.95	3.77	* 0.5%
PKG VS METHOD.....A*B	0.09	3	0.03	0.06	
CYCLES VS METHOD...A*C	4.01	4	1.00	1.94	
PKG VS CYCLES.....B*C	24.41	12	2.03	3.94	* 0.5%
BETWEEN CELLS....A*B*C	17.90	12	1.49	2.89	* 0.5%
RESIDUAL ERROR.....	564.64	1094	0.52		
TOTAL SUM OF SQRS.....	654.01	1133			

THE POOLED MS (RESID+A*B*C)= 0.53
THE POOLED DF= 1106

TABLE IV-35

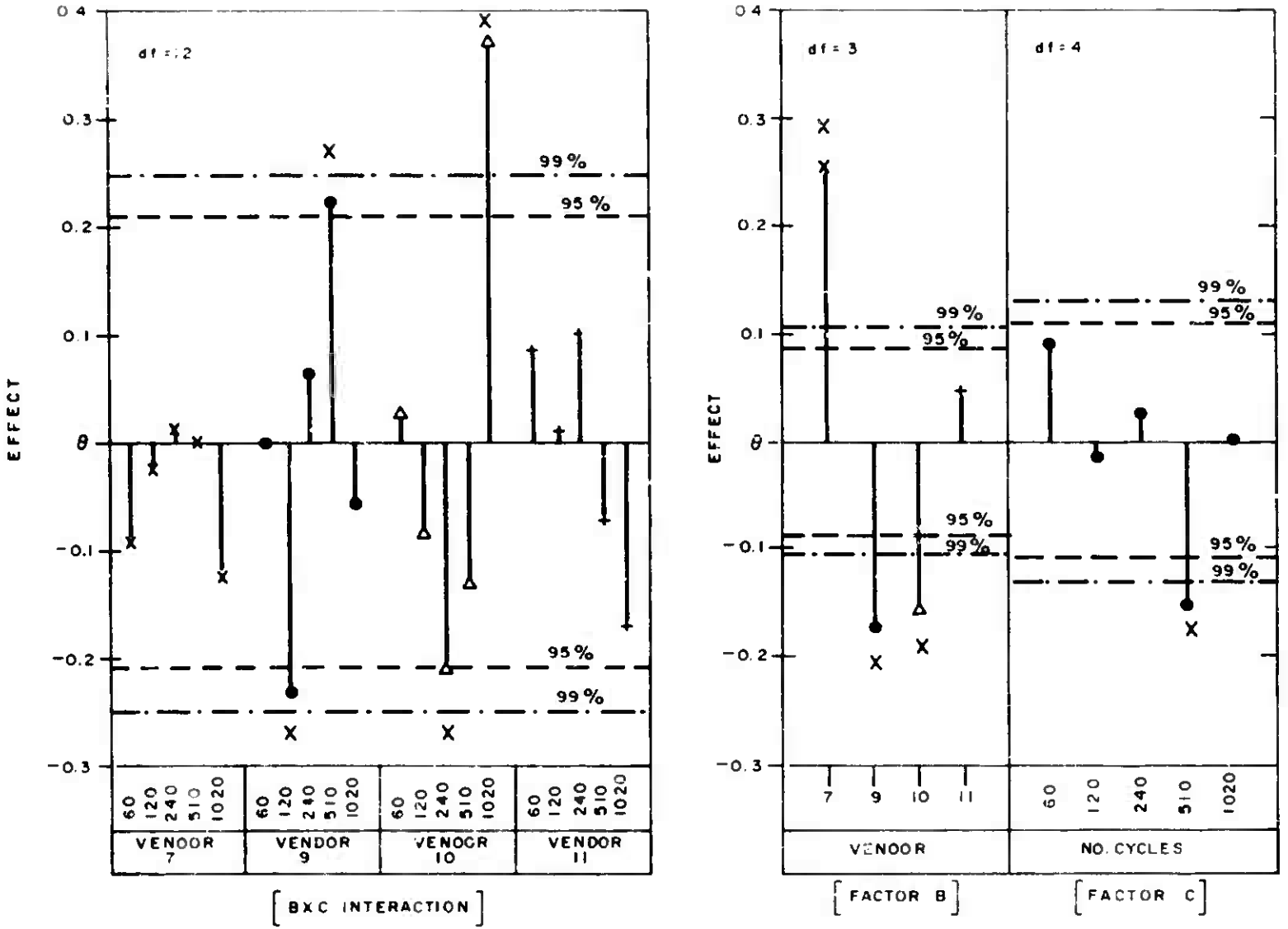

Figure 4-55. Analysis of Means - Wire Pull Strength

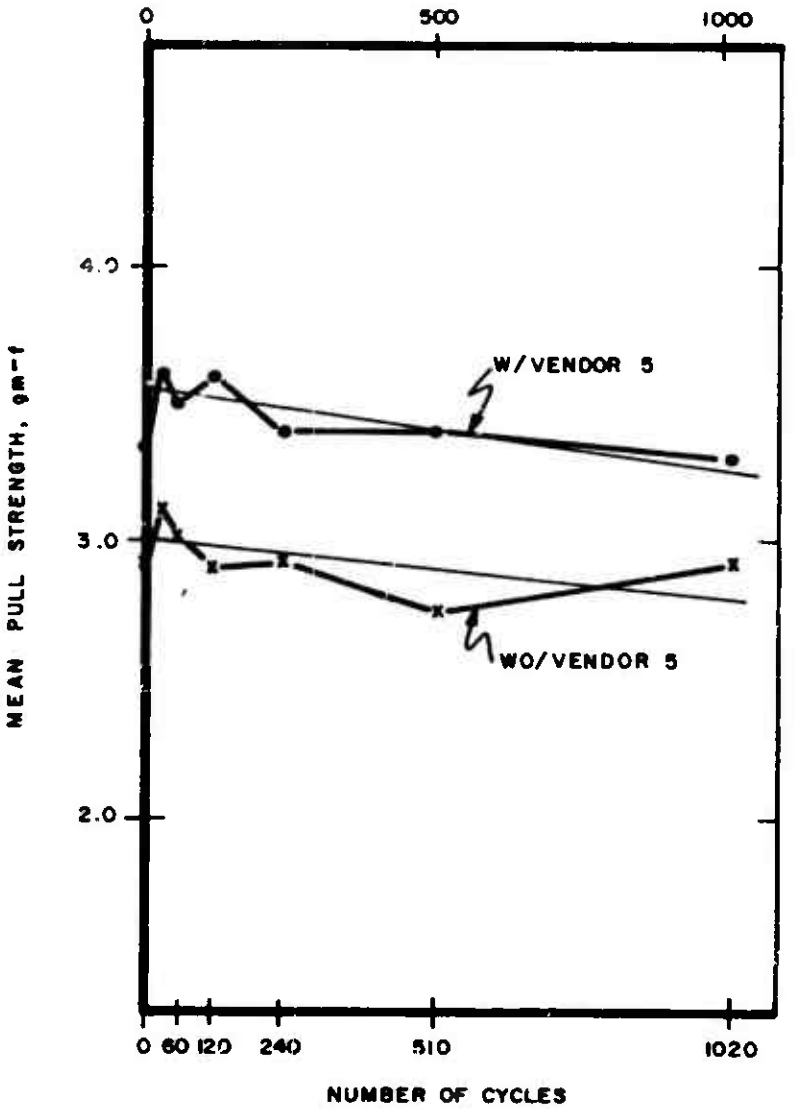

Figure 4-56. Mean Pull Strength vs No. Thermal Cycles

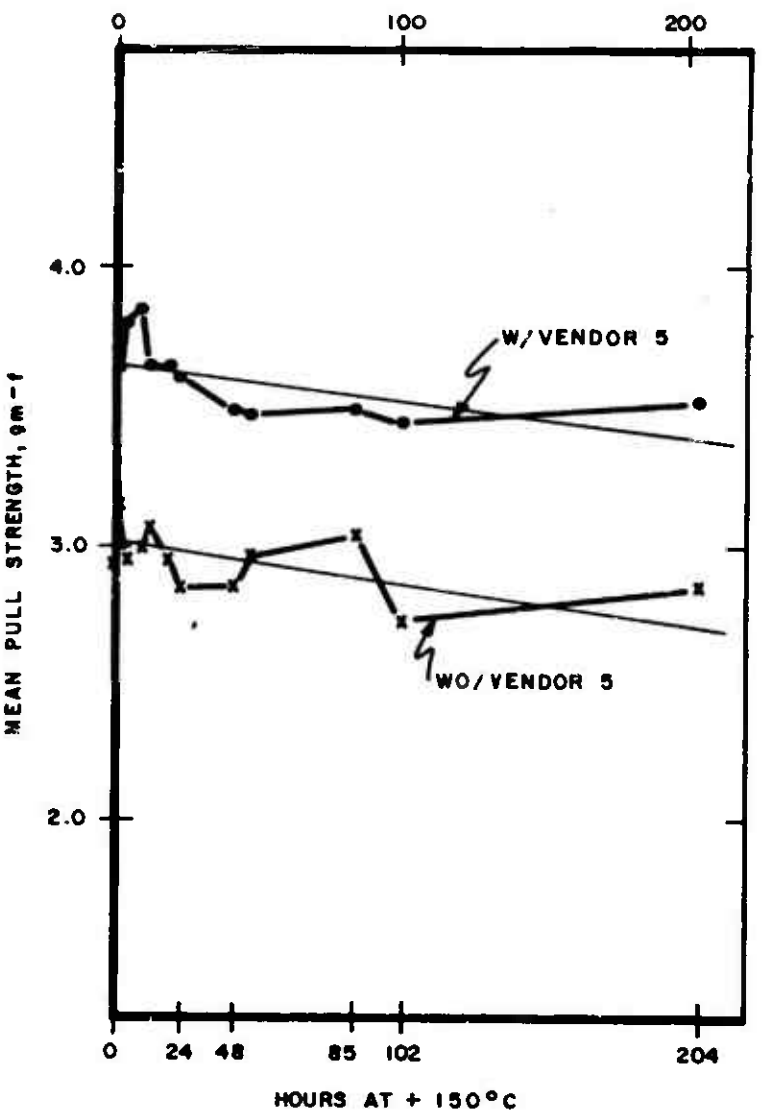

Figure 4-57. Mean Pull Strength vs Hours at +150°C

(2) Mean pull strength vs hours at +150°C
(Figure 4-57)
(3) Mean pull strength vs log (cycles)
(Figure 4-58)
(4) Mean pull strength vs log (hours at 150°C)
(Figure 4-59)

A slight trend does exist both with Vendor 5 (metal flat pack - gold ball bonds) and without Vendor 5.

There is a degradation in wirebond pull strength due to thermal cycling. It is not obvious whether this degradation is linear with cycles, linear with log cycles, linear with hours at 150°C, or linear with log-hours at 150°C. Greater degradation occurs in the temperature cycling cells than in the thermal shock cells as noted in Table IV-36. Also greater degradation occurs to devices with gold-aluminum bonds (Vendors 5 and 11) than to the other CDIP devices.

4.8.3.5 Failure Modes Analysis

Tables WPFM (see Appendix) list all the statistics available on mode of failure for each cell of the wire degradation samples. These data are plotted two ways: Vs log cycles and Vs Log (Hours @ 150°C) for percent BD (Break at the heal of the wirebond to the Die), percent CW (Center Wire between the two heals) and percent BP (Break at the heal of the Post Bond). The percent LD (Loose at the Die bond) and percent LP (Loose at the Post) were also investigated.

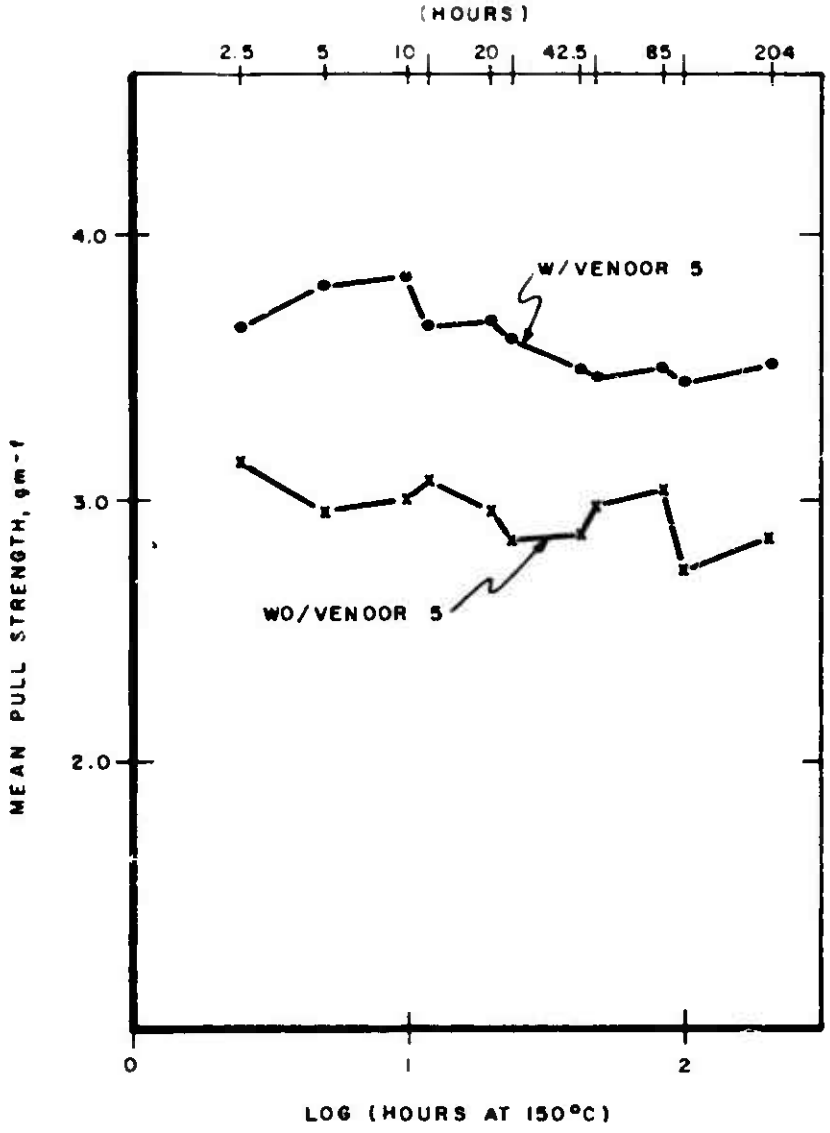

Figure 4-59. Mean Pull Strength vs Log Hours at 150°C

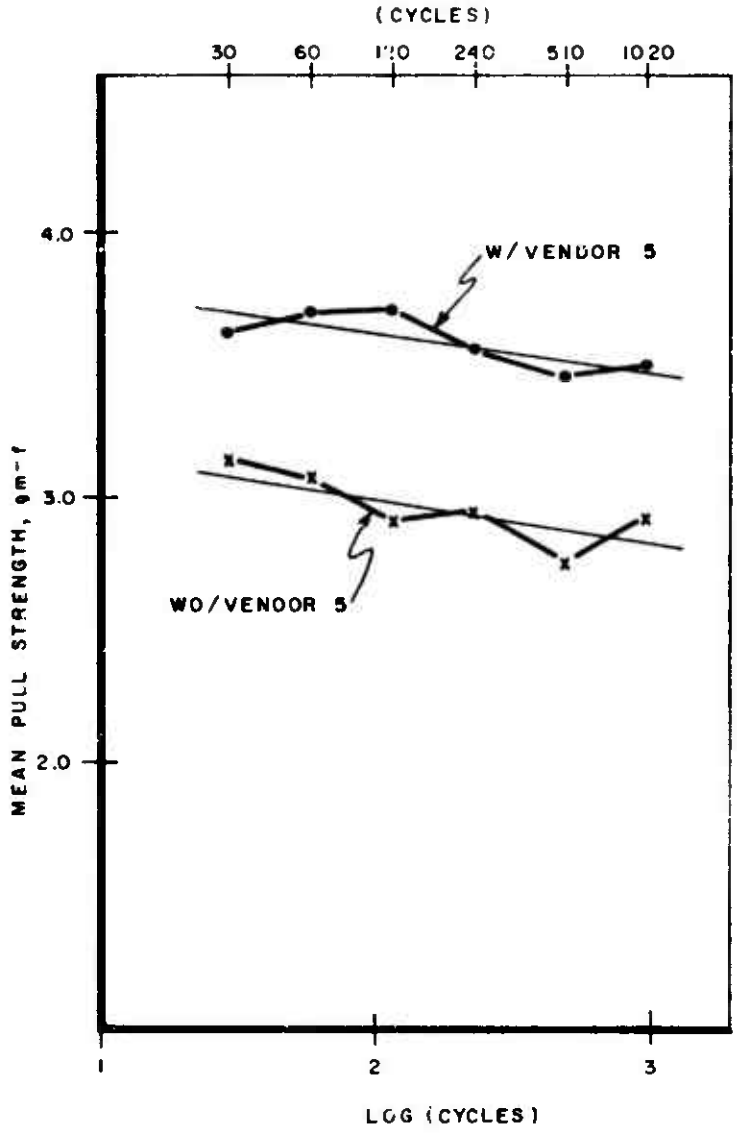

Figure 4-58. Mean Pull Strength vs Log Cycles

SLOPES AND CORRELATION COEFFICIENT Mean Pull Strengths					
Vendor	Temperature Cycling (1010C)		Thermal Shock (1011C)		Combined
	Slope gm-f/Log C	Correl. Coef.	Slope gm-f/Log C	Correl. Coef.	Slope gm-f/Log C
5	-0.089	0.12	-0.464	0.45	-0.276
7	-0.325	0.82	+0.007	0.003	-0.159
9	-0.356	0.56	+0.079	0.15	-0.138
10	+0.295	0.42	-0.139	0.33	-0.078
11	-0.426	0 70	-0.214	0.92	-0.320
Overall	-0.181	0.95	-0.146	0.69	-0.143

TABLE IV-36

4.8.3.5.1 Percent LP

There were only 0.58% LD and 0.23% LP in all samples combined. All of the LD's occurred only on Vendor 11 from 240 cycles through 1020 cycles with 14.81% of the sample having bonds pull loose at the die at the 1020 cycle of temperature cycling. See Figures 4-60 and 4-61.

Each vendor is independent; i.e., his samples were made at different times by different operators from different material than someone else's sample. Since LD's only occurred on Vendor 11, the first conclusion was that this problem is unique to that particular lot of material.

Further microscopic investigation at 100 x - 400 x using Nomarski phase contrast objectives were made of the six failed devices. Comments on this investigation are presented below:

"LP" Failures					Comment
S/N	Group	Cycle	Pin #	P/S	
325	U11	240	12	3.1	Pulled pad metal and big hole in silicon.
343	U11	1020	10	2.5	1 hole in silicon under toe of bond point.
			13	1.4	2 holes in silicon under toe and heal of bond point.
219	V11	510	1	2.2	2 holes in silicon under toe and heal of bond point.
324	U11	1020	6	2.0	Moating - glass on pads - glass under pad visible.
			1	1.3	Moating - glass on pads - glass under pad visible.
227	V11	510	8	1.7	Glass on pads - glass under pad visible.
341	U11	510	8	0.4	Glass on pads.

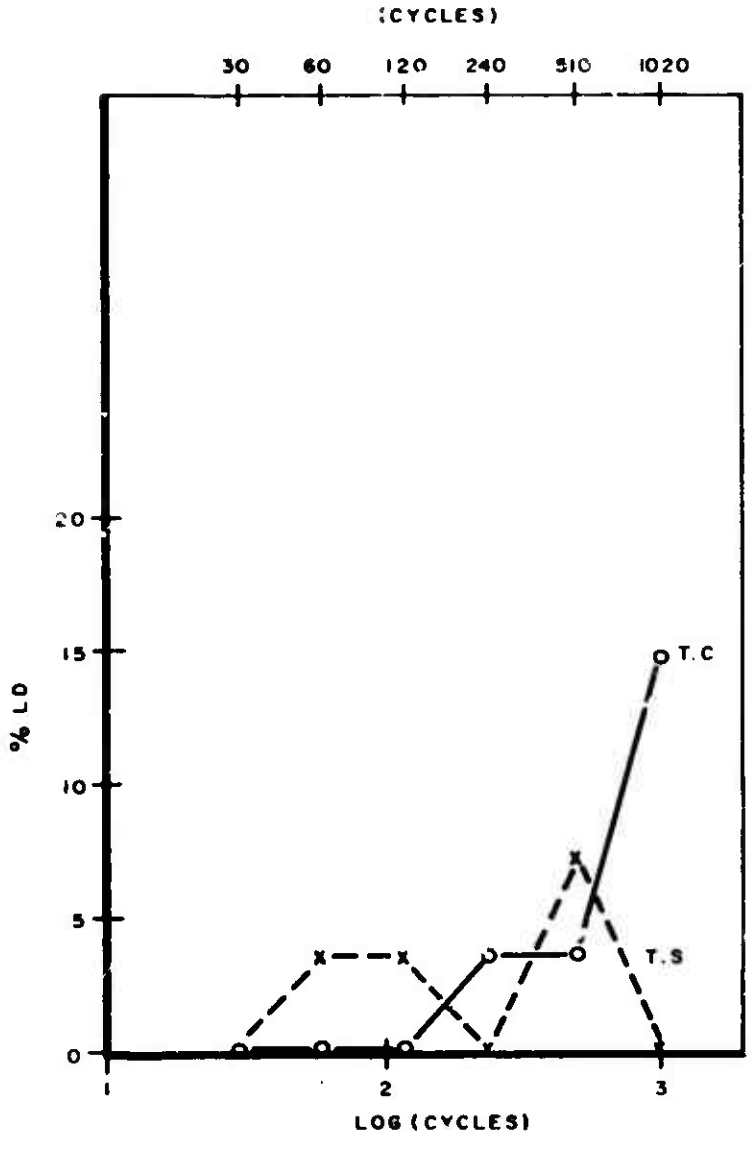

Figure 4-60. Percent LD vs Log Cycles

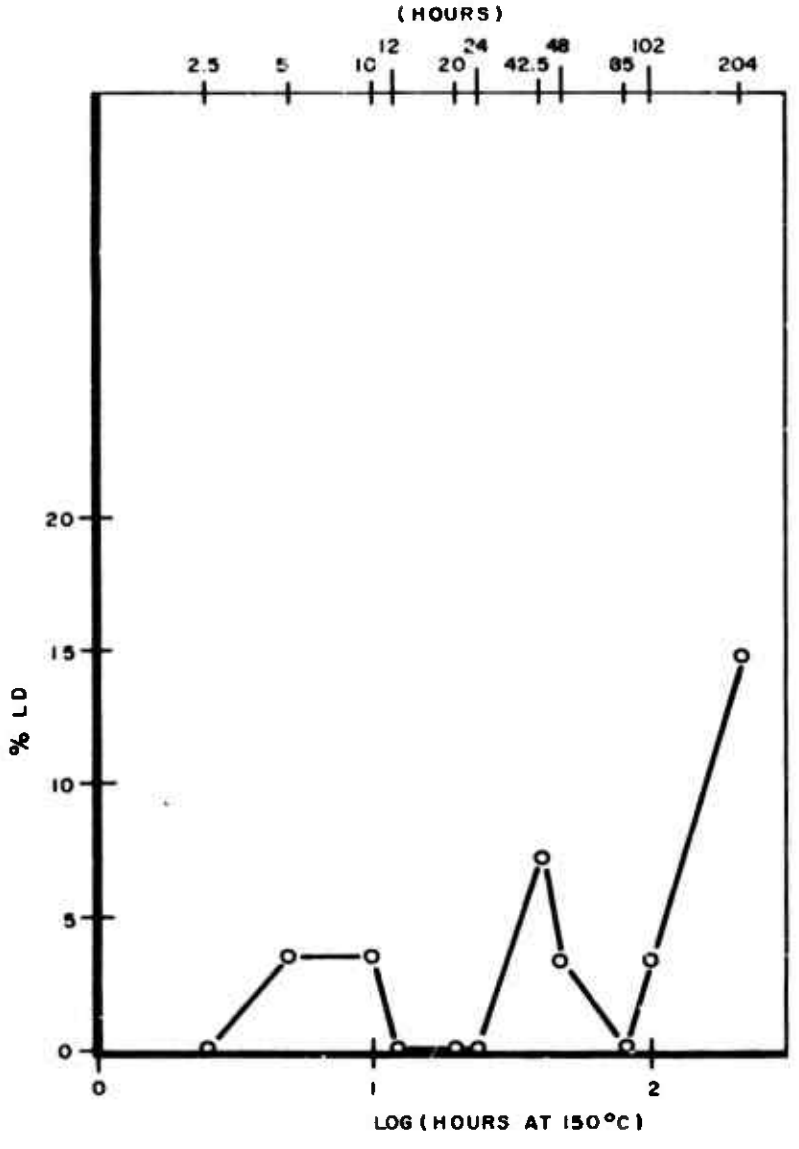

Figure 4-61. Percent Log Hours at 150°C

All devices had dark "mudflat" bonding pads. All bonds to die bonded showed some evidence of high ultrasonic bond energy and/or pressure (moating). All devices failed, leaving some pad metal under the center of the bond.

Therefore, it can be concluded that these devices failed due to faulty wirebonds made through glassivation not completely removed from the bonding pads. Since there was glass on the pads, higher than normal bonding energy had to be used, resulting in ultrasonic "moating" and damage to the pad itself. It is suspected that the initial microcracks under the bonds into the glass and silicon were made during bonding and aggravated by the thermal cycling. The bonds that did have the highest pull strengths (within these 8 readings) also pulled chunks of the pad metal and silicon whereas the lower pull strength samples left exposed glass under and on pads. The 0.4 gm-f sample (S/N 341) had the greatest amount of obvious glass on the bonding pad.

The mechanism of failure is thought to be due to the difference between the relatively high expansion and contraction of the aluminum bond and pad (18-26 x $10^6/^oC$) compared to the much lower expansion and contraction of the glass layer (or wedge) between the bond and pad (0.8 - 1.3 x $10^6/^oC$). The glass contains or restricts the expansion and contraction of the normal bond/pad interface, causing microfracture to occur in the aluminum during thermal cycling - thereby resulting in degradation in pull strength faster at this interface than at the heel of the bond. The major damage should occur during the low temperature excursion (to -65^oC) since the aluminum is trying to contract more than the glass will let it - resulting in a "pulling apart" of the aluminum-to-aluminum interface.

4.8.3.5.2 Percent BD

Break at the die bond was the most common failure mode with some 38% of the bonds exhibiting this failure mode. Figure 4-62 and 4-63 show that no strong trend is evident for this failure mode vs cycles or time.

There were large differences in percent BD from vendor to vendor. These range from 63% (Vendor 9) to 22% for Vendor 10, both CDIP with 1 mil aluminum ultrasonic bonding. Except for Vendor 10 percent BD was more likely than percent BP. This was especially true for Vendors 5 and 9.

4.8.3.5.3 Percent CW

Center wire breaks, breaks in wires between the heels of the bonds, occurred approximately 35% of the time.

The plots in Figures 4-64 and 4-65 show the behavior of percent CW with number of cycles and with time at temperature extreme. No trend is apparent throughout the range of this test.

Again there were gross differences between vendors on percent CW. Vendor 5, using 1 mil gold ball bonds, had twice the percentage of center wire breaks (75%) as any of the aluminum wire samples (36%). Vendor 11, sidebraze DIP, using 1 mil aluminum wire, appears to be more stretchable than the aluminum as well as having a ball bond on the die. The ceramic dual-in-line packages undergo sealing temperatures between 450 - 500°C which causes some annealing of the wire and bonds. Vendor 11 uses a solder sealed lid, attached at about 325°C.

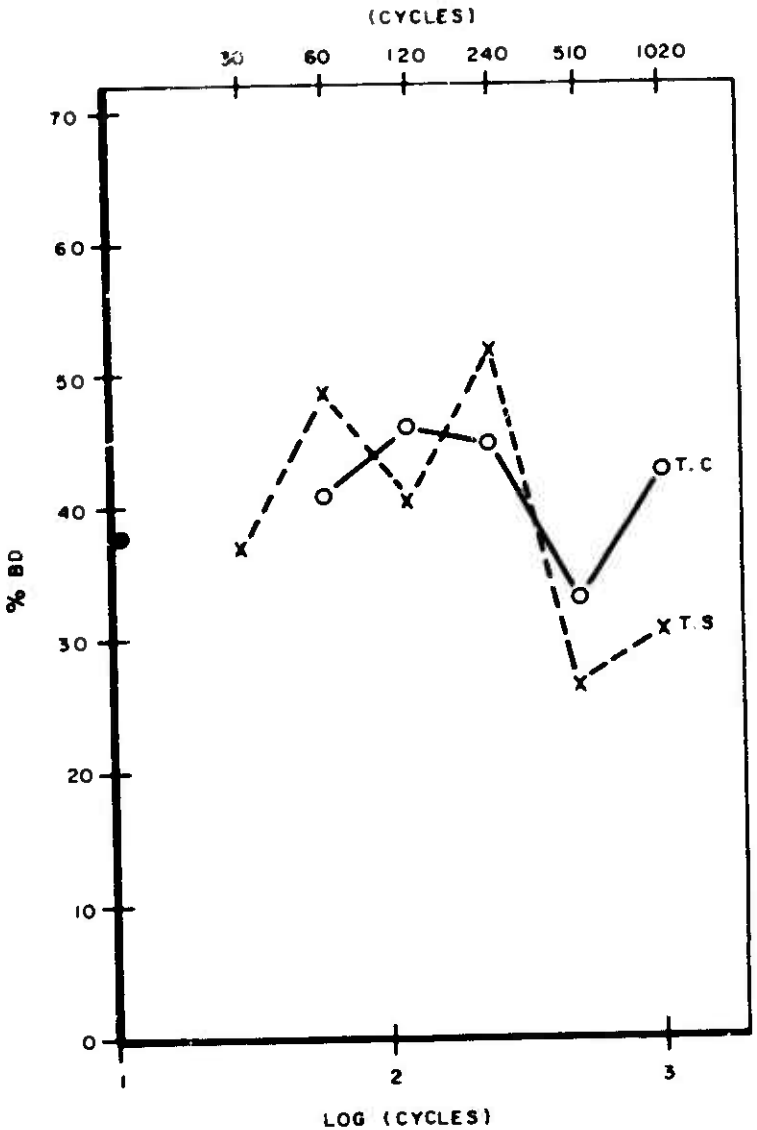

Figure 4-62. Percent BD vs Log Cycles

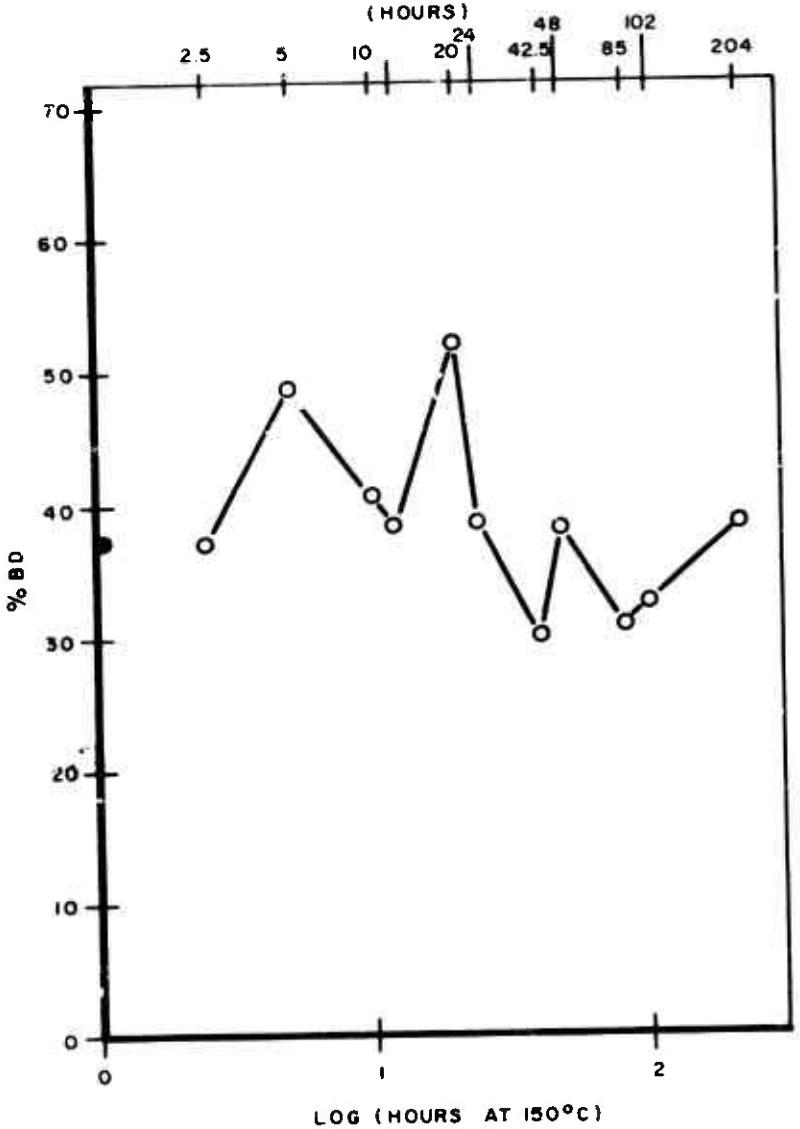

Figure 4-63. Percent BD vs Log Hours at 150°C

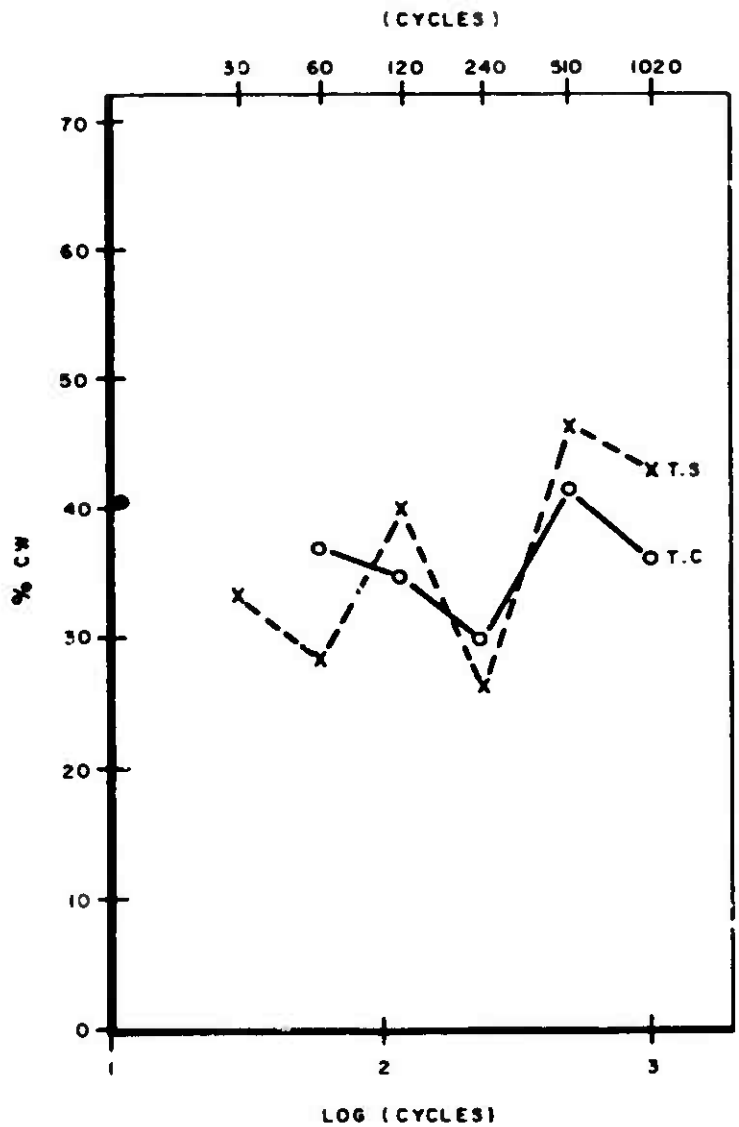

Figure 4-64. Percent CW vs Log Cycles

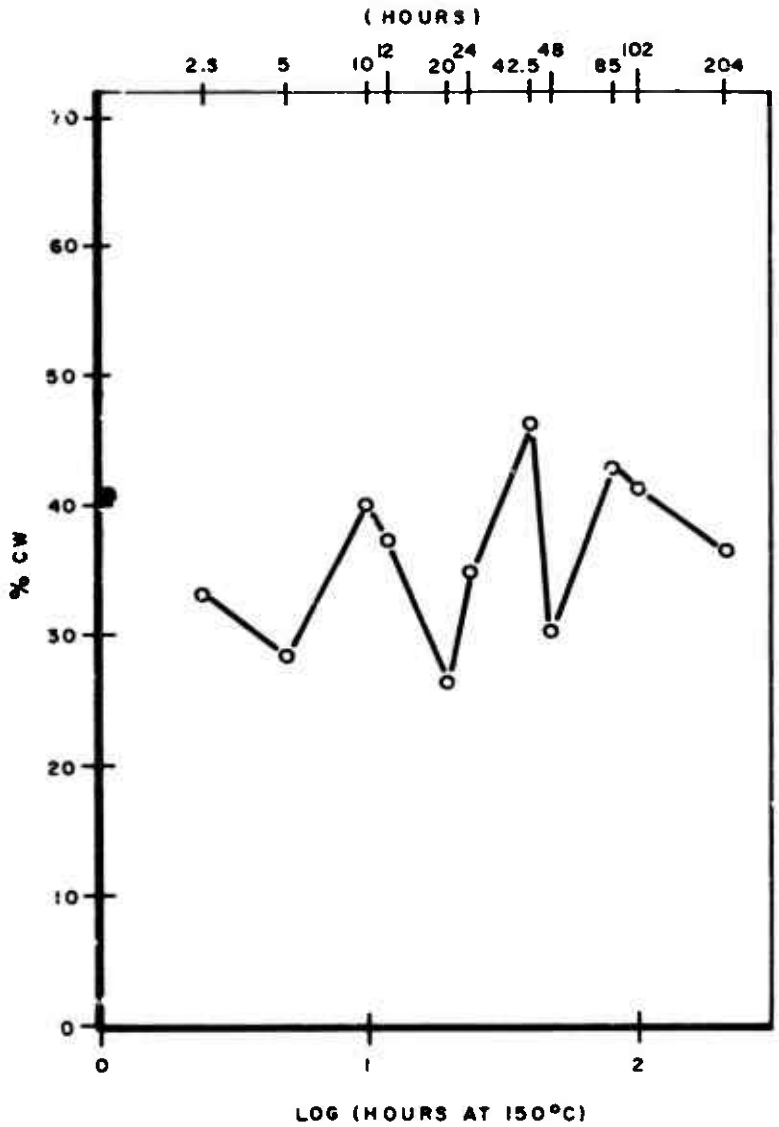

Figure 4-65. Percent CW vs Log Hours at 150°C

Consequently, this product does not see the annealing temperature extremes of the CDIP and thus has far fewer center wire breaks. (Both Vendor 10 and 11 are known to use the same aluminum ultrasonic wire and same bonding machines and bonding schedules.)

4.8.3.5.4 Percent BP

Percent break at the post bond is plotted in Figures 4-66 and 4-67. As with the other failure modes studied, there is no trend effect on this failure mode due to extended thermal cycling or time at temperature extremes over the range of test conditions studied.

4.8.3.5.5 High/Low Values

The most conclusive data showing the degradation of wire-bond strengths with temperature cycling or thermal shock was found by studying the number of low pulls, their lowest values and size of the low pull strength distribution. Figure 4-68 and 4-69 show the response of the highest and lowest values observed over the 1020 thermal cycles and 204 hours at temp extremes. Thermal cycling does not affect the highest value of pull strength observed but definitely affects the lowest value observed. The trend seems to be associated with the increasing number of cycles more than accumulated time at temperature extremes. Although there was a continuous steady degradation from the beginning, zero pulls were not observed prior to the 510 cycle step. There was no obvious difference in response between the gold ball bond sample, the all-aluminum CDIP and sidebraze DIP. Vendor 7, C Flat, was definitely the best performer, and Vendor 11 and 5 the most likely to have

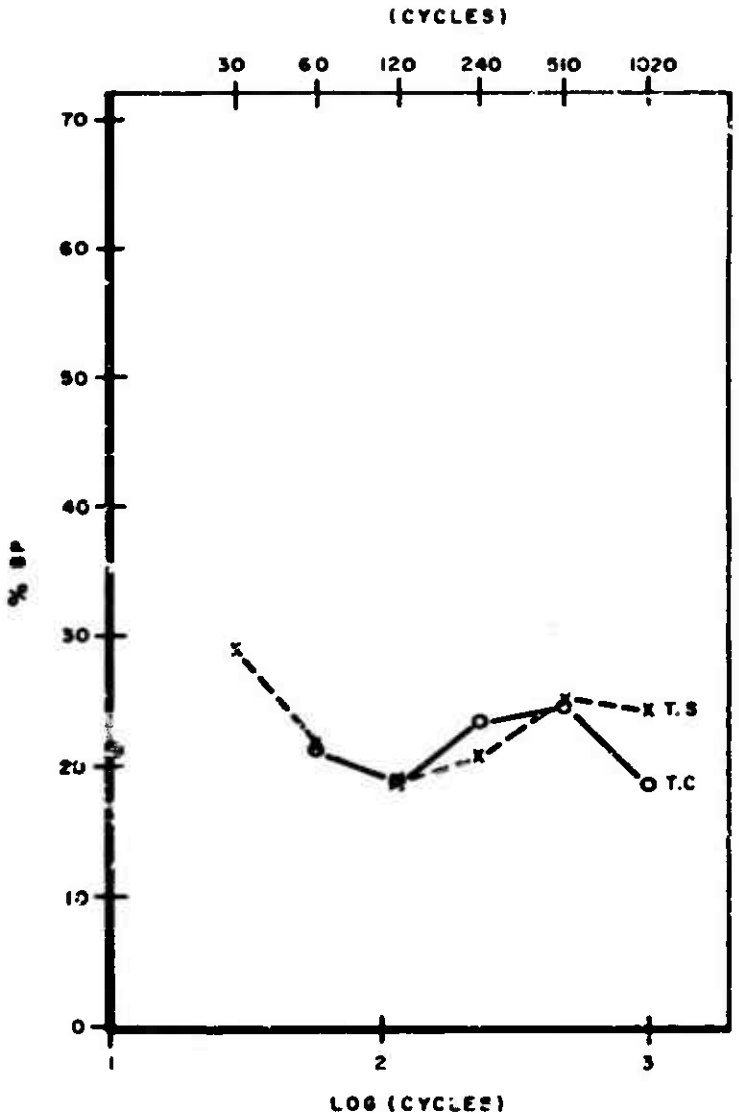

Figure 4-66. Percent BP vs Log Cycles

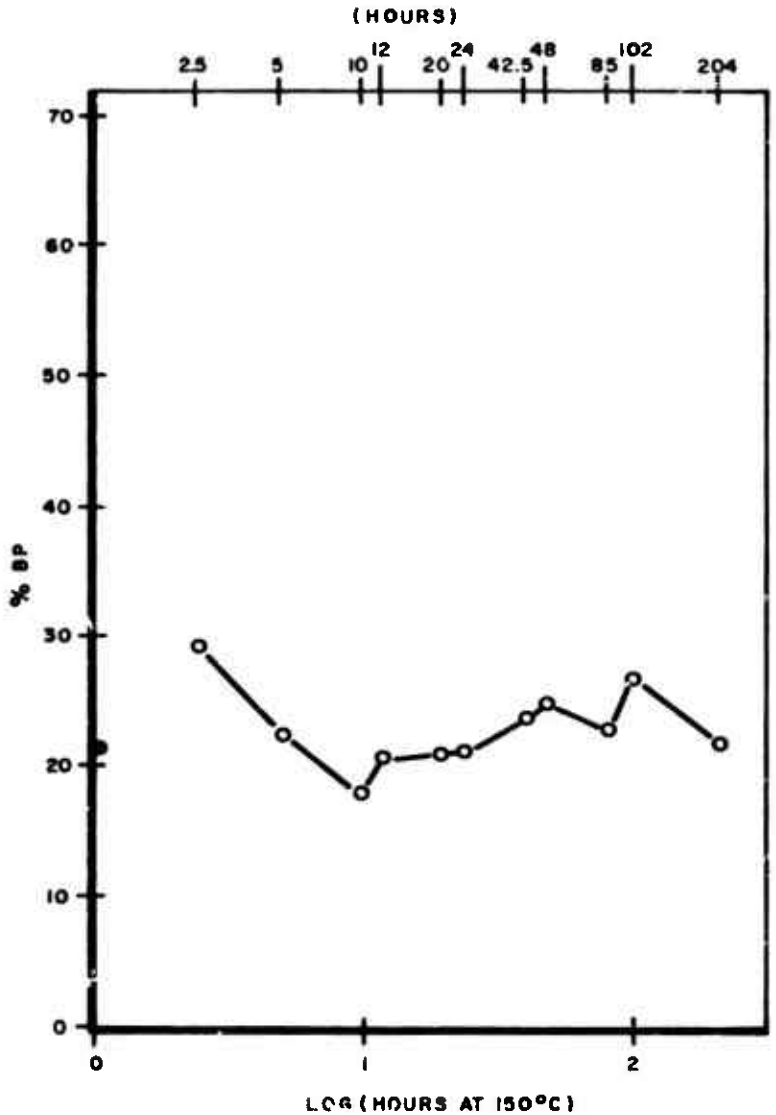

Figure 4-67. Percent BP vs Log Hours at 150°C

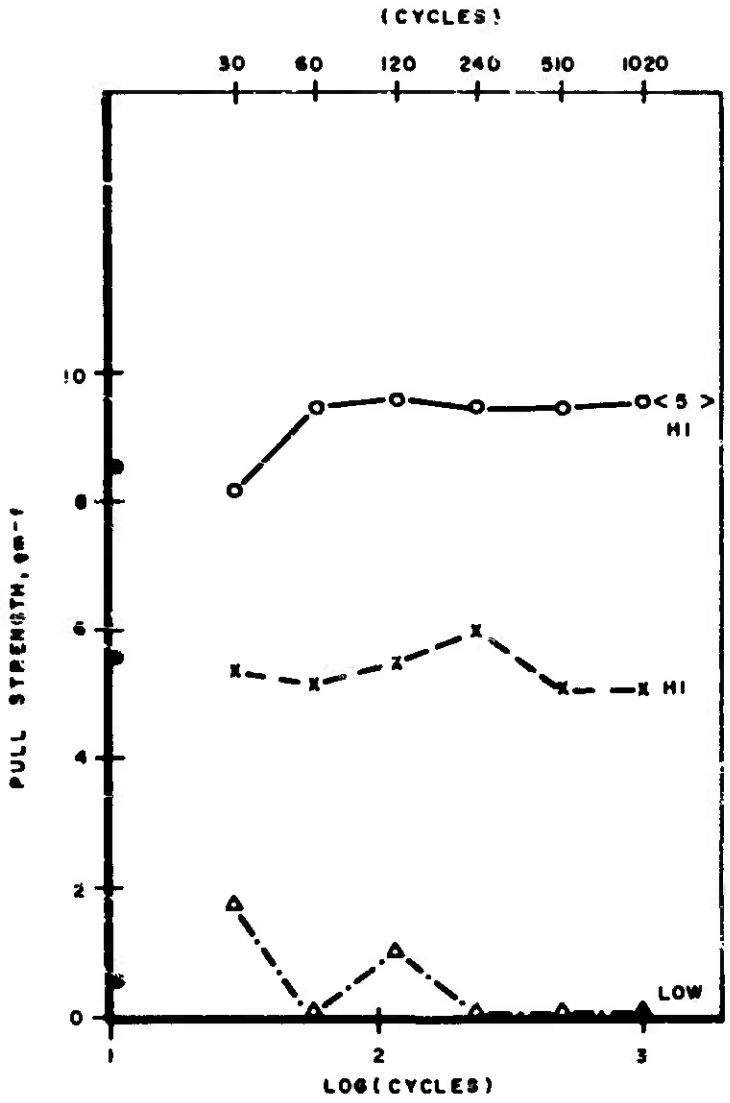

Figure 4-68. Hi/Low Pull Strength vs Log Cycles

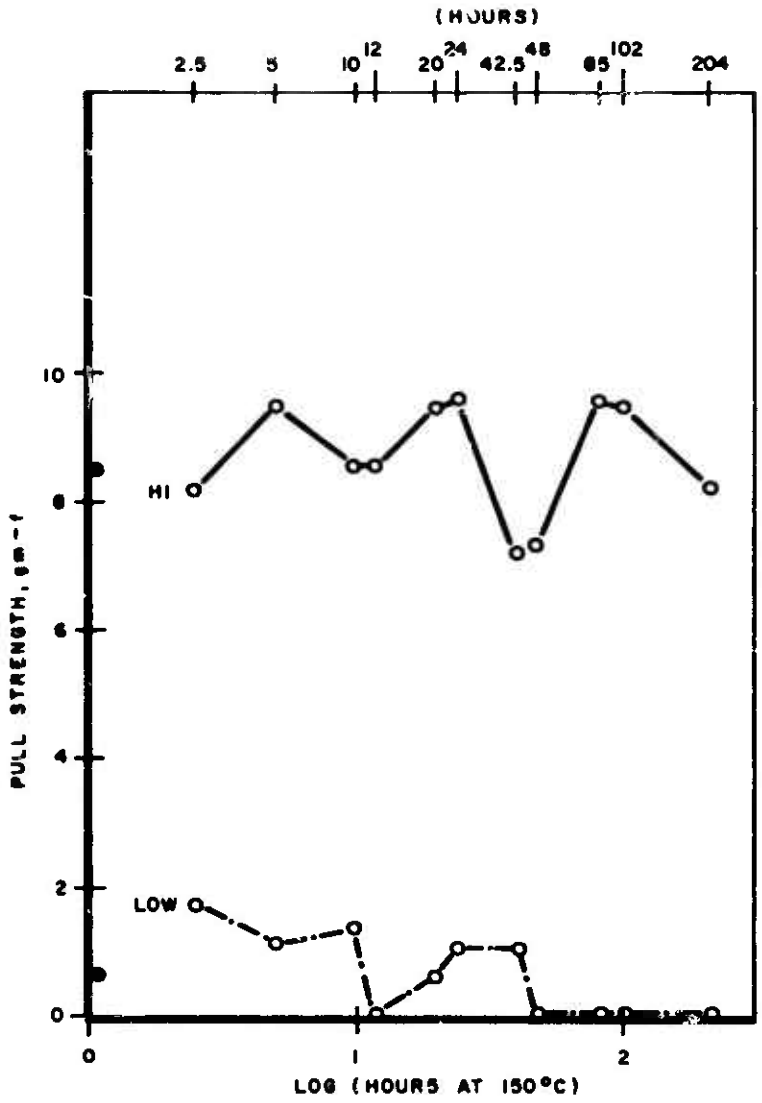

Figure 4-69. Hi/Low Pull Strength vs Log Hours at 150°C

zero pulls. Vendor 9 showed susceptibility to have zero pulls with Vendor 10 having none. The following table (Table IV-37) clearly shows these results. The distribution of low values observed have these mean and standard deviations. There were N = 11 values for each vendor used - one from each cell. Vendors 11 and 5, the ones with the greatest probability of having zero pulls, have gold/aluminum bonds. Vendors 7, 9, and 10 have all aluminum bonding systems. Vendor 9 had "black" posts - possibly indicative of extensive oxidation of the post aluminum. None of the other vendors showed any signs of "black" posts. There was evidence of aluminum directly under each of Vendor 9's post bonds.

4.8.3.5.6 Percent $\leq$ 0.5 Gm-f

If pull strength degraded with increase in stress, there should be more values with very low readings as time passed. This is surely the case as shown in Figures 4-70 and 4-71. Here are plots of the percentage of values less than or equal to 0.5 gm-f - the extreme lower tail of the distributions.

There were no values below 0.5 gm-f for the first 240 cycles; then a positive increase in low values occurred. Again, the best fit seems to be associated with increase in number of thermal cycles.

All failures occurred with Vendors 5, 9, and 11, the same ones shown to have the most susceptibility to zero pulls in the Hi/Low evaluation. In this case, though, additional interesting information surfaced. On Vendors 5 and 11, the failures occurred as BP, Break at the Post, and on Vendor 9, BD, Bread at the Die.

Distribution Statistics of "Lowest" Pull Strengths

Vendor	Mean	S. Dev.	$\bar{x}$ = ( )s
5	3.53	1.76	$\bar{x}$ = 2.01 s
7	1.84	0.29	$\bar{x}$ = 6.34 s
9	1.49	0.64	$\bar{x}$ = 2.33 s
10	1.52	0.43	$\bar{x}$ = 3.53 s
11	1.46	0.83	$\bar{x}$ = 1.75 s

TABLE IV-37

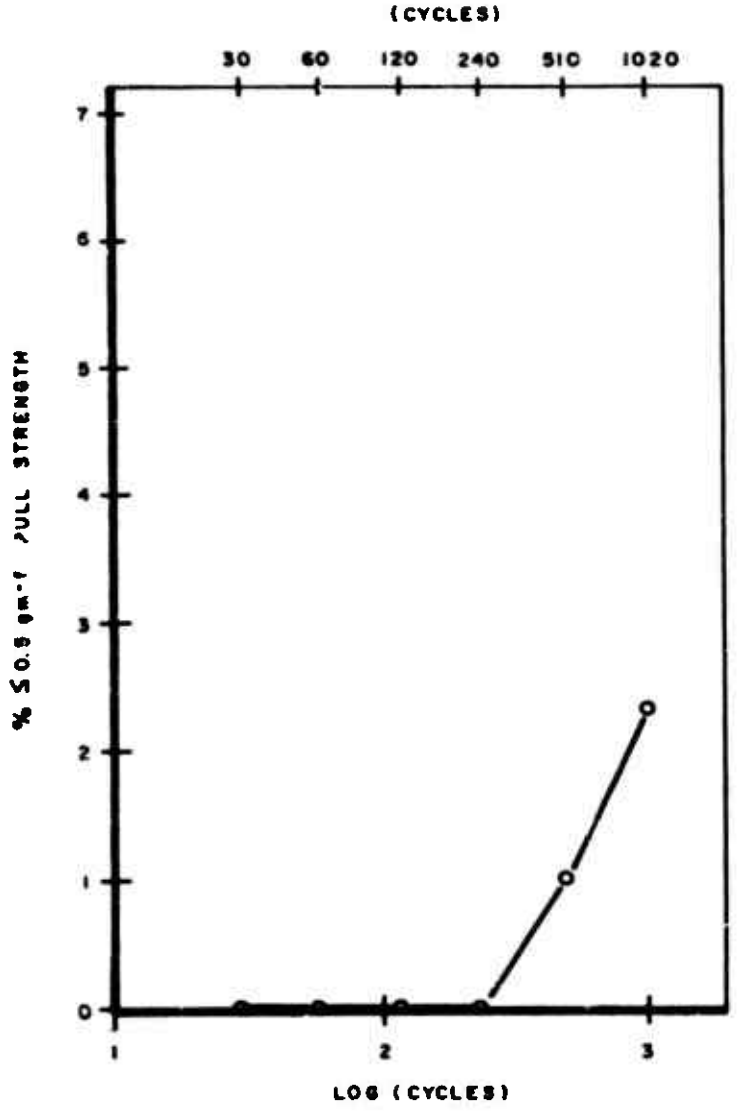

Figure 4-70. Percent ≤ 0.5 gm-f vs Log Cycles

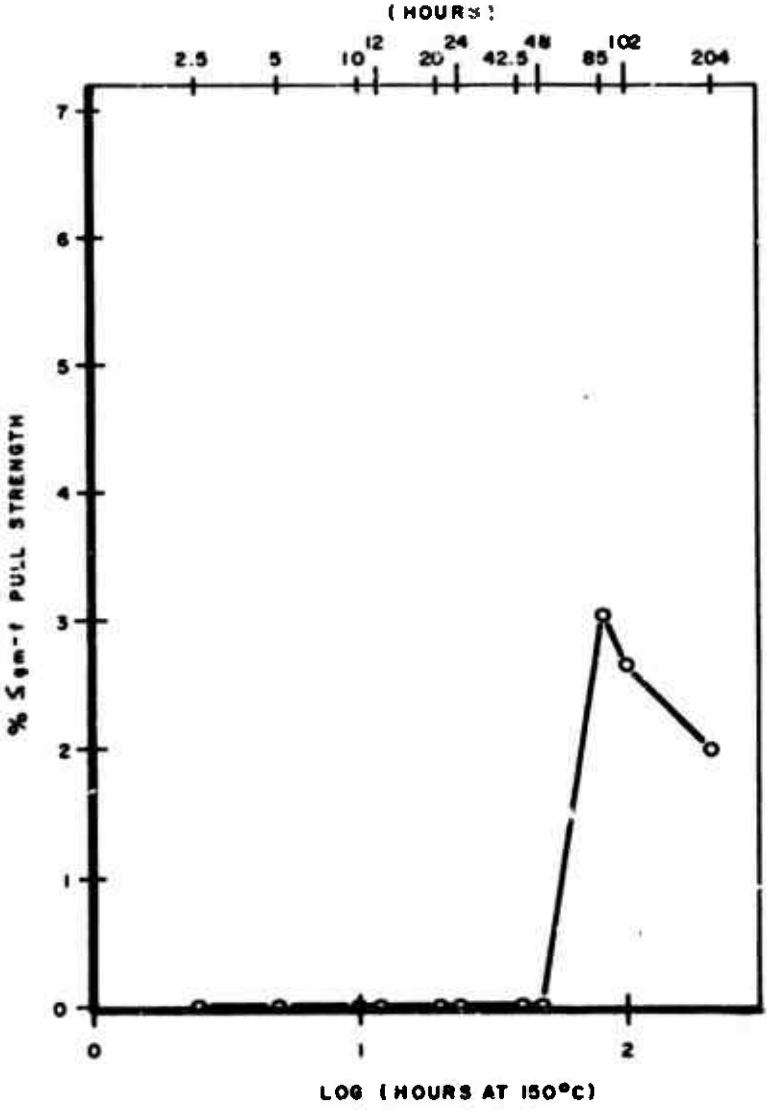

Figure 4-71. Percent ≤ 0.5 gm-f vs Log Hours at 150°C

In all cases, there was no evidence of damage or displacement of the wires prior to obtaining the zero pulls. All these zero pulls are considered true "zero" pulls and are not the result of the decapping operation. Also, all of these failures were on the longest wires in the package. In the case of Vendor 11, all failures were associated with the gold/aluminum ultrasonic post bond; whereas with Vendor 5, the failures were not associated with the gold-aluminum bond but with the gold-to-gold "wedge" type post bond.

The overall conclusion must be that thermal cycling does lead to wire bond strength degradation and that the degradation affects the longest (end) wires first. The probability of zero strength following thermal cycling is greater if the bonding system has a wedge or capillary type bond, rather than a ball type bond.

4.8.3.5.7 Percent < 1.5 gm-f:

Although not as obvious as the % $\leq$ 0.5 gm-f response, the % $\leq$ 1.5 gm-f, Figure 4-72 and 4-73, also show evidence of wirebond strength degradation. The tables show that there were some 46% more wire pull strengths $\leq$ 1.5 gm-f in the temperature cycling groups as in the thermal shock groups.

The following analysis shows how they compare:

% < 1.5 gm-f				
-65/+150°C	60c	1020c	Ave.	Diff. Ratio
Temp. Cycle Thermal Shock	1.84 2.26	6.22 3.25	4.03 2.76	1.27
Ave.	2.05	4.73		
Diff Ratio	2.68 2.30			

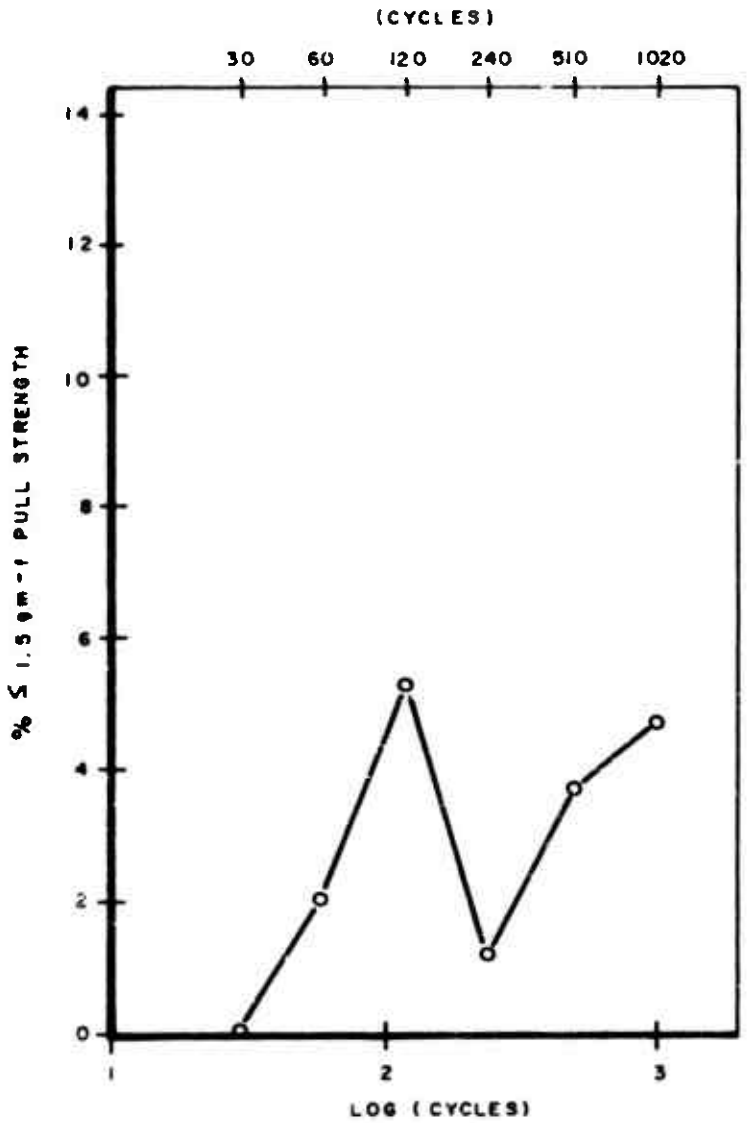

Figure 4-72. Percent ≤ 1.5 gm-f vs Log Cycles

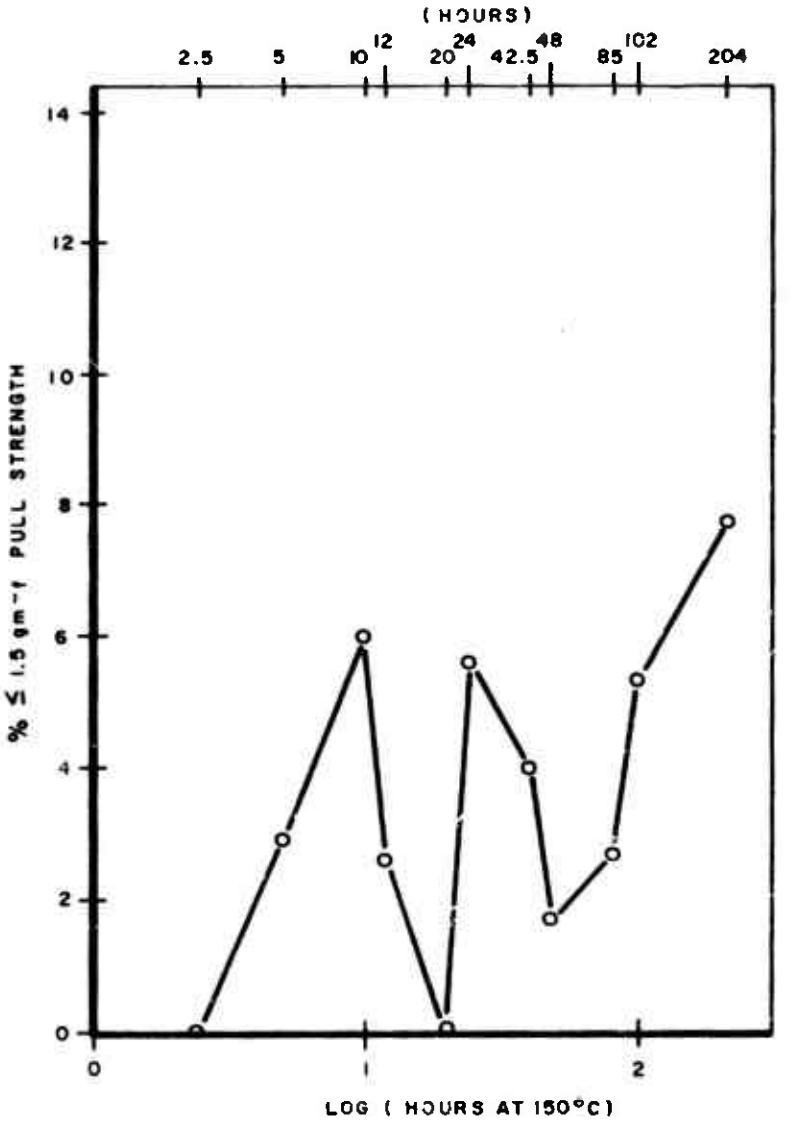

Figure 4-73. Percent ≤ 1.5 gm-f vs Log Hours at 150°C

This table indicates that the thermal shock groups had a greater number of % $\leq$ 1.5 gm-f than did the temperature cycled groups at 60 cycles. By the end of 1020 cycles, this relation had reversed itself. The temperature cycled groups now had much more product less than 1.5 gm-f than did the thermal shock groups.

4.8.4 Overall Conclusions From Wirebond Degradation Study

When integrated circuits, packaged in metal flat packs, ceramic flat packs, ceramic dual-in-lines or sidebraze ceramic dual-in-line packages are subjected to either -65°C/+150°C temperature cycling or thermal shock, degradation of the hermetic seal and wirebonds can result. This degradation starts from the first cycle and is progressive as the number of cycles is increased. If enough cycles are attempted, catastrophic failure will result.

In general, air-to-air temperature cycling affects wirebonds and wirebond strength. Liquid-to-liquid thermal shock affects the hermeticity of the package and to a lesser extent the wirebond strength. In almost all cases, flat packs did better than dual-in-line ceramics, and sidebraze DIP did better than standard ceramic DIPs.

Within the ceramic dual-in-line samples, there were large vendor-to-vendor differences in response. Vendor 9 had the strongest package but weakest bonding. Vendor 8 performed so poorly, it is suspected that our sample was not representative of this vendor's true reliability. Vendor 10 had a weak package seal but good wire bonding.

The CERFLAT. Vendor 7 was the best performer across the board. This package had no hermetic, mechanical, or electrical failures throughout 1020 cycles of temperature cycling or thermal

shock and also had no zero wire pulls. The standard deviation of wirebond strength was the second lowest value, 0.72. This overall good performance is attributed to the following factors:

(1) Small Size: Therefore smaller expansions of the lead frame, body and lid during thermal cycling.
(2) Less ceramic mass: Change temperature more easily - distribute temperature around and through package more uniformly.
(3) Shorter wires: The average wire length was only 56.57 mils with a range of only 12 mils. (The next smallest range was Vendor 8 with 30.)
(4) Square Package: Minimizes expansions and contraction extremes normally associated with long narrow packages. Also allows wires to be more nearly the same length.

If a wedge type bond is thermally cycled, it will probably fail before a ball bond and if it is a gold/aluminum wedge type bond, it will fail more often than an aluminum/aluminum bond.

Gold wire is heavier and softer than aluminum. There are significantly more center wire breaks with the gold wire than with aluminum wire. When aluminum wire is used, it is annealled by the high capping and therefore yields more center wire breaks. The fewest center wire breaks occurred on the sidebraze DIP sealed at a much lower temperature.

The longer the time at temperature extremes, the greater the degradation of the wirebond strength. The rate of change of temperature appears to have little effect on wirebond strength but a pronounced effect on hermeticity and seal strength.

Unfortunately, since separate samples had to be pulled at each step, the "sample" variations masked any obvious break point in the fallout vs cycles response which might indicate a logical 100% screen specification.

4.9 SEAL STRENGTH - TORQUE

From previous experiments, there was reason to believe that the glass to ceramic seal used on ceramic dual-in-line packages would be weakened by exposure of the parts to thermal cycling. It was further proposed that liquid-liquid thermal shock would cause more degradation of the seal strength than would air-air temperature cycling since the ceramic and glass parts would be forced to change temperature faster than the thermal response time of the system would allow. Of particular interest was whether Thermal Shock, Method 1011, Condition A, $0^{\circ}C$ to $100^{\circ}C$, would cause degradation of the seal strength since this condition has been specified for use as a 100% screen on high reliability integrated circuits in the past. With this in mind, the following test plan (Figure 4-74) was proposed and executed.

4.9.1 Procedure

(1) The device is placed in the fixed holding chuck, lid down.
(2) The chuck is hand-tightened so as to just hold the lid without wobble.
(3) The upper socket is lowered over the base and rotated slightly until it seats
(4) The torque wrench indicator is set to zero.

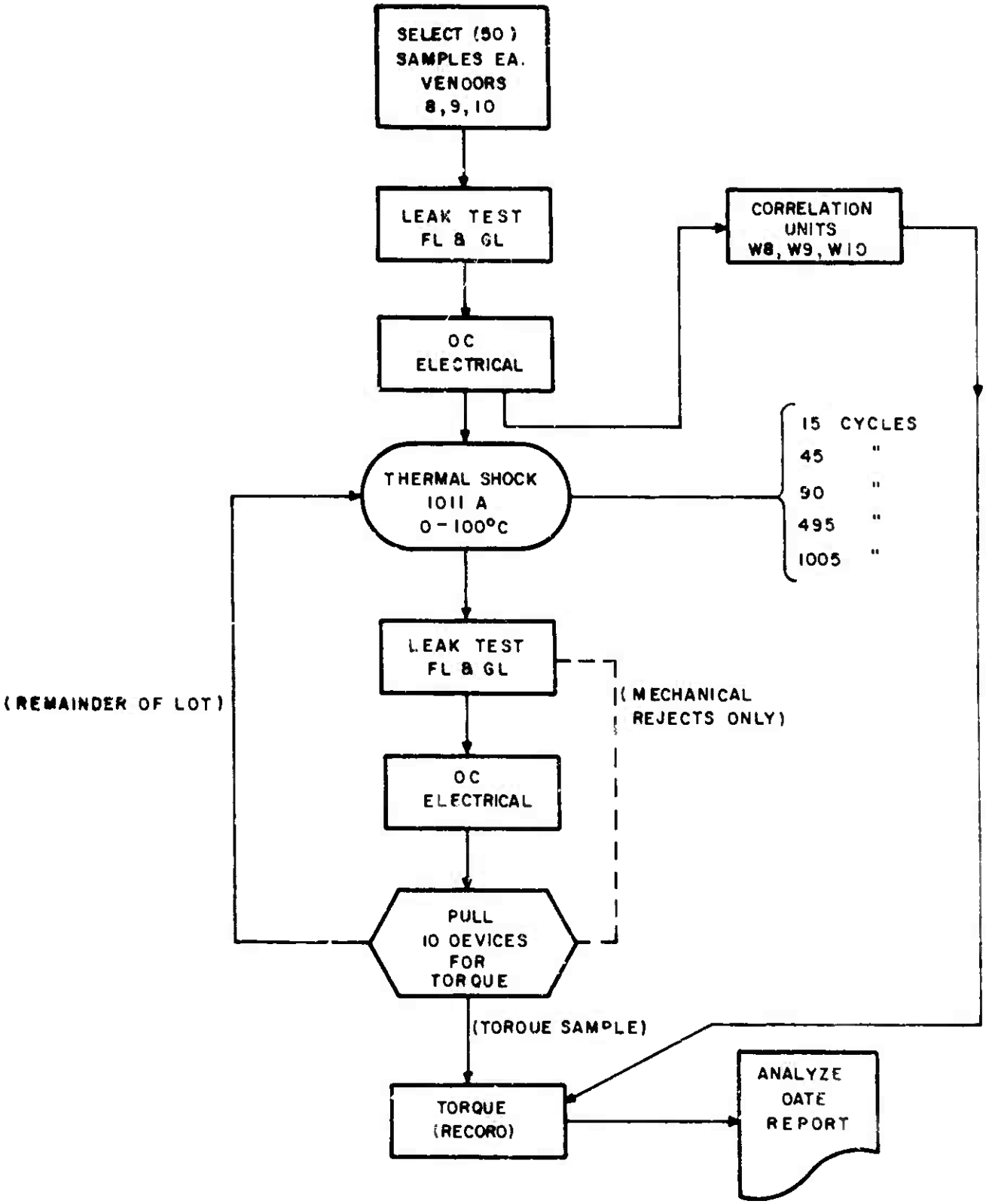

Figure 4-74. Torque Evaluation Test Plan

(5) The torque is applied slowly (approximately 10 inch - lbs/second) until the device fails or the maximum reading on the torque wrench is reached.

(6) If the device failed, the torque value is recorded. If the device did not fail, it was removed and retested later using a higher range torque wrench.

(7) All torque testing was done by the same operator using the same equipment and same torque wrenches. All wrenches had valid calibration stickers.

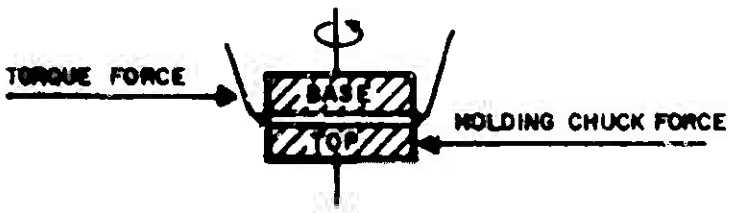

Because of the difficulty with fixturing, only CERDIPS are torqued.

4.9.2 End Point Test Results

The end point tests included hermeticity, DC electrical, mechanical fallout, and torque test results.

4.9.2.1 Hermeticity Results

As the result of subjecting these parts to Thermal Shock, Method 1011A (0 - 100°C), rather than Condition C, all hermeticity fixtures in this test were helium leak failures, > 1×10^{-8} atm cc/sec. Only one gross leak failure occurred - Vendor 8 at 1005 cycles. This result is significantly different from those found in Section 4.8 where the parts were subjected to test Condition C

(-65°C to +150°C). Again, there is an obvious vendor-to-vendor difference with Vendor 9 having a very strong package and Vendors 8 and 10 having a weaker package. Table IV-38 gives these results.

The same general pattern of failure is seen here as in Section 4.8 - a weak population followed by a break in the curve with a normally distributed strong population. The failure rates are not constant (not exponentially distributed) but some comparisons can be made. (See Figures 4-75 and 4-76.)

Helium Leak Failure Rates - Thermal Shock
(0 - 100°C)

Vendor	% in Lower Tail	[%/cycle] in (10-20%) Tail	[%/cycle] in (80-90%) Tail	Ratio
X8	79%	0.37	0.0114	32.6
X9	0%	-	-	-
X10	32%	0.83	0.0357	23.3

The reason for the double distribution is not obvious at this point. Vendor 9 has the best built package with no failures experienced throughout the entire 1005 cycles. Vendor 8 had 79% of the population in the weak distribution with an average failure rate of 0.37%/cycle between the 10% and 20% points. The average failure rate between the 80th and 90th percentiles is only 1/32.6 that of the weak population. In Vendor 10, 32% is in the lower tail with a 0.83%/cycle average failure rate. This failure rate is 23.3 times greater than that of the strong population.

An important observation was noted on all parts, both the "weak" and "strong" distribution units following red dye gross leak verification. All devices showed signs of structural

	Lot X Seal Strength Degradation (1011A, 0°C/100°C)							
	Hermeticity Failures vs Sample Size at Step							
	Vendor #	S.S.	No. of Cycles 15	45	90	495	1005	Total Hermeticity Failures
CDIP	8	50	3/50	4/40	23/30*	2/20	2/9	34
	9	50	0/50	0/40	0/30	0/20	0/10	0
	10	50	4/50	4/40	9/30	8/20	4/10	20
			7/150 4.7%	8/120 6.7%	31/90 34.4%	10/60 16.7%	6/29 20.7%	54

*Indicated fine leakers: 13/23 remained with lot

TABLE IV-38

	Lot X Seal Strength Degradation (1011A, 0°C/100°C)							
	Electrical Failures vs Sample Size at Step							
	Vendor #	S.S.	No. of Cycles 15	45	90	495	1005	Total Electrical Failures
CDIP	8	50	0/50	0/40	0/30	0/20	1/9	1
	9	50	0/50	0/40	0/30	0/20	0/10	0
	10	50	0/50	0/40	0/30	0/20	1/10	1
			0/150 0%	0/120 0%	0/90 0%	0/60 0%	2/29 6.9%	2

TABLE IV-39

Lot X	Seal Strength Degradation (1011A, 0°C/100°C)						
	Mechanical Failures vs Sample Size at Step						
	Vendor #	S.S.	No. of Cycles 15	45	90	495	1005	Total Mechanical Failures
CDIP	8	50	0/50	1/40	0/30	1/20	1/9	3
	9	50	0/50	0/40	0/30	0/20	0/10	0
	10	50	0/50	0/40	0/30	0/20	0/10	0
			0/150 0%	1/120 .8%	0/30 0%	0/20 0%	1/29 3.4%	3

TABLE IV-40

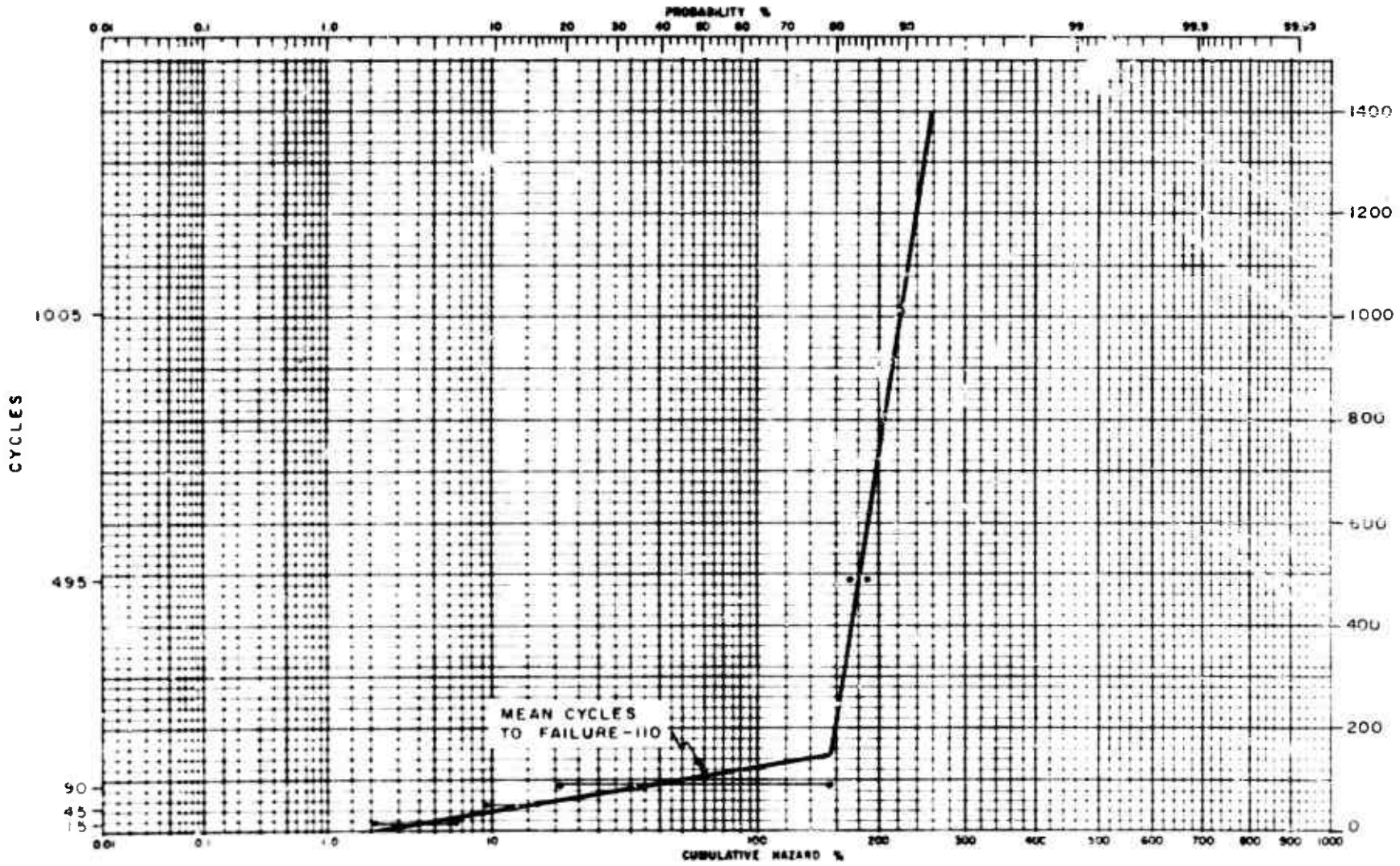

Figure 4-75. Distribution of Fine Leak Failures - Sample X8

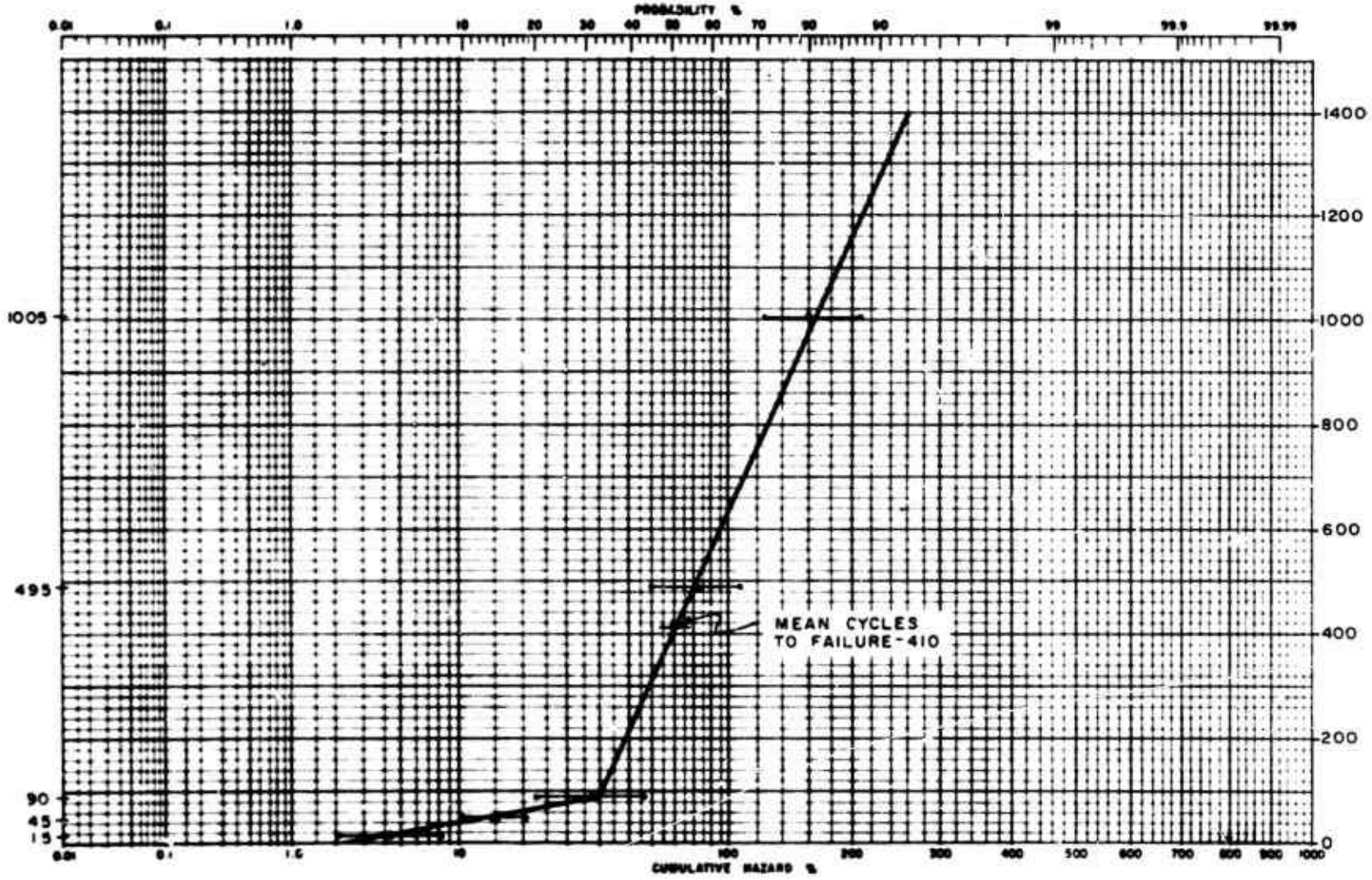

Figure 4-76. Distribution of Fine Leak Failures - Sample X10

seal degradation - microcracks in and around the glass, glass/ ceramic interface. The red dye did not penetrate completely into the package so the devices were not leakers. It is evident, however, that thermal shock does cause glass strain damage, to some extent, to all the CDIP device.

4.9.2.2 Electrical Results

Only two electrical failures occurred throughout the 1005 thermal shocks. These were found at the 1005 cycle readout. This is consistent with previous results and indicates that thermal shock does not cause electrical failures to a significant extent. See Table IV-39.

4.9.2.3 Mechanical Results

Three mechanical failures were noted during this test sequence. All were Vendor 8 and were spaced out over the length of the cycling. The first was a broken external lead found at the 45 cycle readout. The remaining two were fracture at the lead frame seal - causing the parts to fall apart when inserted into a socket. See Table IV-40.

4.9.2.4 Torque Test Results

Histograms of the torque values from samples X 8, X9, and X 10 are plotted in Figure 4-77. This figure shows that Vendor 9 had the most consistant torque distributions except for one maverick (below 3 sigma limit) reading after 90 cycles. Most of the torque values were above 50 inch - lbs and only a few readings taken with the larger torque wrench were less than 50 inch - lbs. This indicates the first 50 inch - lb torque application

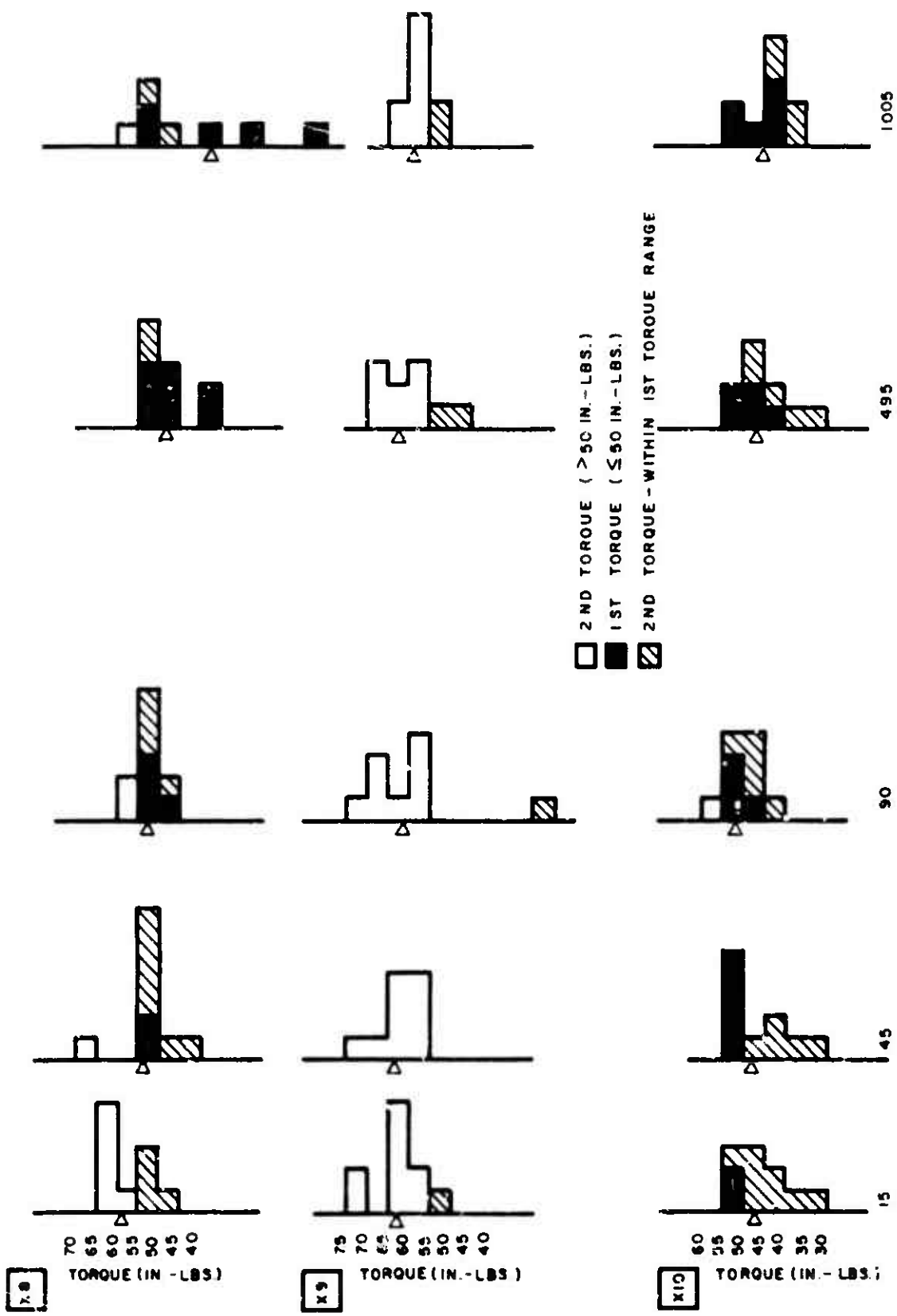

Figure 4-77. Torque Histograms vs No. Thermal Shock Cycles - Vendors 8, 9, and 10

did not weaken the seal so when the higher scale wrench was used, only values greater than 50 inch - lbs were noted. With Vendor 8 and especially Vendor 10, many readings less than 50 inch - lbs were noted after the device had initially passed a 50 inch - lb torque. This weakening of the seal upon application of the 50 inch - lbs torque affects the samples with the least cycles more than it does the samples with 1005 cycles. The thermal shock cycling seems to "stress relieve" the bonds in the glass which would otherwise have been weakened by the first torque application.

Vendor 8 was the only one showing extensive seal strength degradation at 1005 cycles of 0 - 100°C thermal shock. The normal bell shaped distribution seems to fall apart. These low values were all first torque values.

The data codes for these products were:

Vendor 8	7150A, 7127A
Vendor 9	7025
Vendor 10	

4.9.3 Degradation of Mean Torque Strength

The torque values are distributed in reasonably bell-shaped fashion so use of normal mean and standard deviation statistics will be valid. These statistics are given in Table IV-41. The overall mean torque values, average torque for all three vendors, are plotted in Figure 4-78, and the individual responses in Figure 4-79.

Vendor	TORQUE STATISTICS						
		Correlation	15c	45c	90c	495c	1005c
3	$\bar{x}$	48.50	54.40	49.10	48.80	43.30	37.38
	s	6.81	5.25	5.51	4.21	6.00	18.35
	+95%	68.67	64.70	59.89	57.05	55.06	73.35
	-95%	28.33	44.10	38.31	40.55	31.54	1.40
	N	14	10	10	10	10	8
	%<50	57.14	10	50	60	90	62.5
	%<40	7.14	0	0	0	20	37.5
9	$\bar{x}$	52.00	58.60	58.10	60.44*	57.20	54.10
	s	7.22	5.21	5.70	4.17*	6.75	2.85
	+95%	73.37	68.81	69.28	68.61*	70.42	59.68
	-95%	30.63	48.39	46.92	52.28*	43.93	48.52
	N	15	10	10	10	10	10
	%<50	33.33	0	0	0*	10	0
	%<40	6.67	0	0	0*	0	0
10	$\bar{x}$	42.43	42.20	43.00	46.90	41.40	40.60
	s	6.49	6.00	7.42	5.00	5.80	4.95
	+95%	61.64	53.95	57.55	56.70	52.76	50.30
	-95%	23.22	30.45	25.45	37.10	30.04	30.90
	N	14	10	10	10	10	10
	%<50	92.86	90	70	60	90	90
	%<40	21.43	20	20	0	20	30
	$\bar{x}$	47.64	51.73	50.07	50.87	47.30	44.03
	s	6.84	5.49	6.21	7.06	6.18	8.72
	+95%	67.89	62.48	62.24	64.70	59.42	61.11
	-95%	27.39	40.98	37.90	37.04	35.18	26.94
	N	3	3	3	3	3	3

*Not including the maverick failure

TABLE IV-41

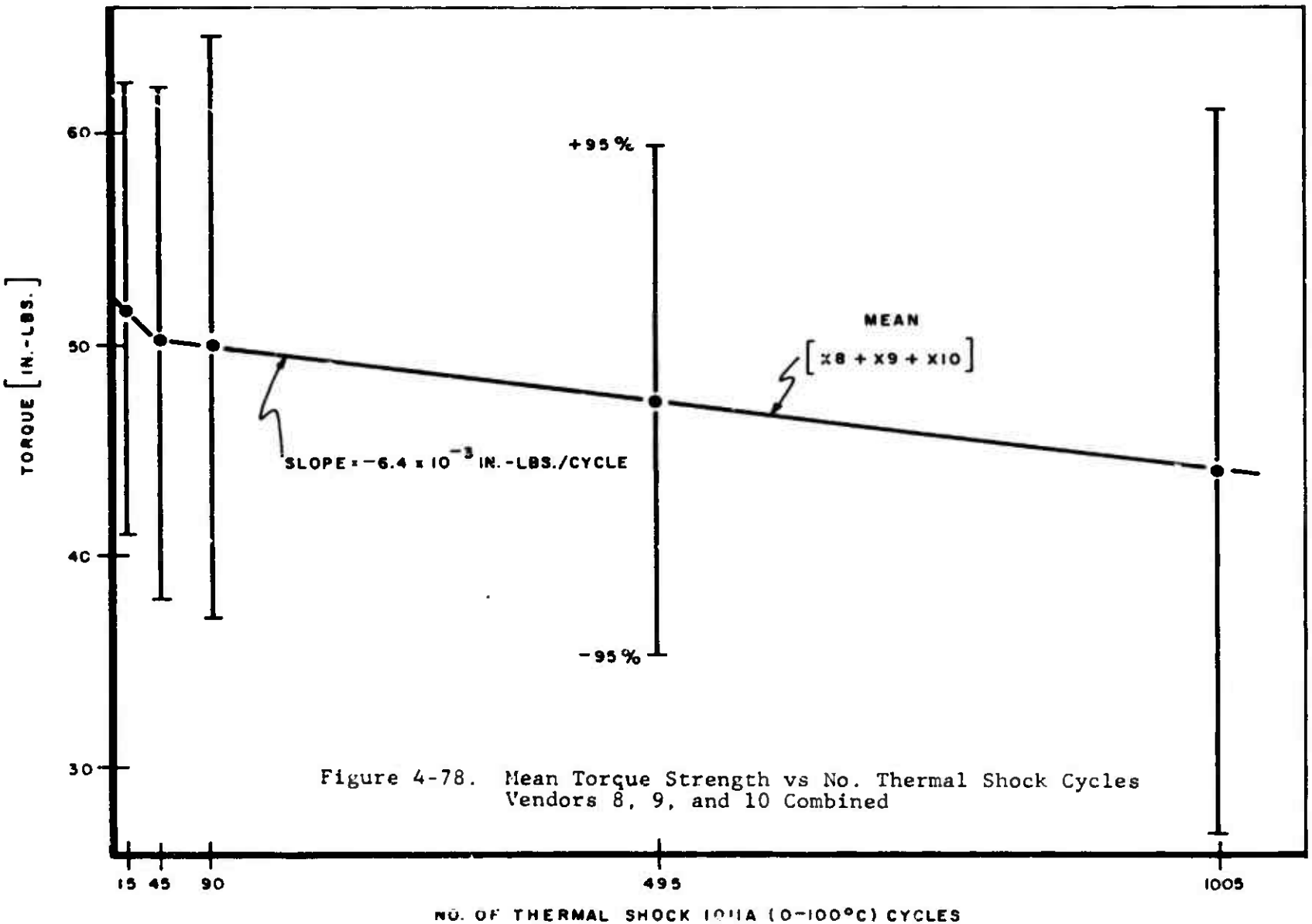

Figure 4-78. Mean Torque Strength vs No. Thermal Shock Cycles Vendors 8, 9, and 10 Combined

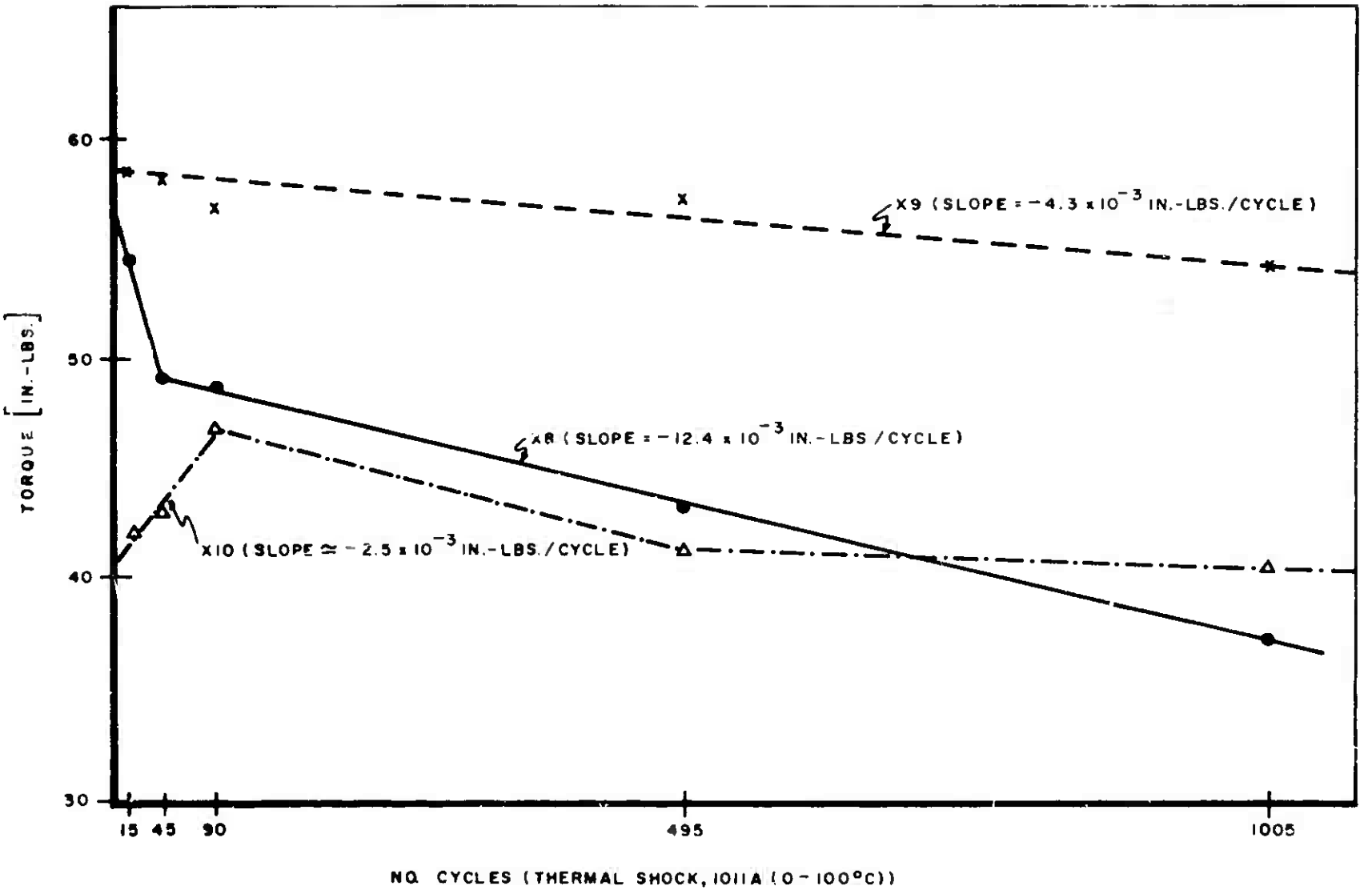

Figure 4-79. Mean Torque Strength vs No. Thermal Shock Cycles by Vendor

The mean torque strength degrades with increasing number of 0 - 100°C thermal shock cycles on all three vendors parts. This degradation is greatest for Vendor 8 and least for Vendor 10. The estimated average degradation of torque values per cycle are as follows:

Torque Degradation per 1000 Cycles
(0 - 100°C) Thermal Shock

	V8	V9	V10	Overall
in-lbs/1000C	-12.4	-4.3	-2.5	-6.4
%/1000C	-24.9%/1000C	-7.3%/1000C	-5.8%/1000C	-12.67%/1000C

Although this degradation does not appear to be too severe, it is quite linear with number of cycles from the first 15 cycles through 1005 cycles termination point.

Visual examination of the fracture surfaces did reveal some minor differences. In Vendor 8, nearly all parts failed at "A" and "E" simultaneously (Figure 4-80); i.e., some glass was still attached to the base and the remainder attached to the lid. At each of these interfaces, the ceramic looked smooth and unwetted. The attached glass was dark gray/black in color and fairly uniform in texture with occasional small bubbles. There were very few devices where the glass broke a "C", the plane of the lead frame. The lead frame looked well bonded in the glass and the frame/glass interface had strong uniform bonding. There was no obvious differences in failure mode with increase in number of cycles of thermal shock.

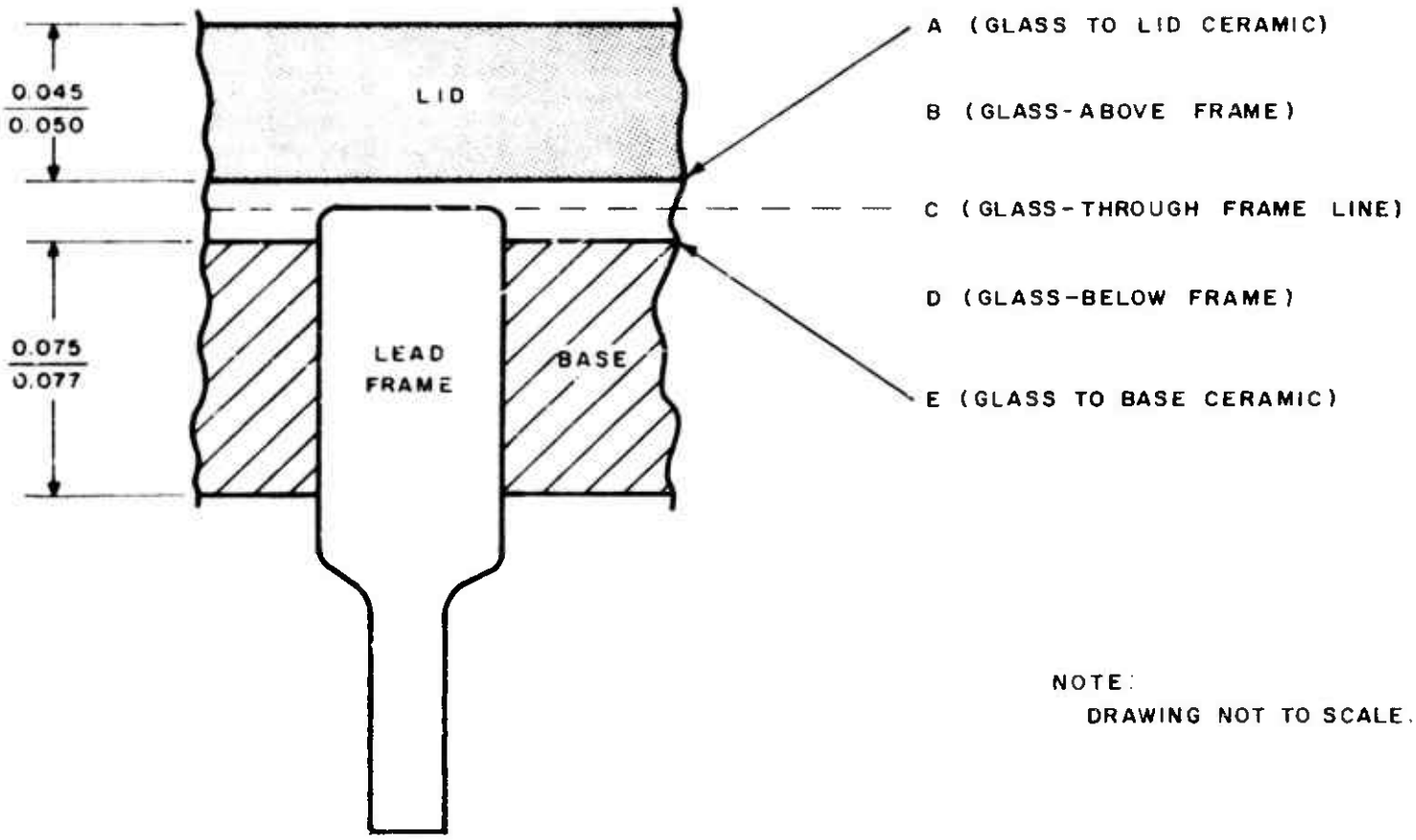

Figure 4-80. CERDIP Torque Failure Locations

Vendor 9 has a different glass than Vendor 8 or 10. His glass looked light gray rather than gray/black. There were some small bubbles in the glass between leads 7 and 8, between pins 6 and 9, on a number of these devices. With this vendor, most of the torque failures occurred at interface "A" with the second largest number at "A" and "E" together as was the case with Vendor 8.

As with Vendor 8, Vendor 9 had no failures along the lead frame or in the glass on either side of the lead frame and there was no obvious shift in failure mode with number of cycles.

Vendor 10 looked like Vendor 8. Almost all failures occurred with separation at "A" and "E" simultaneously and none along the lead frame. There were some bubbles in the glass and the glass looked like it had been more "liquid" than the other two samples. This glass flowed between leads well, but still trapped some bubbles.

4.9.4 Discussion and Conclusion

Thermal Shock, Method 1011A, 0 - 100°C does cause degradation of ceramic dual-in-line packages resulting in fine leak (helium > 1 x 10^{-8} atm cc/sec) failures and a weakening of the strength of the glass seal to the lid and base.

An explanation for this behavior may be as follows. When a CERDIP package is sealed, bonds are formed between the glass and the ceramic lid and base at interfaces "A" and "E". As the device cools down, these bonds are left in a stress condition. Upon subjecting the package to liquid-to-liquid 0 -100°C thermal

shock, some of these bonds fail, allowing small leak paths to be developed into the inner regions of the package. During the helium leak end point test, helium becomes trapped in these "microcrack" regions and internal bubbles in the glass - now connected to the outside world by these fixtures. As additional thermal cycling is imposed, additional bonds fail, creating additional or longer leak paths in the device and creating new "microcracks" in devices not previously detected as fine leakers.

This process continues, resulting in an increase in fine leak failures and a degradation in torque strength values with increased thermal shock cycles until the fine leaker becomes a gross leaker or until the seal strength becomes so weak that the package fails mechanically when handled.

If Method 1011C (-65°C +150°C) Thermal Shock is used instead of 1011A, the failure mode shifts from fine leak to gross leak (as seen in Section 4.8). The results of Section 4.8 and 4.9 appear to be consistent.

SECTION V

5.0 FAILURE ANALYSIS

5.1 PROCEDURES

These procedures were used to verify rejects, open the packages and investigate for failure modes and mechanisms.

5.1.1 General

Any device failing the end-point test sequence was sent to failure analysis. Prior to decapsulation, the reject status was verified electrically by read and record data from the Fairchild 4000 Test Set and by opens and shorts findings using a Tektronix 575/576 curve trace.

In addition, the package was analyzed externally using a low power (approximately 10X) microscope.

5.1.2 Decap - Plastic

Plastic dual-in-line packages were opened by one of these two procedures. The sandblast technique is faster but does destroy the wirebonds as the flag is removed. The chemical decap takes much longer to perform but does leave all parts in place.

5.1.2.1 Sandblast Decap

(A) Flatten the leads, then polish or sandblast the underside of the package to expose the metal flat (diebond pad) and pin or through-bar holding the

die. Do not reduce the flat thickness, as peel-off could occur.

(B) Sandblast a moat around the flag and through-bar. Turn up the ends of the through-bar with a knife blade or pliers, without affecting the flag or disturbing it.

(C) Apply heat gun to the plastic side (top of unit), or place the plastic side on top of a hot plate (500°F or greater).

The plastic will expand sufficiently to release the flag and die by pulling on the through-bar moderately, while applying the heat. Use of a hot plate allows mass decapsulation.

5.1.2.2 Chemical Decap

(A) Solder a holding wire (like a closed-loop paper clip) to all leads of the device.

(B) Heat concentrated sulfuric acid to approximately 200°C.

(C) Lower the part into the acid. Leave until plastic is dissolved (approximately 15 min.).

(D) Remove - let cool - dip into acetone to remove acid.

(E) Carefully blow dry or air dry.

5.1.3 Decap - Hermetic

Several different techniques were used to open hermetic dual-in-line ceramic, ceramic flat packages with recessed lids,

metal flat packages and daul-in-line sidebraze packages with solder seal lids.

5.1.3.1 Vise Grips (Cerdips Only)

(A) Hold leads on one side of the device with a vise.
(B) Grip top ceramic on the sides with vise grips.
(C) Pull straight up. Top will come off along a fracture plane exposing the top surface of the lead frame.
*Wires embedded in the pyroceram sealing glass near the posts attached to the top will be broken upon lid removal.
*This procedure mainly used when interested in die defects examination rather than wires or wire bond examination.

5.1.3.2 Wax Down (Cerdips)

(A) Stand the Cerdip part on the metal plate.
(B) Apply wax under and around the leads so that the entire body and leads of the device are embedded in wax. The wax should not cover the lead frame at the edge of the package.
(C) Hold the metal plate in a vise.
(D) Grip the top with vise grips and pull straight up.
*This procedure was used on the wirebond degradation samples.
*The wax holds the leads and body firmly. generally preventing the lead frame from pulling off with the lid.

5.1.3.3 Lid Grind (Cerflats)

(A) Wax down the flat package to a metal plate with Quartz Sticky Wax.
(B) Using a small hand grinder (such as a Dremel Model 281) with a diamond cutter wheel (Model 35X-P, DENSCO, Denver, Col.), make vertical cuts through the lid along each of the lid's four sides.
(C) Lengthen the cuts using the diamond cutter.
(D) Using a knife blade, pick out the lid material between the cuts leaving a hole in the lid exposing the die, wires, and package posts.
*This procedure used on the wire pull degradation sample - Cerflats.

5.1.3.4 Solder Decap (Sidebraze Dip)

(A) Hold leads along one side of the device with a vise.
(B) Using a sharp pocket knife, cut at the solder at the edge of the lid so as to allow the blade to be inserted under the lid edge.
(C) Pry up the lid to break the solder seal.

5.1.3.5 Solder Seal Decap (Flat Packages)

(A) Wax the flat package down to a metal plate using Quartz Sticky Wax.
(B) File down the lid at a slight angle until a corner of the metal lid is filed through, allowing a knife blade to be inserted under the lid edge.
(C) Pry up the lid to break the solder seal.

5.2 FAILURE MECHANISMS - HERMETIC DEVICES

All hermetic parts had packages with cavities. These cavities were backfilled with a gas - normally nitrogen. The gaseous atmosphere surrounded the die, wires and bonds. Wires were free to move in this atmosphere.

5.2.1 Wireflex (Aluminum Wire)

One of the principal failure modes for devices with aluminum wires was break at the heel of the bond following repeated thermal cycling. The mechanism causing this failure mode is wireflex.[22], [21]

Figure 5-1 shows how this happens. As the device changes temperature, the wires will expand or contract accordingly. This change in wire length causes the angle at which the wire contacts the bond to change. Eventually, the heel of the bond will become "work hardened", brittle, and fracture. The fracture occurs at the thinnest region of the heel of the bond. Many failure analyses call this a "chopped bond" since the fracture does result in a tearing defect at the heel of the bond. Generally, these wireflux failures are not due to chopped bonds, but chopped bonds would fail sooner than those with no tears at the heel. Bonds with normal deformations will fail for wireflex eventually.

Wireflex failures are more likely to occur at the heel of the first bond. This would be the post bond heel when using post-to-pad bonding as shown in Figure 5-1, and the pad bond heel when using pad-to-post bonding. When using post-to-pad bonding, the first bond is placed on the post. The bonding tool tip is

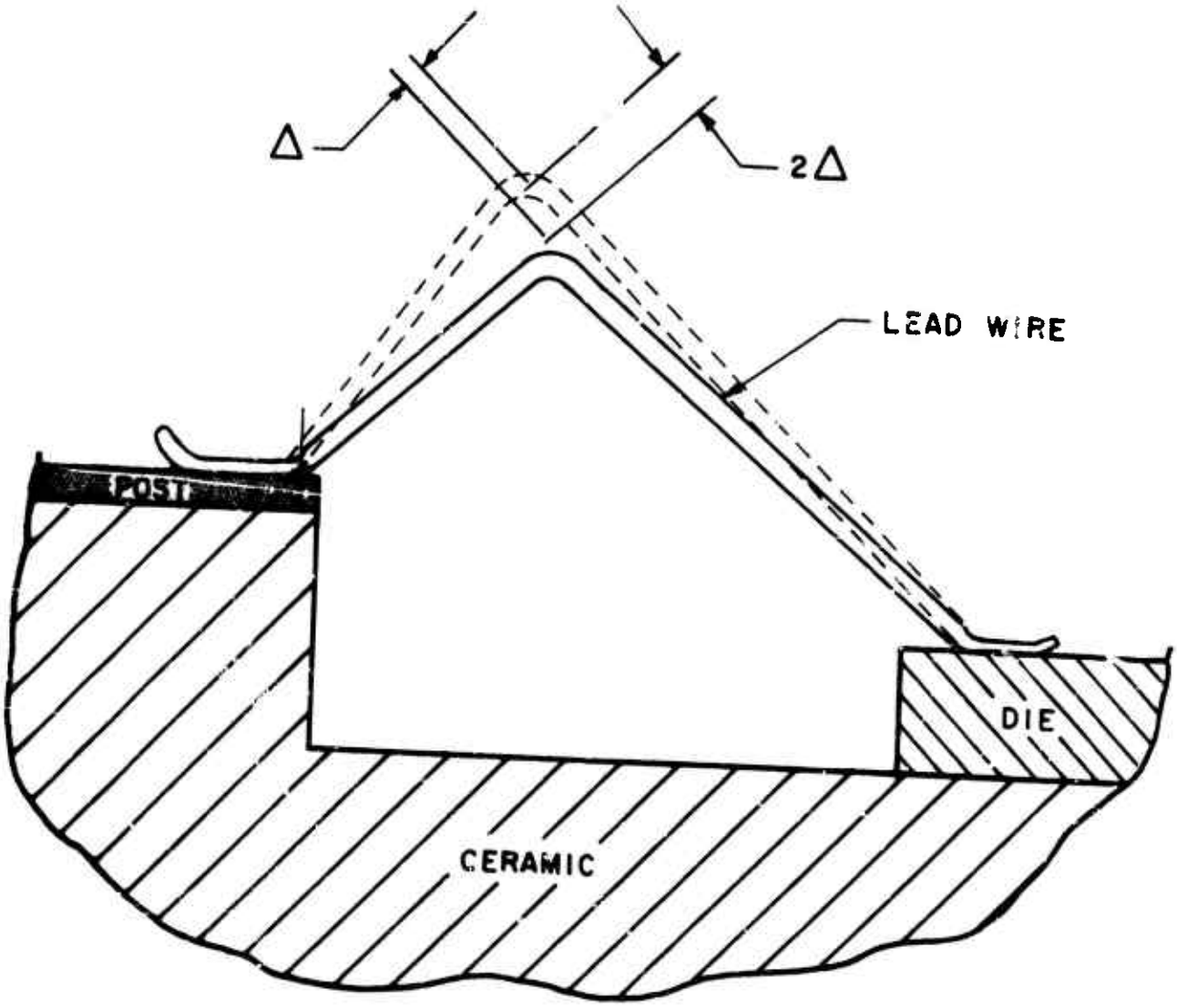

Figure 5-1. Illustration of Wireflex

raised slightly to allow the wire to feed through the needle; then the wire is routed over and down to the bonding pad on the die, where the bond-to-die is made. Two things act to weaken the first bond: First, the lifting and pulling of the wire at the first bond while setting the loop height and routing the wire to the pad; and second, the maximum loop height will normally occur closest to the first bond subsequently experiencing more delta (2Δ) angle flexure during thermal cycling.

It can be shown that a "tight wire", one routed directly from pad-to-post with no loop, is a worst-case condition. As the wire tries to contract, it stretches the wire at the heels, causing them to thin and weaken. Then when the wire expands, it goes under compression. Since it has no loop, it will continue to expand until the wire develops a bow, flexing both bonds at the heels. This flexing will cause the weakest heel to break. Conversly, wires with large loops tend to expand along the loop with very little change in the angle of wire-to-bond and therefore little flexing.[18]

If one end of the aluminum wire is bonded to a gold post, the additional presence of gold-aluminum intermetallics cause this bond to weaken and become brittle sooner than if the bond were made to an aluminum clad post or bare Kovar post. Design limits for gold-aluminum wirebonds are discussed in detail in Reference 13.

Wireflex failures occur primarily with aluminum wires. Gold wires are generally much more ductile and resist "work hardening" unless they are bonded to aluminum metallization. In this case, failure will occur in the intermetallic regions.

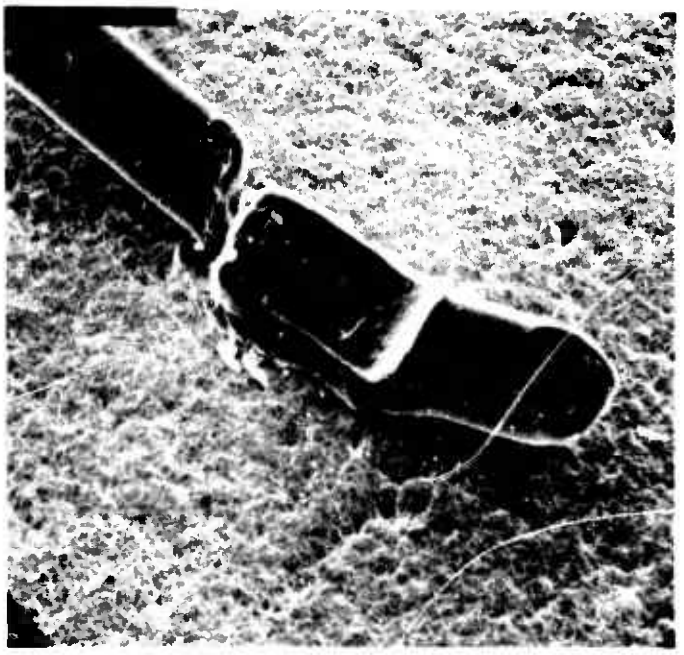

440X

Figure 5-2. Wireflex Break at Heel
(Lot L11, Sidebraze, 3000 Cycles of 1010D)

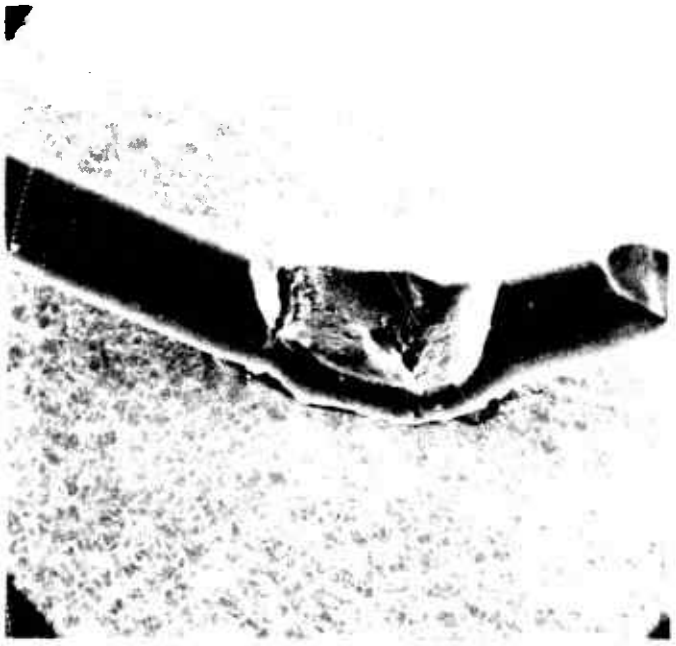

420X

Figure 5-3. Wireflex Break at Heel
(Lot L11, Sidebraze, 3000 Cycles of 1010D)

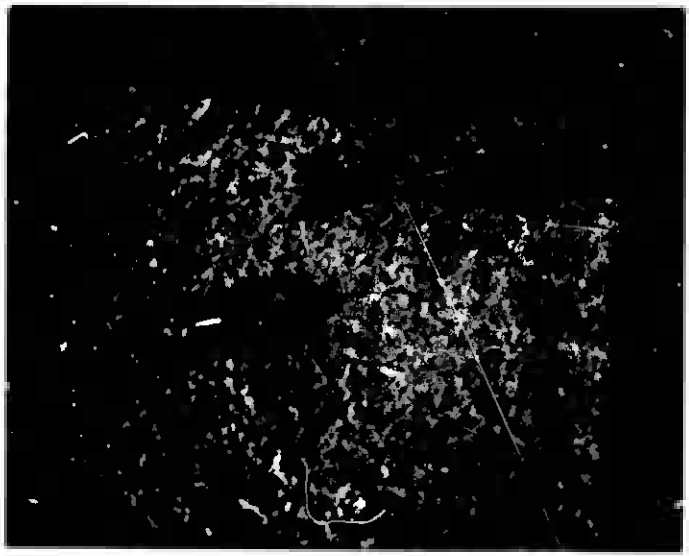

Figure 5-4. Wireflex Intermetallic Failure
Aluminum Wire to Gold Post
(Lot D11, 3500 Cycles of 1010C)

Figure 5-5. Wireflex Failure - Pad Bond
(Lot D6, 4500 Cycles of 1010C)

See Referenees 18, 19, 20, 21, and 22 for further comments.

Figures 5-2, 5-3, 5-4, and 5-5 are examples of wire-flex failures found in one testing.

5.2.2 Intermetallic Failures (Au - Al)

Whenever gold and aluminum are bonded together, sueh as when an aluminum wire is bonded to a gold-plated post or when gold wire is bonded to aluminum metallization, several compounds of gold and aluminum are formed.[13] The two most eommon ones are Au Al_2 (purple color) and Au_5 Al_2 (tan color).

Upon repeated thermal cyeling, differences in coefficient of expansion within the intermetallie region eause miero-eraeks to form in the regions of high stress. These miero-eraeks become Kirkendall voids[13] in the Au_5 Al_2. The failure mode is intermittent or hard opens and zero wirepulls. Figures 5-6, 5-7, 5-8, 5-9, and 5-10 are examples of intermetallie formation under the ball of the bond.

Kirkendall voiding will also oeeur when bonds are aged at temperatures greater than 300°C.[13] These voids are formed in the aluminum due to the higher diffusion rate of aluminum into the intermetallic phase at elevated temperatures.

Reliability performanee may be inereased by keeping the temperature below 300°C; using larger diameter gold wires so as to restriet the formation of the stronger gold rich intermetallics,[13] and keeping the post plating thin in relation to the bond heel thickness.

300X

Figure 5-6. Intermetallic Open (Au/Al) with Surface Reconstruction (Pads) (Lot D5, 4000 Cycles of 1010C)

600X

Figure 5-7. Intermetallic Open (Au/Al) with Surface Reconstruction (Pads) (Lot D5, 4000 Cycles of 1010C)

2,400X

Figure 5-8. Intermetallic Open (Au/Al) with Surface Reconstruction (Pads) (Lot D5, 4000 Cycles of 1010C)

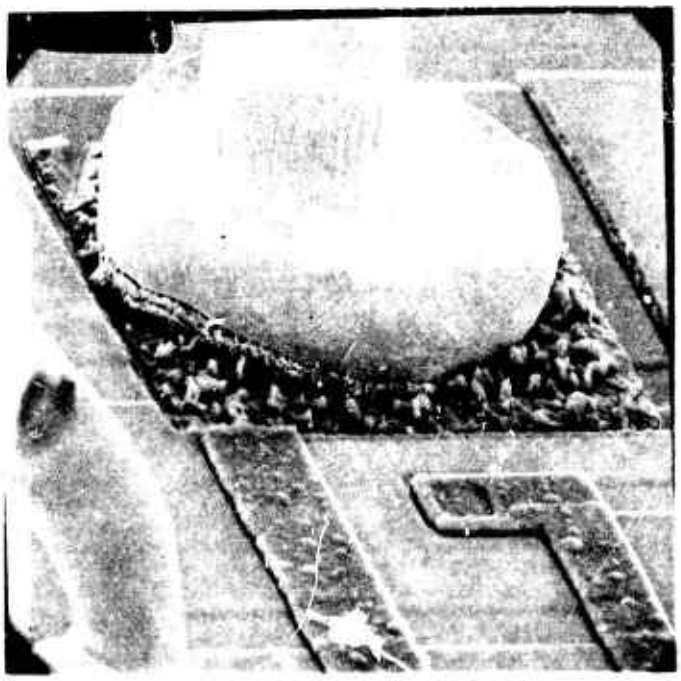

600X

Figure 5-9. Intermetallic Open (Au/Al) with Surface Reconstruction (Pads) (Lot D5, 4000 Cycles of 1010C)

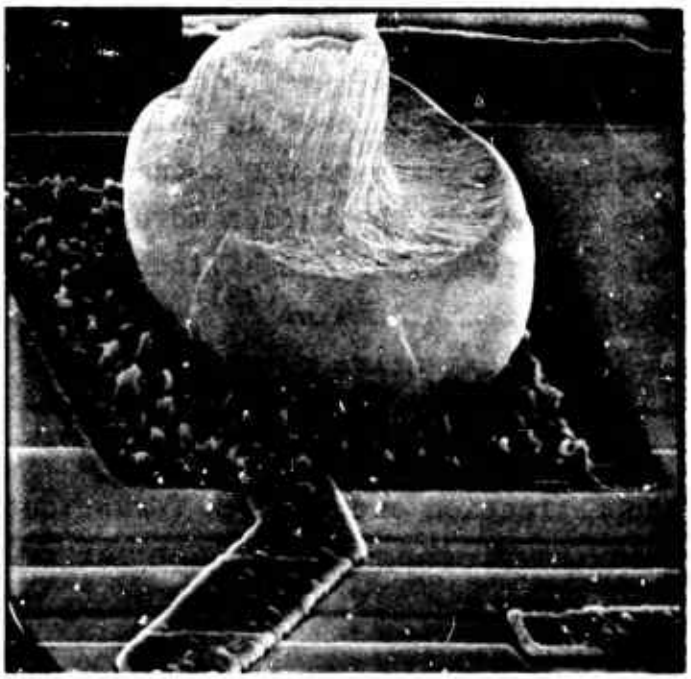

600X

Figure 5-10. Intermetallic Open (Au/Al) with Surface Reconstruction (Pads) (Lot D5, 4000 Cycles of 1010C)

It was noted that Vendors 1 and 4 used 1.5 mil (38μm) gold wire with plastic packaging. All other wire sizes were 1.0 mil (25μm). Of the Cerdip parts, only the sidebraze, Vendor 11, had aluminum wire to gold plated package posts. The LSI packages, Vendors 12 and 14, had gold plated posts.

5.2.3 Metallization/Oxide Defects

Thermal cycling causes changes in volume of structures due to thermal expansion. If these volume changes are great enough, cracks will be formed in the harder more brittle materials and restructuring, electromigration, and hillock formation will be formed in the more ductile materials.[23] (See Figures 5-6, 5-7, 5-8 5-9, and 5-10 for extensive reconstruction on the bonding pads.)

Surface reconstruction and hillock formation are dependent upon grain size in the aluminum films. The larger the grain size, the less hillock formation. Figure 5-11 shows an example of surface reconstruction.

For both small and large grain films, the greater the temperature extremes or number of thermal cycles, the greater the extent and severity of the reconstruction.[23]

Oxide defects most often occur as the result of imperfect wafer masking and etching. The result is a region of oxide insulation which is thinner than normal. Expansion and contraction caused by thermal cycling will cause these thin oxide regions to develop cracks. If metal is over the oxide defect, it can work it's way down the crack, eventually causing a short between the metal and underlying structure. Figures 5-12 and 5-13 show examples of oxide defects.

Figure 5-11. Surface Reconstruction
(Lot F7, Cerflat, 1500 Cycles of 1010E)

Figure 5-12. Oxide Defect
(Lot D6, 2000 Cycles of 1010C)

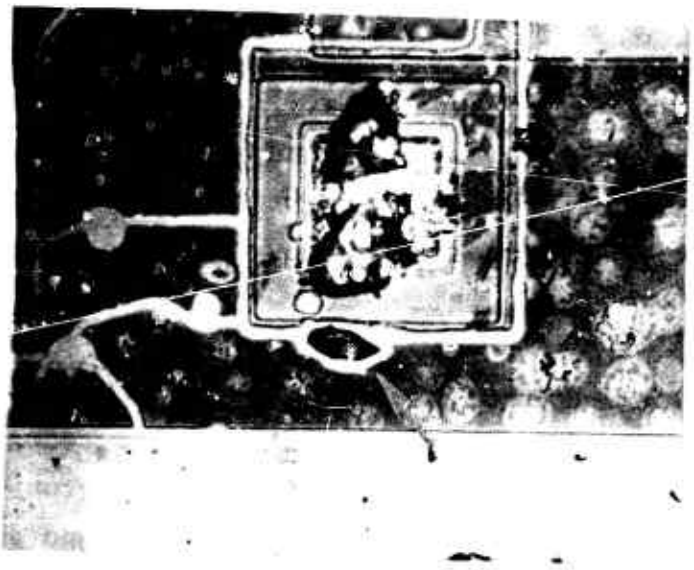

Figure 5-13. Oxide Defect - Damage by U/S Bonder (Lot D6, 4500 Cycles of 1010C)

5.2.4 Hermetic Seal Defects

All hermetic devices received seal testing per MIL-STD-883, Method 1014, Condition A (Fine Leak - Helium) and Condition C (Fluorocarbon Bubble Test) initially and at every readout thereafter.

A device was considered a fine leaker if it had a reading greater than 5×10^{-8} atm. cc/sec. and a gross leaker if it exhibited a stream of bubbles or one big bubble. All indicated gross leakers were subjected to red dye verification.[31] See Figure 5-14 for a red dye failure.

Several leak responses were noted. First ceramic devices subjected to thermal cycling would become fine leakers after some number of cycles. These devices, which passed gross leak but repeated as fine leakers, were left in the lot and given additional thermal cycling. At each subsequent readout, these same devices would fail fine leak until eventually they failed gross leak, were removed from the test and verified with red dye. All indications were that thermal cycling, especially thermal shock, Method 1011, caused micro-cracks to form between the bubbles on voids in the sealing glass material. Section 4.3 shows that the sealing glass is the weak material. As more and more micro-cracks were formed, more helium was trapped in the connected voids, increasing the measured leak value. After sufficient thermal cycling, the amount of micro-cracking became great enough to cause the trapping of enough fluorocarbon to cause a failure indication to this test Red dye verification showed that the dye often penetrated only halfway to the cavity. The internal cavity was still hermetic but the device failed both fine and gross leak tests. This progressive deterioration in leak test performance correlates well with the torque test results of Section 4.9. The amount of micro cracking seems to correspond to the decrease in mean torque value.

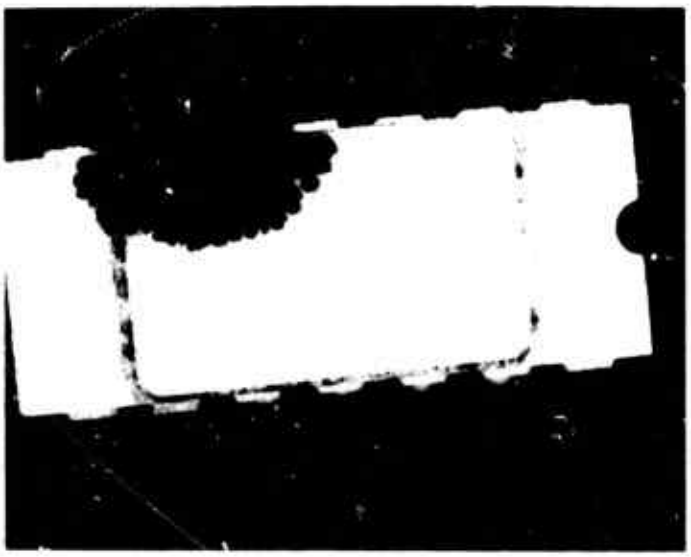

Figure 5-14. Gross Leak (Red Dye) at Cap Seal
(Lot All, Sidebraze, 10 Cycles of 1010E)

Second, a device would become a fine leaker and repeat as one for the next two or three readouts, and then appear to be good. Upon further thermal cycling and seal testing, the device would fail gross leak. There appeared to be a gap between being a fine leaker and becoming a gross leaker. These devices went through the transition region between fine and gross leak more slowly. At the transition point, where they tested good, they were large enough fine leakers to be flushed of helium prior to measurement, but small enough to be missed in the gross leak test. There definitely appeared to be a gap between fine and gross leak responses.

Third, a device following exposure to a severe thermal shock would indicate a gross leaker directly. Occasionally, the lid would come off and the parts would disintegrate. These devices had been subjected to thermal shock which exceeded their critical value and they were destroyed by the test (see Section 4.5.3).

Fourth, solder sealed devices failed if subjected to temperature extremes greater than 325°C. At these temperatures the solder melted and the lid would be free to move. It was possible to cause the lid to "float" on molten solder but "resolder" itself upon cool-down, retaining it's hermeticity.

Section 4.3 shows that hermeticity failures are most likely to occur during the heating from low temperature or at thermal equilibrium at the low extreme.

5.3 FAILURE MECHANISMS - PLASTIC DEVICES

All plastic parts are molded into a solid block with no cavity. Plastic material surrounds the die, wires and bonds. The wires are not free to move. They are constrained by the plastic.

5.3.1 Wirebond Failures

5.3.1.1 Intermetallic Failures

All plastic parts in this experiment had gold wire bonded to aluminum metallization on the die and to gold plating on the posts. Vendors 2, 3 and 14 used ball bonding on the die, and 1.0 mil diameter wire. Vendors 1 and 4 used thermo-compression bonding and 1.5 mil diameter wire.

Gold-aluminum intermetallics were formed in the pad bonds which were weakened by thermal cycling. The failure mode was "opens" between the metal stripe and the gold bonding wire due to Kirkendall voiding around the outer edge of the bond between the bond and the metal stripe.[13] These failures often failed for intermittents first before the wire was moved enough to indicate a hard open.

Section 4.6.2 verifies that 1.5 mil diameter wire is more reliable than 1.0 mil wire as recommended in Reference 13 and 14. In all cases, the 1.5 mil samples out-performed the 1.0 mil diameter wire samples.

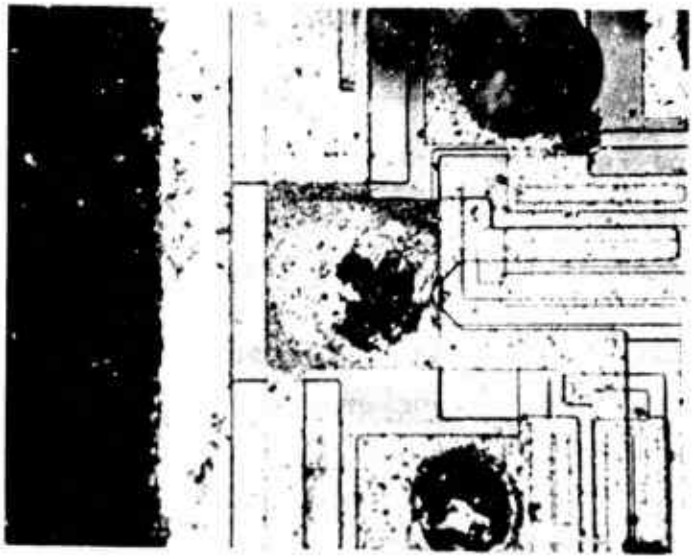

Figure 5-15. Intermetallic Open - Bond to Pad (Lot B2, 10 Cycles of 1011C)

Figure 5-16. Intermetallic (Au/Al) - Gold Wire to Aluminum Pad (Lot G4, 3005 Cycles of 1011A)

In terms of wire bond failure mode, intermetallics failures occur as LD, lift at the die, and BD, break at the heel of the bond to the die. Figure 5-15 and 5-16 show examples of intermetallics failures on plastic devices.

5.3.1.2 Chopped Bonds

Occasionally, a thermocompression bond will be formed with excessive deformation of the wire resulting in a bond with a thin heel region. This thin heel region may also be nicked or damaged by the bonding needle.[18] As the plastic package expands and contracts during thermal cycling, the plastic-enclosed wires will undergo extensive tension stress in the wire due to the difference in coefficient of thermal expansion between the plastic and the wire. These tension forces, which normally act on a different part of the wire (see Section 5.3.2.1), can stretch the thin bond heel until it breaks. This failure mode is normally associated with the gold wire to gold plated post bond, not subject to intermetallic formations.

5.3.2 Wire Failures

5.3.2.1 Grain Boundry Fracture[24]

The most common failure observed with extended thermal cycled plastic parts was grain boundry fracture.[24] This failure mode manifests itself as a thinning down of the gold wire a few mils up from the bond combined with "open" wire along the grain boundries in the wire.[14] This failure mode is due to the

difference between the coefficient of thermal expansion between the gold wire and the plastic. Thermal cycling subjects the wires to extreme tension, causing excessive grain growth to occur across the wire - eventually causing the wire to fracture along the grain boundry. The fracture mode is intermittent or hard opens. This failure mode is only found in plastic devices where the wires are physically constrained by the plastic. Both elevated temperature and stress are required to cause the failure. Failures occur quickly when the plastics glass transition point is exceeded due to the sharp increase in coefficient of thermal expansion. Figures 5-17 through 5-23 show examples of grain boundry fracture failures.

Reliability can be enhanced by keeping the temperature excursions small, never exceeding the glass transition point, using plastics of low coefficient of thermal expansion and use of plastic with high shrinkage.

5.3.2.2 Intergranular Cracking[24]

This failure mode is very similar to grain boundry fracture (see Section 4.3.2.1) except that the tension stress in the wire causes slip planes at nearly 45° to the axis of the wire. These slip planes can allow the wire to slide relative to one another, creating a "bamboo" effect in the wire. There is less noticeable thinning of the wire with this failure mode.

5.3.3 Corrosion

Plastic packages are not as hermetic as ceramic packages when subjected to thermal shock. As the package expands, the thermal shock liquid can enter the body of the device along the lead frame and come into contact with the die surface.

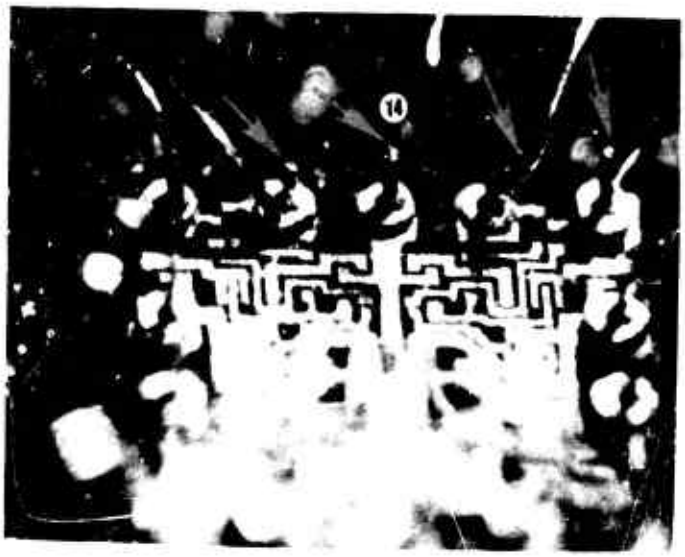

Figure 5-17. Crain Boundry Fracture
(Lot P3, 30 Cycles of 1010D)

Figure 5-18. Grain Boundry Fracture
(Lot P3, 30 Cycles of 1010D)

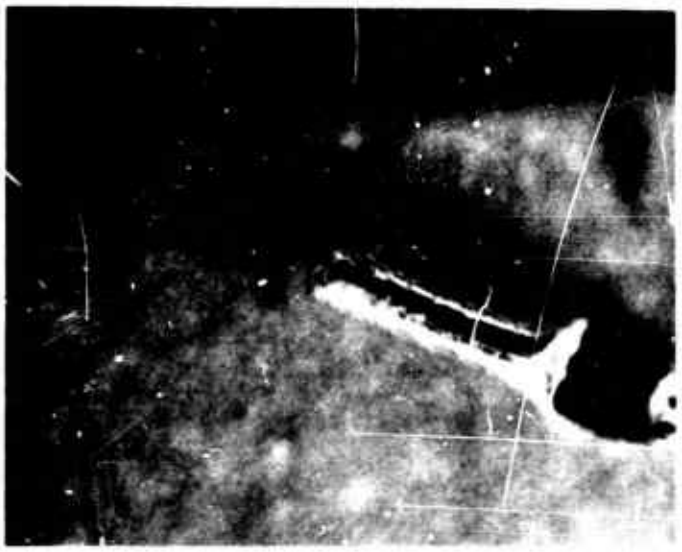

Figure 5-19. Grain Boundry Fracture
(Lot L1, Epoxy, 500 Cycles of 1010D)

350X

Figure 5-20. Grain Boundry Fracture
(Lot L1, Epoxy, 500 Cycles of 1010D)

1,000X

Figure 5-21. Grain Boundry Fracture
(Lot L1, Epoxy, 500 Cycles of 1010D)

2,000X

Figure 5-22. Grain Boundry Fracture
(Lot L1, Epoxy, 500 Cycles of 1010D)

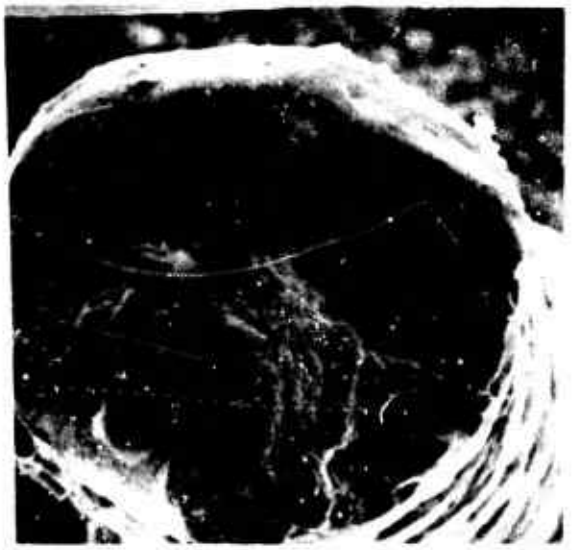

2,000X

Figure 5-23. Grain Boundry Fracture
(Lot L1, Epoxy, 500 Cycles of 1010D)

Figure 5-24. Corrosion
(Lot G4, 3005 Cycles of 1011A)

When the device is then biased, any moisture in contact with the aluminum pad metallization can interact, causing corrosion of the aluminum pad material.[33] The product formed is generally aluminum hydroxide. This aluminum hydroxide has about three times the molar volume of all-aluminum which is enough to cause damage to glassivation.[32] Figure 5-24 shows a stripe corrosion failure.

The presence of water also reacts with excess phosphorus (2 - 10 wt pct) to cause increased corrosion of aluminum. The amount of absorbed water increases with increasing P_2O_5, this water reacting with the aluminum to form $Al(OH)_3$ corrosion.

Thermal shock, Method 1011, Condition A is particularly destructive to plastic parts since water baths are used.

5.3.4 Temperature Coefficient of Thermal Expansion vs Wire Size

All other factors being equal, reliability of plastic integrated circuits increases with increase in wire size from 1.0 mil to 1.5 mil diameter. This increased reliability is due to the following:

(A) Larger, stronger bonds - withstands molding better.
(B) Greater tensile strength of the larger wire - therefore reduced susceptability to grain boundry fracture.
(C) Thicker heel regions - therefore reduced intermetallic voiding and fewer chopped bonds.

5.4 STRESS RELAXATION

One of the anomalies found in temperature cycling hermetic integrated circuits at various conditions was an apparent increase in reliability at test Condition D (-65/+200°C) compared to both test Condition C (-65/+150°C) and test Condition E (-65/+350°C). This anomally in electrical failure rate was consistent across all vendors except Vendor 11. This result is thought to be due to stress relaxation.[30, 35]

When wire bonds are formed, the actual bond is made at a temperature above room temperature. As the part cools, stress begins to increase in deformed parts of the bond as it contracts. As the part undergoes thermal cycling, the bonds heat up, reducing the stress inherent in the structure. Each time it heats up and cools down, the bond loses some of its inherent stress. The closer the heat-up temperature comes to the initial formation temperature, the greater the degree of stress relaxation. The upper temperature must be high enough to cause plastic deformation in the materials.

Stress relaxation is essentially a decrease in initial stress with time and temperature. In hermetic devices this stress reduction is measured as a decrease in bond pull strength combined with an annealing of the stress part of the bond, i.e., the bond heel. This annealing of the bond heel causes a change in location of failure from break at the heel to centerwire breaks but with a decrease in pull strength.[38] The end result of stress relaxation in use conditions is the formation of slightly weaker but more flexible wires and bonds, resulting in lower thermal cycling failure rates.

The amount of stress relaxation goes up with time and temperature but so does the formation of gold-aluminum intermetallics. Above 200°C intermetallics become weaker than the stress relaxed bonds and the failure rate increases again. (See Section 4.6.3.3 - Vendor 11.)

As seen in Section 4.6.3.2, Extended Thermal Cycling of Dual-In-Line Ceramic Packages, the next level above test Condition D (-65/+200°C) was test Condition E (-65/+350°C). The results at Condition D show evidence of stress relaxation. Since the wire bonding was aluminum-to-aluminum in the parts, failure mode for Condition E was die attach failures, rather than intermetallics as experienced by Vendor 11 with its aluminum wire-to-gold plated posts. Stress relaxation normally is found in tin lead solder such as the die attach.[30] Figure 5-25 shows a floating die due to test Condition E.

It should be noted that an increase in failure rate occurs with plastic packages. The stress relaxed bonds and wires are weakened and cannot stand the tension in the wires resulting from the expansion of the surrounding plastic.

Stress relaxation can increase the reliability of hermetic parts having monometallic metal bonding but decrease the reliability of plastic parts whose internal wires are enclosed in plastic and hermetic parts with intermetallic bond structures.

Figure 5-25. Floating Die
(Lot F7, Cerflat, 1500 Cycles of 1010E)

REFERENCES

1 Intro. to Scientific Computing - G. A. Pall, Appleton-Century-Crofts, New York, 1971, p. 311-312.

2 Dielectric Bath Promotes Togetherness in IC's - Dupont Technical Bulletin EL-12.

3 UCON Fluids and Lubricants - Technical Bulletin by Union Carbide, 1971.

4 Handbook of Industrial Statistics - Bowker & Lieberman, Prentice Hall Inc. 1955.

5 Quality Control and Industrial Statistics - Duncan, Richard D. Irwin, Inc. 1952.

6 Fundamentals of Analysis of Variance - Charles R. Hicks Reprint from: Industrial Quality Control 1956.

7 Statistical Theory and Methodology in Science and Engineering - K. A. Brownlee, 2nd Ed., John Wiley & Son 1965.

8 A Systematic Approach to the Analysis of Means - Edward G. Shilling, Journal of Quality Technology, July 1973, October 1973.

9 Hazard Plotting for Incomplete Failure Data - Wayne Nelson, Journal of Quality Technology, January 1969.

10 Probability Charts for Decision Making - James R. King, Industrial Press, Inc. 1971.

11 Statistics Manual - Edwin Crow, Frances Davis, Margret Marfield, Dover Publications, Inc. 1960.

12 ASTM Manual on Quality Control of Materials - American Society for Testing Materials 1951.

13 Design Limits When Using Gold-Aluminum Bonds - Elliot Philofsky, 9th Annual Proceedings-Reliability Physics, 1971.

14 Metallurgical Behavior of Gold Wire In Thermal Compression Bonding - T. H. Ramsey, Solid State Technology, October 1973.

15 Failure Mechanisms Associated with Thermo-Compression Bonds in Integrated Circuits - G. Browning, L. Cotteryman, D. Cummings, Physics of Failure in Electronics, 4 (June 1966).

REFERENCES (Cont.)

16 Moisture in SC Packages - Robert W. Thomas, Donald E. Meyer, Solid State Technology, Sept. 1974.

17 Critical Parameters in Glass Sealed Ceramic Packages - T. H. Ramsey, Jr., Solid State Technology, Sept. 1974.

18 Metallurgical Failure Modes of Wire Bonds - G. G. Harmon, 12th Annual Proceedings - Reliability Physics, 1974, IEEE Catalog No. 74 CHO 839-1 Phy.

19 A Metallurgical Basis For the Non-Destructive Wire Bond Pull Test - G. G. Harmon, 12th Annual Proceedings - Reliability Physics, 1974.

20 Failure Analysis of Wire Bonds - Harry A. Schafft, 11th Annual Proceedings - Reliability Physics, 1974.

21 Thermal Excursion Can Cause Bond Problems - M. F. Nowakowski, F. Villalla, 9th Annual Proceedings, Reliability Physics, 1971.

22 Reliability Improvements of Wire Bonds Subjected to Fatigue Stresses - K. V. Ravi, E. M. Philofsky, 10th Annual Proceedings - Reliability Physics, 1972.

23 Surface Reconstruction of Aluminum Metallization - A Potential Wearout Mechanism - E. Philofsky, K. Ravi, E. Hall, and J. Black, 9th Annual Proceedings Reliability Physics, 1972.

24 A Bonding-Wire Failure Mode in Plastic Encapsulated Integrated Circuits - Clark N. Adams, 11th Annual Proceedings, Reliability Physics, 1973.

25 On Measuring the Mechanical Properties of Aluminum Metallization and Their Relationship to Reliability Problems - E. M. Philofsky and K. V. Ravi, 11th Annual Proceedings - Reliability Physics, 1973.

26 Temperature-Humidity Acceleration of Metal-Electrolysis Failure in Semiconductor Devices - D. S. Peck and C. H. Zierdt, Jr., 11th Annual Proceeding - Reliability Physics, 1973.

27 Stress Induced Intermittent Failures in Encapsulated Microcircuits - RADC - TR- 70-213, October 1970 (AD715984).

28 Reliability Evaluation of Plastic Integrated Circuits Delco Electronics Division of GMC - RADC - TR- 71 - 8, January 1971 (AD722043).

29 Controlling the Material Property Variable in Al-1% Si Bonding Wire - E. Philofsky and K. V. Ravi, Motorola, Inc., Central Research Report No. 123, Feb. 1970.

30 Some Effects of Temperature on Material Properties and Device Reliability - Earl Baker, IEEE Transactions on Parts, Hybrids, and Packaging Vol. PHP-8 no. 4, Dec. 1972.

31 Package Hermeticity - George E. Adams, 11th Annual Proceedings, Reliability Physics 1973, IEEE Catalog No. 73 CHO 755-9-Phy.

32 The Effect of Phosphorus-Doped Passivation Glass on the Corrosion of Aluminum - W. M. Paulson and R. W. Kirk, 12th Annual Proceedings, Reliability Physics, 1974.

33 Principles of Corrosion - Stephen C. Kosesar, 12th Annual Proceedings, Reliability Physics, 1974.

34 Principles of Electromigration - James R. Black, 12th Annual Proceedings - Reliability Physics, 1974.

35 Calculation of Thermally Induced Mechanical Stresses in Encapsulated Assemblies - Earl Baker, IEEE Transactions on Parts, Materials, and Packaging, Vol. PMP-6, No. 4, Dec. 1970.

36 Anticipatory Test Monitors I/C Suppliers Process Control - Gene Thoennes, 9th Annual Proceedings, Reliability Physics, 1971.

37 Purple Plague Revisited - Elliot Philofsky, 8th Annual Proceedings, Reliability Physics, 1970.

38 A Comparison of 1% Mg Al and 1% Si Al Wire Interconnects - J. M. Pankratz and D. R. Collins, 8th Annual Proceedings, Reliability Physics, 1970.

APPENDIX

DATA REDUCTION

A problem of variable sample size and missing data was evident. A timeshare program was written to obtain summary statistics from all these wirepull readings. These data are given by cell number in three tables

WPMV = Wirepull Strength Statistics
WPFM = Wirepull Failure Mode Statistics
WPCP = Wirepull Lower Distribution Statistics

In these tables, the coding is:

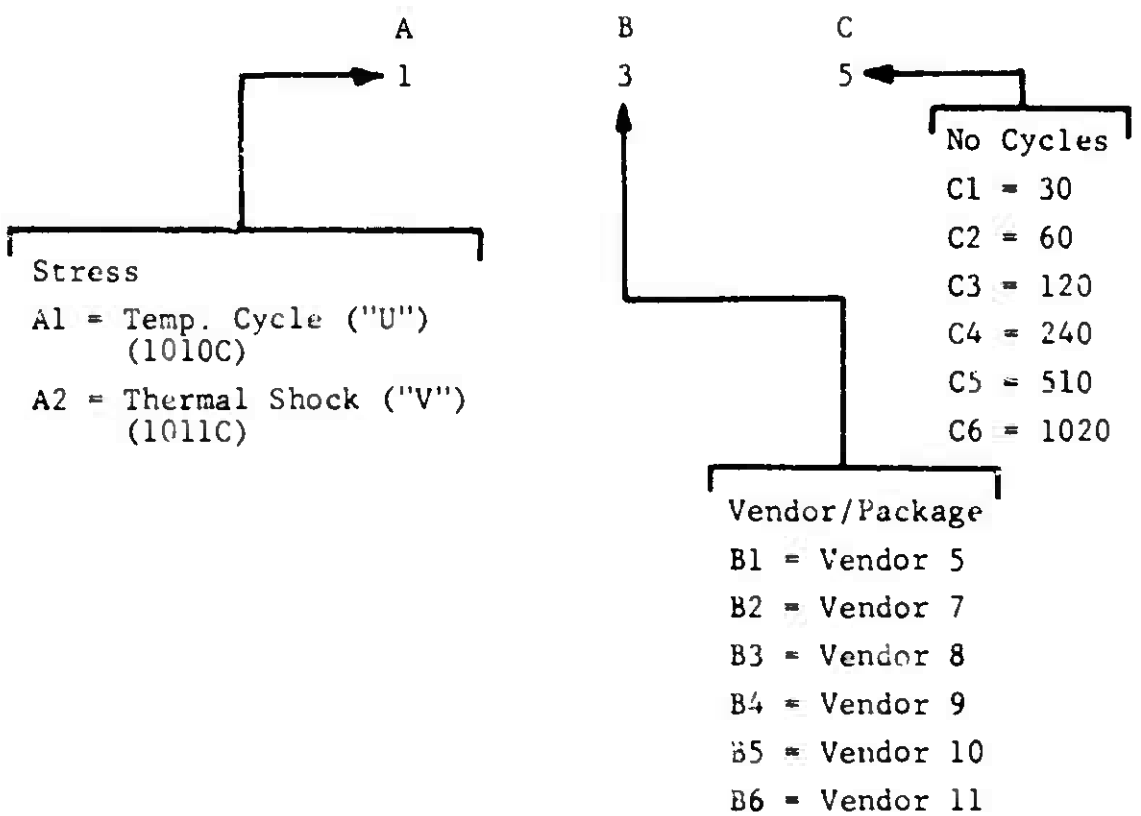

Example = Temp. Cycle - Vendor 8 510 Cycle Step
or U8 - 510 Cycle Step

The sums appear below a dotted line after the last cell summed over. In order to obtain all the sums, the data is sorted three ways within each table. (The individual cell data is repeated for ease of tracking and verification.)

The statistics available are:

WPMV

H = Highest value observed within the cell
M = Mean (Arithmetic Average)
L = Lowest value observed
R = Range (H - L)
S.D. = Standard Deviation ($=\sqrt{\text{Variance}}$)
Var = Variance
SS = Sample Size (= no wires pulled)

WPFM

% BD = % Break at the Die - wire breaks at the heel of the bond to die
% LD = % Lift at die - bond to die lifts off the pad with or without pad metal
% CW = % Center Wire - wire breaks between heel of bond to die and heel of bond to post.
% LP = % Lift at Post - bond to post lifts off the post - bond still attached to wire
% BP = % Break at post - wire breaks at the heel of the bond to post

WPCP

% $\leq$ 0.5 = % of pull strengths less than or equal to 0.5 grams force.
% $\leq$ 1.0 = % of pull strengths less than or equal to 1.0 grams force.

$\% \leq 1.5$ = % of pull strengths less than or equal to 1.5 grams force.

$\% \leq 2.0$ = % of pull strengths less than or equal to 2.0 grams force.

$\% \leq 3.0$ = % of pull strengths less than or equal to 3.0 grams - force.

These tables formed the data bank for further analyses.

PHASE II DATA REDUCTION:

Using the data from WPMV, WPFM, and WPCP, selected data were placed in arrays to facilitate comparisons while looking for trends.

Data was ordered two different ways. First by test - by number of cycles within Vendor/Package within stress. This is a conventional matrix for three variables: stress (at 2 levels); packages (at 6 levels); and cycle blocks (at 6 levels). This matrix allows direct analysis of vendors vs stress; vendor vs cycles; and stress vs cycles.

The second ordering is by total length of time at temperature extremes - mixing temperature cycling and thermal shock according to increase in exposure time at temperature extremes. This ordering dictates the following sequence:

A2C1, A2C2, A2C3, A1C2, A2C4, A1C3, A2C5,
A1C4, A2C6, A1C5, A1C6

and results in a two-way table rather than three-way.